



UNIVERSITAT POLITÈCNICA
DE CATALUNYA
BARCELONATECH

*Synthesis of acoustic wave filters.
Ladder and transversal topologies:
towards a practical complementation*

Alberto Hueltes Escobar

ADVERTIMENT La consulta d'aquesta tesi queda condicionada a l'acceptació de les següents condicions d'ús: La difusió d'aquesta tesi per mitjà del repositori institucional UPCommons (<http://upcommons.upc.edu/tesis>) i el repositori cooperatiu TDX (<http://www.tdx.cat/>) ha estat autoritzada pels titulars dels drets de propietat intel·lectual **únicament per a usos privats** emmarcats en activitats d'investigació i docència. No s'autoritza la seva reproducció amb finalitats de lucre ni la seva difusió i posada a disposició des d'un lloc aliè al servei UPCommons o TDX. No s'autoritza la presentació del seu contingut en una finestra o marc aliè a UPCommons (*framing*). Aquesta reserva de drets afecta tant al resum de presentació de la tesi com als seus continguts. En la utilització o cita de parts de la tesi és obligat indicar el nom de la persona autora.

ADVERTENCIA La consulta de esta tesis queda condicionada a la aceptación de las siguientes condiciones de uso: La difusión de esta tesis por medio del repositorio institucional UPCommons (<http://upcommons.upc.edu/tesis>) y el repositorio cooperativo TDR (<http://www.tdx.cat/?locale-attribute=es>) ha sido autorizada por los titulares de los derechos de propiedad intelectual **únicamente para usos privados enmarcados** en actividades de investigación y docencia. No se autoriza su reproducción con finalidades de lucro ni su difusión y puesta a disposición desde un sitio ajeno al servicio UPCommons No se autoriza la presentación de su contenido en una ventana o marco ajeno a UPCommons (*framing*). Esta reserva de derechos afecta tanto al resumen de presentación de la tesis como a sus contenidos. En la utilización o cita de partes de la tesis es obligado indicar el nombre de la persona autora.

WARNING On having consulted this thesis you're accepting the following use conditions: Spreading this thesis by the institutional repository UPCommons (<http://upcommons.upc.edu/tesis>) and the cooperative repository TDX (<http://www.tdx.cat/?locale-attribute=en>) has been authorized by the titular of the intellectual property rights **only for private uses** placed in investigation and teaching activities. Reproduction with lucrative aims is not authorized neither its spreading nor availability from a site foreign to the UPCommons service. Introducing its content in a window or frame foreign to the UPCommons service is not authorized (*framing*). These rights affect to the presentation summary of the thesis as well as to its contents. In the using or citation of parts of the thesis it's obliged to indicate the name of the author.



Departament de Teoria
del Senyal i Comunicacions



UNIVERSITAT POLITECNICA DE CATALUNYA

DEPARTAMENT DE TEORIA DEL SENYAL I COMUNICACIONS

SYNTHESIS OF ACOUSTIC WAVE FILTERS.
LADDER AND TRANSVERSAL TOPOLOGIES.

Towards a practical implementation

PH.D DISSERTATION

Author: Alberto Hueltes Escobar

Thesis Advisor(s):

Prof. Jordi Mateu Mateu

Prof. Carlos Collado Gomez



Acta de calificación de tesis doctoral

Curso académico:

Nombre y apellidos
Programa de doctorado
Unidad estructural responsable del programa

Resolución del Tribunal

Reunido el Tribunal designado a tal efecto, el doctorando / la doctoranda expone el tema de la su tesis doctoral titulada _____.

Acabada la lectura y después de dar respuesta a las cuestiones formuladas por los miembros titulares del tribunal, éste otorga la calificación:

- NO APTO
 APROBADO
 NOTABLE
 SOBRESALIENTE

(Nombre, apellidos y firma)		(Nombre, apellidos y firma)	
Presidente/a		Secretario/a	
(Nombre, apellidos y firma)	(Nombre, apellidos y firma)	(Nombre, apellidos y firma)	(Nombre, apellidos y firma)
Vocal	Vocal	Vocal	Vocal

_____, _____ de _____ de _____

El resultado del escrutinio de los votos emitidos por los miembros titulares del tribunal, efectuado por la Escuela de Doctorado, a instancia de la Comisión de Doctorado de la UPC, otorga la MENCIÓN CUM LAUDE:

- SÍ
 NO

(Nombre, apellidos y firma)		(Nombre, apellidos y firma)	
Presidente de la Comisión Permanente de la Escuela de Doctorado		Secretario de la Comisión Permanente de la Escuela de Doctorado	

Barcelona a _____ de _____ de _____

ABSTRACT

The meteoric growth of the mobile communication market for the last three decades has been strongly related with the evolution of the electroacoustic (EA) filter technology. With way over 5 billion cell phone users worldwide in 2017 and 5G standard in the horizon, the radiofrequency spectrum is becoming increasingly crowded whereas demand for mobile data has no expected limits in the short to medium term.

In this scenario, where a unique filter needs to be designed for each band of operation, requirements for advanced filtering solutions continue to grow as well as the average value of the RF solutions and the RF content per mobile device.

RF and microwave devices based on EA resonators such as Bulk Acoustic Wave (BAW) and Surface Acoustic Wave (SAW) filters overcame the limitations of the existent technologies back in the 1980's thanks to its compatibility with the manufacturing process of standard Silicon Integrated Circuits (Si-IC).

Nowadays sophisticated RF Front-End (RFFE) Modules based on System-in-Package (SiP) are the key solution to integrate the increasing number of electronic parts - Power Amplifiers (PAs), Low Noise Amplifiers (LNAs) and switches - that accompanies acoustic filtering devices like filters, duplexers and multiplexers.

Even though the level of complexity and accuracy present on the current EA devices is extraordinary, the design procedures for acoustic filters are still based on the optimization of built-in performance parameters from behavior-based compact models of resonators and the success on this duty relies mostly on the expertise of the designers.

However due to the stringent technological constrains and the increasing complexity of the RFFE module architectures devoted to satisfy demanding specifications of the current and forthcoming communications standards, the challenging work of the designers is never getting easier.

The aim of this work is focused on providing valuable insights that might help to overcome some of the existent limitations in the design of EA filters. Wider bandwidths, prescribed inclusion of external elements or multiplexing features are taken into consideration. On one hand we show a synthesis formulation and an automated procedure to carry out the synthesis

for current well-known topologies, i.e. ladder, taking into consideration realistic values and specifications. On the other hand, a synthesis formulation for novel topologies, named here *transversal*, is provided. Success of this novel topology will certainly help to guarantee the prevalence of EA filters in the future communication standards, along with the extension to other applications with more stringent requirements and different operating frequencies.

The first part of the work is devoted to explain the basic theory related to filter synthesis and its applicability to filters based on EA resonators.

Subsequent chapters elaborate the theory to explain the procedures followed to obtain both synthesis and their limitations. Finally, a Chapter devoted to study cases shows the results of applying the filter synthesis to real case scenarios.

LIST OF FIGURES

Figure 1. Nowadays smartphones integrate different front-ends modules to cover (a) low bands (b) mid bands and (c) high bands. Image Source: [5]	17
Figure 2. Filter response with referred parameters	25
Figure 3. Equivalent circuit of a two-port network.....	25
Figure 4. Ladder topology of a 3rd order Chebyshev lowpass prototype filter.....	29
Figure 5. Coupled resonators topology of a 3rd order Chebyshev lowpass prototype filter.	30
Figure 6. Nodal notation of an in-line three order filter. S stands for source, R_i stands for resonant node, L stands for load and M_{ij} is the notation used for the couplings between nodes.....	32
Figure 7. a) Equivalent network of a transversal filter of order N. The empty circles S and L represent the source and the load, the black filled-in circles (from R_1 to R_N) represent the resonators and the lines connecting the circles represent the mainline couplings from each resonator to the source and load. b) Equivalent circuit of the k -th resonator and its couplings to the source and load.....	35
Figure 8. Transfer and reflection coefficients of a polynomial bandpass filtering response as a function of its Q factor.	37
Figure 9. Outline of an acoustic wave resonator on its BAW (Bulk Acoustic wave) configuration.....	38
Figure 10. Outline of an acoustic wave resonator on its SAW (Surface Acoustic wave) configuration.....	38
Figure 11. BVD equivalent circuit model.....	39
Figure 12. Magnitude and phase response of an acoustic resonator, throughout evaluation of the BVD model.....	41
Figure 13. BVD equivalent circuit model.....	42
Figure 14. mBVD circuit model including acoustic and electrode losses.....	42
Figure 15. a) lowpass prototype corresponding to the BVD reciprocal circuit model. b) lowpass prototype corresponding to the BVD model.....	45
Figure 16. Lowpass prototype (mapped at the operating frequency) and bandpass prototype performance of a single acoustic wave resonator.....	46
Figure 17. Typical representation of an acoustic resonator.....	47
Figure 18. Outline of a ladder network.	50

Figure 19. S-parameters of a 7 th order (4 series, 3parallel -4s3p-) AW ladder filter (Figure 18), and input impedance of the isolated resonators. Note that due to the symmetry of the response only two of the four series resonators are different and two of the three shunt resonators are equal.	50
Figure 20. Working principle of a ladder network based on acoustic resonators a) TZ created by the shunt resonators b) behavior in the in-band region and c) TZ created by the series resonators.....	51
Figure 21. Lowpass filter response (transmission in solid black and reflection in dashed black) typical logarithmic representation of the impedance magnitude of the resonators (series resonators in blue and shunt resonators in red). Filter network is outlined below.	57
Figure 22. Lowpass prototype topology of an order 5 filter with 3 Transmission Zeros (TZ) at the lower side band and 2 at the upper side band.....	58
Figure 23. Network topology of an N even order filter, a) starting with a shunt resonator, b) starting with a series resonator.....	59
Figure 24. Synthesized network of a 7 th order filter with 4 transmission zeros at the upper side band and 3 transmission zeros at the lower side band.....	59
Figure 25. Impedance of the synthesized resonators. Blue lines correspond to series resonators, and red lines correspond to shunt resonators (above). Synthesized frequency response of the 7th order filter (below).	61
Figure 26. Filter response of a 5th order filter for a) 50 MHz bandwidth, b) 200 MHz bandwidth, c) 400 MHz bandwidth.	62
Figure 27. BVD model with the inclusion of external elements in order to modify the coupling coefficient. a) inclusion of a series capacitor, b) inclusion of a shunt capacitor, c) inclusion of a shunt inductor, and d) inclusion of a series inductor.....	64
Figure 28. Impedance response of BVD resonator with the inclusion of external capacitors. Legend details on each of the lines in the figure.....	65
Figure 29. Impedance response of BVD resonator with the inclusion of external inductors. Legend details on each of the lines in the figure. Effects of the inclusion of external elements in the broadband response can be seen in the inset at the lower right side.	66
Figure 30. First stage on the extraction element process. a) Shunt susceptance and series BVD lowpass prototype. b) Series susceptance and series BVD lowpass prototype. a) Shunt inductance and series BVD resonator. b) Series inductance and series BVD resonator.....	69
Figure 31. Screen shot of the GUI Synthesis Software outlining the input filter parameters.....	71
Figure 32. Frequency responses corresponding to the topologies of Table 2. Details on the in-band and band-edges of the filter (above). Details on the wideband response (below).	72
Figure 33. Ladder filter topology with inclusion of series ground inductors in the shunt resonators.....	74
Figure 34. Typical circuit scheme of the path to ground consisting on a shunt resonator followed by a ground inductor.	74
Figure 35. a) BVD model, b) equivalent BVD model, c) equivalent BVD model with the inclusion of the ground inductance, d) resulting BVD model with the inclusion of the parasitic inductance.	76

Figure 36. In-band transmission and reflection coefficient of a 7 th order filter with the effects of a parasitic inductance.	78
Figure 37: Filter response for two different location of the transmission zeros prescribed in the synthesis	79
Figure 38. Transmission and reflection coefficient of a 7 th order filter with the effects of including a ground inductor in the first shunt resonator. The additional transmission zero is fixed to 2.5 GHz.	80
Figure 39. Ladder filter network where each node is connected to an external parasitic network.	81
Figure 40. Ladder network of a 5-th order filter with parasitic cross couplings between nodes 1 and 4, and between nodes 2 and 4. Connections of the shunt resonators with the laminate have not been considered here.	82
Figure 41. a) and b) Filter responses for different position of transmission zeros and the effects of a given parasitic network.	83
Figure 42. a) and b) Filter responses for different position of the parasitic cross-coupling.	84
Figure 43. Filter performance for a) -80 dB cross-coupling, b) Filter performance for -50 dB cross-coupling.	85
Figure 44. Filter network of the synthesized topology	86
Figure 45. Measured and synthesized response of the B40 receiver band.	87
Figure 46. Overall filter network including the laminate representation with the ground inductors.	88
Figure 47. Simulated (blue) and measured (black) S-parameters. Top left figure: input reflection coefficient. Top right figure: output reflection coefficient. Bottom left figure: narrow band transmission coefficient. Bottom right figure: broadband transmission coefficient.	89
Figure 48. Outline of a transversal network, a) without direct source-load coupling, b) with direct source-load coupling.	93
Figure 49. Single path of a conventional transversal network. a) non-normalized values, b) scaling transformation has been applied to obtain unitary coupling coefficients.	94
Figure 50. Outlined of the two paths existing in a 2-port filter with symmetric response and without transmission zeros.	95
Figure 51. Outlined of the two paths existing in a two-port filter with symmetric response and without transmission zeros, with additional inverters included.	95
Figure 52. Outlined of the two paths, with additional inverters included, after initial transformation	96
Figure 53. Outlined of the two paths, with additional inverters included, after initial transformation	96
Figure 54. Lowpass prototype of the BVD model	97
Figure 55. Value of k as a function of ke_2	101
Figure 56. Transversal filter topology based on acoustic wave resonators.	102
Figure 57. a) Filter response, b) impedance of each individual resonator.	104

Figure 58. a) BVD circuit, b) equivalent BVD circuit, c) equivalent BVD circuit by splitting the $C3$ component, d) transformation from the equivalent BVD ($C2, L2, C4$) to the BVD, $L3, C6, C7$, with a series capacitance $C5$. e) BVD with a series capacitance BVD.	105
Figure 59. Transversal filter topology based on acoustic BAW resonators, after the transformation outlined in this section.	109
Figure 60. a) Filter response, b) impedance of each individual resonator.	112
Figure 61. a) Filter response, b) impedance of each individual resonator.	115
Figure 62. a) Filter response, b) impedance of each individual resonator.	115
Figure 63. Series resonant frequency of each resonator as a function of its impedance.	116
Figure 64. Impedance of each resonator.	117
Figure 65. Filter response.	118
Figure 66. Filter response of a 200 MHz filter with arbitrary position of transmission zeros.	119
Figure 68. a) initially synthesized BVD with acoustic losses, b) initially synthesized BVD with acoustic losses and electrode losses, c) BVD after transformation with acoustic losses, d) BVD transformation with acoustic losses and electrode losses.	120
Figure 69. a) in-band effect due to only acoustic losses, b) in-band effect due to acoustic losses and electrode losses, c) effect on selectivity due to only acoustic losses, d) effect on selectivity due to acoustic losses and electrode losses.	122
Figure 70. Frequency response considering a uniform variation of 1% and 5% of the impedance of the resonators and all other components of the filter. Legends are used to identify each response. The blue lines correspond to the characteristic polynomial response with none deviation of the impedances.	124
Figure 71. In-band details of the responses of Figure 70.	125
Figure 72. Frequency response considering a uniform variation of 1% and 5% of only the impedance of the resonators. Legends are used to identify each response. The blue lines correspond to the characteristic polynomial response with none deviation of the impedances.	125
Figure 73.- Filter responses when a) + 1MHz variation is applied to the 1st and 6th resonator. Legends are used to identify each response.	127
Figure 74. Filter responses when a) +1MHz variation is applied to the 1st and -1MHz variation is applied to the 6th resonator Legends are used to identify each response.	127
Figure 75. Filter responses when a) -1 MHz variation is applied to the 1st and 6th resonator. Legends are used to identify each response.	128
Figure 76. Filter responses when a) +1MHz variation is applied to the 3rd and 4th resonator, and a -1MHz variation is applied to the 1st and 6th resonator Legends are used to identify each response.	128
Figure 77. Filter responses when a) +1MHz variation is applied to the 2nd, 3th and 4th resonator and a -1MHz variation is applied to the 1st, 5th and 6th resonator. Legends are used to identify each response.	129
Figure 78. Equivalent circuit of the BALUN.	130
Figure 79. Response of a 6 th order filter for coupling coefficients of $k_b=1, 0.95, 0.8$ and 0.75	131
Figure 80. In-band details of the filter of Figure 80.	131
Figure 81.- In-band details of the filter when matching output impedance has been changed.	132

Figure 82.- Response of a sixth order filter for balance signal ratio $a= 1, 0.98, 0.96, 0.94$. The corresponding lines for the transmission coefficient are red, cyan, purple and dark green, respectively.	133
Figure 83. Return losses details for the responses of Figure 83.	133
Figure 84.- Response of a sixth order filter for unbalanced signal ratio $a= 1, 0.95, 0.9, 0.75$. .	134
Figure 85.- Return losses details for the responses of Figure 85. The corresponding lines for the reflection coefficient are blue ($a=1$), pink ($a=0.95$), green ($a=0.9$) and brown ($a=0.75$). .	134
Figure 86. Impedance of each resonator as a function of the return losses (dB). Four order filter with 200 MHz bandwidth.	136
Figure 87. Impedance of each resonator as a function of the filter order.	137
Figure 88. Cascaded transversal networks.	138
Figure 89. Series resonant frequency as a function of the impedance of the resonator. In square marks are indicated the resonant frequencies and impedances when no external components are required.	139
Figure 90. $C5$ values as a function of the impedance of each resonator.	139
Figure 91. Details $C5$ values as a function of the impedance of each resonator.	140
Figure 92. Lshunted value as a function of the impedance of the resonators (assumes a uniform impedance).	141
Figure 94 Settings Section.	146
Figure 95. Frequency Response (right)	147
Figure 96. Topology Section (above)	147
Figure 97. Screen shot for the input parameters of Section 4	148
Figure 98. In-band frequency response (above) and Wide-Band response (below) of the synthesized B39 Wideband filter (solid red and blue) compared to the AWR simulation including the in-house Qorvo resonator model (dashed orange and purple) and also with the same model with the <i>inac</i> and <i>qdeg</i> variables disabled (dotted green and black) [44].	150
Figure 99. Synthesized topology for the B39 Wideband filter.	151
Figure 100. Synthesized network for filter #1.	153
Figure 101. Synthesized network for filter #2.	154
Figure 102. In-band frequency response of the synthesized steep filter #1.	154
Figure 103. Out-of-band frequency response of the synthesized steep filter #1.	155
Figure 104. In-band frequency response of the synthesized steep filter #2.	155
Figure 105 Out-of-band frequency response of the synthesized steep filter #2.	156
Figure 106. Scheme of an N-order multiplexer.	157
Figure 107. Equivalent circuit of an N-order multiplexer outlining the input impedance seen from the filter number 1.	158
Figure 108. Scheme of the B3UL-B3DL-B39DL/UL triplexer.	160
Figure 109. B3UL-B3DL-B39DL/UL triplexer topology following the approach described in paragraphs above. The following table, Table 13, details on the values of circuit components, where the output port is the antenna. The numbering starts by the input ports. Note as well that the overall output shunt capacitance corresponds to the addition of all output shunt capacitances.	161

Figure 110. B3UL-B3DL-B39DL/UL triplexer response following the approach above.....	162
Figure 111. Quadplexer topology following the approach described in paragraphs above. The following table, Table 14, details on the values of circuit components, where the output port is the antenna. The numbering starts by the input ports. Note as well that the overall output shunt capacitance corresponds to the addition of all output shunt capacitances..	163
Figure 112. B3UL-B3DL-B39DL/UL+New filter Quadplexer.....	164
Figure 113. B3UL-B3DL-B39DL/UL+New filter Quadplexer. Losses are evaluated afterwards.	164
Figure 114. Detailed circuit of the synthesized triplexer.....	166
Figure 115. In-band and Inter-band Frequency response of the synthesized triplexer (above). Wide-band Frequency response of the synthesized triplexer (below).....	167
Figure 116. In-band and Inter-band Frequency response of the synthesized quadplexer (above). Wide-band Frequency response of the synthesized quadplexer (below).....	169
Figure 117. Detailed circuit of the synthesized quadplexer.....	170
Figure 118. Series resonant frequency as a function of the impedance of the resonator. In square marks are indicated the resonant frequencies and impedances when no external components are required.	172
Figure 119. C_5 values as a function of the impedance of each resonator.....	173
Figure 120. Details C_5 values as a function of the impedance of each resonator.....	173
Figure 121. $L_{shunted}$ value as a function of the impedance of the resonators (assumes a uniform impedance).	174
Figure 122. Synthesis response by means of a transversal topology. In blue and red solid line are, respectively, indicated S_{21} and S_{11} by evaluating the lossless distributed parameters. Pink and black dashed lines correspond to S_{21} and S_{11} the synthesized response with Approach I. Blue and green dashed thick lines correspond to S_{21} and S_{11} the synthesized response with Approach IV.....	175
Figure 123. Series resonant frequency as a function of the impedance of the resonator. In square marks are indicated the resonant frequencies and impedances when no external components are required.....	178
Figure 124. a) Details C_5 values as a function of the impedance of each resonator. b) $L_{shunted}$ value as a function of the impedance of the resonators (assumes a uniform impedance).	178
Figure 125. Synthesis response by means of a transversal topology. In blue and red solid line are, respectively, indicated S_{21} and S_{11} by evaluating the lossless distributed parameters. Pink and black dashed lines correspond to S_{21} and S_{11} the synthesized response with Approach I. Blue and green dashed thick lines correspond to S_{21} and S_{11} the synthesized response with Approach IV.....	179
Figure 126. Broad band response of the synthesized response (blue), along with the lossy characteristic polynomials in red. The electrical filter requirements are indicated in black.	180
Figure 127. Details on the in-band insertion losses.....	180
Figure 128. Broad band response of the synthesized response (blue), along with the lossy characteristic polynomials in red. The electrical filter requirements are indicated in black.	183

Figure 129. Details on the in-band insertion losses	183
Figure 130. Hybrid transversal-lattice filters with balanced input/output.....	189
Figure 131. Alternative transversal filters without BALUN	190
Figure 132. Hybrid transversal-ladder AW filters.	191
Figure 133. Alternative topologies for AW transversal-shunt filters.	191
Figure 134. Multiplexers based on AW Transversal Filters.	192

LIST OF TABLES

Table 1. Characteristic polynomials of the 3 rd order filter example.....	28
Table 2. Values resulting from the synthesis and circuit transformation.....	73
Table 3: Summary of the circuit parameters for the synthesis responses of Figure 36.....	79
Table 4. RX band 40 specifications.....	86
Table 5. Values of the circuit parameters corresponding to the synthesized and implemented values.....	87
Table 6. Values of Q and resonator impedance related to the different examples assessed for the losses evaluation of the transversal topologies.....	121
Table 7. Specifications for the B39 Wideband filter and simulated values for the resonator stack and ground inductor losses.....	149
Table 8. Specifications for the very demanding skirt steepness filters.....	152
Table 9. Simulation values of the resonator stack and ground inductor losses for the filters of the case study 4.2.2.....	152
Table 10. Circuit parameters corresponding to the synthesized topologies in Figures 100 and 101.....	153
Table 11. B3-B39 Triplexer Frequency Specifications.....	159
Table 12. Simulation values for the stack of each band, and constrains related to the area of the resonators as well as to the external components for the Triplexer case study.....	160
Table 13. Summary of the resultant values of all the filters synthesized for the triplexer example, including ke_2 , C_0 and f_s of each resonator and values of the external elements.....	162
Table 14. Summary of the new filter parameters.....	163
Table 15. Summary of the resultant values of all the filters synthesized for the triplexer example, including ke_2 , C_0 and f_s of each resonator and values of the external elements.....	165
Table 16. Summary of the resultant values of the additional filter and the modified B3UL filter synthesized for the quadplexer example, including ke_2 , C_0 and f_s of each resonator and values of the external elements.....	168
Table 17. B41 Filter Frequency Specifications.....	176
Table 18. Simulation values for the stack of the Band 41 filter.....	177

Table 19. Constrains related to the area and f_s of the resonators as well as to the external components for the Band 41 filter.	177
Table 20. Summary of the resultant values of the synthesized Band 41 filter, including ke_2 , C_5 , impedance and f_s of each resonator and values of the external elements.	181
Table 21. B25 Filter Frequency Specifications.....	181
Table 22. Simulation values for the stack of the Band 25 filter.....	182
Table 23. Constrains related to the area and f_s of the resonators as well as to the external components for the Band 25 filter.	182
Table 24. Summary of the resultant values of the synthesized Band 25 filter, including ke_2 , C_5 , impedance and f_s of each resonator and values of the external elements.	184

CONTENTS

ABSTRACT	i
LIST OF FIGURES	x
LIST OF TABLES	xi
CONTENTS	xiii
INTRODUCTION	16
0.1 Objectives of the thesis	19
0.2 Contents.....	21
THEORETICAL BACKGROUND	23
1.1 Filter transfer function.....	24
1.2 Principles of Synthesis Techniques: Mathematical formulation	25
1.3 Element extraction synthesis approach	26
1.4 Coupling matrix representation	30
1.5 Coupling Matrix Synthesis approach	32
1.6 Dissipation effects	35
1.7 Electro-acoustic resonators and technology.....	37
1.8 Summary.....	47
DEVELOPMENT OF LADDER TOPOLOGIES IN ACOUSTIC FILTERS	49
2.1 Acoustic wave ladder filter topology and concept.....	50
2.2 Characteristic polynomials for ladder acoustic filters.....	51
2.3 Synthesis procedure. Element extraction	52
2.4 Circuit transformation	63
2.5 Input series inductance	69
2.6 Ground inductors effects	73
2.7 General modeling of parasitic effects.....	80

2.8	Synthesis of a filter for the Band 40	85
2.9	Conclusions	89
DEVELOPMENT OF TRANSVERSAL FILTERS IN BAW TECHNOLOGY		91
3.1	Transversal Coupling Matrix. Conventional network	92
3.2	Transformation to Transversal Topology Based on acoustic wave resonators	93
3.3	Procedure to extract the required cross coupling for a given coupling coefficient ke_2 ..	97
3.4	From lowpass prototype to bandpass prototype	99
3.5	Synthesis and Design procedure: Approach I. Prescribed ke_2	103
3.6	Flexible Approaches	104
3.7	Synthesis Procedure: Approach II. Prescribed Impedance.	109
3.8	Synthesis Procedure Approach III. Prescribed Resonant Frequency	112
3.9	Synthesis Procedure: Approach IV. Trade-off	116
3.10	Advanced filter performances	118
3.11	Evaluation of the losses in a transversal filter configuration	119
3.12	Sensitivity analysis on transversal topologies	123
3.13	Effects of a non-ideal BALUN stage on the overall filter	129
3.14	Practical considerations	135
3.15	Practical considerations - External capacitors and shunt inductors	138
3.16	Conclusions	141
CASE STUDIES		143
4.1	Software for the synthesis of ladder filters	143
4.2	Case studies of ladder filters	148
4.3	Case studies on transversal filters	171
4.4	Conclusions	184
CONCLUSIONS AND FUTURE RESEARCH LINES		186
5.1	Conclusions	186
5.2	Future research lines	188
PUBLICATIONS AND OUTCOMES		194
APPENDIX 1: Demonstration of Equivalent Circuits		198
References		202

INTRODUCTION

Current technological challenges

The requirements in mobile communication technologies nowadays are tremendous due to the worldwide steady growth in mobile devices [1] [2] [3] [4]. Every new mobile communications standard is aiming for enabling more demanding applications thus increasing the needed data transmission rates. Requirements for reduced power consumption, low latency, spectrum efficiency and shrinking device footprint are other concerns typically reflected in communication standards. Just a glimpse of what is discussed here: 4G-LTE defined up to more than forty frequency bands together with Carrier Aggregation (CA) and MIMO technology as some of its most notable features. This increased the complexity of the RFFE Module up to unbelievable limits. Hundreds of possible CA combinations are available inside the RFFE modules existing in the market, meaning standalone filters are being replaced by all sorts of complex multiplexers - including BAW and SAW filter technology – that have to cover low, middle and high frequency bands along with switches for numerous different purposes, diplexers, power amplifiers (PA) or Low Noise Amplifiers (LNA) and antennas. Besides new mobile phone standards must often coexist with both, older mobile phone standards i.e. GSM/3G and different purpose mobile communications standards i.e. Bluetooth, Wi-Fi, GNSS, WiMAX and so on, all of them in a single, light and slim portable device. Therefore integration issues are a nightmare for design engineers and in turn set a lot of pressure on the scientific community and the ICT wireless industry in order to find new solutions that help facing the challenge.

Among the RF components, the filtering stage is one of the more critical components, which usually has to be individual for each communication band. Adding to that, many of these bands are very close together and therefore require highly selective filters. When this happens it is crucial to operate without detrimental of mutual interference. Currently modern 4G smart phones may include more than 40 RF filters with very demanding specifications [6]. In fact, more than 100 filters in a phone could be a reality in a near future. The increasing complexity is expected to stay on the forthcoming 5G devices [7] [8] [9], which will operate in an environment that will include many new bands especially at higher portions of the spectrum. This goes along the requirement of enhanced performance demands, smaller size and lower cost as the driving forces for RF enabled products. Natural questions arise then: How does one fit 100+ filters and all the additional RF components into a cell phone considering the ever-tighter size restrictions? And, how can they be integrated for an efficient solution without losing performance?

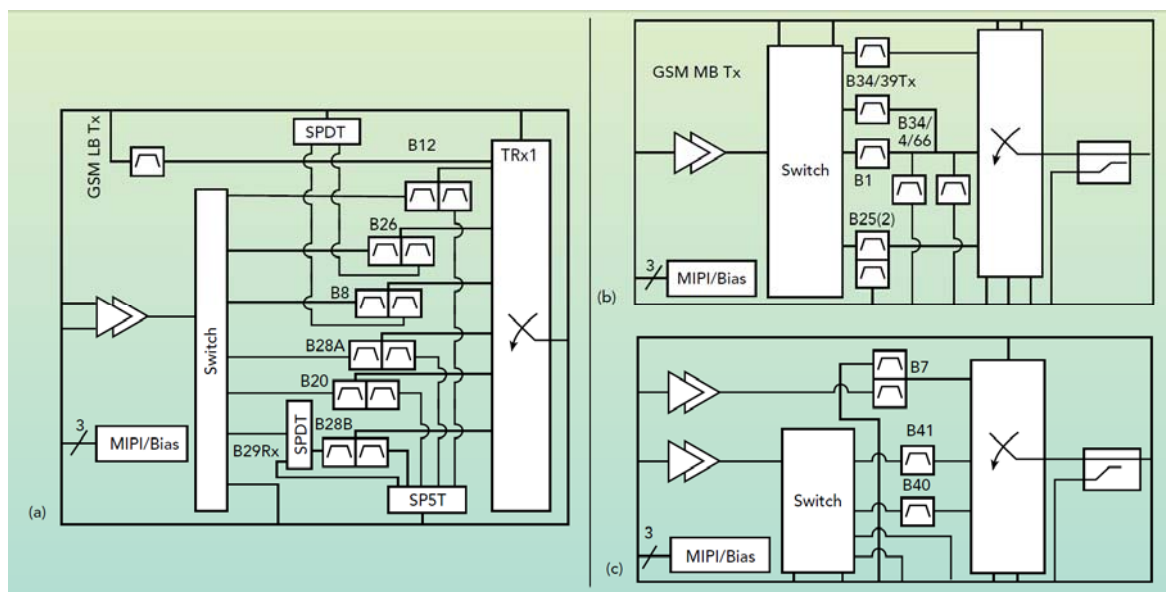


Figure 1. Nowadays smartphones integrate different front-ends modules to cover (a) low bands (b) mid bands and (c) high bands. Image Source: [5]

In the last two decades, electro-acoustic wave filters have been, without any doubt, the key technology for the development of highly miniature high-performance RF/Microwave filters [3]. Such a technological and engineering effort has been one of the driving forces for expansion of handset wireless devices, such as smartphones, tablets and other portable gadgets. The main features of current AW filters are low insertion loss, sharp frequency response and highly miniaturized, in comparison with other technologies.

To cope with the worldwide global transition to 4G/5G networks, a demand for even more exceptional high-performance filters is significantly increasing and may become the technological bottleneck in the definition of new advanced services in future standards. This challenge demands for continuous research in the RF acoustic technology to drastically improve the performance of the current filtering structures, reduce further their area, and lower their cost and time-to-market as much as possible. The most critical aspects that limit the performance of Acoustic Wave (AW) filters go from intrinsic limitations of the technology itself, to the filter design and manufacturing process.

Despite these huge efforts, achievements and expansion on the development of AW filters, there are still some important drawbacks that limit their transition to even more enhanced responses, their complete expansion into other domains, and the certainty that those will give response to the near future demands.

The limitations go from:

- Lack of mathematical formulation of the filter responses based on AW filter, even for well-established topologies.

- Systematic procedure to go from the mathematical formulation to the network configuration.
- Poor prediction of degrading undesired parasitic effects.
- Achievable response:
 - Limited achievable filter bandwidth.
 - Non-arbitrary location and number of transmission zeros.
 - Non (or hardly) achievable advance filter performances such as multiband response, and the always desired self-equalized filter response, required for space applications.
- Strong dependence on technological constrains. The achievable response mainly depends on:
 - The electro-acoustic coupling coefficients,
 - The impedance of the resonators,
 - The amount of different resonant frequencies of the resonators and their position.

Those limitations come mostly from the filter synthesis and the resulting topology used in conventional AW filters. Note that due to the nature of the AW configuration, which gives rise to a pole/zero performance in a single resonator, makes the synthesis and circuit transformation used on conventional technology might not always be applicable.

State of the art

Even though the contributions of two pioneers like K. S. Van Dyke and W. P. Mason [10] on the characterization of piezoelectric resonators and their integration in electric networks such as filters were published between the late '20s and the '40s of the past century it wasn't until the late '70s and early '80s when the work of K.M. Lakin, J.S. Wang and G.R. Kline - among others - on thin film SAW and BAW started to become more significant for the manufacturers of filtering devices. Their work was the precursor of the nowadays existent technology and made remarkable advancements in the miniaturization of filters [11] [12] [13], involving fabrication techniques, suitability of materials, piezoelectric film growth and characterization of electromechanical resonators for microwave frequencies. Later in the early '90s R. Ruby started out a program for the development of FBAR technology at Hewlett Packard Labs and officially laid the first stone of what currently is a multi-billion dollar industry [6] [9] [14] [15]. It does not come as a surprise that some authors have employed expressions like the "Golden Age" [16] [17] to refer to the acoustic filter design industry nowadays.

Major contributors to the technology, like R. Aigner [18] [19] [20] [21] [22], showed their concern as well on the issues related to the performance optimization and practical manufacturing for high-volume production having a key role on the success of the technology and enabling it for today's advanced performance wireless applications.

Thus, this technology has been under development for decades in one form or another, and it has required very significant advances in integrated circuit processing and high-volume manufacturing procedures to become what it is currently.

In addition to [17], [6], there are in the literature some readings that are highly recommended for those interested in this topic. They comprehend a good overview and provide the reader with bright insights regarding key aspects of the thin film acoustic filter technology, helping to follow the path from the filtering circuits used within the first existing wireless cellphones (GSM and before) to the complex multiplexer architectures within the modern RF front-end modules (4G-LTE) as well as foreseen trends (5G and tunable filters) [23]- [22].

In parallel, the evolution of filter synthesis techniques has reached outstanding results and many researchers have worked on it for many decades now. The filter transfer function synthesis date back to the late '40s and early '50s and some of the most significant contributions, also considering the early published works, may be attributable to G. L. Matthaei [24] . More recent authors like R. J. Cameron, C. M. Kudsia and R. R. Mansour were very prolific generalizing the coupling matrix synthesis method [25], first introduced by A.E. Atia et al. [26] and therefore providing with a very flexible and powerful tool to obtain all sort of filter topologies and filtering responses. Other distinguished authors like J-S. Hong, M. J. Lancaster [27] or I. Hunter [28], also made significant contributions in order to apply the filter synthesis concept to all sort of applications and technologies. Filter synthesis not only helps making easier and more flexible the filter design procedure but also covering all sorts of features regarding filtering requirements, i.e. multiplexing architectures, group delay equalization, predistortion [29], multiband, lossy [30] [31] [32] [33] or tunable. In turn, being such a generalized procedure, it is suitable for any kind of technology where two fundamental pieces coexist, resonators (cavity, waveguide, lumped element, planar, etc.) and couplings mechanisms between them.

Oddly enough the paths of filter synthesis and acoustic wave filters had not cross until recent years. Actually, the first works related to the topic didn't use closed-form expression synthesis techniques but optimization methods of lumped element models based on preliminary given data related to the acoustic technology [34], [35] and [36]. The coupling matrix used to synthesize acoustic filters appears in [37], however the related results are only valid for Coupled Resonators Filters (CRF), which have a very particular working principle and are still a residual percentage of all the EA filters in the market. Finally, in [38] a method to synthesize BAW and SAW filters using the coupling matrix is discussed for the first time. Some more recent works [39], [40] and [41] give a natural continuation to the prior work.

0.1 Objectives of the thesis

The goal of this work is to contribute to overcome the above limitations and significantly help to the achievement of higher performance filters to give response to future requirements and further expansion of the application of AW filters.

Current methodologies on the filters and multiplexer design rely on an initial design of the basic resonator and a given ladder pre-existing filter topology from a previous design. Iterations over the initial design are performed until the final filter design reaches the electrical and implementation requirements.

This limits the achievable filter performance since does not consider all possible solutions, and makes the procedure very time consuming and with lack of flexibility.

To this end the general objective of the thesis is to establish a synthesis procedure for designing BAW filters under the technological constraints given by the technology. The synthesis procedure will allow design novel filter topologies, beyond the conventional ladder topology, which better fulfills given requirements.

The specific objectives are:

- Develop a mathematical description of the AW filter response based on an equivalent low pass prototype model of the AW filters.
- Develop a synthesis procedure for the design of the most commonly used filter and multiplexer topologies. Those are based on ladder configurations.
- Develop a new synthesis procedure to obtain novel topologies and generate a solution-space of filters (different topologies that are complaint with the required specifications)
- Propose and demonstrate the synthesis of an innovative topology for the design of AW filters, in both SAW and BAW configurations, which allows to obtain high performance filter with arbitrary response, not achievable with the current state of the art electro-acoustic topologies.
- Account for the technological constrains of the filter synthesis from the very beginning.

This thesis will perform activities on:

- Achieving a good knowledge of the current design procedures of BAW filters, the manufacturing process and the technological constraints.
- Mathematical formulation to:
 - Obtain the characteristic polynomials of the lowpass prototype of AW filters.
 - Define the lowpass prototype of an AW resonator
- Synthesis of ladder filters.
 - Define a procedure based on the element extraction approach to automatically synthesize conventional ladder filters with prescribed topology.
 - Use in the synthesis of multiplexers.

Since those activities will focus on existing and widely used topologies a software tool has been developed along the mathematical formulation and synthesis procedure. This software tools not only provides the synthesized network but also it allows for the evaluation of

undesired effects, like parasitic effects, nonlinearities [42] [43] and effects of lateral modes [44] and border ring modes [45].

The major contribution of this work is the novel filter topologies based on a transversal arrangement of the AW resonators forming the filter [47] [48]. The objectives on this last topic are:

- Define a new filter topology along with a tailored synthesis procedure.
- Evaluate the electrical filter performance of the new topology and its limitations due to its particular nature.
- Evaluate the technological requirements of the topology according to the available materials and manufacturing processes.
- Provide a design process based on useful designing curves

The above objectives and activities define the content of this work.

0.2 Contents

This thesis is divided into five chapter in addition of this introductory initial chapter. Among those five chapter we also include the chapter gathering the conclusions of this work and the outline of future research lines. We consider this last chapter very significant since the novel proposed topology opens up a new way of designing acoustic filters and therefore the existence of many different topologies, applications and the possibility of using other materials.

Chapter 1 is referred as a background chapter that presents the previous required knowledge for contributing on the synthesis of AW filters. In that sense, this chapter essentially outlines the initial concepts and formulation for the definition of microwave filters along with some of the existing synthesis methodologies that will be used along the thesis.

This chapter also includes the description of a BVD (Butterworth-Van-Dike) model which is the basic building block describing the behaviour of an AW resonator around the resonant frequency. The equivalent lowpass prototype circuit model of the BVD is also presented and evaluated. Note that the lowpass prototype is the initially required circuit in a synthesis procedure [24].

Chapter 2 presents all the mathematical formulation and detailed development of the synthesis procedure used for obtaining the ladder networks based on AW resonators. Practical considerations on the filter implementation such as the existence of shunt inductances to ground, or the way the filters need to be ended for a proper connection to the antenna even when the filter will be part of a multiplexer, will be also considered on the synthesis process. Examples of designed filters are shown in this chapter.

All the formulation and synthesis procedure detailed in this chapter are then used to create a comprehensive software tool for the synthesis of ladder filters. The tool showed to be very

useful to provide a quick design of an AW filter. The code also includes the features to provide the design of multiplexing structures. Some details and examples of real case studies designed with this tool, will be shown in Chapter 4.

Chapter 3 proposes a novel filter topology, referred along the thesis as *transversal network*, which allows to overcome many of the limitations observed in the ladder topologies of Chapter 2. This new topology essentially can be used to implement any transfer function without restriction on the electro-acoustic coupling coefficient of each individual resonator. The mathematical details and synthesis procedure to go from the filter characteristic polynomials to the novel transversal network are fully detailed. This method shows to be very flexible and several examples of enhanced performance filters are illustrated at the end of the chapter.

As done for ladder filters developed in Chapter 2, this chapter is supplemented with the case studies resorted in Chapter 4.

Chapter 4 applies the synthesis procedures developed in previous chapters, 2 and 3, respectively for ladder and transversal topologies to evaluate some practical cases, this is using real electrical requirements and implementation constrains. These cases correspond to scenarios of existing systems and/or bands specificifications but also to some cases which are under definition for future systems. This chapter clearly illustrates the validity of the methodology proposed in this thesis and briefly details on the implemented software that includes all the mathematical formulation and features detailed in Chapter 2.

Finally, Chapter 5 summarizes the conclusions and outlines future research activities that are consequence of the findings of this work. At this point, it is worth to mention that the novel topologies presented in Chapter 3 opens up the possibility of developing other novel topology based on the transversal concept. Also the advantages of this topology in terms of implementation constrains give rise to the possibility of using those topologies for novel applications or for being suitable to be used with other material or resonator configuration where the coupling coefficient it is not an issue.

CHAPTER 1

THEORETICAL BACKGROUND

The following chapter provides the tools and theoretical background used throughout the thesis for the development of synthesis techniques for filter networks where the basic building block is an acoustic wave resonator. This does not attempt to fully comprehend all the details of the required background and some of the mathematical formulation and concepts will be properly referred in technical references. Nevertheless, it offers a previous content for a self-contained and through reading of this work.

To this end, the chapter presents aspects of both branches of this work, theoretical basics of filter synthesis techniques and the initial aspects of the acoustic technology required on the filter synthesis. It starts by presenting the conventional parameters that defines the filter response, and their mathematical formulation by means of the characteristic polynomials. The basic existing synthesis techniques based on the element extraction approach and on the matrix approach are introduced. For the element extraction approach, only a brief introduction is outlined since fully details for the case addressed in this work (ladder filter configuration based on acoustic devices) will be provided in Chapter 2. The matrix approach is outlined as well since it sets the basics for the development of the novel transversal networks [25].

On the acoustic technology part, we simply detail on the compact equivalent circuit emulating the behavior of an acoustic wave resonator. This equivalent circuit is referred as BVD (Butterworth-Van-Dike) [23] model and it is a key model widely used on the development of the synthesis procedures, and crucial for the understanding of these processes. Along with the BVD model, its equivalent circuit is also presented.

Last section of this chapter develops an equivalent lowpass prototype circuit model required on the synthesis procedure.

1.1 Filter transfer function

This section outlines the general specification parameters that are used to define the performance of any filter. These parameters will be widely used along the thesis and although those are very well-known, their definition may differ from the conventional one by considering the scope of acoustic wave filters. Specific aspects of these parameters into the acoustic technology will be also mentioned in this section. See also Figure 2 as a reference.

- Passband (#1) defines the frequency range where the filter allows signal transmission. In acoustic technology, the passband is usually limited by the acoustic coupling coefficient, which is inherent to a single resonator itself, including the material and configuration behind [23].
- Insertion loss (#2) defines the minimum value of the transmission parameter in the passband. This can be also referred to a certain frequency range of the passband.
- Passband attenuation ripple (#3) defines the insertion loss variation of the filter through the passband. In the particular case of acoustic technology such ripple might not be solely due to the partial reflected signal but also due to the existence of lateral mode effects [44].
- Flatness in the passband or rounding in the passband (#4) refers to the insertion losses in the passband versus frequency. In conventional filters this figure of merit is set by the Quality factor (Q) of the resonator, and therefore it is directly obtained from a polynomial mathematical description of the filter response. In acoustic filters, due to the nature of the AW resonators - with the resonant and anti-resonant frequencies, - and the existence of external elements (i.e., input and output resistances and inductances or ground parasitic capacitances and inductances), the effects of losses in the synthesized response requires of special attention.
- Stopband (#5) refers to the portion of the frequency spectrum that is blocked by the filter.
- Out-of-band attenuation (#6) is defined as the amount of energy that is reflected by the filter at a certain frequency in the stopband. It is also called rejection. This value might be affected by the spurious longitudinal modes due to configuration of the layer stack of the resonator [23].
- Return loss (#7) defines the maximum value of the reflection parameter in the passband of the filter.
- Transmission zeros (#8). They may exist or not and consist on the inclusion of zero transmission frequency points in order to increase the rejection in a certain frequency range. In the case of *acoustic ladder filter configuration* transmission zeros always exist and their location is essentially set by the coupling coefficient of the series and shunt resonators [23].

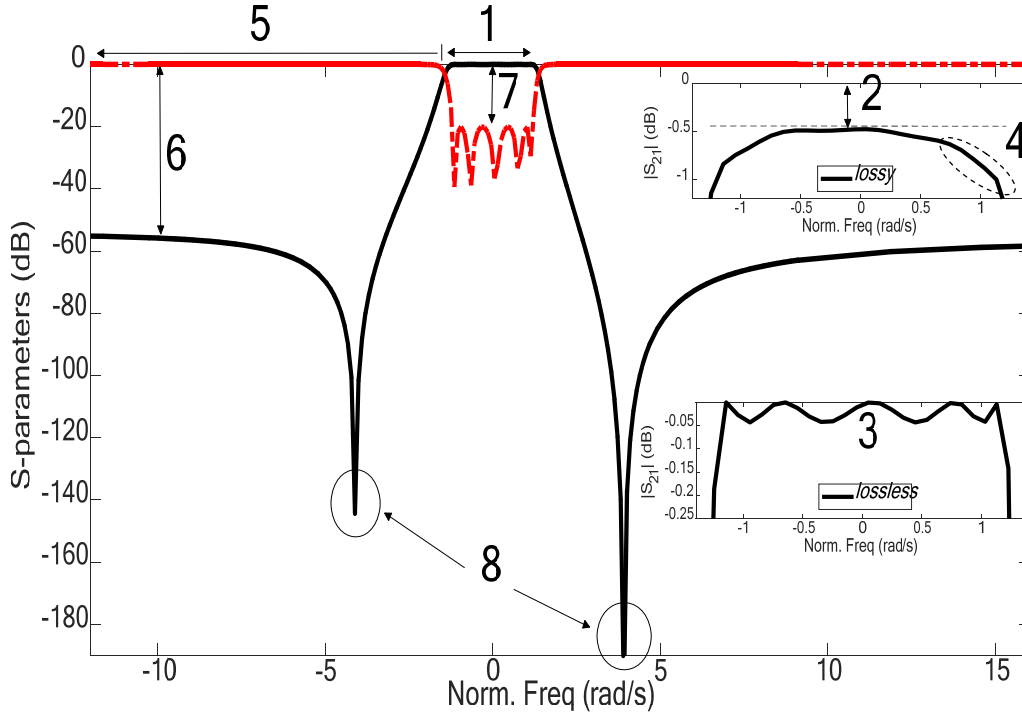


Figure 2. Filter response with referred parameters

1.2 Principles of Synthesis Techniques: Mathematical formulation

Most standalone microwave filters can be represented by a two-port network as outlined in [28] [25] [27]. For the majority of existing synthesis techniques, this network is assumed to be lossless. In other words, the filter would be composed by non-dissipative components.

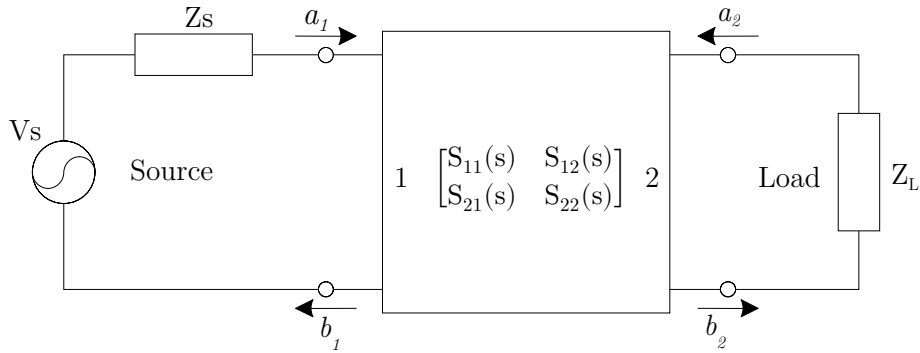


Figure 3. Equivalent circuit of a two-port network

As usually done in microwave technology the two-port network can be characterized by its scattering matrix, which can be represented by the filter *characteristic polynomials*, $P(s)$, $F(s)$ and $E(s)$ [25].

$$\begin{bmatrix} S_{11}(s) & S_{12}(s) \\ S_{21}(s) & S_{22}(s) \end{bmatrix} = \frac{1}{E(s)} \begin{bmatrix} \frac{F(s)}{\epsilon_r} & \frac{P(s)}{\epsilon} \\ \frac{P(s)}{\epsilon} & \frac{(-1)^N F(s)^*}{\epsilon_r} \end{bmatrix} \quad (1)$$

Where ϵ and ϵ_r are constant values and N is the order of the filter. The roots of $P(s)$ and $F(s)$ correspond to the transmission and reflection zeros respectively, and all their roots lie along the imaginary axis in conjugate pairs. The polynomial $E(s)$ is the denominator of the reflection and transmission coefficients and it must be strictly Hurwitz, i.e., all its roots must lie in the left half side of the s plane.

At this point it is also worth to mention that the *characteristic polynomials* are defined in the lowpass prototype, being therefore the variable s the Laplace operator, which is related with the normalized frequency as $s=j\Omega$.

This latter statement will force to find a lowpass prototype of the basic building block of an acoustic filter, this is for the *AW resonator*. In contrast with conventional filter synthesis where the basic resonator is defined by a series or shunt *LC* (Inductance-capacitance) circuit, whose lowpass prototype consists in coupled series inductances or shunt capacitances, the equivalent circuit of an AW resonator is defined by the well-known BVD model [23]. Later in this chapter (section 1.7.5), the BVD model is presented and its corresponding lowpass prototype is defined. The presented lowpass prototype will be used throughout all the synthesis procedures developed in this work.

The synthesis will therefore consist in the process to define a 2-port network with a scattering matrix in the form of (1). Following in this section, two of the most often used synthesis approaches are presented: *element extraction approach* and *coupling matrix approach*.

Element extraction approach will be used, in chapter two, to develop the synthesis procedure of *Ladder filters*, whereas the coupling matrix synthesis approach, in chapter 3, will be used to develop the novel *Transversal topologies*. Although the basic of these two approaches are outlined below, further details will be presented throughout the corresponding chapters when necessary.

1.3 Element extraction synthesis approach

Using the notation above, the synthesis of a filter network by means of a circuit approach or element extraction approach may be outlined as follows:

1. From the filter requirements, the transfer function is defined as the scattering parameter S_{21} :

$$S_{21}(s) = \frac{P(s)/\varepsilon}{E(s)} \quad (2)$$

Using the unitary condition of a lossless network, $|S_{11}|^2 + |S_{21}|^2 = 1$, the reflection coefficient results in the fractional form

$$S_{11}(s) = \frac{F(s)/\varepsilon_r}{E(s)} \quad (3)$$

2. From the reflection coefficient, the input impedance $Z(s)$ or admittance $Y(s)$ of the filter network is obtained. **This assumes unitary input and output port impedances, this means equal impedance at the input and output ports.** Scaling to the right impedances will be latter applied in the frequency and circuit transformation process, always existing in filter synthesis. For this case the input impedance as a function of the *characteristic polynomials* results:

$$Z(s) = \frac{E(s) + F(s)/\varepsilon_R}{E(s) - F(s)/\varepsilon_R} \quad (4)$$

It is worth to mention that differences between input and output impedances must be considered at this point. Note that in a situation where the filter goes from another part of the RF chain to the antenna, this is very much like a common case.

3. Once the input impedance (or admittance) is known, one can determine the type and value of the circuit elements using the well-known *element extraction* method [28] [24].

Using this technique engineers have developed many direct synthesis methods, that is, obtaining specific network topologies for a given type of transfer functions. For example, the conventional ladder networks based on conventional LC resonators, or even more complicated configurations, as the cascaded quadruplet sections are used to obtain symmetric transmission zeros [27].

This work, in chapter 2, will use the element extraction approach to synthesize circuit networks based on the lowpass equivalent circuit of a BVD model. Although this section shows the basis of the element extraction technique, details corresponding to the especial case of acoustic filters is fully reported in section 2.3, and corresponds to a novel contribution of this thesis.

1.3.1 Example of Element extraction approach: third order filter

As an illustrative example, the synthesis of a conventional ladder network (corresponding to a filter based on conventional –non-acoustic- resonators) by using the element extraction circuit approach is shown below. Although this is a widely reported procedure, here it is also used to introduce the following section on coupling matrix approach.

The procedure starts by the selection of the characteristic polynomials. This case considers a 3rd order Chebyshev filter with 15 dB return losses, without any transmission zero:

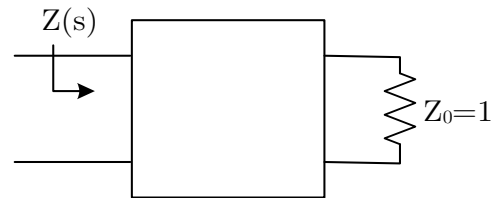
$F(s)=s^3+0.75s$
$E(s)=s^3+1.787s^2+2.34s+1.38$
$P(s)=1$, Note that this value is 1 because there is not transmission zeros

Table 1. Characteristic polynomials of the 3rd order filter example.

The way to obtain the characteristic polynomials is very well defined in many references [49] [25]. Use of these characteristic polynomials will be further discussed along this work, when necessary.

Equation (4) is used to write down the input impedance:

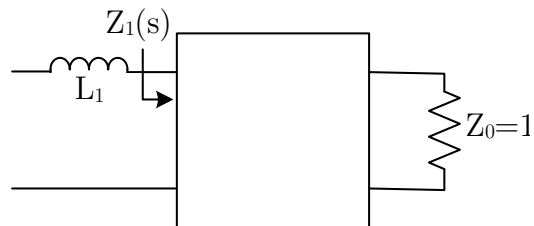
$$Z(s) = \frac{2s^3 + 1.787s^2 + 3.096s + 1.383}{1.787s^2 + 1.596s + 1.383}$$



By inspection of the input impedance, note that the numerator is defined by a higher order polynomial than the denominator, we can extract a series inductance as:

$$\left. \frac{Z(s)}{s} \right|_{s \rightarrow \infty} = 1.12 \rightarrow L_1 = 1.12 \text{ H}$$

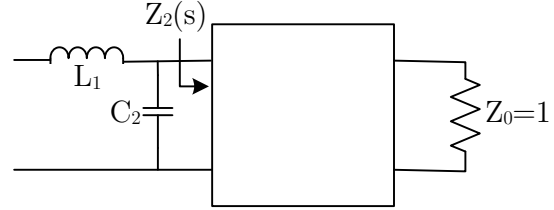
$$Z_1(s) = Z(s) - L_1 s = \frac{1.548s + 1.383}{1.787s^2 + 1.596s + 1.383}$$



By doing so the remaining admittance is $Y_1(s) = 1/Z_1(s)$. Analogously, and since the remaining input admittance has a numerator defined by polynomial of one order higher than the denominator, we can extract a shunt capacitor as:

$$\frac{Y_1(s)}{s} \Big|_{s \rightarrow \infty} = 1.154 \rightarrow C_2 = 1.154 \text{ F}$$

$$Y_2(s) = Y_1(s) - C_2 s = \frac{1.383}{1.548s + 1.383}$$



Now, from the remaining impedance $Z_2(s)$ we can again extract a series inductance as:

$$\frac{Z_2(s)}{s} \Big|_{s \rightarrow \infty} = 1.12 \rightarrow L_3 = 1.12 \text{ H}$$

Then, we can write down $Z_3(s)$ as:

$$Z_3(s) = Z_2(s) - L_3 s = 1$$

Which results in a non-dependent frequency component, a resistor to a normalized unitary value, that is the output impedance. The element extraction technique results in a ladder network as in figure below.

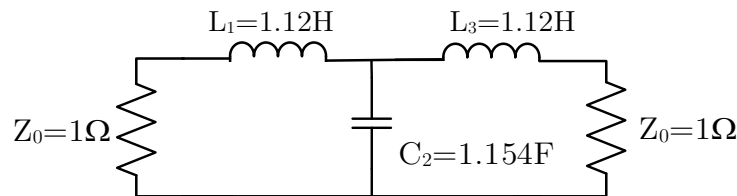


Figure 4. Ladder topology of a 3rd order Chebyshev lowpass prototype filter.

This example, although a very simple one, clearly illustrates the element extraction process. It is worth to emphasize that the extraction of each component at each step of the procedure is not unique and different filter networks could give rise to the same filter performance [28].

Note that this corresponds to the lowpass prototype, which would become the bandpass filter based on LC series and LC shunt resonators by applying circuit transformations [24].

1.4 Coupling matrix representation

As any network the synthesized filter of Figure 5 allows for a matrix representation. In order to introduce the Coupling matrix synthesis approach, detailed section 1.5 and used for the development of novel filter topologies based on acoustic filters in chapter 3, this subsection uses the network of Figure 5 above to find the coupling matrix representation.

Coupling matrix representation requires of the existence of couplings between resonators, thus a circuit transformation needs to be applied to the circuit of Figure 5 for the inclusion of those couplings. This transformation consists on the introduction of impedance/admittance inverters in order to transform the ladder topology in a coupled resonators topology [25]. This results in the filter topology shown in Fig. 5.

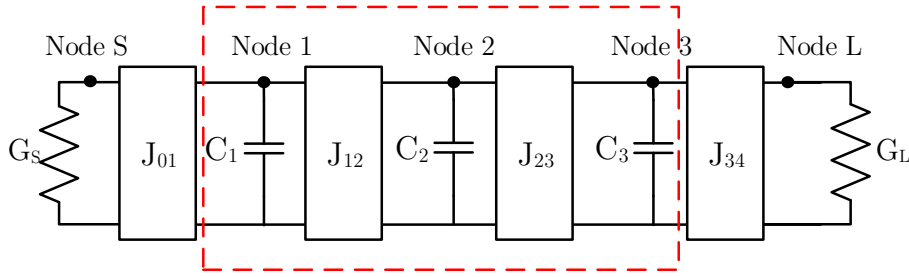


Figure 5. Coupled resonators topology of a 3rd order Chebyshev lowpass prototype filter.

The general admittance matrix of a 3x3 network relates the current getting into the node I_i with the voltage dropped at the corresponding node V_i .

$$\begin{bmatrix} I_1 \\ I_2 \\ I_3 \end{bmatrix} = \begin{bmatrix} Y_{11} & Y_{12} & Y_{13} \\ Y_{21} & Y_{22} & Y_{23} \\ Y_{31} & Y_{32} & Y_{33} \end{bmatrix} \begin{bmatrix} V_1 \\ V_2 \\ V_3 \end{bmatrix}$$

The resulting admittance matrix of the red-squared circuit in Fig. 5, without including the source and load impedances neither the input-output couplings (admittance inverters), is:

$$\begin{bmatrix} I_1 \\ I_2 \\ I_3 \end{bmatrix} = \begin{bmatrix} sC_1 & -jJ_{12} & 0 \\ -jJ_{12} & sC_2 & -jJ_{23} \\ 0 & -jJ_{23} & sC_3 \end{bmatrix} \begin{bmatrix} V_1 \\ V_2 \\ V_3 \end{bmatrix}$$

Which can be extended to include the source and the load as:

$$\begin{bmatrix} I_s \\ I_1 \\ I_2 \\ I_3 \\ I_L \end{bmatrix} = \begin{bmatrix} G_s & -jJ_{01} & 0 & 0 & 0 \\ -jJ_{01} & sC_1 & -jJ_{12} & 0 & 0 \\ 0 & -jJ_{12} & sC_2 & -jJ_{23} & 0 \\ 0 & 0 & -jJ_{23} & sC_3 & -jJ_{34} \\ 0 & 0 & 0 & -jJ_{34} & G_L \end{bmatrix} \begin{bmatrix} V_s \\ V_1 \\ V_2 \\ V_3 \\ V_L \end{bmatrix}$$

This admittance matrix is also referred as the $(N+2) \times (N+2)$ admittance matrix, where N is the order of the filter, $N=3$ in this case. The $(N+2) \times (N+2)$ admittance matrix can then be written down as the summation of three matrices,

$$\begin{bmatrix} G_s & 0 & 0 & 0 & 0 \\ 0 & 0 & 0 & 0 & 0 \\ 0 & 0 & 0 & 0 & 0 \\ 0 & 0 & 0 & 0 & 0 \\ 0 & 0 & 0 & 0 & G_L \end{bmatrix} - j \begin{bmatrix} 0 & J_{01} & 0 & 0 & 0 \\ J_{01} & 0 & J_{12} & 0 & 0 \\ 0 & J_{12} & 0 & J_{23} & 0 \\ 0 & 0 & J_{23} & 0 & J_{34} \\ 0 & 0 & 0 & J_{34} & 0 \end{bmatrix} + s \begin{bmatrix} 0 & 0 & 0 & 0 & 0 \\ 0 & C_1 & 0 & 0 & 0 \\ 0 & 0 & C_2 & 0 & 0 \\ 0 & 0 & 0 & C_3 & 0 \\ 0 & 0 & 0 & 0 & 0 \end{bmatrix}$$

Where the first matrix includes the source and the load impedances, the second matrix include the coupling between resonators and the third matrix accounts for the frequency dependence. The values of the matrices above can be scaled without affecting the relation between I_i and V_i [25] therefore without affecting the filter performance and obtaining the following matrices:

$$\begin{bmatrix} 1 & 0 & 0 & 0 & 0 \\ 0 & 0 & 0 & 0 & 0 \\ 0 & 0 & 0 & 0 & 0 \\ 0 & 0 & 0 & 0 & 0 \\ 0 & 0 & 0 & 0 & 1 \end{bmatrix} - j \begin{bmatrix} 0 & M_{01} & 0 & 0 & 0 \\ M_{01} & 0 & M_{12} & 0 & 0 \\ 0 & M_{12} & 0 & M_{23} & 0 \\ 0 & 0 & M_{23} & 0 & M_{34} \\ 0 & 0 & 0 & M_{34} & 0 \end{bmatrix} + s \begin{bmatrix} 0 & 0 & 0 & 0 & 0 \\ 0 & 1 & 0 & 0 & 0 \\ 0 & 0 & 1 & 0 & 0 \\ 0 & 0 & 0 & 1 & 0 \\ 0 & 0 & 0 & 0 & 0 \end{bmatrix}$$

It is now clear, from this notation, that all the information on the filter can be gathered into the coupling matrix, whose values M_{ij} are the normalized coupling values.

The resulting coupling matrix for the characteristic polynomials of Section 1.3.1 would be

$$[M] = \begin{bmatrix} 0 & 0.9453 & 0 & 0 & 0 \\ 0.9453 & 0 & 0.8779 & 0 & 0 \\ 0 & 0.8779 & 0 & 0.8779 & 0 \\ 0 & 0 & 0.8779 & 0 & 0.9453 \\ 0 & 0 & 0 & 0.9453 & 0 \end{bmatrix}$$

Although more details will be given in the following section, during this thesis the filter topologies will be represented with the conventional scheme that appears in Figure 6, where the

filled-in black circles corresponds to the resonators (R_i) forming the filter, the empty circles represent the source (S) and load (L), and the connecting lines indicate the coupling mechanisms (M_{ij}). Note that in this topology there are no cross-couplings, this is coupling between non-adjacent nodes, and therefore results in an *in-line* topology [25].

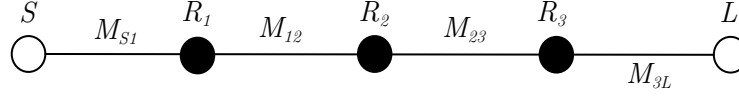


Figure 6. Nodal notation of an in-line three order filter. S stands for source, R_i stands for resonant node, L stands for load and M_{ij} is the notation used for the couplings between nodes.

1.5 Coupling Matrix Synthesis approach

In contrast with the *element extraction approach* where the *characteristic polynomials* of (1) are used to obtain the input impedance and its circuit network afterwards, the matrix approach uses these polynomials to obtain the coupling matrix of the filter. As in the example above (section 1.3.1) we will use the coupling matrix in its $(N+2) \times (N+2)$ format, instead of the $N \times N$ format. Note that the $N \times N$ matrix does not consider possible couplings between the source and the load, and as will be seen in Chapter 3, the existence of the source and load nodes in the coupling matrix might be convenient on the synthesis of novel topologies based on a transversal configuration.

The synthesis procedure starts by recalling the scattering parameters of the network as a function of the characteristic polynomials (1). The 2-port scattering matrix can then be transformed to the 2-port Y matrix, by following matrix conversion from S to Y [50]. Doing so, the admittance matrix of a 2-port network can be written as:

$$\begin{bmatrix} Y_{11}(s) & Y_{12}(s) \\ Y_{21}(s) & Y_{22}(s) \end{bmatrix} = \frac{1}{Y_d(s)} \begin{bmatrix} Y_{11n}(s) & Y_{12n}(s) \\ Y_{21n}(s) & Y_{22n}(s) \end{bmatrix} \quad (5)$$

Where the numerators and denominator of the admittance matrix may be written as a function of the characteristic polynomials as detailed in the following set of equation:

$$\begin{aligned}
Y_d(s) &= \frac{\left(E(s) + \frac{F(s)}{\varepsilon_r}\right) \left(E(s) + \frac{(-1)^N F^*(s)}{\varepsilon_r}\right) - \left(\frac{P(s)}{\varepsilon}\right)^2}{2E(s)} \\
Y_{21n}(s) &= Y_{12n}(s) = P(s)/\varepsilon \\
Y_{d11n}(s) &= \frac{(E(s) - F(s)/\varepsilon_r)(E(s) + (-1)^N F^*(s)/\varepsilon_r) + (P(s)/\varepsilon)^2}{2E(s)} \\
Y_{d22n}(s) &= \frac{(E(s) + F(s)/\varepsilon_r)(E(s) - (-1)^N F^*(s)/\varepsilon_r) + (P(s)/\varepsilon)^2}{2E(s)}
\end{aligned} \tag{6}$$

* Note that we used a normalized source and load impedance to 1.

As outlined in (6), it results in a set of rational fractions where both the numerator and the denominator are polynomials. In such case, we may perform *partial fraction expansion* (also known as *partial fraction decomposition*) [51]. This operation consists in expressing the fraction as a sum of polynomials with a simpler denominator. From the nature of the characteristic polynomials, the resulting rational fraction above can be decomposed in a sum of polynomials where the numerators are residuals and the denominators are first order polynomials. This is illustrated in the expression below, where r_i are the residuals and p_i are the poles of the rational function.

$$\frac{B(s)}{A(s)} = \frac{r_1}{s - p_1} + \frac{r_2}{s - p_2} + \frac{r_3}{s - p_3} + \dots + \frac{r_4}{s - p_4} \tag{7}$$

By applying this to the rational functions of the 2-port admittance matrix the decomposition results on:

$$\begin{bmatrix} Y_{11}(s) & Y_{12}(s) \\ Y_{21}(s) & Y_{22}(s) \end{bmatrix} = \frac{1}{Y_d(s)} \begin{bmatrix} Y_{11n}(s) & Y_{12n}(s) \\ Y_{21n}(s) & Y_{22n}(s) \end{bmatrix} = \sum_{k=1}^N \frac{1}{(s - j\lambda_k)} \begin{bmatrix} r_{11k} & r_{12k} \\ r_{21k} & r_{22k} \end{bmatrix} \tag{8},$$

where r_{ijk} are the residues and λ_k are the eigenvalues. The eigenvalues are obtained from the roots of $Y_d(s)$ and, in case of characteristic polynomials corresponding to an ideal lossless response, they result in purely imaginary roots, therefore purely real eigenvalues.

The residues can be obtained from:

$$r_{ijk} = \left. \frac{Y_{ijn}(s)}{Y'_d(s)} \right|_{s=j\lambda_k} \quad (9),$$

where $Y'_d(s)$ is the first derivative of $Y_d(s)$.

The conclusions of that procedure is very significant and states that any response following the performance of the characteristic polynomials in (1) can be synthesized by a network consisting on transversal connections of first order filters, i.e., resonators. This type of topology is known as *transversal topology* (see Figure 7a, below). This well-known transversal topology is the basis for the new developed **AW transversal topology**.

As an example (10) shows the coupling matrix of a 4th order canonical transversal filter.

$$[M] = \begin{bmatrix} 0 & M_{S1} & M_{S2} & M_{S3} & M_{S4} & M_{SL} \\ M_{1S} & M_{11} & 0 & 0 & 0 & M_{1L} \\ M_{2S} & 0 & M_{22} & 0 & 0 & M_{2L} \\ M_{3S} & 0 & 0 & M_{33} & 0 & M_{3L} \\ M_{4S} & 0 & 0 & 0 & M_{44} & M_{4L} \\ M_{LS} & M_{L1} & M_{L2} & M_{L3} & M_{L4} & 0 \end{bmatrix} \quad (10)$$

where each resonator is only coupled to the source (M_{Si} or M_{iS}) and load (M_{Li} or M_{iL}), and there are no couplings between resonators. The terms M_{ii} on the diagonal indicate the mutual coupling, which defines the resonant frequency of each individual resonator .

Considering the equivalent circuit model of each resonator coupled to the source and load of Figure 7.b, we can obtain the 2-port admittance matrix of the network as:

$$[Y] = \begin{bmatrix} Y_{11}(s) & Y(s) \\ Y_{21}(s) & Y_{22}(s) \end{bmatrix} = j \begin{bmatrix} 0 & M_{LS} \\ M_{SL} & 0 \end{bmatrix} + \sum_{k=1}^N \frac{1}{sC_k + jB_k} \begin{bmatrix} M_{Sk}^2 & M_{Sk}M_{Lk} \\ M_{Sk}M_{Lk} & M_{Lk}^2 \end{bmatrix} \quad (11)$$

Note that the elements of the admittance matrix $Y_{ij}(s)$ can be obtained as a function of the *characteristic polynomials*.

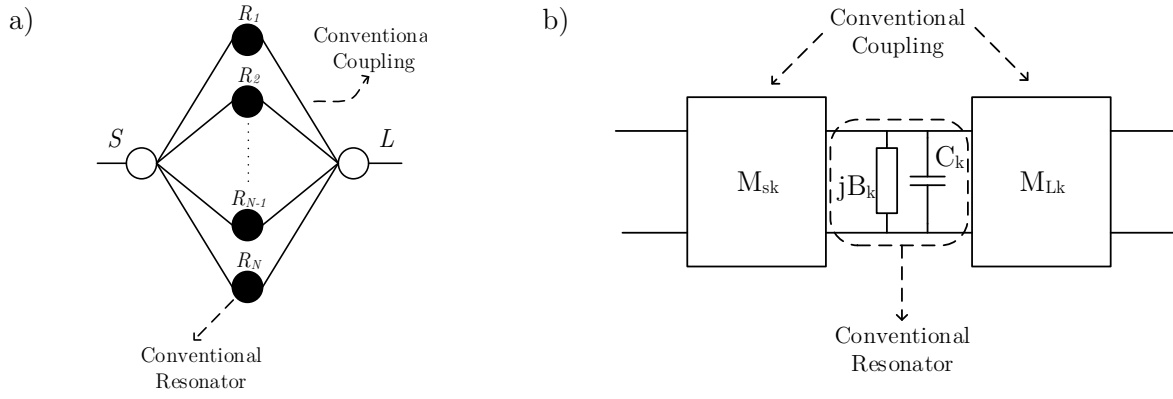


Figure 7. a) Equivalent network of a transversal filter of order N . The empty circles S and L represent the source and the load, the black filled-in circles (from R_1 to R_N) represent the resonators and the lines connecting the circles represent the mainline couplings from each resonator to the source and load. b) Equivalent circuit of the k -th resonator and its couplings to the source and load.

Now the outer terms of the coupling matrix M_{kS} , M_{Sk} , M_{kL} and M_{Lk} can be found from the residues of the admittance matrix terms, using (9).

The other elements in matrix M , the diagonal elements M_{kk} , can be found by equating the real and imaginary part of the elements of (8) and (11), respectively. Doing so results in:

$$C_k = 1, \quad B_k (\equiv M_{kk}) = -\lambda_k \quad (12)$$

Therefore, the diagonal of the coupling matrix is formed by the eigenvalues of the coupling matrix.

As previously mentioned the conclusions resulting from this section are very significant and **will be also valid when applied to acoustic wave filters**. This means that any filter response could be synthesized as a transversal network. This concept will imply a significant advantage over the conventional responses achievable with AW ladder filters.

1.6 Dissipation effects

Dissipation effects produce degradation of the filter response, mainly in the in-band and on the roll-off skirts of the band-edges. These effects are due to existence of *lossy* components on the ultimate designed filter network. In filters based on conventional coupled resonators the major contribution of the losses are due to the limited Q of the resonators, being the couplings between resonators usually negligible on the overall dissipation effect. In that case, and when the limited Q of the resonators is uniform, i.e., all the resonators have identical Q , the

dissipation effects can be predicted in advance from the characteristic polynomials, without needing to perform the synthesis of the filter [24].

This is not the case of most acoustic implemented filters, where the resonators forming the filter have different Q (non-uniform Q), and the overall losses of each resonator needs to account for the Q of both resonances (resonance and anti-resonant) and the external losses elements like electrodes and additional inductors and capacitors which are very common on the resulting topologies. Despite of that, the possibility to account for the losses in advance (prior to the synthesis), sets the best filter achievable performance. Note that the accurate modeling of those losses needs to evaluate the resulting network topology and account for the losses of each individual component. Further details of the losses in an AW resonator are presented in section 1.6.

The text below outlines how to account for the dissipative effects into the characteristic polynomials. This method will be used along the thesis and compared with the accurate modeling that considers all the lossy sources when needed.

To do that one could simply add a positive real factor σ to the purely imaginary variable $s = j\omega$, on the transfer function expression $S_{21}(s)$. This is equivalent to move all the poles of the transfer function to the left, in the s -plane representation. The value of σ for a bandpass filter can be expressed as:

$$\sigma = \frac{1}{Q \cdot FBW} \quad (13),$$

where FBW is the fractional bandwidth of the filter. Then the scattering parameters can be evaluated at $s = \sigma + j\omega$.

Figure 8 depicts the effects of losses in the transfer function and reflection coefficient for a 4th order Quasi-Elliptic filter of 2.5% fractional bandwidth, with a single pair of transmission zeros. The black curve corresponds to the ideal response of the filter, whereas the blue, green and red curves represent the filter response for finites Q s of 1000, 500 and 250, respectively.

In any case, the effects of dissipation in a bandpass filter are:

- The insertion loss increases
- A rounding off of the insertion loss curve at the band edges occurs. This diminishes the width of the passband and reduces the selectivity of the filter.
- Transmission and reflection zeros are less distinct.

These three features are more prominent when the losses increase or when the fractional bandwidth of the filters decreases.

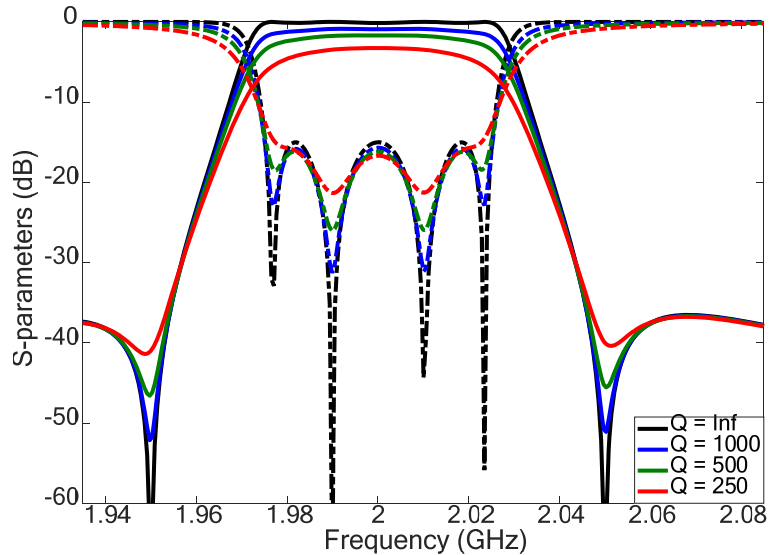


Figure 8. Transfer and reflection coefficients of a polynomial bandpass filtering response as a function of its Q factor.

1.7 Electro-acoustic resonators and technology

This work frames on the electro-acoustic technology and in particular in the electro-acoustic filters and its application into the telecommunication industry. Although an extensive and detailed description of the electro-acoustic technology is not necessary for a full comprehension of the work developed during this thesis, outlining the most common AW resonator configuration is a must. In particular, a detailed description of the equivalent circuits describing the AW resonators, is necessary.

The synthesis techniques developed in this work are based on a basic building block described by the BVD equivalent circuit model. This model is detailed in this section and it is used to describe the performance of AW resonator in both configuration: Surface Acoustic Wave (SAW) resonators and Bulk Acoustic Wave (BAW) resonators.

1.7.1 Bulk Acoustic Wave Resonator

The BAW resonator is widely used on filter development for wireless applications operating at frequency nearly and above 2 GHz. Figure 9 sketches the configuration of a BAW resonator, which consists of a piezoelectric plate sandwiched between two metallic electrodes. Additional layers (or air gaps) are included on at bottom and/or top of the piezoelectric layer to define the boundary conditions that confine the acoustic wave and therefore define the resonant mode.

As in a conventional resonator the resonant mode occurs when a standing wave is patterned inside the resonator, which defines the resonant frequency. The fundamental resonant frequency also known as longitudinal frequency in BAW resonators is mainly defined by the thickness and material properties of the piezo-electric layer. This happens approximately when

the piezo-electric thickness is half-wavelength. Note however, the resonant frequency is strongly affected by any additional layer, including those used as reflector layers.

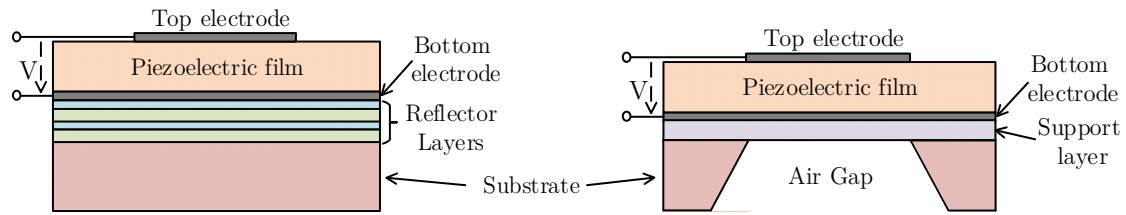


Figure 9. Outline of an acoustic wave resonator on its BAW (Bulk Acoustic wave) configuration.

Note that the configuration of Figure 9 corresponds to a parallel plate capacitor, where the dielectric constant of the piezo-electric defines the capacitance between electrodes. Being a piezo-electric material, a voltage applied between the top and bottom electrodes gives rise to an acoustic wave.

1.7.2 Surface Acoustic Wave Resonator

In contrast with BAW resonators where the acoustic wave travels through the thickness of the piezo-electric layer, the acoustic wave travels along the surface of the piezo-electric. A conventional configuration of a SAW resonator consists of an interdigitated capacitor (IDC), as outlined in Figure 10. The resonant frequency in this case is defined by the separation between the fingers of the IDC. The feasibility of manufacturing these structures with very small gap between the fingers, limits the application of this configuration to frequencies below 2 GHz.

As occurs in the BAW configuration, an external voltage is applied to create a travelling acoustic wave, note as well that an electric capacitor also exists between the two ports where the voltage is applied.

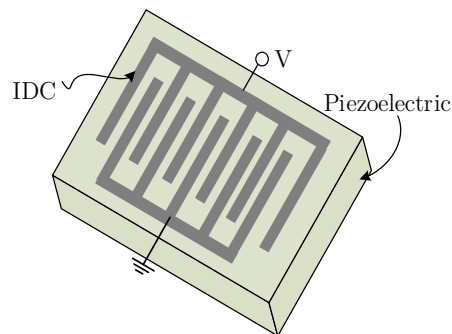


Figure 10. Outline of an acoustic wave resonator on its SAW (Surface Acoustic wave) configuration.

1.7.3 BVD circuit model. Lossless

Figure 11 shows a Butterworth-Van-Dike (BVD) circuit model that describes the main resonances of an acoustic wave resonator, for both, the BAW and SAW configuration. The

equivalent circuit described below corresponds to the lossless case, this is when no losses are considered neither in the metallic or electrodes part, nor in the acoustic wave propagation path. Although losses introduce significant effect on the filter performance (see section 1.6), as conventionally done on filter synthesis, those are not considered in the initial synthesized network, and are usually evaluated afterwards.

Note as well that the corresponding equivalent circuit emulates the acoustic resonator response only near the resonant frequency as it is required in the synthesis of acoustic filters. Evaluation of the filter spurious response can be performed afterwards by the use of a distributed circuit model - such as the Mason model [10], or extended BVD models that account for additional resonances [23].

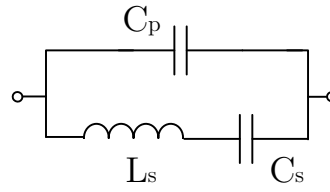


Figure 11. BVD equivalent circuit model

From the acoustic configurations outlined in Figures 9 and 10, we can identify a capacitive structure due to the electrodes confrontation and a traveling wave section where the acoustic standing wave occurs, creating a resonance. Both effect are explained by the equivalent circuit above.

Regarding this equivalent circuit the total capacitance, which corresponds to the "low frequency" capacitance results from:

$$C_0 = C_p + C_s \quad (14)$$

And could be extracted from the impedance of the resonator as $C_0 = \frac{1}{2\pi f \text{Im}(Z)} \Big|_{f < f_0/2}$, where f_0 would correspond to the operating frequency.

A fundamental property of this circuit model is the existence of two resonances known as, series resonance f_s , also known as acoustic resonance, and shunt resonance f_p , also known as anti-resonance. Those two resonances can be clearly identified in the impedance of the resonator outlined in Figure 12. This figure also details on the impedance phase performance, which exhibits a 180° degrees shift in the frequency range between the two resonances. Expressions of both resonances as a function of the circuit parameters of Figure 11 can be read as:

$$\begin{aligned}
f_s &= \frac{1}{2\pi\sqrt{L_s C_s}} \\
f_p &= \frac{1}{2\pi} \sqrt{\frac{C_p + C_s}{L_s C_s C_p}}
\end{aligned} \tag{15}$$

Useful expression on how the circuit parameters relates with the series and shunt resonances, f_s and f_p , are:

$$\begin{aligned}
C_p &= C_0 \left(\frac{f_s}{f_p} \right)^2 \\
C_s &= C_0 \left[1 - \left(\frac{f_s}{f_p} \right)^2 \right] \\
L_s &= \frac{1}{(2\pi f_s)^2 C_s}
\end{aligned} \tag{16}$$

The characteristic impedance of the resonator is defined as:

$$Z_0 = \frac{1}{\omega_s \cdot C_0} \tag{17}$$

A significant parameter of an AW resonator, which is crucial in the filter design, is the widely mentioned coupling coefficient k_e^2 , which is related with the energy conversion between the electric and acoustic domains, and it is related to the two resonances f_s and f_p . The coupling coefficient can be expressed as:

$$k_e^2 = \frac{\pi f_s}{2 f_p} \frac{1}{\tan\left(\frac{\pi f_s}{2 f_p}\right)} \cong \frac{\pi^2 f_s}{4 f_p} \left(1 - \frac{f_s}{f_p}\right) \tag{18}$$

Where the last term in (18) corresponds to the Taylor series 2nd order expansion of the coupling coefficient. Now the series and shunt resonance frequencies can be rewritten as a function of the coupling coefficient, resulting in the following expression:

$$f_p \cong \frac{f_s}{1 - \frac{4}{\pi^2} k_e^2 \left(1 + \frac{4}{\pi^2} k_e^2\right)} \quad (19)$$

The expressions presented in this section will be used throughout the following chapters, where the resonator performance and parameters will be related with the filter performance.

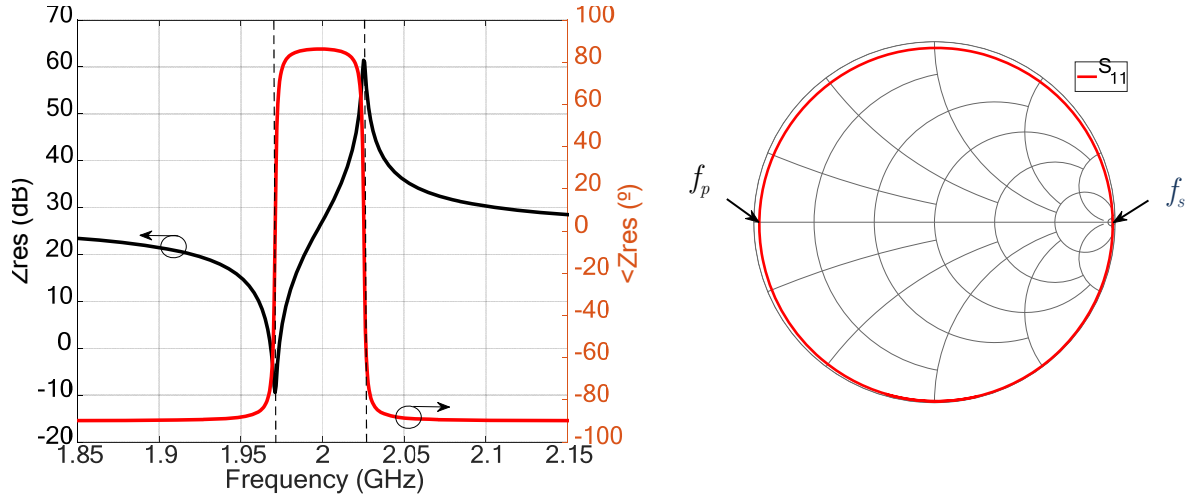


Figure 12. Magnitude and phase response of an acoustic resonator, throughout evaluation of the BVD model.

Figure 12 (a) shows the phase and module representation of the impedance corresponding to an acoustic resonator centered at 2 GHz, with reference impedance 51Ω and BVD circuit parameters: $f_s = 1.97\text{GHz}$, $C_0 = 1.58\text{pF}$, and $k_e^2 = 6.44\%$ and Figure 12 (b) shows its reflection coefficient on the Smith Chart.

Equivalent circuit model

The BVD circuit model of Figure 11 has its equivalent circuit model [27] as shown in Figure 13. This is a circuit that provides exactly the same frequency response by means of a different network. Such a transformation is very well established and allows to define the new circuit parameters, C_2 , L_2 and C_3 . The values of the series and shunt resonance now can be obtained from the circuit parameters defining the equivalent circuit. The set of equations are:

will determine if the losses of the C_0 branch needs to be accounted (when $Q_p < Q_a$) through the following expression:

1.7.5 Lowpass prototype

As indicated in section 1.1, the synthesis procedure occurs at the lowpass domain, this is in the normalized frequency Ω , instead of f . This process implies a frequency transformation and a circuit transformation [25], which reproduces the filter performance at the normalized frequency and centered at $\Omega=0$ instead of $f = f_0$, where f_0 , is the central operating frequency.

Although the frequency transformation from lowpass to bandpass is very well-known, it is recalled in (27), where Ω_c is the normalized cut-off frequency, which is set to 1 if not said otherwise, and FBW is the fractional bandwidth defined as f_0/BW , where BW is the bandpass bandwidth of the filter.

$$\Omega = \frac{\Omega_c}{FBW} \left(\frac{f}{f_0} - \frac{f_0}{f} \right) \quad (27)$$

Along with the frequency transformation, operating in the lowpass prototype domain requires the definition of the equivalent lowpass circuit and the circuit transformation between lowpass and bandpass. Note that these circuit transformations are very well established for conventional LC series or shunt resonators, however such transformation is not defined for the case of an AW resonator, assuming the bandpass circuit models as the ones defined in section 1.7.3 , and outlined in Figure 11 and Figure 13.

The circuit of Figure 15.a is the lowpass prototype corresponding to the circuit of Figure 13. This circuit consists in a capacitor C_{LP} , shunted with an independent frequency susceptance B_{LP} , and all in series with a frequency independent reactance X_{LP} . These circuit parameters need to be related with the parameters defining the circuit model of Figure 13, C_2 , L_2 and L_3 .

On the other hand, the circuit of Figure 15.b, is the lowpass prototype of the BVD model outlined in Figure 11. Following the configuration of a BVD model, it consists on an inductance L_{LP} in series with a reactance B'_{LP} , and all shunt connected to a susceptance X'_{LP} .

Now, those parameters need to be related with the circuit parameters of the BVD model, L_s , C_s and C_p .

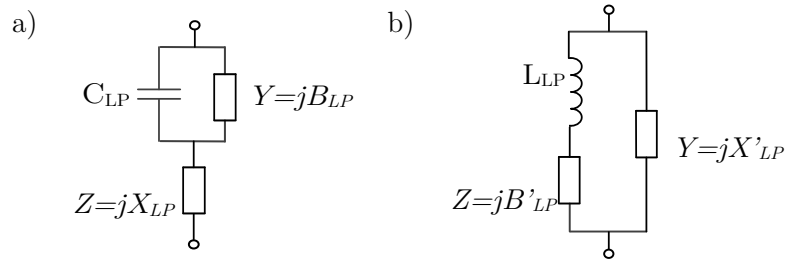


Figure 15. a) lowpass prototype corresponding to the BVD reciprocal circuit model. b) lowpass prototype corresponding to the BVD model.

Each of these normalized frequencies can be related with their corresponding bandpass frequencies, f_s and f_p , by following the frequency transformation equation of (27). Note that, this results in a second order equation as $f_s^2 - f_s \cdot FBW \cdot f_0 \cdot \Omega_s - f_0^2 = 0$, for the case of f_s , with two solutions.

In practice, and as will be shown in chapter 2 in the synthesis of ladder filters, the equivalent circuit of Figure 15.a is extracted as a series resonator, and its de-normalized shunt resonance f_p , should result in a transmission zeros at the upper bandpass. Note that this value is prescribed on the definition of the characteristic polynomials. Then, its counterpart, circuit of Figure 15.b, is extracted as a shunt resonator whose de-normalized series resonance f_s should match the prescribed transmission zeros at the lower passband.

By applying circuit transformation and frequency transformation to the lowpass prototypes above, we can relate the parameters of the pass band prototypes with the circuit parameters defining the lowpass prototype. The two set of equations corresponding to both circuits are detailed in (30) and (31), below:

$$\begin{aligned}
C_2 &= \frac{C_{LP}}{FBW\omega_0} & L_s &= \frac{L_{LP}}{FBW\omega_0} \\
L_2 &= \frac{1}{C_2(2\pi f_p)^2} & C_s &= \frac{1}{L_s(2\pi f_s)^2} \\
C_3 &= C_2 \left[\left(\frac{f_p}{f_s} \right)^2 - 1 \right] & C_p &= C_s \left(\frac{f_s}{f_p} \right)^2 \left[1 - \left(\frac{f_s}{f_p} \right)^2 \right]^{-1}
\end{aligned}
\tag{30} \tag{31}$$

Figure 16, shows the frequency response of a BVD model mapped down and normalized in frequency to overlap the frequency response of the lowpass prototypes defined in the current section.

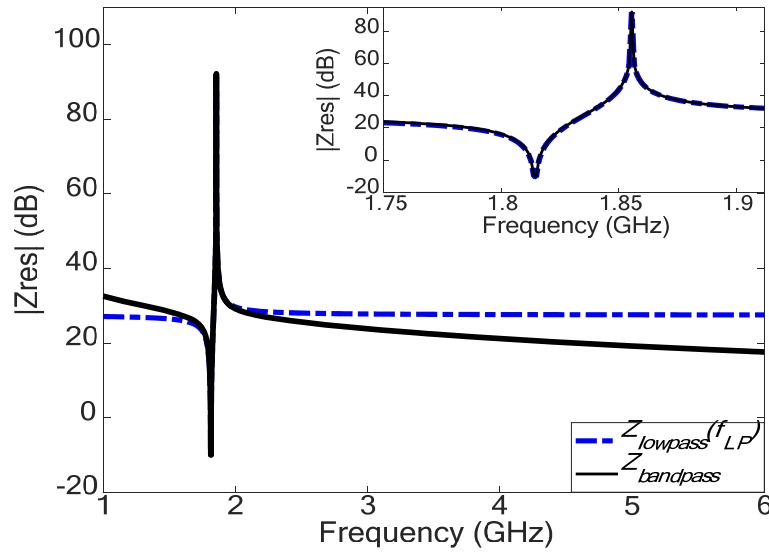


Figure 16. Lowpass prototype (mapped at the operating frequency) and bandpass prototype performance of a single acoustic wave resonator.

In contrast with conventional passband circuit transformation to lowpass prototype of conventional LC resonators, - both in its series and shunt configuration -, where the overlap is perfect all over the frequency range, this is not the case for the lowpass prototypes presented in this section. The reason for that is because in the conventional case the circuit transformation is consistent with the frequency transformation, whereas in the present case the developed lowpass prototypes are simply circuit artifacts to emulate a resonator with a resonant and anti-resonant frequency, but does not fully follow the same frequency response. In spite of that the proposed circuit model has the advantage of having only one frequency dependent component (C_{LP} or L_{LP}), being therefore an order one resonator. This implies a suitable formulation of filters based on acoustic wave resonators by means of the presented characteristic polynomials, where an N order polynomial requires of N order 1 resonators. It is also worth to mention at this point that both lowpass circuit prototypes of Figure 15, do not follow the exact same frequency dependence.

On the other hand, the fact that passband and lowpass circuits do not follow exactly the same frequency dependence will result in differences between the lowpass prototype filter and the bandpass filter (based on BVD resonators). Although these effects will be mentioned along the thesis when synthesis and case studies will be shown, its major effects occur in the in-band of very wideband filters and in the out-of-band rejection. In the latter case, the final bandpass filter shows actually a better rejection than the lowpass prototype, due to the frequency dependence of the resonators itself.

Despite this latter explanation, the proposed lowpass prototype shows to be very useful for the mathematical formulation, synthesis and to provide good designs at passband frequencies.

To finalize this chapter, Figure 17 shows the conventional representation of an acoustic resonator, which will be used along the whole document. This representation corresponds to any of the equivalent circuits presented in previous sections, for both the lowpass prototypes, Figure 15.a and Figure 15.b, and for the bandpass prototypes, Figure 11 and Figure 13, and even if we refer to SAW or BAW configurations.



Figure 17. Typical representation of an acoustic resonator.

1.8 Summary

This chapter presented most of the theoretical background to track on the mathematical development reported in following Chapters 2 and 3, where the synthesis of ladder filters and transversal acoustic wave filters are developed. To this end, the main topics have been addressed: the mathematical formulation required on the synthesis procedure, which is included in sections 1.2 - 1.6, and the circuit modelling of acoustic resonators, which is described in section 1.7. This chapter is complemented with further details on the mathematical description of the characteristic polynomials in the references provided along the document. Despite the existence of this initial chapter, all the mathematical details and procedures are carefully detailed throughout this thesis.

CHAPTER 2

DEVELOPMENT OF LADDER TOPOLOGIES IN ACOUSTIC FILTERS

Ladder configuration is probably the most common topology used on the development of acoustic filters, for both SAW and BAW configurations. In spite of that, there is barely none straightforward reported methods for the synthesis of this type of filters. This chapter develops a direct synthesis method based on the very well-known *extraction element* process, described in section 1.3. Due to the nature of the acoustic resonator, and the fact of performing a resonant and anti-resonant response in a single resonator, some considerations need to be accounted for the application of the element extraction method.

The chapter starts by outlining the concept of a ladder topology detailing the way the filter performance is profiled. From this, we identify a kind of characteristic polynomials that can be synthesized through a ladder network based on AW resonators as a main building block. Then the element extraction synthesis procedure is described for these particular polynomials. Previous considerations for the application of this method are described along the text. Additional circuit transformations are latter applied to the resulting synthesized topology in order to address and provided further useful topology from the technological point of view.

Some illustrative examples will be shown at the end of this chapter. Additional examples considering real case studies, including multiplexing structures will be detailed in Chapter 4. Chapter 4 will also describe the user-friendly software tool created for the application of the current synthesis technique.

2.1 Acoustic wave ladder filter topology and concept

Figure 18 outlines the ladder filter topology based on acoustic resonators. As occurs in a conventional ladder filter configuration, this topology consists on cascading series and shunt AW resonators.

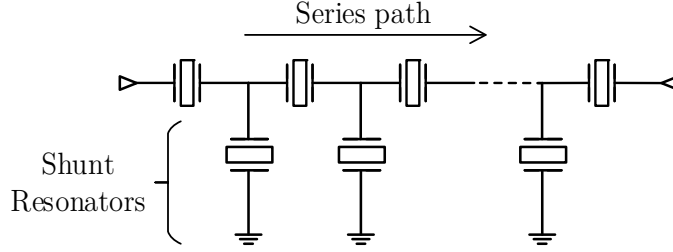


Figure 18. Outline of a ladder network.

In contrast with conventional resonators, AW resonators exhibit a pole/zero response. This singular characteristic allows to achieve sharper filter responses due to the existence of transmission zeros without the need of including cross-coupling effects [28]. Nevertheless this also limits the type of responses that can be achieved with this configuration, and therefore, it will set the characteristic polynomials that define the filter responses.

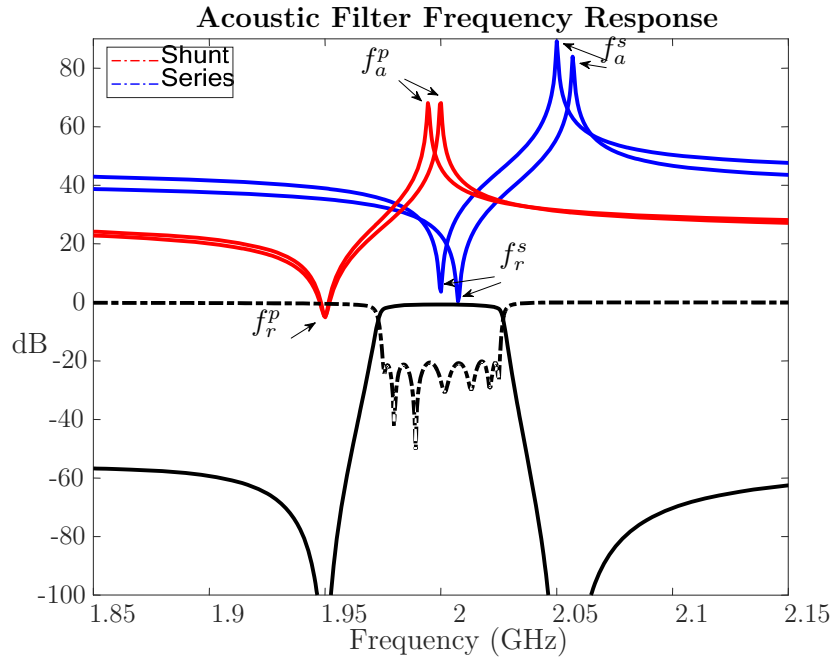


Figure 19. S-parameters of a 7th order (4 series, 3parallel -4s3p-) AW ladder filter (Figure 18), and input impedance of the isolated resonators. Note that due to the symmetry of the response only two of the four series resonators are different and two of the three shunt resonators are equal.

Figure 19 shows the S-parameters (black lines) corresponding to a 7th order ladder filter based on acoustic resonators and the resonators impedances (blue & red lines). This figure clearly shows how due to the nature of acoustic resonators, that is, each of them creating a transmission zero, the transfer response offers a pronounced selectivity.

The transmission zeros at the lower side band are created at the frequency point where the shunt resonator offers a very small impedance (short circuit - known as resonance or series resonance), whereas the transmission zeros at the upper side band are created by the series resonator at the frequency point where the impedance of the resonator is very large (open circuit - known as anti-resonance or shunt resonance). To better illustrate this concept, Figure 20 depicts the circuit behavior for different frequencies. Note that, in general, impedance of series resonators are higher than impedances of shunt resonators at the out-of-band, $Z_{R_{ser}} \gg Z_{R_{shu}}$ and just the other way around, $Z_{R_{shu}} \gg Z_{R_{ser}}$ for most of the in-band frequency range, especially around f_0 where the difference is especially significant.

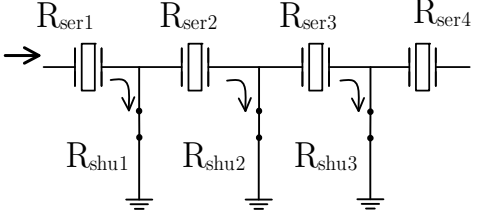
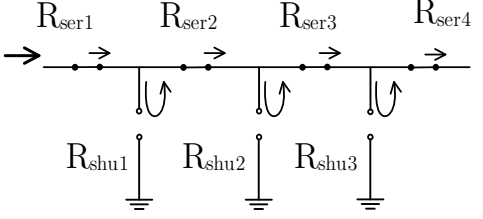
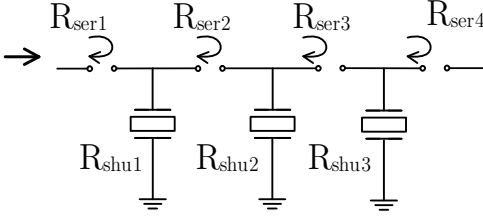
	<p>Assuming all shunt resonators have the same f_r^p, (which here is an approximation and not always necessarily true), when $f = f_r^p$, the impedances of the shunt resonators are very low (they act as a short-circuit). The signal finds a clearer path to the ground.</p>
	<p>Around the center frequency of the filter we are close to two singular frequency points, $f \cong f_r^s$, where all $Z_{R_{ser}}$ are very low (SC) and $f \cong f_a^p$, where the impedances of the shunt resonators are very high (OC). The signal finds a clear straight path to the output port.</p>
	<p>Assuming all series resonators have the same f_a^s (which again is not always necessarily true), when $f = f_a^s$, the impedances of the series resonators are very high (they act as an open circuit). The signal sees a very high impedance series path and gets reflected to the input port.</p>

Figure 20. Working principle of a ladder network based on acoustic resonators a) TZ created by the shunt resonators b) behavior in the in-band region and c) TZ created by the series resonators.

2.2 Characteristic polynomials for ladder acoustic filters

As outlined in section 1.2, general Chebyshev characteristic polynomials offers the flexibility to propose the type of filter responses that can be implemented by means of ladder

configurations. Although it may exist other types of characteristic polynomials for this purpose, the nature of an AW resonator and the arrangement in a ladder configuration, requires characteristic polynomials with:

- Equal number of transmission zeros than number of resonators forming the filter
- The location of the transmission zeros is defined by the number of series or shunt resonators:
 - In a filter of order N odd that starts with a series resonator (and therefore ends with a series resonators), the number of transmission zeros above the upper band edge are $(N+1)/2$, and at the lower side band are $(N-1)/2$.
 - In a filter of order N odd that starts with a shunt resonator (and therefore ends with a shunt resonators), the number of transmission zeros below the lower band edge are $(N+1)/2$, and at the upper side band are $(N-1)/2$.
 - In a filter of order N even, the number of transmission zeros in both, below the lower band edge and above the upper band edge are $N/2$. In this case two filter configuration exist:
 - Starting with series resonator.
 - Starting with shunt resonator.

Those polynomials will be used to synthesize the ladder network based on AW resonators and they can define any position of transmission zeros and reflection zeros. In practice, this will offer many designs that can meet certain filter specifications and requirements, by means of proposing different sets of characteristic polynomials.

As presented in previous chapter, the characteristic polynomials are defined in the lowpass frequency domain, and the equivalent lowpass circuit models of the AW resonators of Figures 15a and 15b will be extracted from the synthesis.

2.3 Synthesis procedure. Element extraction

Element extraction is applied for the type of polynomials described above. This results in a recipe that can always be followed and only slight variations need to be considered depending if an even or an odd order filter is synthesized and on the location of the transmission zeros. As indicated above, this results in variations of the filter configuration and, therefore, this directly affects the extraction procedure.

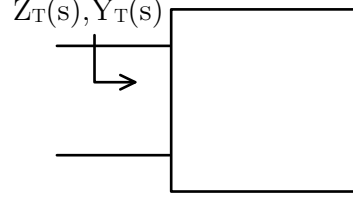
This section outlines the procedure for the case of an N odd order filter where the number of transmission zeros above the upper band edge are $(N+1)/2$, and in the lower side band are $(N-1)/2$. Despite this particular case the concept and rules to be followed at each step are completely general.

Procedure:

1) Define the characteristic polynomials according the rules of previous section. The transmission zeros above the upper band edge band are located at Ω_i , where $i=1, 3, 5 \dots N$, and the transmission zeros below the lower band edge band are located at Ω_j , where $j=2, 4 \dots N-1$.

2) Obtain the input filter impedance, $Z_T(s)$, following (4). Recall that this assumes a 2-port network loaded with a 1Ω normalized impedance.

$$Z_T(s) = \frac{E(s) + F(s)/\varepsilon_R}{E(s) - F(s)/\varepsilon_R} = \frac{Z_n(s)}{Z_d(s)}$$

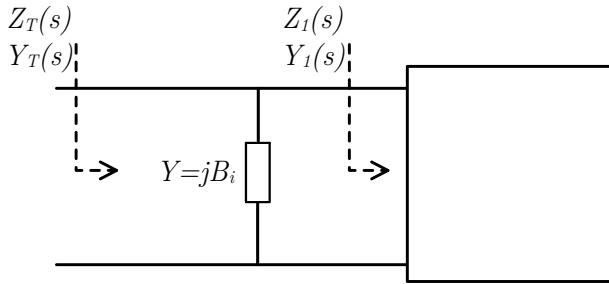


where $Z_n(s)$ and $Z_d(s)$ represent, respectively, the numerator and denominator.

3) The first element to extract, is a susceptance jB_i , which is extracted to obtain a remaining admittance $Y_i(s)$ such that exhibits a transmission zero at Ω_i of the upper side band (anti-resonance of a series resonator). This value can be obtained by evaluating the admittance $Y_T(s)$ at the normalized frequency of the transmission zero, as:

$$B_i = \text{imag}(Y_T(j\Omega_1))$$

Although the real part is zero, this process forces to take only the imaginary part, to avoid numerical problems. **Note that flexibility exists on selecting the transmission zero to be extracted**, which could be any of the ones located above the upper band edge. Selection of a different transmission zero would result in a different acoustic resonator. Then, the resulting network is:



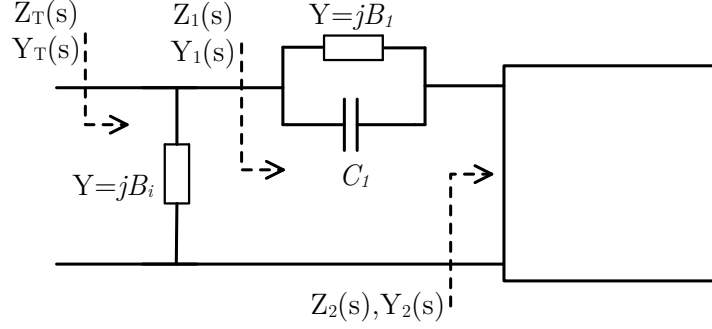
Where $Y_i(s)$, is obtained as:

$$Y_1(s) = Y_T(s) - jB_i$$

4) Due to the condition of 3), the resulting admittance $Y_i(s)$ exhibits a zero at Ω_i , therefore the impedance $Z_i(s)$ could be written as [54]:

$$Z_1(s) = \frac{K_1}{s - j\Omega_1} + Z_2(s)$$

Which would result in the following network:



Where the value of C_1 and B_1 are:

$$C_1 = \frac{1}{K_1}, \quad B_1 = \frac{-\Omega_1}{K_1}$$

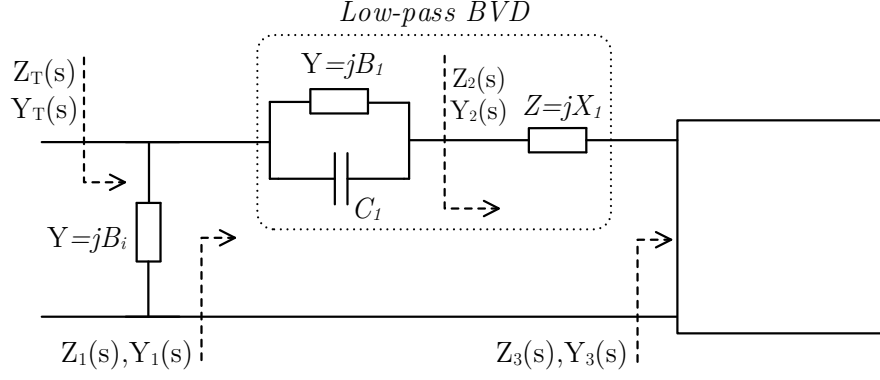
and K_1 can be easily obtained by applying:

$$K_1 = Z_1(s)(s - j\Omega_1)|_{s=j\Omega_1}$$

5) Extract a reactive element jX_1 to obtain a remaining impedance with a transmission zero at Ω_2 of the lower side band (resonance of the shunt resonator). This value can be obtained by evaluating the impedance $Z_2(s)$ at the normalized frequency of the transmission zero, as:

$$X_1 = \text{imag}(Z_2(j\Omega_2))$$

Again, flexibility exists on selecting the transmission zero to be extracted, as long as this is located below the lower band edge. This results in the following network:



Now at this point, it is worth to note that the first stage of this extraction reveals a lowpass prototype of an acoustic resonator (dash-squared in the circuit), as the one in Figure 15.a. Formulation on how to go from this lowpass prototype to a bandpass acoustic resonator was clearly detailed in section 1.7.5.

The remaining impedance $Z_3(s)$ is given by $Z_3(s) = Z_2(s) - jX_1$.

6) Due to the condition of 5) the resulting impedance $Z_3(s)$ exhibits a zero at Ω_2 , therefore the admittance $Y_3(s)$ could be written as [9]:

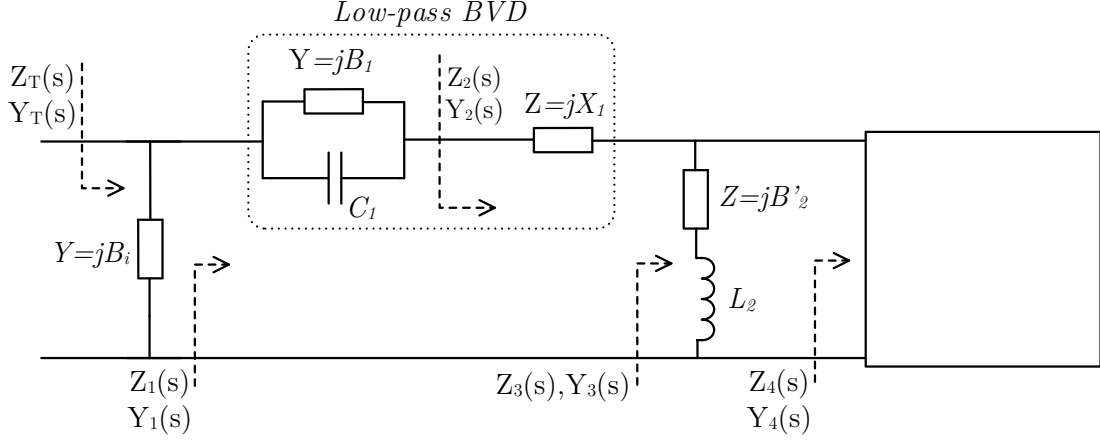
$$Y_3(s) = \frac{K_2}{s - j\Omega_2} + Y_4(s)$$

Analogously as in step 4) L_2 and the reactance B'_2 of the following network can be found as:

$$L_2 = \frac{1}{K_2}, \quad B'_2 = \frac{-\Omega_2}{K_2}$$

where K_2 can be easily obtained by applying:

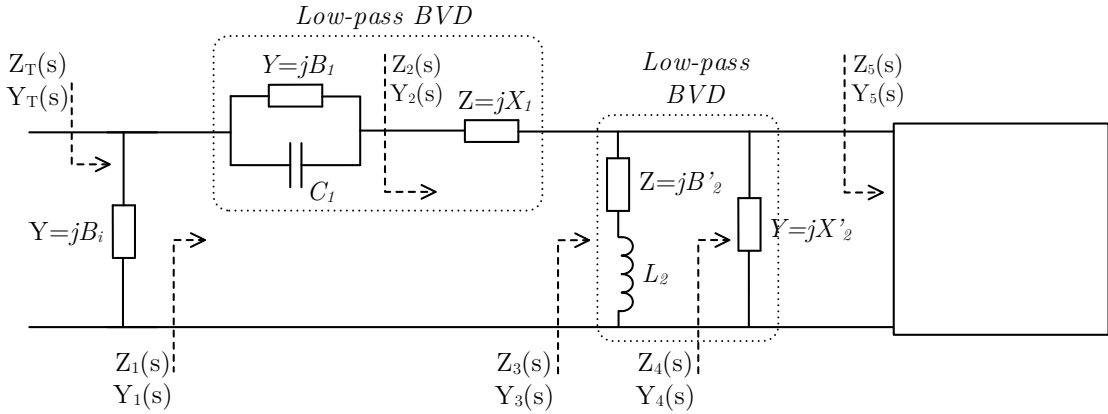
$$K_2 = Y_3(s)(s - j\Omega_2)|_{s=j\Omega_2}$$



7) The next element to extract is a susceptance jX'_2 to obtain a remaining admittance $Y_5(s)$ such that exhibits a transmission zero at Ω_3 of the upper side band (anti-resonance of a series resonator). This value can be obtained by evaluating the admittance $Y_4(s)$ at the normalized frequency of the transmission zero, as:

$$X'_2 = \text{imag}(Y_4(j\Omega_3))$$

Then, the resulting network is:



At this stage of the extraction, the first shunt acoustic resonator can be clearly identified as the circuit model of Figure 15 b.

This procedure will continue until all transmission zeros are extracted and the remaining impedance is a single loading impedance to the normalized value 1Ω . In that sense, note that the last series susceptance (see figure below) would not need to be extracted since it is directly the imaginary part of the remaining admittance.

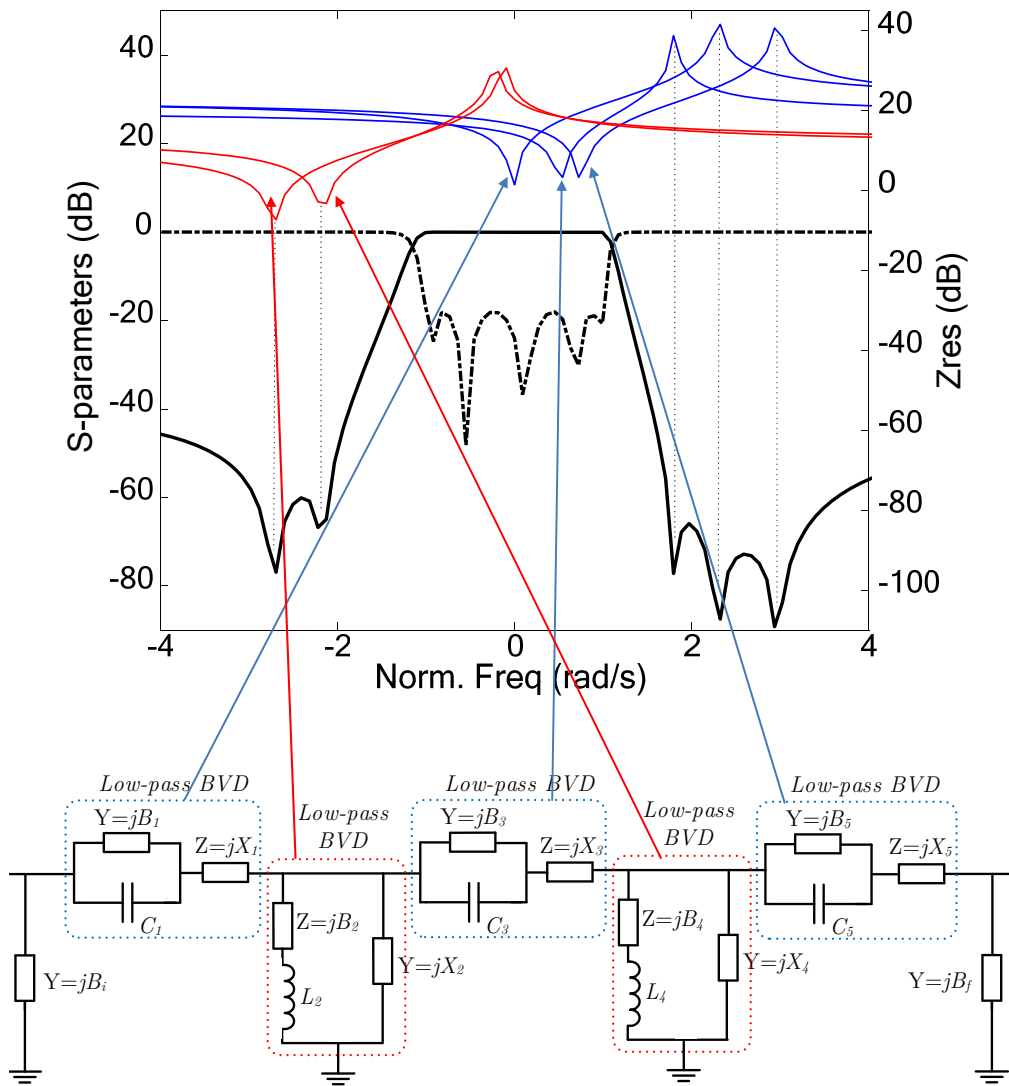


Figure 21. Lowpass filter response (transmission in solid black and reflection in dashed black) typical logarithmic representation of the impedance magnitude of the resonators (series resonators in blue and shunt resonators in red). Filter network is outlined below.

Figure 21 shows the final synthesized filter corresponding to an example of order 5. The figure also shows the frequency response of the filter and the impedance of each of the extracted resonators. Note that this correspond to the lowpass prototype.

Before moving to the next section, where the lowpass equivalent circuit will be transformed to the bandpass frequency, it is necessary to mention that in the case of proposing a filter response where the number of transmission zeros at the upper side of the passband are $(N+1)/2$ and at the lower side band are $(N-1)/2$, the resulting equivalent circuit for $N=5$ would result in the circuit topology of the figure below, Figure 22. In this case the element extraction procedure starts by obtaining a series reactance instead, followed by a shunt

resonator. Since in this case we still consider an odd order filter, the synthesized network ends with a series reactance, which will be connected to the normalized loading impedance.

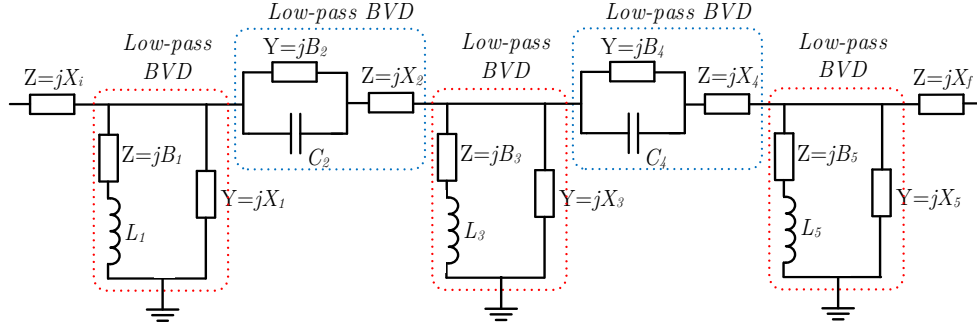
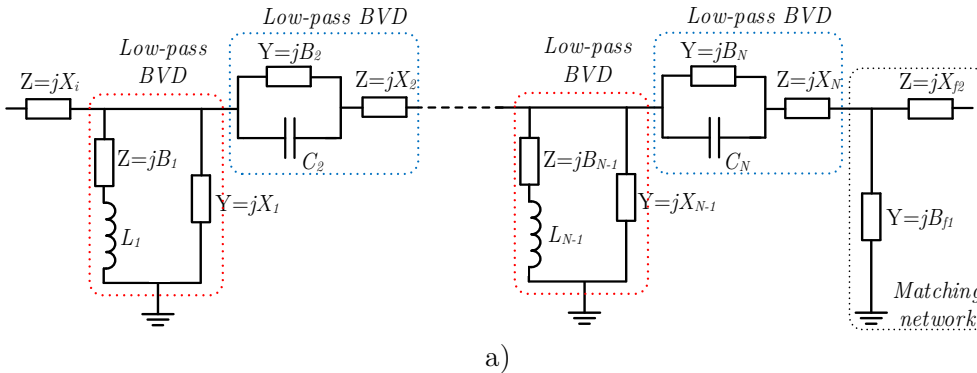


Figure 22. Lowpass prototype topology of an order 5 filter with 3 Transmission Zeros (TZ) at the lower side band and 2 at the upper side band

One of the major concerns on acoustic filter design is the goal of providing the best possible solution for a given response. In that sense, the element extraction procedure described is subject to the proposed characteristic polynomials, and for given characteristic polynomials, a certain degree of flexibility is given by selecting the transmission zero extracted by each resonator. In practice, the required flexibility to achieve the final design will be given by the different characteristic polynomials meeting the required specifications. As mentioned above, the general Chebyshev polynomials allows changes on the position of transmission zeros and reflection zeros, which offer different values of the resonators for a given synthesized network.

In contrast with the cases above, for even order filters with equal number of transmission zeros at the lower and upper side bands of the filter, the synthesis procedure has the additional flexibility of extracting a series acoustic resonator to perform a transmission zero at the upper side band, as a first stage, as in Figure 23.b, or extracting a shunt resonator to perform a transmission zero at the lower side band, as in Figure 23.a. Therefore, two different topologies (Figure 23) can provide the same exact response (in the lowpass domain).



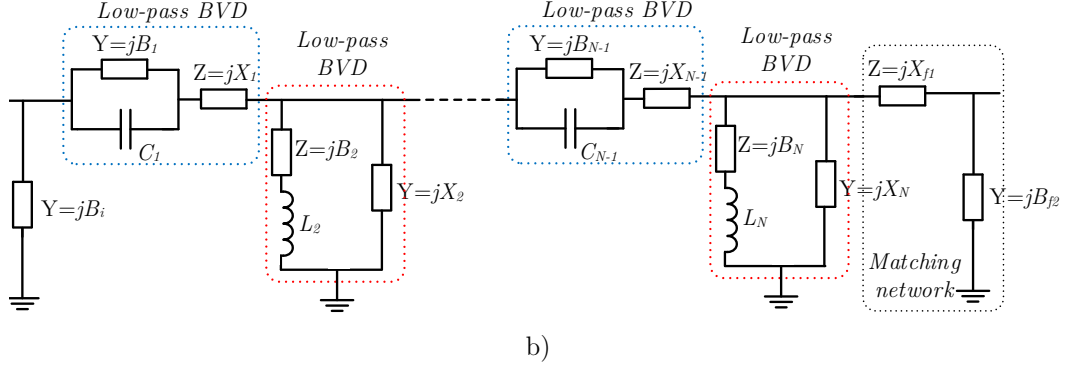


Figure 23. Network topology of an N even order filter, a) starting with a shunt resonator, b) starting with a series resonator.

A particular consideration on the two previous configurations is that they require a matching network to match the normalized output impedance. Note that in the cases of Figure 23, when the resulting networks are transformed to the bandpass prototype (see section 2.3.2, below), they would exhibit differences on their responses.

2.3.1 Example: synthesis of a 7th order filter.

The following example contains the numerical details of the procedure described above for a:

- Filter order $N = 7$
- Prescribed transmission zeros: 4 transmission zeros at $\Omega_{UB}=1.4835j$ and 3 transmission zeros at $\Omega_{LB}=-1.5173j$. Note that the position the transmission zeros are indicated in normalized frequency.
- Passband ripple = 0.04dB (\rightarrow Return Losses = 20.3 dB)

Note that since the number of transmission zeros is higher at the upper side band than at the lower side band, the ladder filter topology starts and ends with a series resonator, as indicated in Figure 24.

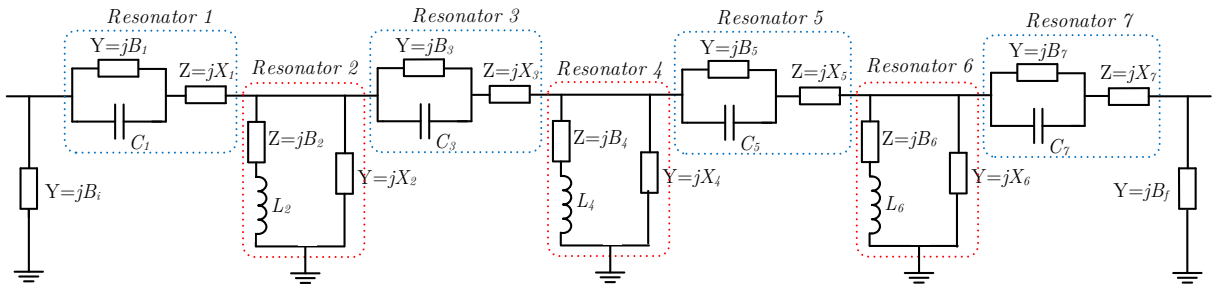


Figure 24. Synthesized network of a 7th order filter with 4 transmission zeros at the upper side band and 3 transmission zeros at the lower side band.

From the filter parameters above and following the described synthesis procedure we obtain the normalized values:

- Resonator 1 (series): $C_1=1.7217$, $B_1=-2.5542$, $X_1=-0.687$.
- Resonator 2 (shunt): $L_2=0.3152$, $B_2=2.0909$, $X_2=0.3491$.
- Resonator 3 (series): $C_3=0.5785$, $B_3=-0.8582$, $X_3=-1.1877$.
- Resonator 4 (shunt): $L_4=0.2026$, $B_4=3.2523$, $X_4=0.3029$.
- Resonator 5 (series): $C_5 = C_3$, $B_5 = B_3$, $X_5 = X_3$.
- Resonator 6 (shunt): $L_6 = L_2$, $B_6 = B_2$, $X_6 = X_2$.
- Resonator 7 (series): $C_7 = C_1$, $B_7 = B_1$, $X_7 = X_1$.
- Input and output susceptances: $B_i = B_f = -1.0332$

Figure 25 shows the lowpass frequency response by evaluating the synthesized lowpass prototype. Note that this response is identical to the one reproduced by evaluating the characteristic polynomials. Same figure also shows the impedance of the resulting lowpass BVD resonators. Resonators in series are indicated in blue whereas the shunt resonators are indicated in red.

Also note how for this example, all series resonant frequencies of shunt resonators (TZ at the lower band edge) were set to the same value and all shunt resonant frequencies of the series resonators (TZ at the upper band edge) were set to the same value, the resulting synthesized resonators from the synthesis may have different k_e^2 (by simple inspection it can be observed that the separation between f_s and f_p of each resonator is different), which is generally a drawback since all resonators in a same die would have almost identical coupling. The synthesis outcome follows the desired frequency response nevertheless it does not necessarily provide a network were all technological issues are considered per se. In general, some iterations shall be necessary in order to obtain the particular synthesis that fulfills both, desired frequency response and technological constrains.

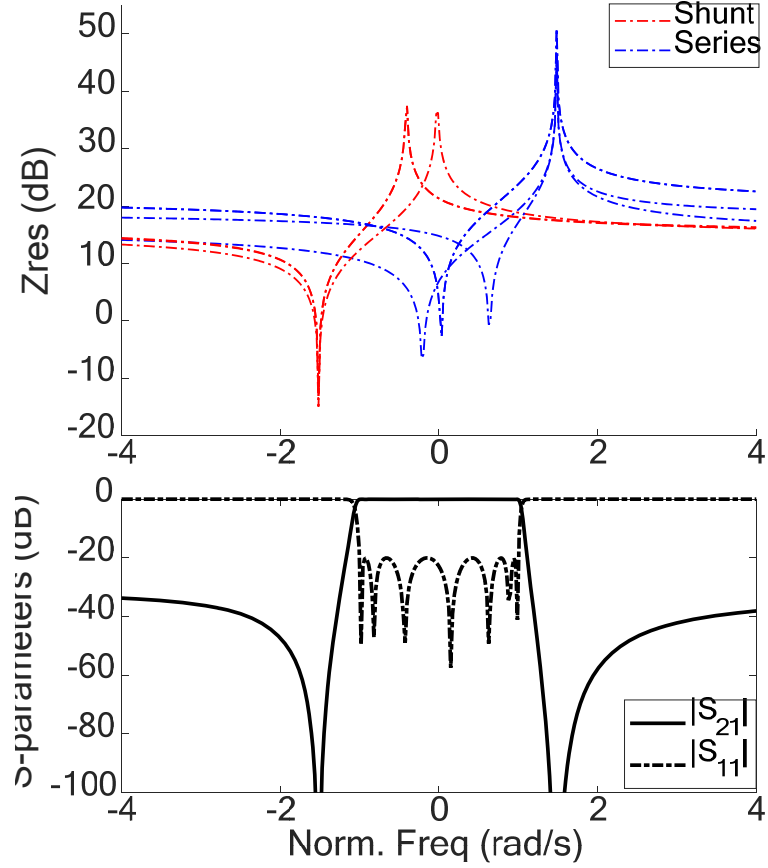


Figure 25. Impedance of the synthesized resonators. Blue lines correspond to series resonators, and red lines correspond to shunt resonators (above). Synthesized frequency response of the 7th order filter (below).

2.3.2 Bandpass transformation

The synthesized responses presented so far correspond to the lowpass prototype evaluated at the normalized frequency domain Ω . Those responses result from the evaluation of the characteristic polynomials or by evaluating the lowpass prototype. As occurs in conventional (non-acoustic) filters both responses overlap all over the frequency range.

To obtain the bandpass responses one can evaluate the characteristic polynomials considering the frequency transformation of equation (27), at f , or by evaluating the resulting synthesized network after circuit transformation to the bandpass circuit model [24]. Recall at this point that the transformation from the lowpass prototype to the bandpass circuit model uses the circuit transformation outlined in section 1.7.5. In contrast with conventional (non-acoustic) resonators, where the response of the lowpass prototype matches the response of the bandpass prototype but a shift in frequency, in this case, certain disagreement at both in-band and out-of-band response exists. As mentioned in section 1.7.5, this is because the circuit transformation from lowpass to bandpass is not fully consistent with the frequency transformation.

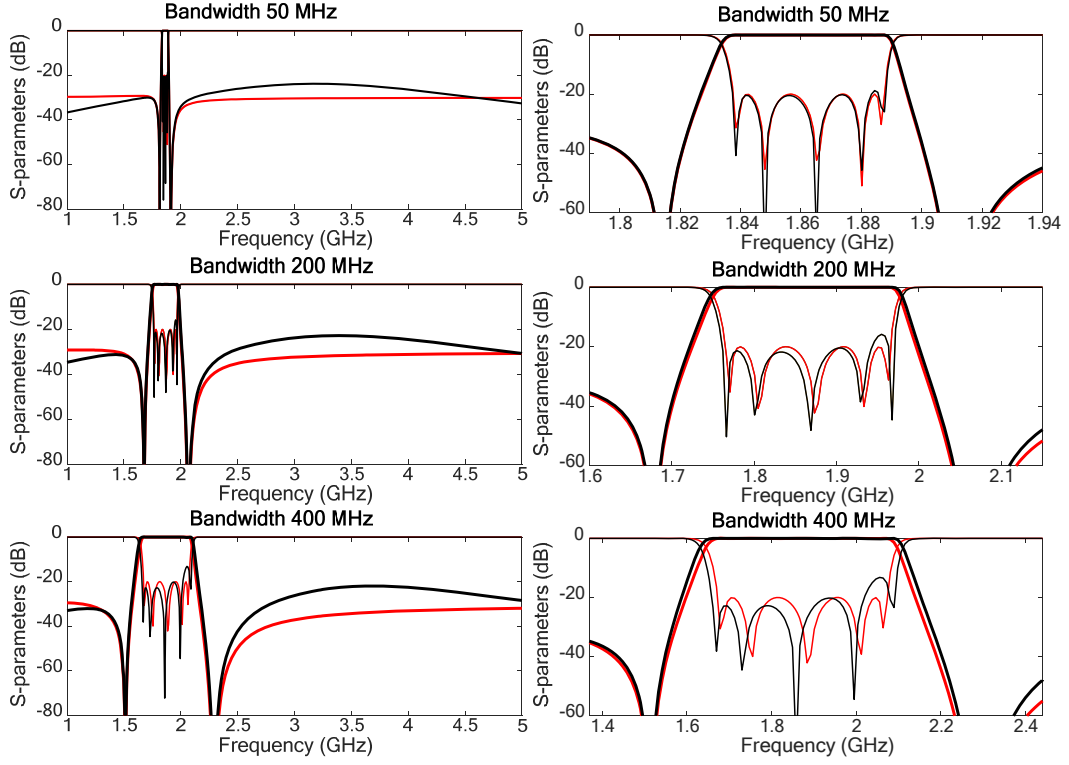


Figure 26. Filter response of a 5th order filter for a) 50 MHz bandwidth, b) 200 MHz bandwidth, c) 400 MHz bandwidth.

In order to illustrate this point, which will be observed and referred along the designs presented in this work, the figure above shows the frequency responses of three filter, whose lowpass response is the same and therefore the same lowpass prototype and characteristic polynomials, which correspond to a 5th order filter, with three transmission zeros at the upper side band and two transmission zeros at the lower side band, and 20 dB return losses. The filter responses differ on their bandwidth, being 50 MHz, 200 MHz and 400 MHz, corresponding respectively to Figure 26.a, Figure 26.b and Figure 26.c. Red lines outline the response of the characteristic polynomials, and black line correspond to the bandpass synthesized network.

The results of Figure 26 reveal that when the filter bandwidth increases, the disagreement between the ideally synthesized response and the bandpass responses increases, both at the in-band and at the out-of-band frequency ranges. Despite of that, all the filter responses in all cases are still very good, which demonstrates the validity of the synthesis procedure and circuit transformations proposed.

At this point, it is very important to mention that in all the responses above no restriction have been considered on the value of the coupling coefficient of the resonators, and that their values increase as the bandwidth increases.

2.4 Circuit transformation

The synthesis method above does not offer the flexibility of selecting the coupling coefficient of the resonators in advance, and for a given characteristic polynomials the unique flexibility, for instance, in an odd order filter is the transmission zero assigned to each resonator. The flexibility of this method lays on the fact that a ladder filter topology can be proposed for any general Chebyshev set of polynomials, and it is well-known that there are many sets of polynomials that fulfill given filter specifications. This allows for selecting the most convenient polynomials for the implementation.

Despite of that, full flexibility on the *a priori* selection of the resonator parameters does not exist. The present section recalls and formulates the circuit transformation applied at the resonator level in order to obtain the desired coupling coefficient. Those transformations are very well established on the design of acoustic filters and require the inclusion of external elements. However, the inclusion of external elements is uncommonly desired from a practical point of view, since increases volume, introduces losses and further complicates the design and manufacturing procedure. Regarding this latter statement then, the ultimate goal would be to provide a filter network without external elements and with desired values of coupling coefficients.

Similar arguments can be exposed on the selection of the resonant frequency of the resonators. As occurs with the coupling coefficients those cannot be prescribed in advanced and result from the proposed characteristic polynomials and the way the transmission zeros are extracted. Although the manufacturing techniques allow for full flexibility on the selection of the resonant frequency, in practice, a maximum of four to six resonant frequencies might be tailored if need it in a single wafer. Note that increasing the number of the available resonant frequencies in a single chip, would complicate the fabrication process and substantially increase the cost. Additionally, the differences between all the resonant frequencies to be implemented in a single chip cannot significantly differ.

Figure 27 shows the possible circuit transformations to be applied in a single resonator. Figure 27.a1 and Figure 27.a2 show how a series capacitance would be added to a BVD resonator. Figure 27.b1 and Figure 27.b2 include a shunt capacitor, Figure 27.c1 and Figure 27.c2 includes a shunt inductor, and Figure 27.d1 and Figure 27.d2 include a series inductor.

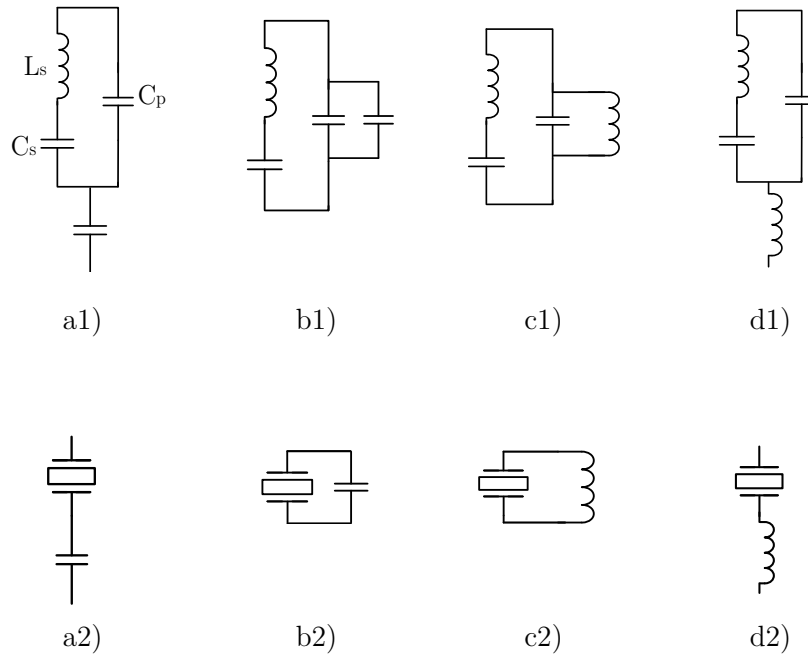


Figure 27. BVD model with the inclusion of external elements in order to modify the coupling coefficient. a) inclusion of a series capacitor, b) inclusion of a shunt capacitor, c) inclusion of a shunt inductor, and d) inclusion of a series inductor.

From simple inspection of the external elements above along with the BVD circuit model (Figure 11), and also the equivalent BVD model (Figure 13), one can easily conclude that the frequency performance of a BVD circuit model with the inclusion of a series or shunt capacitance is not affected and this new circuit emulates exactly an acoustic BVD circuit performance with an equivalent coupling coefficient and different series or shunt resonance [23] [13]. This is clearly illustrated in Figure 28.

Figure 28 shows the impedance frequency performance of a 4.1% coupling coefficient BVD model. This would be the value resulting from the synthesis. Since in practice the coupling coefficient of the resonator cannot be freely selected, we would need to transform it to a 4.1% coupling coefficient equivalent resonator, by means of suitable acoustic resonators, 6.7% for instance in this case (whose impedance is indicated in black), with an additional external element, a shunt or series capacitor. By doing so, the impedance of a 6.7% acoustic resonator is shown in dashed red line in Figure 28, where the series resonator f_s remains as in the synthesized resonator and the shunt resonance f_p is moved to lower frequencies. If the series capacitor is connected at this resonator, it emulates a 4.1% resonator, indicated in dotted red line. Note that this perfectly overlaps the synthesized resonator response.

In solid black line the required 6.7% resonator would perform with identical f_p as in the synthesized resonator and f_s is moved to higher frequencies. Again, when this resonator is connected to a shunt capacitor this exactly emulates the 4.1% synthesized resonator, indicated in red line.

This concludes therefore that a series or shunt capacitor results on an equivalent acoustic resonator with lower coupling coefficient.

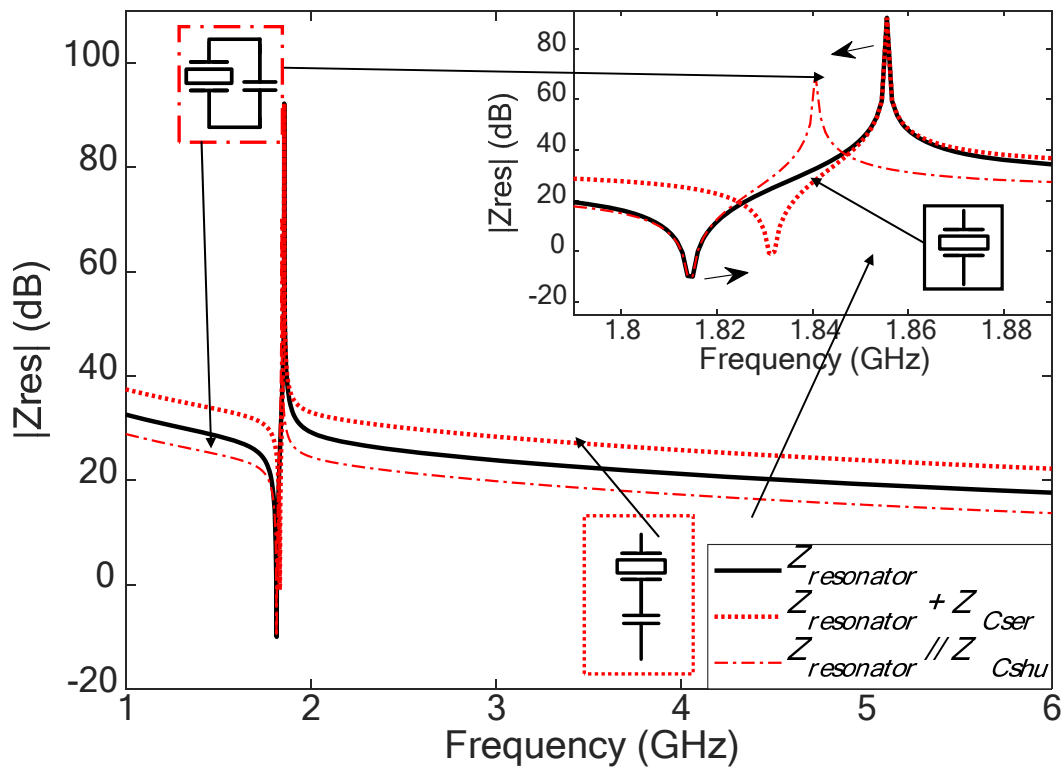


Figure 28. Impedance response of BVD resonator with the inclusion of external capacitors. Legend details on each of the lines in the figure.

In contrast with the previous cases, when an additional inductance is added in shunt or series to the acoustic resonator, as shown in Figure 27.c2 and Figure 27.d2, the resulting circuit emulates an acoustic resonator with larger coupling coefficient. The example to illustrate this statement assumes a target coupling coefficient of 7.5% to be implemented with acoustic resonators of 6.7% and additional inductors. Results of that are summarized in Figure 29.

When a shunt inductor is added to get the required 7.5%, the overall impedance exhibits the same f_s and the f_p is shifted to higher frequencies. Whereas in the case of a series inductor, the impedance will have now identical f_p and the f_s is shifted to lower frequencies. Both cases allow to emulate a higher coupling coefficient resonator. Nevertheless, this approach is only valid in a certain frequency range. The inset of Figure 29 shows the broadband behavior of these equivalent circuits. In the case of adding a shunt inductance the impedance gives rise to a pole at lower frequencies, and in the case of adding a series inductance a zero-impedance point occurs at higher frequencies. Note that this might have important implications in the broadband response of the filter, and this fact should be considered in advance.

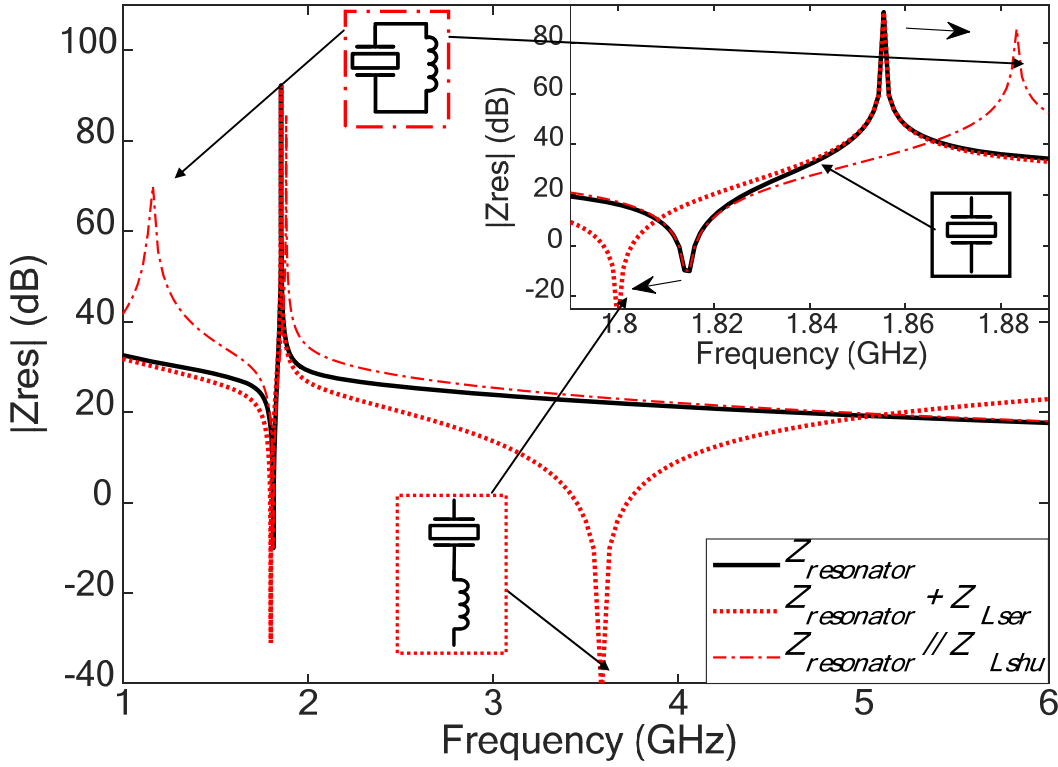


Figure 29. Impedance response of BVD resonator with the inclusion of external inductors. Legend details on each of the lines in the figure. Effects of the inclusion of external elements in the broadband response can be seen in the inset at the lower right side.

Formulation to find the values of the equivalent circuit, this is the values of the BVD model and external components for a given targeted coupling $k_{e_target}^2$ is detailed below for the four circuit transformations above. First, we assume as initially synthesized values, f_s , f_p , and C_s , C_p , L_s defining the BVD circuit, or C_2 , L_2 and C_3 for the equivalent BVD circuit.

$C_{add_shunted}$

- f_s , L_s and C_s remain as in the synthesis
- f_{p_new} is obtained as:

$$f_{p_new} = \frac{f_s}{0.5 + \sqrt{0.25 - \frac{4}{\pi^2} k_{e_target}^2}} \quad (32)$$

- C_{p_new} is obtained as:

$$C_{p_new} = \frac{C_s}{(2\pi f_{p_new})^2 L_s C_s - 1} \quad (33)$$

- C_{add} is obtained as:

$$C_{add} = C_p - C_{p_new} \quad (34)$$

C_{add} series

- f_p , L_2 and C_2 remain as in the synthesis

- f_{s_new} is obtained as:

$$f_{s_new} = f_p \left(0.5 + \sqrt{0.25 - \frac{4}{\pi^2} k_{e_target}^2} \right) \quad (35)$$

- C_{3_new} is obtained as:

$$C_{3_new} = \frac{1}{(2\pi f_{s_new})^2 L_2} - C_2 \quad (36)$$

- C_{add} is obtained as:

$$C_{add} = \frac{1}{\frac{1}{C_3} - \frac{1}{C_{3_new}}} \quad (37)$$

- Now we use C_2 , L_2 and C_{3_new} to obtain the new values of the conventional BVD resonator by applying the formulation in section 1.7.3.

L_{add} shunted

- f_s , L_s and C_s remain as in the synthesis

- f_{p_new} is obtained as:

$$f_{p_new} = \frac{f_s}{0.5 + \sqrt{0.25 - \frac{4}{\pi^2} k_{e_target}^2}} \quad (38)$$

- C_{p_new} is obtained as:

$$C_{p_new} = \frac{C_s}{(2\pi f_{p_new})^2 L_s C_s - 1} \quad (39)$$

- L_{add} is obtained as:

$$L_{add} = \frac{1}{(2\pi f_{p_new})^2 (C_{p_new} - C_p)} \quad (1)$$

L_{add} series

- f_p , L_2 and C_2 remain as in the synthesis

- f_{s_new} is obtained as:

$$f_{s_new} = f_p \left(0.5 + \sqrt{0.25 - \frac{4}{\pi^2} k_{e_target}^2} \right) \quad (40)$$

- C_{3_new} is obtained as:

$$C_{3_new} = \frac{1}{(2\pi f_{s_new})^2 L_2} - C_2 \quad (41)$$

- C_{add} is obtained as:

$$L_{add} = \frac{1}{(2\pi f_{s_new})^2} \left(\frac{1}{C_3} - \frac{1}{C_{3_new}} \right) \quad (42)$$

- Now, we use C_2 , L_2 and C_{3_new} to obtain the new values of the conventional BVD resonator by applying the formulation in Section 1.7.3.

2.5 Input series inductance



•



2.5.1 Example: 7th order filter.

This example corresponds to a 7th order filter whose input filter parameters are detailed in Figure 31 (screen shot of the software described in Chapter 4). The filter parameters indicate, input and output impedances, bandwidth, central frequency and position of the transmission zeros. From these parameters, we follow the synthesis procedure outlined in section 2.3. The values resulting from the synthesis are summarized in Table 2. Note that this table considers the values for both topologies, the one directly synthesized, which starts and ends with a shunt inductance, and the one starting and ending with a series inductance.

The screenshot shows a software interface for filter synthesis. It is divided into several sections:

- Settings:** Contains input fields for Order [N] (7), Return Losses [dB] (13), Bandwidth [MHz] (150), and Center frequency [GHz] (2.35). There are 'Load', 'Save', and 'Set' buttons.
- Prescribed Transmission Zeros:** Shows '# lower band TZ' as 3 and '# upper band TZ' as 4.
- Input & Output Impedances:** Shows 'Zs [Ohm]' as 50 + j* 0 and 'Zl [Ohm]' as 50 + j* 0.
- TZ Tuning:** A table with two columns: 'Lower Band [GHz]' and 'Upper Band [GHz]'. It lists transmission zeros PR1, PR2, PR3 and SR1, SR2, SR3, SR4 with their respective frequencies.

Lower Band [GHz]		Upper Band [GHz]	
PR1	2.2585	SR1	2.4559
PR2	2.2705	SR2	2.434
PR3	2.2585	SR3	2.434
		SR4	2.4559

Figure 31. Screen shot of the GUI Synthesis Software outlining the input filter parameters.

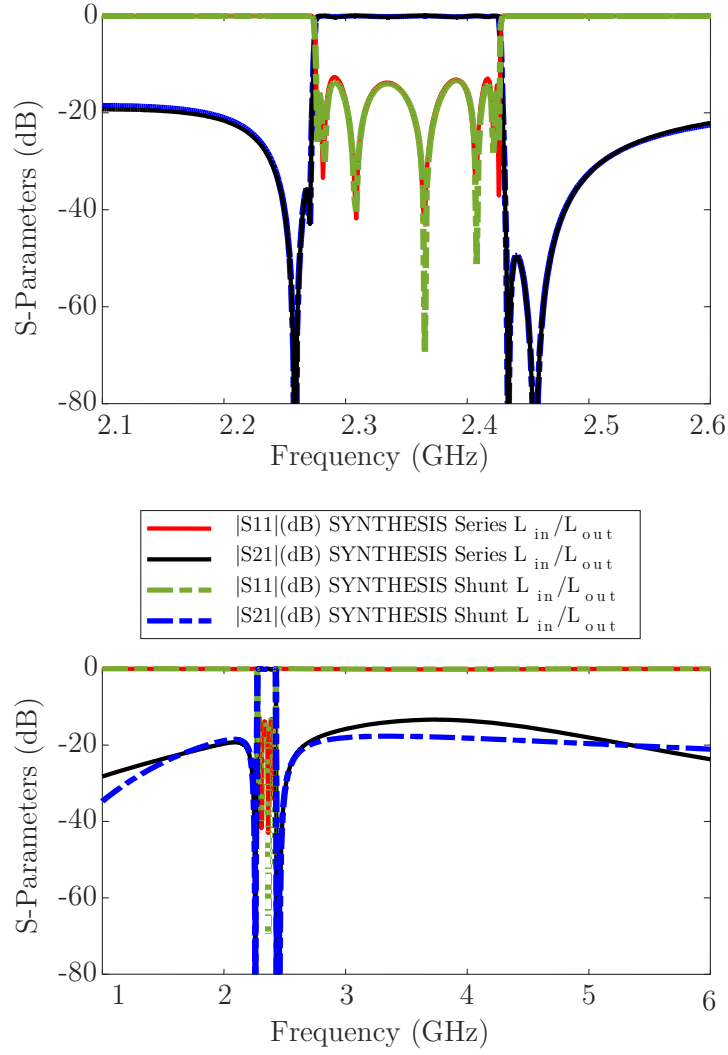


Figure 32. Frequency responses corresponding to the topologies of Table 2. Details on the in-band and band-edges of the filter (above). Details on the wideband response (below).

Responses of both topologies, in the bandpass domain, are depicted in Figure 32. Black and red correspond to the transmission and reflection coefficients respectively, for the series inductance case. Blue and green, correspond to the shunt inductance topology for the transmission and reflection coefficients, respectively. These responses reveal that both topologies result in an equal response in the in-band of the filter, and the reflective coefficient only show negligible deviations. Regarding the transmission coefficients (black and blue lines) in the out-of-band regime, the two responses differ on the attenuation that they exhibit. At the upper side of the passband, the shunt inductance case (blue line) shows better rejection close the passband of the filter, due to the higher side lobe performance of the series inductance case (black line), at frequencies further from the passband edges, the series inductance case exhibits

higher rejection. These performances are in the other way around in the lower side band of the passband, being the series inductance case less stringent at frequencies far from the passband and more rejective closer to the passband.

Parameter	Value
Order N	7
RL	13 dB
BW	150 MHz
f_0	2.35 GHz
Transmission	LB 2258.5MHz, 2270.5MHz, 2258.5MHz
Zeros	UB 2455.9MHz, 2434MHz, 2434MHz, 2455.9MHz
f_s	Ser 2384.4MHz, 2362.3MHz, 2362.3MHz, 2384.4MHz Shu 2258.5MHz, 2270.5MHz, 2258.5MHz
k_e^2	Ser 6.974%, 7.053%, 7.053%, 6.974% Shu 6.998%, 6.953%, 6.998%
L series @ in/out	
C_p	Ser 0.976pF, 1.199pF, 1.199pF, 0.976pF Shu 1.19pF, 0.758pF, 1.19pF
C_{ser}/C_{shu}	$\sim 1 - 1.5$ pF
L shunt@ in/out	
C_p	Ser 1.518pF, 1.865pF, 1.865pF, 1.518pF Shu 1.851pF, 1.179pF, 1.851pF
C_{ser}/C_{shu}	$\sim 0.8 - 1.5$ pF

Table 2. Values resulting from the synthesis and circuit transformation

2.6 Ground inductors effects

The filter networks proposed so far result from the synthesis procedure where additional circuit transformations may have to be applied afterwards in order to obtain more suitable configuration for a final filter implementation. As a matter of fact, the previous networks do not consider the effect of the ground inductors that appear integrated in the laminate of acoustic filters.

The existence of these ground inductors is illustrated in Figure 33. Although the inclusion of ground inductors are not mandatory per se in the filter design (absence of inductor would mean an ideal via that directly connects the bottom electrode of the resonator to the common ground at the bottom of the laminate) it has been proven that their presence may help to increase the achievable bandwidth, by means of a virtually higher resonator effective coupling k_e^2 , and meet the near-out-of-band as well as the far-out-of-band rejection specifications.

These inductances are required to be very small, in the range of $\sim 0.5\text{-}3\text{nH}$. Larger inductors will introduce more losses and they may also be too big in size making difficult to fit them in the laminate due to lack of space.

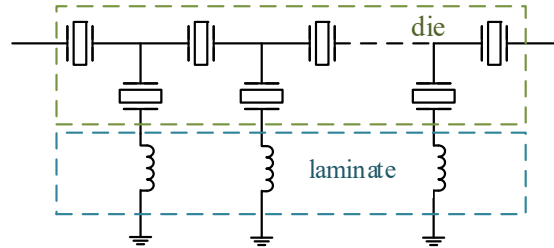


Figure 33. Ladder filter topology with inclusion of series ground inductors in the shunt resonators

The addition of these inductors in such configuration (Figure 27.d1 and Figure 27.d2) will affect the corresponding shunt branch behavior as depicted in Figure 29. The equivalent impedance of the pair “resonator - series inductor” will describe an electrical frequency-dependent behavior with two important differences with respect to the resonator in absence of inductor: on one hand, the f_s frequency will experience a shift to lower frequencies and on the other hand, a new resonant frequency will appear at higher frequencies, in turn causing an additional notch (or transmission zero) on the ladder filter transmission. Inevitably, the in-band performance of the shunt branch initially provided by the resonator alone will no longer be the same with the inclusion of the inductor although this deviation will be acceptable in most cases. The downwards shift in f_s may help achieving better rejection in the proximity of the lower band edge, meanwhile the notch at higher frequencies may help improving the out-of-band rejection at given frequencies. The cost of these improvements would be the worsening of the in-band insertion losses and most likely degradation of the return losses. Other issues may arise in the out-of-band frequency range if the chosen value for the inductance is not appropriate, i.e. undesired “fly-backs” which may ruin the out-of-band rejection.

At resonator level, the location of the two new resonant frequencies will depend directly on the inductance value of the ground inductor. At filter level, we will be able to displace two notches along the frequency range.

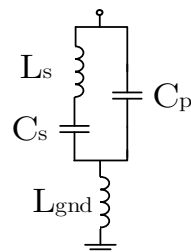


Figure 34. Typical circuit scheme of the path to ground consisting on a shunt resonator followed by a ground inductor.

Figure 34 shows the new circuit with the addition of the inductor in series, L_{gnd} . So far, we have described qualitatively the effect of this addition but a more rigorous explanation is detailed hereinafter.



the new f_s value after the downwards shift. The second solution corresponds to the new transmission zero in the far-band and will be referred here as $f_{OoB,TZ}$.

Integration into the synthesized network

From a filter designer classical perspective, an inductor will most likely hang from every shunt resonator of the circuit from the very early design steps. During the conventional optimization using CAD tools, the inductance values will be used as adjustable parameters in the simulation, with only two conditions to fulfill: 1) the overall filter performance meets the filter specifications, and 2) the inductance values stay within a certain suitable range.

Nevertheless, a different approach can be done thanks to the synthesis presented here. The circuit modification can be included in the outcome of the synthesis procedure and electrically modeled in such a way we have control on the location of the two new resonant frequencies.

For the sake of taking profit of the advantages related to the inclusion of such ground inductors, one can modify the synthesized shunt resonator in order to *absorb* it. That means, an equivalent circuit that includes the ground inductance and behaves electrically similar to the previous BVD in absence of inductor, mainly in the in-band range, is figured out. In some cases the subsequent results will deviate significantly from those provided by the synthesis.

The following procedure aims to essentially maintain as much as possible the in-band flatness filter response and rejection on the sides of the passband, as they were before any modification to the BVD circuit was done. For this, we recall Figure 11 and Figure 13 in Figure 35.a (with circuit parameters L_s , C_s and C_p) and the equivalent BVD model in Figure 35.b (with circuit parameters L_2 , C_2 , C_3), respectively. Figure 35.c represents the modified equivalent BVD model together with the ground inductance L_{gnd} . Finally, Figure 35.d corresponds to the final BVD model, which is a direct result from the reverse transformation of the equivalent BVD circuit in Figure 35.c.

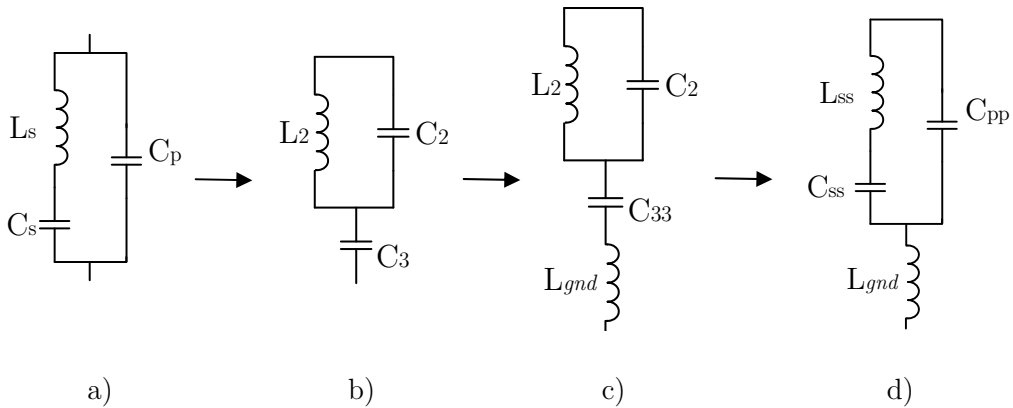
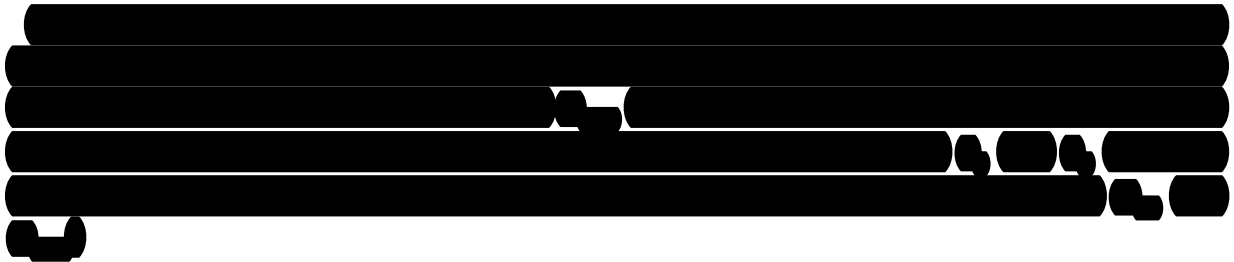


Figure 35. a) BVD model, b) equivalent BVD model, c) equivalent BVD model with the inclusion of the ground inductance, d) resulting BVD model with the inclusion of the parasitic inductance.



Therefore, if we compare the frequency dependence between the original BVD impedance response Z_{BVD} (47) and the Z_T impedance response (49), corresponding to $BVD+L_{gnd}$, the differences will become more significant as long as we keep moving far from the frequency point that sets the equation (51) and also as long as the value of L_{gnd} increases.

From the circuit perspective, since L_2 , C_2 in Figure 35.b define the anti-resonance of the resonator and these are not modified, we know that even if we add a ground inductance, f_p will remain the same. This is consistent with the solutions obtained from the impedance expression (49). In addition, since we already set $f = f_s$ we assure the impedance will achieve the same value in both singular frequency points (f_s , f_p). Otherwise, for any other condition $f \neq f_s$, the near-out-of-band notch created by our shunt branch would appear at a location different from our prescribed transmission zeros.

Finally we will transform the circuit in Figure 35.c to the one in Figure 35.d obtaining thus a new BVD resonator in series with the calculated L_{gnd} .

The example we display in Figure 36 shows the performance of a 100 MHz lossless filter centered at 2.35 GHz by means of synthesizing a 7th order filter. The filter topology consists on a ladder network with four series resonators and three shunt resonators. This filter produces four transmission zeros at the upper side band at 2.4225 GHz and three transmission zeros at the lower side band at 2.2776 GHz. The initially synthesizes return losses are 18dB.

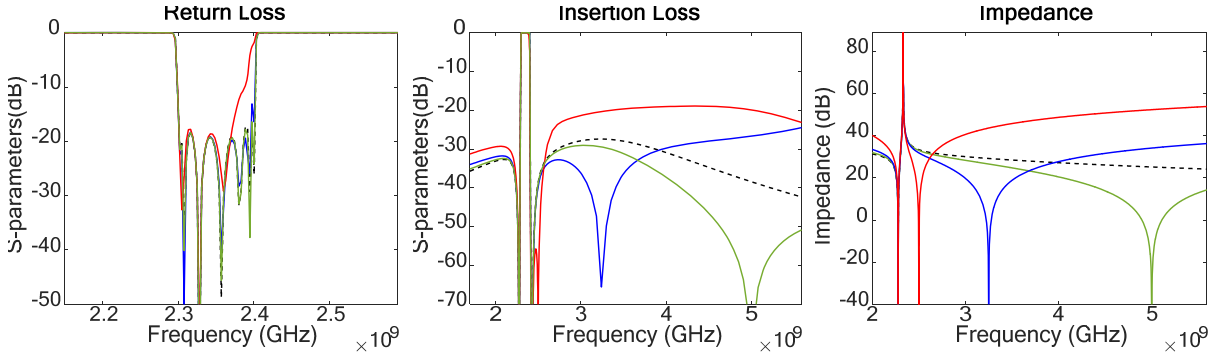


Figure 36. In-band transmission and reflection coefficient of a 7th order filter with the effects of a parasitic inductance.

Using this filter as an example, we evaluate the effects of having a ground inductance at only the first shunt resonator of the filter. We consider three different cases: 1) the effect of including an additional transmission zero very close to the passband, $f_{OoB_TZ} = 2.5$ GHz, 2) at an arbitrary intermediate frequency $f_{OoB_TZ} = 3.25$ GHz and 3) at $f_{OoB_TZ} = 4.5$ GHz, thus far from the passband. Once f_{OoB_TZ} is set we use (51) to solve (52) obtaining C_{33} and L_{gnd} . Results of these three cases are outlined in the Table 3 and Figure 36, where we can clearly identify the position of the additional transmission zeros, in red, blue and green, respectively. Dashed black lines depict the response of the resonator and the filter with no ground inductor whatsoever. Note that the position of the initial transmission zeros produced by the shunt branch at the lower band edge remains always the same as per the condition of (51) $f = f_s = 1/(2\pi\sqrt{L_s C_s})$.

Even though solution values for C_{33} are not relevant, they are shown in the Table 3 along with solution values for L_{gnd} and the other parameters involved in each step of the procedure. It is worth to pay attention to what is happening to the coupling value of this new BVD, $k_{e_new}^2$, due to these circuit transformations. Since the synthesized resonator is absorbing the ground inductance, it behaves as an equivalent resonator (defined by L_{ss} , C_{ss} , C_{pp}) with a much lower k_e^2 that makes use of the inductor to virtually increase its value up to the one achieved before the “absorption”. Now, our resonator is therefore very impractical in terms of feasibility. Fortunately, to counteract this situation the synthesis allows much flexibility to play with both, $f_s (=TZ_{lb})$ and f_{TZ_OoB} in order to reestablish a proper k_e^2 value.

	Figure 35.a)	Figure 35.b)	Figure 35.c)	Figure 35.d)
f_{OoB_TZ}	$k_e^2 = 5.53\%$, $f_s = 2.2776\text{GHz}$			
		$L_2 = 0.12\text{nH}$ $C_2 = 39\text{pF}$		
2.5GHz	$L_s = 58.07\text{nH}$ $C_s = 0.084\text{pF}$ $C_p = 1.77\text{pF}$	$C_3 = 1.85\text{pF}$	$C_{33} = 0.242\text{pF}$	$L_{ss} = 3.14\mu\text{H}$, $C_{ss} = 1.49\text{fF}$ $C_{pp} = 0.24\text{pF}$
			$L_{gnd} = 17.54\text{nH}$	
			$k_{e_new}^2 = 0.7596\%$, $f_{s_BVDnew} = 2.3239\text{GHz}$	
3.25GHz			$C_{33} = 0.9\text{pF}$	$L_{ss} = 0.235\mu\text{H}$, $C_{ss} = 0.02\text{pF}$ $C_{pp} = 0.88\text{pF}$
			$L_{gnd} = 2.79\text{nH}$	
			$k_{e_new}^2 = 2.79\%$, $f_{s_BVDnew} = 2.3046\text{GHz}$	
5GHz	$C_{33} = 1.45\text{pF}$	$L_{ss} = 92.9\text{nH}$, $C_{ss} = 0.05\text{pF}$ $C_{pp} = 1.4\text{pF}$		
	$L_{gnd} = 0.73\text{nH}$			
	$k_{e_new}^2 = 4.3834\%$, $f_{s_BVDnew} = 2.2889\text{GHz}$			

Table 3: Summary of the circuit parameters for the synthesis responses of Figure 36.

Figure 37 demonstrates that we can counteract the in-band degradation by means of relocating our transmission zero, TZ_{lb} to a new place and recover the initial coupling value. We run the example with the worst case scenario simulated before and set f_{TZ_OoB} at 2.5GHz.

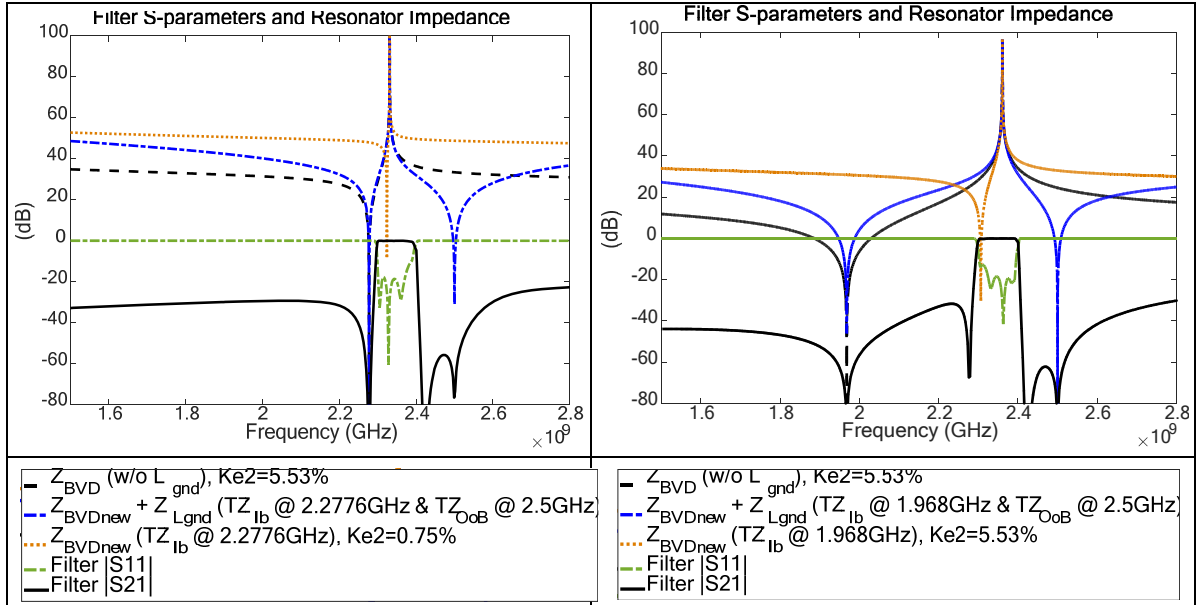


Figure 37: Filter response for two different location of the transmission zeros prescribed in the synthesis

In conclusion, the procedure outlined creates a new transmission zero integrating the ground inductor to the original BVD. It provides with very good results unless the selected f_{OoB_TZ} was very close to the passband, in which case, it may degrade the in-band response spoiling the return losses at the upper band edge. In addition, by inspection of (53) we can see that in order to keep fulfilling the equality, if we place f_{OoB_TZ} far from the band, L_{gnd} will be necessarily small.

$$L_{gnd} = \frac{1}{\frac{1}{L_2} - (2\pi f_{OoB_TZ})^2 C_2} + \frac{1}{(2\pi f_{OoB_TZ})^2 C_{33}} \quad (53)$$

Therefore, it is also clear that the closer we set f_{OoB_TZ} to the passband, the higher is the value of the ground inductor needed, and the lower is the k_e^2 of the resultant BVD (Figure 35.d).

This situation can be improved by changing the frequency value used to set (51). For this particular case, several different frequency values have been tested to this purpose as indicated in the legend of Figure 38. Differences on the in-band response can be observed. Note that this affects to the position of the transmission zero initially synthesized to 2.2776 GHz. These results foresee the idea of avoiding major degradation in the in-band frequency response and try to remark the flexibility provided by the synthesis.

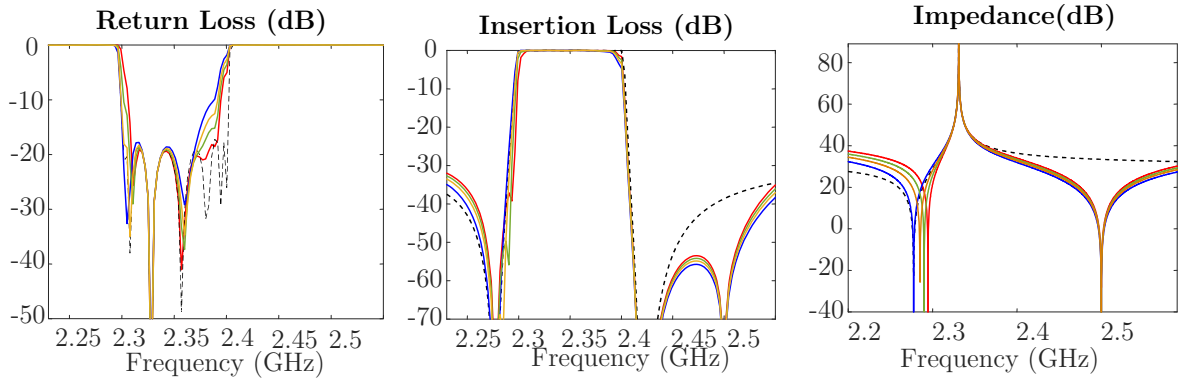


Figure 38. Transmission and reflection coefficient of a 7th order filter with the effects of including a ground inductor in the first shunt resonator. The additional transmission zero is fixed to 2.5 GHz.

2.7 General modeling of parasitic effects

The synthesis procedure presented in this chapter provides a quick extraction of a filter network that fulfills the system requirements. This fast procedure allows the integration of this method into a more complex system analysis that for instance accounts for the parasitic effects.

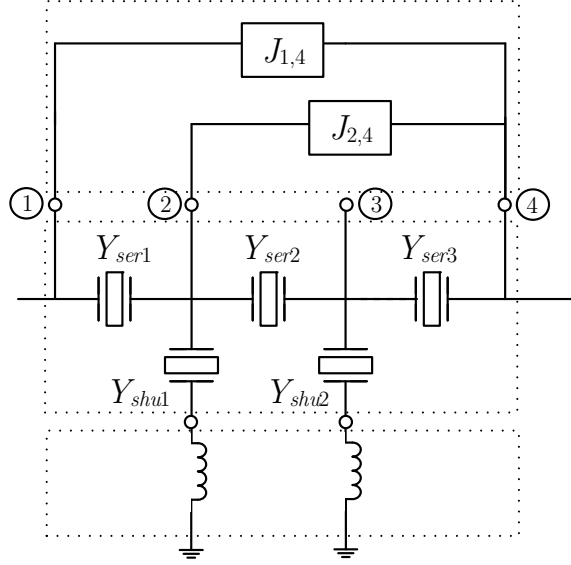


Figure 40. Ladder network of a 5-th order filter with parasitic cross couplings between nodes 1 and 4, and between nodes 2 and 4. Connections of the shunt resonators with the laminate have not been considered here.

By analogy to the general nodal admittance matrix above (54), and considering the different nodal definition of the example, we can write down the new matrix that describes the ladder network of Figure 40, without the inclusion of parasitic effects neither the ground inductors, as:

$$[Y] = \begin{bmatrix} -Y_{ser1} & -Y_{ser1} & 0 & 0 \\ -Y_{ser1} & Y_{ser1} + Y_{shu1} + Y_{ser2} & -Y_{ser2} & 0 \\ 0 & -Y_{ser2} & Y_{ser2} + Y_{shu2} + Y_{ser3} & -Y_{ser3} \\ 0 & 0 & -Y_{ser3} & -Y_{ser3} \end{bmatrix} \quad (55)$$

And a corresponding admittance matrix describing the parasitic network of Figure 40 like (56):

$$[Y_{parasitic}] = \begin{bmatrix} 0 & 0 & 0 & -jJ_{14} \\ 0 & 0 & 0 & -jJ_{24} \\ 0 & 0 & 0 & 0 \\ -jJ_{14} & -jJ_{24} & 0 & 0 \end{bmatrix} \quad (56)$$

Then both admittance matrix can be added together to evaluate the filter performance under the existence of parasitic effects, which are modeled as ideal frequency invariant admittance inverters:

$$[Y_{total}] = [Y] + [Y_{parasitic}] = \begin{bmatrix} -Y_{ser1} & -Y_{ser1} & 0 & -jJ_{14} \\ -Y_{ser1} & Y_{ser1} + Y_{shu1} + Y_{ser2} & -Y_{ser2} & -jJ_{24} \\ 0 & -Y_{ser2} & Y_{ser2} + Y_{shu2} + Y_{ser3} & -Y_{ser3} \\ -jJ_{14} & -jJ_{24} & -Y_{ser3} & -Y_{ser3} \end{bmatrix} \quad (57)$$

The approach above, which is based on conventional circuit analysis, is used to illustrate several cases. The first one consists in a 5th order lossless filter centered at 1.95 GHz, with 75 MHz bandwidth, and synthesized on its ladder configuration. In this case, only a cross coupling between the input and the output is evaluated by means of including an admittance inverter, J_{14} , as in Figure 40. The filter is evaluated for a -80 dB cross coupling. This effect is evaluated when the filter is synthesized for two different position of transmission zeros. Results for each of those cases are detailed in Figure 41.a and Figure 41.b, respectively. Blue line corresponds to the synthesized response and black line outlines the filter performance under parasitic effects. For these two cases the parasitic effects do not degrade the in-band response, this can be seen on the reflection coefficient (pink lines).

From this example, we can conclude that the effects of identical parasitic effects might be very different depending on the initial filter network. Under this consideration, it becomes very usefull to have a procedure that can directly evaluate the parasitic effects.

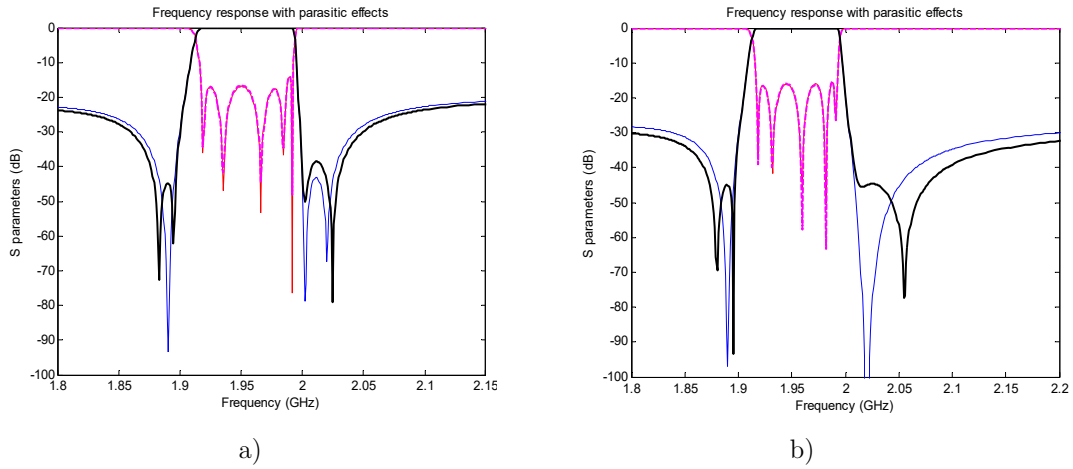


Figure 41. a) and b) Filter responses for different position of transmission zeros and the effects of a given parasitic network.

To further illustrate this capability, the following example considers a 7th order lossless filter evaluated under two different cross-couplings. Both cross-couplings are fix to -80dB. In one case, Figure 42.a, the parasitic cross coupling is set between node 1 (source) and 4 (just before the last series resonator). The other case, Figure 42.b, considers the cross-coupling between node 2 (just after the first series resonator) and node 4. As occurred in previous example the effects in the in-band are negligible, and these parasitic mainly affects the position of the transmission zeros. This example allows to conclude that the position of the cross-coupling, and

therefore the arrangement of the resonators on the chip, might be an important issue for the final filter response. Again, the ability to have a fast synthesis procedure might be very useful to determine in advance the most robust response to parasitic effects and help on the definition of the filter layout.

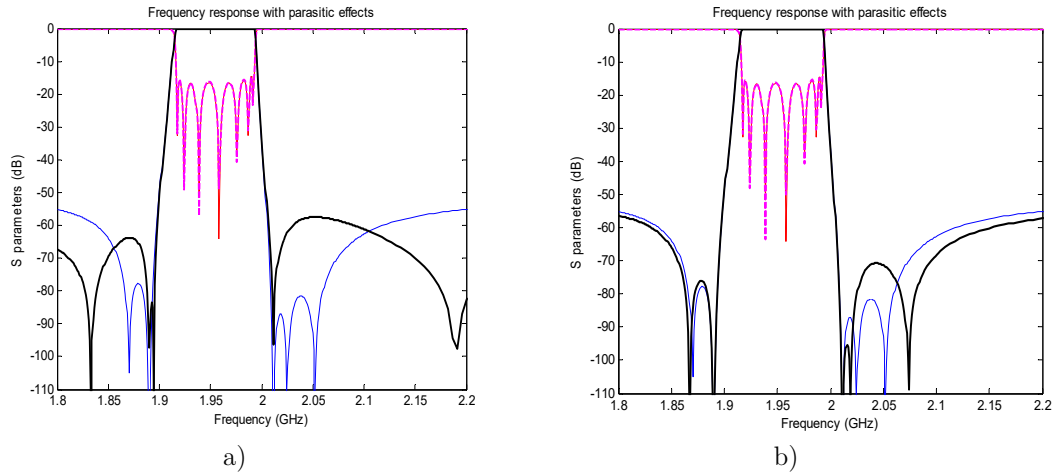


Figure 42. a) and b) Filter responses for different position of the parasitic cross-coupling.

The last example considers the filter above where now the parasitic cross coupling is set between nodes 2 (just after the first series resonator) and 3 (after the second series resonator). In this case two different values of cross-coupling are evaluated. Figure 43.a shows the effects when a -80 dB cross-coupling is inserted, and Figure 43.b when a -50 dB cross-coupling is inserted. In the first case the effects of the parasitic are negligible, whereas in the second case this affects both the in-band and out-of-band response. However, even in the latter case, the filter response is not much degraded, being therefore, this particular filter significantly robust to undesired parasitic effects (within the tested range of values) between nodes 2 and 3. This might conclude that those two resonators could be arranged physically close in the layout.

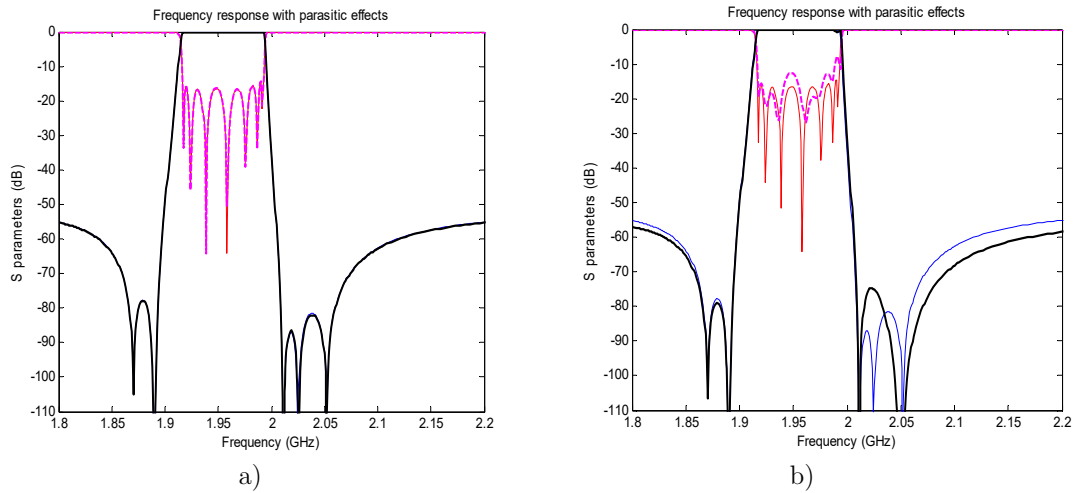


Figure 43. Filter performance for a) -80 dB cross-coupling, b) Filter performance for -50 dB cross-coupling.

2.8 Synthesis of a filter for the Band 40

The last section of this chapter presents the synthesis of a filter following real requirements. The result of the synthesized filter is then compared to the final manufactured filter. Both synthesized and implemented filters follow the same topology and with very similar values on their components. This example therefore validates the utility of the synthesis procedure as a tool to highly contribute in the process of acoustic filter development.

The filter requirements correspond to the receiver band 40, and are listed in the Table 4.

Frequency (MHz)	Min (dB)	Typ (dB)	Max (dB)	Parameter	Notes
2300 – 2400		-1.2	-1.8	S(2,1)	<i>Insertion Loss</i>
2300 – 2400	9.5			S(1,1) S(2,2)	<i>Return Loss</i> <i>(VSWR 2:1)</i>
1 – 2215	20				
2215 – 2240	10				
2240 – 2275	5			S(2,1)	<i>Out-of-Band</i>
2428 – 2471	30				<i>Attenuation</i>
2471 - 2481	30	40			
2481 - 12500	20				

Table 4. RX band 40 specifications.

To meet the specification above we propose the following filter parameters:

- Order: 7
- Bandwidth: 100 MHz
- Central frequency: 2350 MHz
- Return losses: 15 dB
- Transmission zeros at the upper band (4) in MHz: 2447, 2429, 2429, 2447
- Transmission zeros at the lower band (3) in MHz: 2266, 2266, 2266

The synthesis procedure is applied with these filter parameters. As mentioned in the synthesis procedure, even for a given input filter parameters, flexibility exists on the order in which the transmission zeros are extracted. For the current synthesis the extraction of the transmission zeros is performed as they are listed above. This results in the following network, whose circuit parameters are detailed in Table 5.

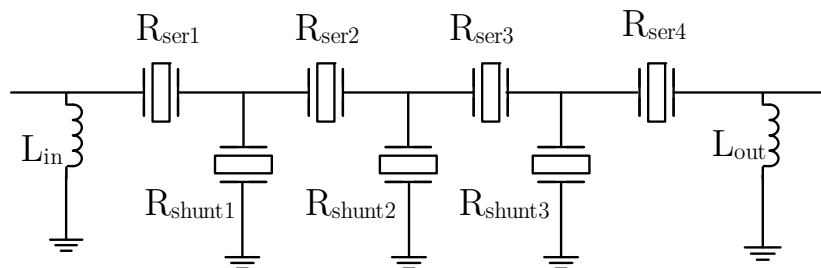


Figure 44. Filter network of the synthesized topology

Synthesized							
$L_{in}=L_{out}= 5.3$ nH							
	R_{ser1}	R_{ser2}	R_{ser3}	R_{ser4}	R_{shu1}	R_{shu2}	R_{shu3}
f_s (GHz)	2.3764	2.36	2.36	2.3464	2.266	2.266	2.266
f_p (GHz)	2.447	2.429	2.429	2.447	2.3404	2.3583	2.3404
k_e^2 (%)	6.9	6.8	6.8	6.9	7.5	9.27	7.5
C_p (pF)	1.18	1.01	1.01	1.18	2.75	2.95	2.75
Implementation							
$L_{in}=L_{out}= 4.3$ nH							
	R_{ser1}	R_{ser2}	R_{ser3}	R_{ser4}	R_{shu1}	R_{shu2}	R_{shu3}
f_s (GHz)	2.378	2.361	2.361	2.378	2.2815	2.268	2.2815
k_e^2 (%)	6.65	6.65	6.65	6.65	6.55	6.55	6.55
C_p (pF)	1.369	1.332	1.517	1.367	2.678	1.731	2.338

Table 5. Values of the circuit parameters corresponding to the synthesized and implemented values.

Note that although differences between the synthesized and implemented values exist, they are all very close, and most importantly they follow exactly the same topology. Note as well that in this initial synthesis we did not consider any implementation constrain, which certainly are taking into consideration along the design flow. Therefore, this concludes that the synthesis method can indeed be used at least as a first step in the design process.

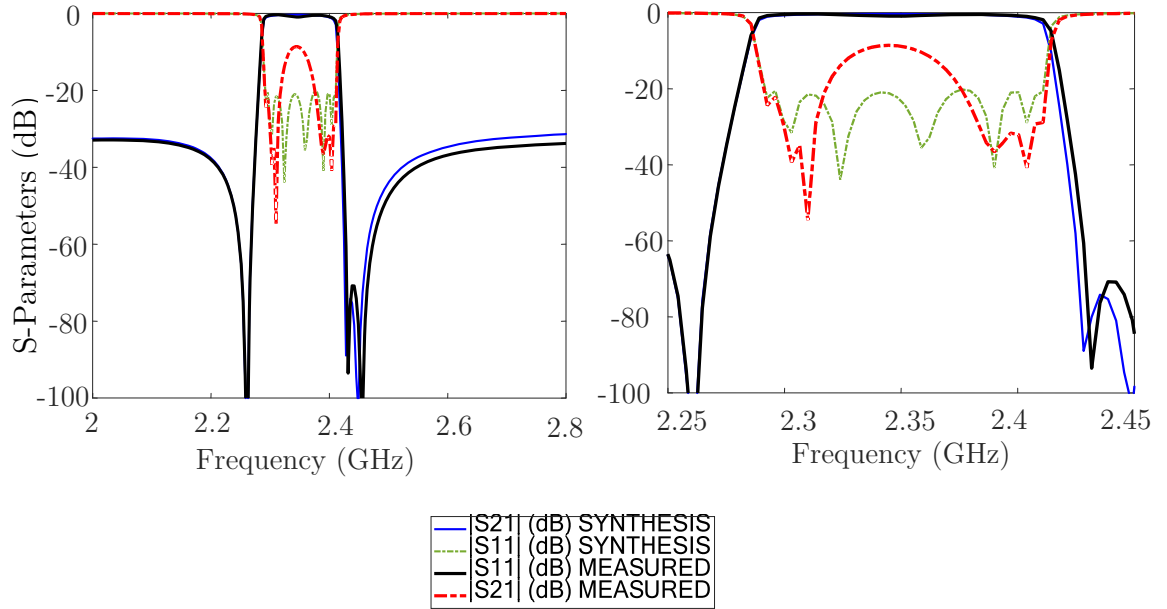


Figure 45. Measured and synthesized response of the B40 receiver band.

Figure 45 shows the frequency response of both the synthesized and the implemented filter, with details on the in-band flatness. Note that losses are considered in both cases, showing very good agreement in the in-band response. Black lines correspond the transmission and reflection coefficient of the implemented and measured filter, whereas blue and red correspond, respectively, to the transmission and reflection coefficient of the bandpass synthesized response.

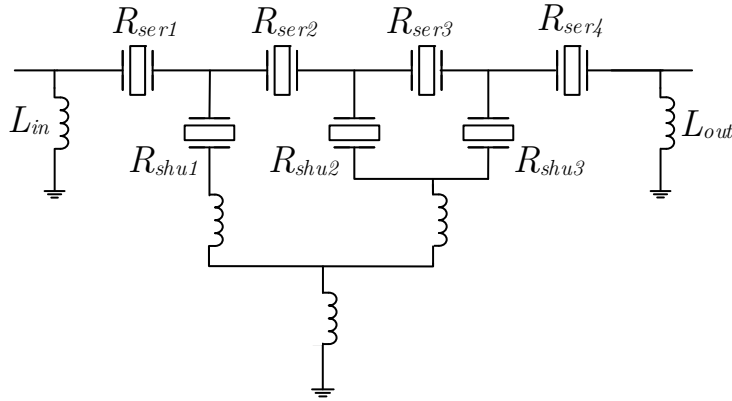


Figure 46. Overall filter network including the laminate representation with the ground inductors.

As outlined in the section 2.7, inclusion of parasitic effects can be easily performed by the description of the synthesized network as its nodal admittance matrix which can be then connected to the external parasitic network. To further illustrate this concept the following filter network shows the overall filter network including the parasitic effects. In this case, an inductive network to connect the shunt resonators to the ground, see Figure 46.

Using this overall filter network, Figure 47 shows the simulated S parameters of the simulated response in dashed blue, along with the measured response in solid black. Broadband measurements are also shown in this case. Note that by accounting for the parasitic effect, good agreement exist now at both in-band and out-of band response.

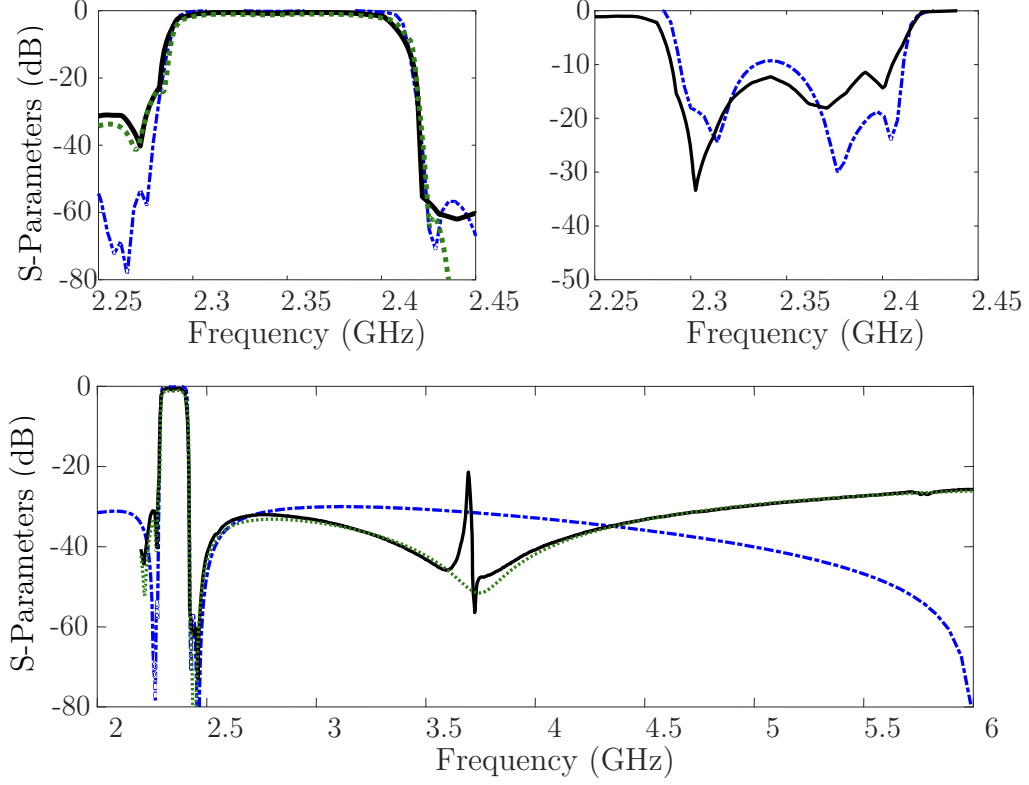


Figure 47. Simulated (blue) and measured (black) S-parameters. Top left figure: input reflection coefficient. Top right figure: output reflection coefficient. Bottom left figure: narrow band transmission coefficient. Bottom right figure: broadband transmission coefficient

2.9 Conclusions

This chapter described one of the major contributions of this thesis, this is the development of a synthesis procedure to obtain the very common ladder networks based on acoustic wave filters. At this point, it is worth to mention that no novelty has been applied for the synthesis procedure and we use the well-known element extraction approach. The novelty therefore relies on the identification of the characteristic polynomials that can later be implemented by means of ladder networks based on acoustic wave filters. Those polynomials are the general Chebyshev, where the number of transmission zeros is the same that the order of the filter. The location of those transmission zeros is not arbitrary in a ladder network and for an N order filter have to be distributed $N/2$ at each side, for N even, and $(N+1)/2$ and $(N-1)/2$, at each side respectively for an odd order filter.

The extraction procedure uses the lowpass prototype version of both the BVD model and the equivalent BVD model, presented in Chapter 1. Note that those lowpass prototypes are not pure equivalent to the bandpass prototypes but they are very valid to achieve the synthesized response in the band pass domain. Mention that these are also one of the artifacts properly chose on the development of this work.

Further practical considerations have been applied to move forward into a real implementation. In particular, the circuit transformation to obtain a network with series input and output impedance and the consideration of the always existing shunt inductors to ground.

The resulting synthesized network can then be used for the final design or as initial step to find out other networks by means of applying circuit transformations as the ones shown in this chapter. This is illustrated in the last section of this chapter with the design of a standalone filter at the B41 band.

All the procedures outlined in this chapter have been implemented into a software tool successfully applied to a several case studies, including duplexers, triplexers and quadplexers, all detailed in Chapter 4.

CHAPTER 3

DEVELOPMENT OF TRANSVERSAL FILTERS IN BAW TECHNOLOGY

This chapter details the development of the synthesis procedure to obtain acoustic wave filters based on a transversal configuration, this includes mathematical formulation, circuit transformations, considerations of practical issues and the definition of several step by step synthesis approaches. Finally, the synthesis procedure is used to synthesize advanced filtering responses, such as very wideband filters, filters with arbitrary position of transmission zeros and multiband filters.

It starts by outlining those mathematical details used on the synthesis procedure of conventional filters and required for the development of this new approach for acoustic filters. Then, we present, with full details, all the circuit transformations to go from the transversal conventional topology to the transversal topology based on acoustic wave resonators. These circuit transformations also include the required transformation to define the impedance and resonant frequencies forming the filter as the prescribed input variables of the designer. These later transformations give rise to several topologies for a given filter response, providing flexibility on the filter design.

The synthesis technique is used to demonstrate the ability of this approach to provide enhanced filter responses, in particular responses with very wide passband, with arbitrary position of transmission zeros and responses with multiband performance. Evaluation of its application into real stringent problems, as broadband frontend receivers and MIMO architectures will be presented in the case studies of chapter 4.

Further development of acoustic filters includes practical considerations on the realization of transversal topologies. In particular, this document evaluates the effect of the losses and the

sensitivity of the filter performance to the variation of the impedance and resonances of each resonator.

Practical considerations also assess the effect of having a non-ideal transformer. This is an additional circuit component required for these topologies as it will be shown in next sections.

3.1 Transversal Coupling Matrix. Conventional network

Before detailing the circuit transformation to develop transversal topologies based on acoustic wave resonators, this section recalls and extends part of the mathematical details shown in section 1.5. The initial 2-port scattering matrix of (1) was transformed into its counterpart 2-port admittance matrix (5). Below we recall (5):

$$[Y(s)] = \frac{1}{Y_d(s)} \begin{bmatrix} Y_{11n}(s) & Y_{12n}(s) \\ Y_{21n}(s) & Y_{22n}(s) \end{bmatrix} \quad (58)$$

Each rational term of the 2-port matrix is then expanded as (see section 1.5):

$$[Y(s)] = \frac{1}{Y_d(s)} \begin{bmatrix} Y_{11n}(s) & Y_{12n}(s) \\ Y_{21n}(s) & Y_{22n}(s) \end{bmatrix} = \sum_{k=1}^N \frac{1}{s - j\lambda_k} \begin{bmatrix} r_{11k} & r_{12k} \\ r_{21k} & r_{22k} \end{bmatrix} + j \begin{bmatrix} 0 & K \\ K & 0 \end{bmatrix} \quad (59)$$

In contrast with (8), (59) includes an additional 2x2 matrix, where the real term K is equal to zero, except for the fully canonical case, i.e., the number of finite transmission zeros, n_{fz} is equal to the order of the filter N .

The equation (59) reveals that any transfer function as in (58) results in a transversal network as indicated in Figure 48. The circles labeled with S and L , correspond to the source and load of the filter. The filled circles indicate a conventional resonator and the connecting lines correspond to the coupling between the resonators and the source or load. In Figure 48.b, a direct coupling from the source and load is required to generate $n_{fz}=N$.

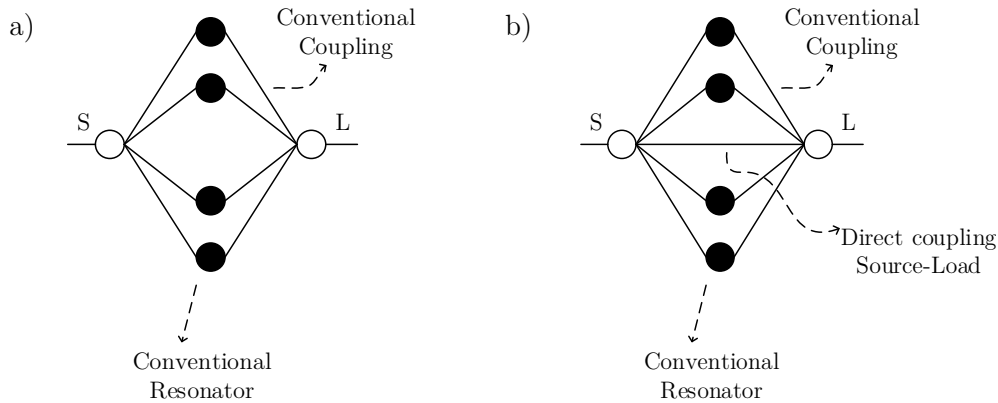


Figure 48. Outline of a transversal network, a) without direct source-load coupling, b) with direct source-load coupling.

A well-known significant conclusion is that **any transfer function can be synthesized as a transversal topology:**

- For any number of transmission zeros
- For complex transmission zeros (for instance in case of phase equalization)
- For any position of transmission zeros
- For multiband filter responses

Note that the features listed above are not compliant with a conventional ladder topology based on acoustic wave filter, where the number of transmission zeros is equal to the number of resonators and their positions are basically defined by the material coupling coefficient. Additionally, in a ladder acoustic wave filter topology the achievable bandwidth is limited by the coupling coefficient of the resonators and performing dual band, for not saying multiband, are not trivial.

3.2 Transformation to Transversal Topology Based on acoustic wave resonators

The following section describes the steps and circuit transformations applied to a transversal network as the one in Figure 48, to result in a network based on acoustic wave resonators.

Let start considering a single signal path, this is input port, coupling, resonator, coupling and output port, which would correspond to one branch of the outlined transversal network above. Details on the single signal path are in Figure 49.

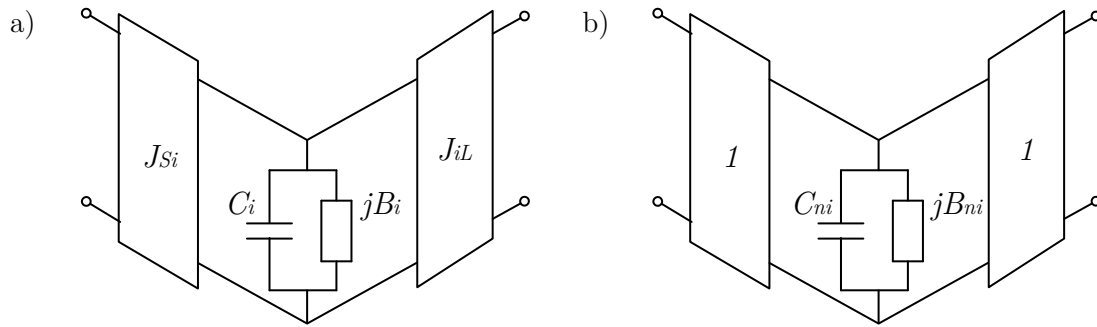


Figure 49. Single path of a conventional transversal network. a) non-normalized values, b) scaling transformation has been applied to obtain unitary coupling coefficients.

The values of J_{Si} , J_{iL} , C_i and B_i can be related to the values resulting in (59), (see (11), (12)). Note that J_{Si} and J_{iL} , correspond to the coupling from the source to the resonator and to the resonator to the load by means of an admittance inverter. C_i and B_i are the lowpass capacitance and frequency independent reactance, which set the lowpass resonant frequency of the corresponding branch.

In a general Chebyshev type response with equal input and output impedances, J_{Si} and J_{iL} are equal in magnitude and can differ only on 180 degrees on phase.

Scaling factors into the resulting coupling matrix, this is multiplying a given row and column by the same value, can be applied without affecting the final filter response. By doing this on each resonator node, the equivalent circuit of Figure 49.b is obtained, where the admittance transformers are set to 1 (or -1 in the case of a 180°).

For the sake of clarity, we present the concept of going from a conventional transversal topology (see Figure 48) to a transversal topology based on acoustic wave resonators, in a symmetric 2nd order filter without transmission zeros. In that case the initial conventional transversal topology would consist only on two branches without any direct coupling between the source and the load. Additionally, due to properties of the general Chebyshev polynomials, these two branches will be detailed as in Figure 50.

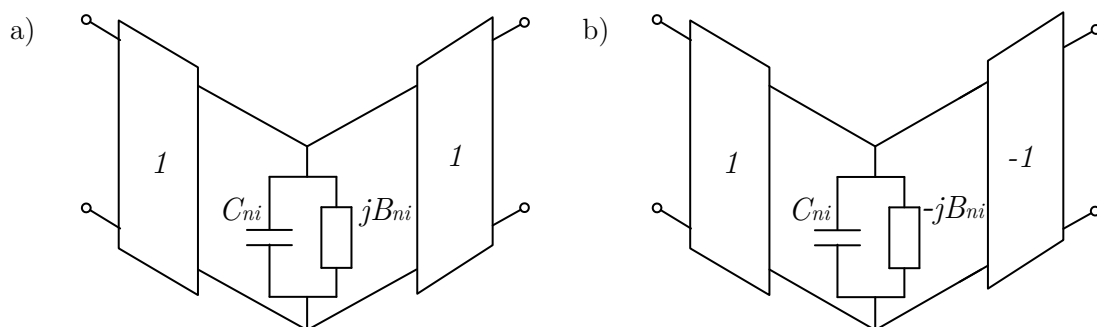


Figure 50. Outlined of the two paths existing in a 2-port filter with symmetric response and without transmission zeros.

Figure 50 reveals that in these conditions the impedance of the resonator of each branch (defined by C_{ni}) are equal, and the mutual couplings [27], defined by the shunt reactance term, are also equal in magnitude and have opposite phase. Figure 50 also shows that one of the inverters has opposite phase. It is worth to mention, that these conditions and properties fulfill, in path pairs, as long as the frequency response is symmetric, the order of the filter is even and the number of transmission zeros is lower that the order of the filter. For an odd order filter this also fulfills with an additional branch whose resonance frequency equals to the central frequency of the filter ($\Omega=0$, in the low pass prototype).

Taking therefore the branches of Figure 50, we can add at each branch an admittance inverter of opposite sing, without affecting the frequency response, as detailed in the figure below Figure 51. Note that, since the branches are connected in parallel they simply add, therefore cancelling the effect of the inserted inverters.

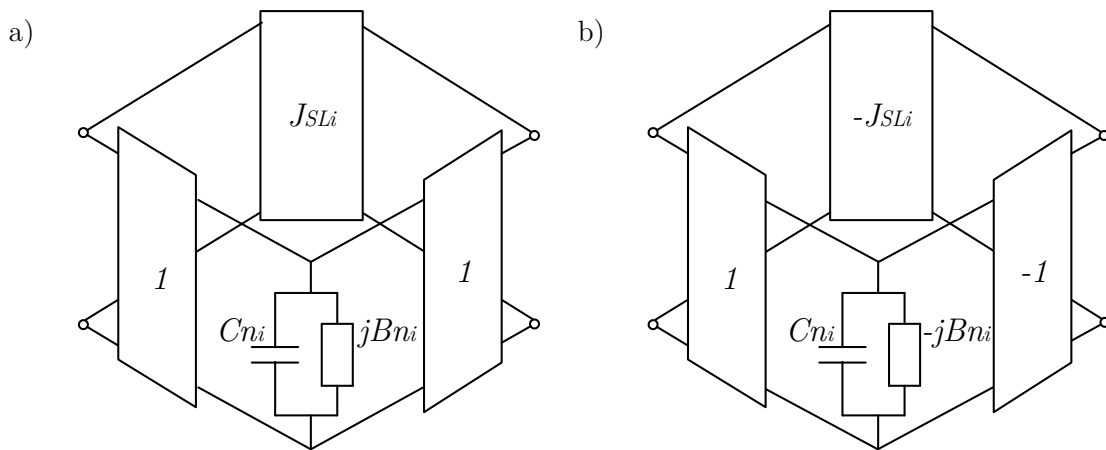


Figure 51. Outlined of the two paths existing in a two-port filter with symmetric response and without transmission zeros, with additional inverters included.

Each of the branches sketched in Figure 51 can be transformed into individual lowpass prototypes of acoustic resonators, detailed in Figure 15 in Chapter 1. Although detailed in [57], [25], below we outline this procedure.

The first step would consist on transforming the shunt admittance (defined by C_{ni} and B_{ni}) into series impedances (defined by L_{Si} and X_{Si}), where $L_{Si}=C_{ni}$ and $X_{Si}=B_{ni}$. The resulting circuits from such transformation are outlined in Figure 52. The term T, in the circuit of Figure 52.b corresponds to a transformer of -1 (or a phase shift of 180 degrees).

From Figure 52, and using the π -network circuit model defining an admittance inverter [27], is then straightforward to obtain the equivalent circuits of Figure 53. Details on such transformation can be found in Appendix 1.

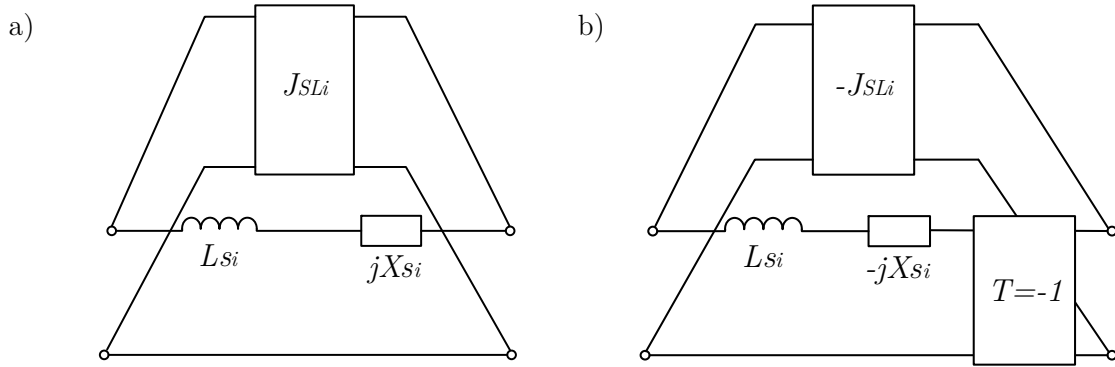


Figure 52. Outlined of the two paths, with additional inverters included, after initial transformation

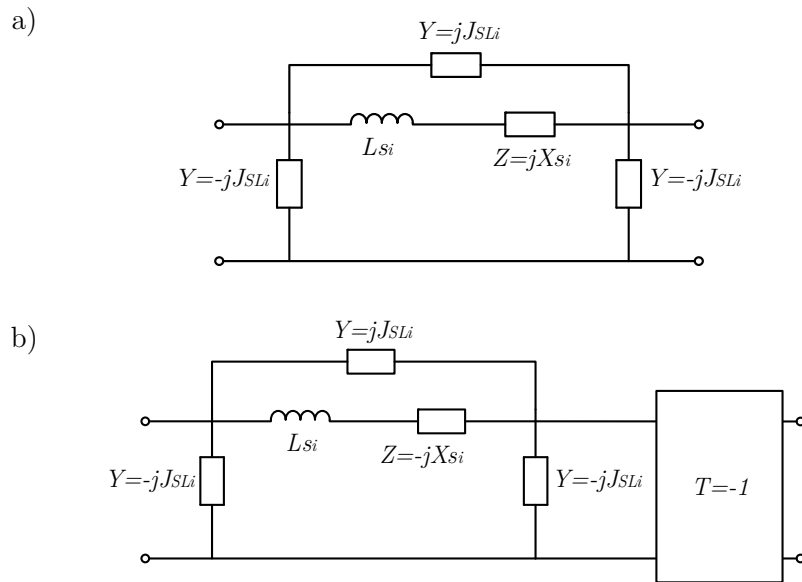


Figure 53. Outlined of the two paths, with additional inverters included, after initial transformation

For this particular case the two branches result on identical resonators, with the same electro-acoustic coupling coefficient and impedance, and they only differ on their resonant frequencies, which are distributed along the bandwidth.

The section above detailed the steps to go from a conventional transversal network based on single resonant frequency resonators into a transversal network based on acoustic wave resonators.

Note that in the procedure above no conditions have been set on the values of J_{SL_i} . This value can be arbitrary selected, as long as the summation of all new introduced admittance

inverters is zero, or equal to the initially defined by the synthesis (for the case of a canonical synthesis, Figure 48.b).

The section below details on how to select the proper inserted admittance inverter to obtain the desired coupling coefficient.

3.3 Procedure to extract the required cross coupling for a given coupling coefficient k_e^2 .

The process starts by recalling the lowpass prototype of a BVD model of Figure 15b, in Figure 54. Note that in this case we use a different notation on the circuit parameters to be consistent with the notation in section 3.2.

Below we reproduce part of the formulation in section 1.7.5, using the notation of Figure 54.

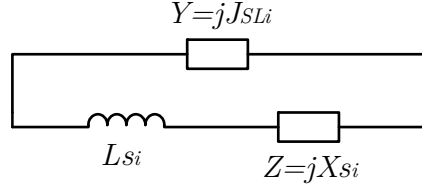


Figure 54. Lowpass prototype of the BVD model

From the circuit model we can identify the series resonant frequency, Ω_s , of the lowpass prototype when the impedance of the acoustic branch Z_s equals 0:

$$Z_s = j\Omega_s L_s + jX_s = 0 \quad (60)$$

From this, we can set the following relation between the acoustic inductance and the acoustic reactance:

$$X_{Si} = -\Omega_s L_{Si} \quad (61)$$

Now we can obtain the parallel resonant frequency, Ω_p , of the lowpass prototype when the admittance of the resonator Y_{BVD_LP} , equals 0

$$Y_{BVD_LP} = jJ_{SLi} + \frac{1}{j\Omega_p L_{Si} + jX_{Si}} = 0 \quad (62)$$

Now by substituting (61) into (62), results in the following relation:

$$J_{SLi} = \frac{-1}{(\Omega_s - \Omega_p)L_{Si}} \quad (63)$$

From the conventional frequency transformation lowpass-to-bandpass, we can also write down:

$$\begin{aligned} \Omega_s &= \frac{1}{\text{FBW}} \left(\frac{f_s}{f_0} - \frac{f_0}{f_s} \right) \\ \Omega_p &= \frac{1}{\text{FBW}} \left(\frac{f_p}{f_0} - \frac{f_0}{f_p} \right) \end{aligned} \quad (64)$$

and

$$\Omega_s - \Omega_p = \frac{1}{\text{FBW}} \left[\left(\frac{f_s}{f_0} - \frac{f_0}{f_s} \right) - \left(\frac{f_p}{f_0} - \frac{f_0}{f_p} \right) \right] \quad (65)$$

which can be re-written as:

$$\Omega_s - \Omega_p = \frac{1}{\text{FBW}} \left(\frac{f_s - f_p}{f_0} - \frac{f_0 f_p - f_0 f_s}{f_s f_p} \right) = \frac{2}{\text{FBW}} \left(\frac{f_s - f_p}{f_0} \right) \quad (66)$$

where we have considered that $f_0 = \sqrt{f_s f_p}$, and then $\frac{f_0 f_p - f_0 f_s}{f_s f_p} = \frac{f_p - f_s}{f_0}$.

Now, from the expression of the coupling coefficient k_e^2 [53] (also in (19)), $\frac{f_s}{f_p} \cong 1 - \frac{4}{\pi^2} k_e^2 (1 + \frac{4}{\pi^2} k_e^2)$, we can obtain the following relation:

$$\frac{f_p - f_s}{f_p} \cong \frac{4}{\pi^2} k_e^2 \left(1 + \frac{4}{\pi^2} k_e^2 \right) \quad (67)$$

which can be approximated, as:

$$\frac{f_p - f_s}{f_0} \cong \frac{4}{\pi^2} k_e^2 \left(1 + \frac{4}{\pi^2} k_e^2 \right) \quad (68)$$

[REDACTED]

[REDACTED]

[REDACTED]

[REDACTED]

[REDACTED]

3.4 From lowpass prototype to bandpass prototype

To evaluate the practical values of the resulting filters, we need to apply frequency and element transformation to go from the lowpass prototype to the bandpass prototype.

[REDACTED]

[REDACTED]

[REDACTED]



$$\frac{C_p}{C_s} = \frac{1}{\left(1 - \frac{4}{\pi^2} k 2e \left(1 + \frac{4}{\pi^2} k 2e\right)\right)^{-2} - 1} = k \quad (78)$$

We call this value k , and it will be extensively used on the design procedures defined above. Note that k is constant for a given value of coupling coefficient (for a certain operation frequency). From (78), we may conclude that the ratio between the static and acoustic capacitances is fixed by the synthesis value and the prescribed coupling coefficient k_e^2 .

For values of $k_e^2 \approx 6.8\%$ we would obtain $\frac{C_p}{C_s} \approx 17$, no matter the fractional bandwidth of the filter. Equation (78) also indicates that the ratio C_p/C_s would increase for smaller k_e^2 . This is illustrated in Figure 55, below.

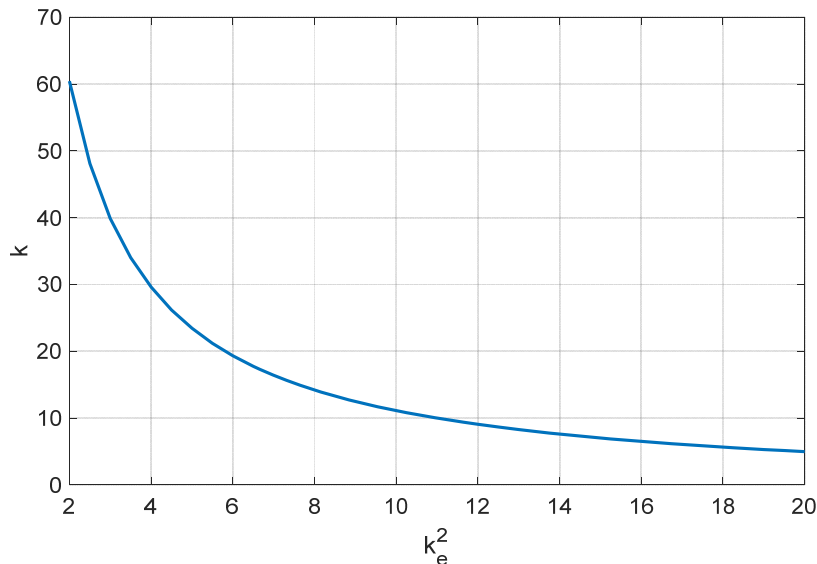


Figure 55. Value of k as a function of k_e^2

Once all the circuit parameters of the BVD model of the acoustic wave resonators are fixed, its impedance is also defined. Following the conventional definition [53] and using the transformation from lowpass prototype and pass band prototype the resulting impedance might be written as:

$$Z_0 = \frac{1}{\omega_s \cdot (C_p + C_s)} = \frac{L_{Si}}{FBW(k+1)} \quad (79)$$

This expression reveals that the resulting impedance of each resonator is defined by the synthesized lowpass values, L_{Si} (so the characteristic polynomials), the prescribed coupling coefficient (which is related with k) and the fractional bandwidth of the filter FBW .

The formulation described in this section might be used to provide a transversal topology based on acoustic wave resonators, for a given prescribed k_e^2 coefficient. This allows to conclude that a transversal topology based on acoustic wave resonators might be used to obtain:

- The filter bandwidth is not limited by the k_e^2 of the resonators
- The k_e^2 could be prescribed by the designer
- The filter transmission zeros are not defined by f_s or f_p of the resonators
- It is possible to place transmission zeros from the filter bandwidth without the need of including additional inductances
- The number of transmission zeros might be different than the number of acoustic resonators
- It is possible to synthesize any transfer function:
 - Multiband responses
 - Responses with equalization zeros

The resulting figure configuration would be:

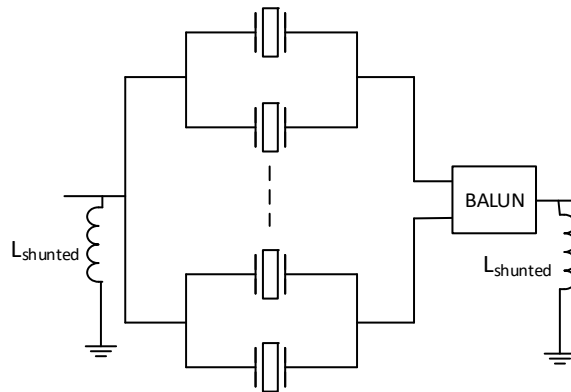


Figure 56. Transversal filter topology based on acoustic wave resonators.

The topology of Figure 56 shows the need of including a BALUN at the output (or input) of the filter to account for the desired 180 phase shift required in some branches (see Figure 53.b). Figure 53 also reveals the need of having shunt reactive elements at the input and at the output, which results in shunt inductances ($L_{shunted}$) at the input and output ports of the filter, as we will see in the following sections.

In spite of the significant advantages of this procedure over the conventional ladder designs we would also mention the potential drawbacks:

- Need of including a BALUN/Transformer at the input or output of the filter.
- The resulting values of the resonators (L_s , C_s and C_p) are in part defined by the initially synthesized parameters, L_{S_i} and X_{S_i} . This results in very high impedance resonators. This statement will be illustrated in the following example.
- The series frequency f_s of the resonators are all different.

Following, the procedure outlined for the synthesis of transversal configurations based on AW resonators is presented along with a particular example.

3.5 Synthesis and Design procedure: Approach I. Prescribed k_e^2 .

The synthesis procedure of this approach corresponds to the case where the designer has full control to prescribe the coupling coefficient of each individual resonator forming the transversal topology of Figure 56. At the same time no control over some other important parameters from the implementation point of view, such as the resonant frequency and impedance of the resonators, exists. We name this initial approach as Approach I, whose most significant steps can be read as:

1. Apply a conventional synthesis procedure - as outlined in (1), (58) and (59) to a general Chebyshev type response, to obtain a conventional transversal network, see Figure 48.
2. Add the additional cross coupling J_{SLi} at each branch following the expression (70)
3. Apply circuit transformation on the branches (Figure 51), to obtain the equivalent circuit of Figure 53 for each branch. This is L_{Si} and X_{Si} for each resonator, along with J_{SLi}
4. Apply element and frequency transformation from lowpass to bandpass following the set of equations (71)-(76), in order to obtain L_s , C_s and C_p for each resonator.
5. To obtain a good in-band matched response, each transversal branch would need to introduce, at the input and at the output, a shunt inductance of $L_{shunted_i} = \frac{1}{2\pi f_{oi} C_{p_i}}$, where f_{oi} is the frequency of the corresponding branch, and C_{p_i} is the C_p value of the branch. The overall shunt inductance $L_{shunted}$ results from the shunt connection of all the individual inductances.

At this point, it is worth to mention that the characteristic impedance of each resonator is defined by (79), and that for typical values of FBW, and a coupling coefficient of 6.8% result in resonators with very high impedance, thus resonators very small in size, which might not be convenient for practical implementation.

3.5.1 Example: Approach I

The following example corresponds to a 6th order filter with 100 MHz bandwidth and centered at 2 GHz. The filter frequency responses are detailed in Figure 57a. Red and blue lines correspond, respectively, to the transmission and reflection coefficients described by the characteristic polynomials, whereas in dash black and green, the transmission and reflection coefficients of the resulting topology are shown. Note that both responses are in very good agreement. The filter response exhibits four transmission zeros, two at the upper band and two at the lower band. The normalized location of the transmission zeros are: $j1.56$, $j1.66$, $-j1.6$, $-j1.71$. Figure 57b shows the impedance of each individual resonator. This figure allow to observe that all resonators have the same coupling coefficient, but different impedances and resonant frequencies.

The resulting characteristic impedances in this particular case are: 697Ω , 320Ω , 231Ω , 229Ω , 310Ω , and 667Ω , respectively, which as previously state gives rise to impractical small resonators.

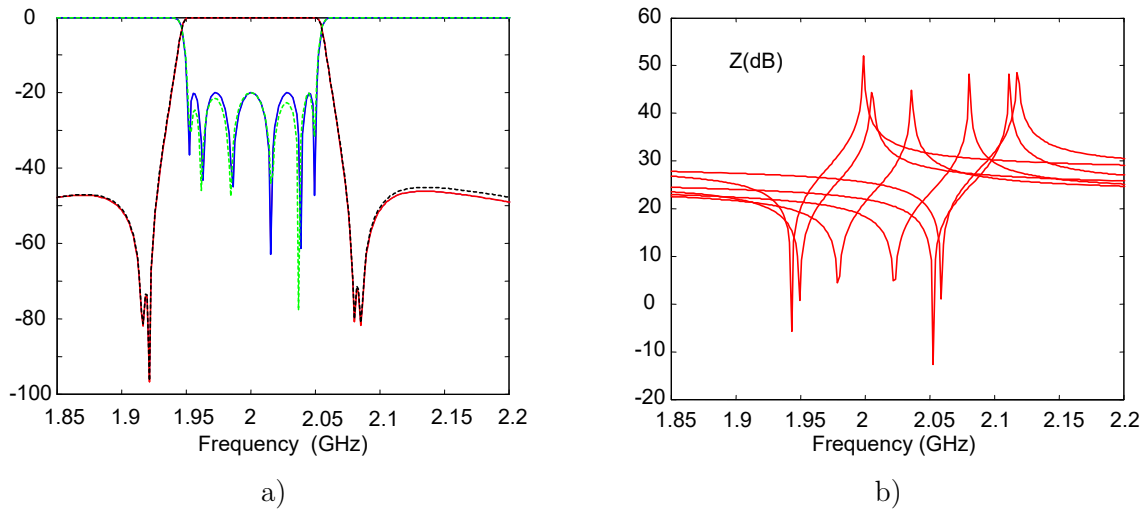
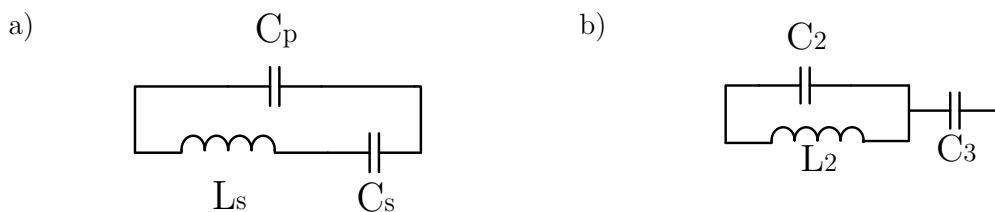


Figure 57. a) Filter response, b) impedance of each individual resonator.

This example unveils the necessity of controlling the impedance of the acoustic resonators, this is therefore the area of the resonator, and the series resonant frequency. Additional flexibility will be added into the design procedure in the following sections.

3.6 Flexible Approaches

In order to obtain more suitable acoustic resonators to be used in the transversal topologies, we introduce further flexibility on the selection of their characteristic parameters. To do that we start by taking the BVD model of an AW resonator, Figure 58a, and we transform it to its equivalent circuit depicted in Figure 58.b (see section 1.7.3). The values of the circuit elements of Figure 58.b, C_2 , L_2 and C_3 , are defined from the initial values of the BVD, C_s , L_s and C_p , as outlined in (20):



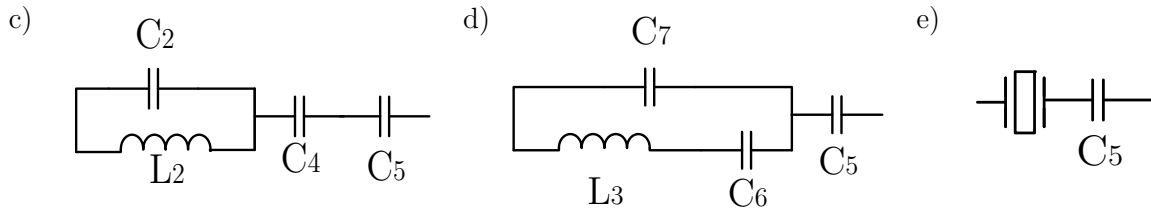


Figure 58. a) BVD circuit, b) equivalent BVD circuit, c) equivalent BVD circuit by splitting the C_3 component, d) transformation from the equivalent BVD (C_2 , L_2 , C_4) to the BVD, L_3 , C_6 , C_7 , with a series capacitance C_5 . e) BVD with a series capacitance BVD.



Now, by substituting (20) and (80) into (81), we obtain:

[REDACTED]

At this point, it is worth to mention that the f_s frequency of the initial BVD model (Figure 58.a) is defined by L_s and C_s , whereas the f_s frequency of the resulting BVD model is defined by L_3 and C_6 (Figure 58.d). Therefore, the new BVD has a different f_s . On the other hand, the f_p of the initial BVD is defined by L_2 and C_2 , (Figure 58.b), and the f_p of the new BVD is also defined by L_2 and C_2 , (Figure 58.c), so the new BVD has the same f_p that the initially synthesized resonator. And also recall here that the f_p of each resonator can be selected by the designer by the inclusion of J_{SLi} , see Section 3.2, providing therefore the required flexibility for the filter design.

In order to take advantage of the flexibility resulting from the transformation above, we continue reformulating the equations above in order to define practical designing parameters.

[REDACTED]

[REDACTED]





The formulation developed in this section, relates the values of the initially synthesized filter values with the values of the new resonators and their parameters. Using therefore the set of relations in this section, following we present a new synthesis procedure approach.

By following the above transformations, the resulting filter topology of Figure 56, will be modified to the new filter topology outlined in Figure 59.

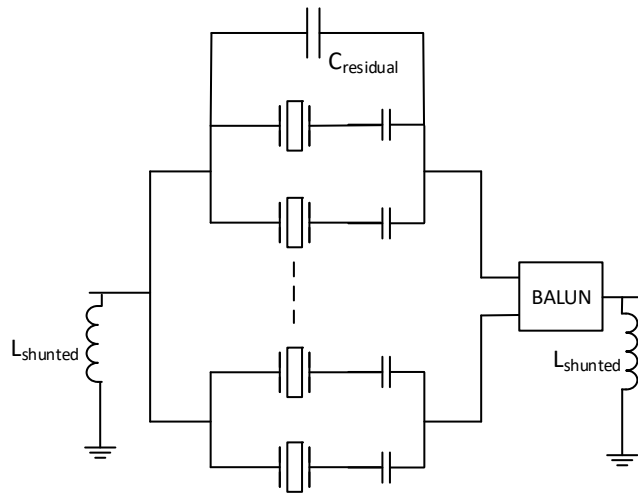


Figure 59. Transversal filter topology based on acoustic BAW resonators, after the transformation outlined in this section.

In addition to the direct transformation from Figure 58.a to Figure 58.e, the resulting topology of Figure 59 also exhibits an additional capacitance transversal to all the resonators. Existence of this capacitance is not always required and its value would depend on the synthesized network. Details on that will be found in the following section. We will call this capacitance as residual capacitances, $C_{residual}$:


3.7 Synthesis Procedure: Approach II. Prescribed Impedance.

The following approach uses the formulation in previous section to transform from the equivalent circuit of Figure 58.a to the equivalent circuit of Figure 58.d, where the coupling of each resonators and their impedances, a therefore size of the resonator are set by the filter designer.

The steps for the corresponding approach are:

1. Apply a conventional synthesis procedure - as outlined in (1), (58) and (59) to a general Chebyshev type response, to obtain a conventional transversal network, see Figure 48.
2. Apply circuit transformation on Figure 51, branches, to obtain the equivalent circuit of Figure 53 for each branch. This is L_{S_i} and X_{S_i} for each resonator.
3. Apply element and frequency transformation from lowpass to bandpass following the set of equations (71)-(76), in order to obtain L_s , C_s , for each resonator.
4. Set the desired impedance of each resonator through equation (94), and the desired coupling (recall that it is related with the k_l value (usually $k_l=17$, for $k_e^2=6.8\%$), see

equation (78) from equation (88). This defines a set of two equations (94) and (88) and two unknowns C_6 and C_7


$$(101)$$

where

$$\bullet \tag{102}$$

7. The last step is to calculate the residual capacitances $C_{residual}$, if any. The procedure is defined on the following steps:
- a. Calculate the value of C_p , Figure 58.a, that would be needed in case of the synthesis Approach I:
 - i. \bullet



$$\tag{104}$$

- b. From the initial values of C_p , we can calculate the required value of the matching inductances $L_{shunted}$ by following step 5 of the procedure described in section 3.5.
- c. From the initial, conventional synthesized network, it is clear that the summation of all C_p of one branch of the BALUN, should compensate all the C_p on the other branch of the BALUN. If this is not happening we need to include some additional capacitance ($C_{residual}$) in one of the branches, to perfectly match the synthesized response.

Note as well, that since this additional $C_{residual}$ is introduced in the lowpass prototype, as a π -network admittance inverter from the source to the load additional shunt inductors should be added at the input and output ports. We call these inductances as residual inductances, $L_{residual}$. This value can be directly calculated as:

$$L_{residual} = \frac{1}{2\pi f_0 C_{residual}} \tag{105}$$

which is shunt connected to $L_{shunted}$.

Strictly speaking only, a $C_{residual}$ is required in one of the branches, nevertheless in practical application, having additional capacitances at each

branch might help to compensate the out-of-band performance. Details of that will be seen along the examples shown at the end of this document.

3.7.1 Example Approach II

The following example synthesizes the same frequency response that has been synthesized on the synthesis Approach I. The filter frequency responses are detailed in Figure 60.a. Red and blue correspond to the filter response described by the characteristic polynomials, whereas in thick dash blue and red, it is shown the response of the resulting filter topology. Note that both responses are in very good agreement. Figure 60.b shows the impedance of each individual resonator. This figure reveals that all resonators have the same coupling coefficient (6.8%) and also the same impedance. In this example the impedance of each resonator has been set to 60Ω . Can also be observed that the f_s of each resonator are different.

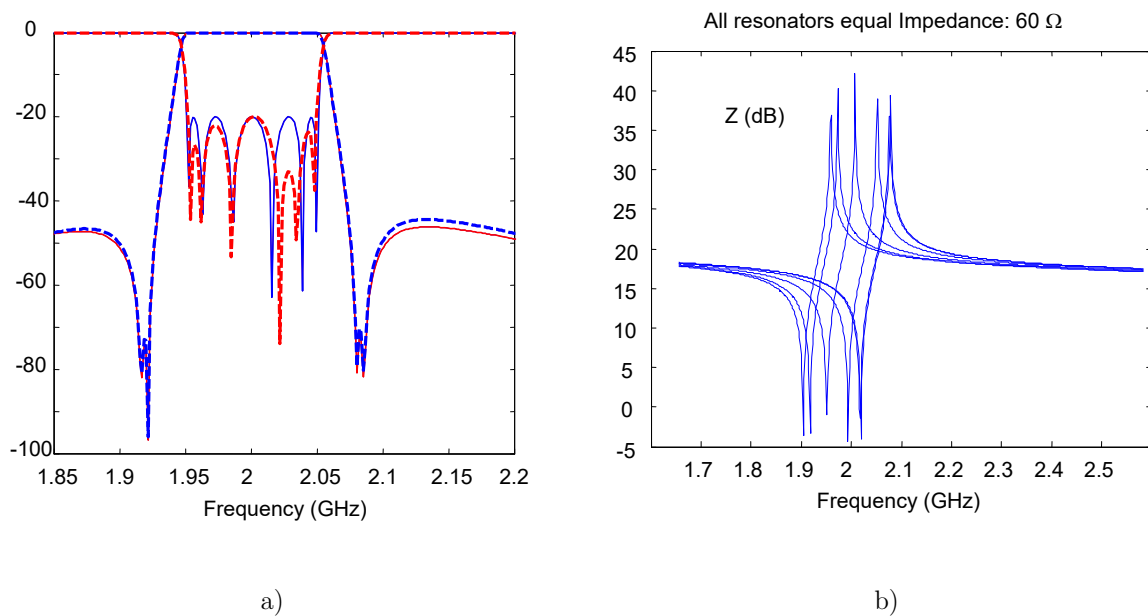


Figure 60. a) Filter response, b) impedance of each individual resonator.

3.8 Synthesis Procedure Approach III. Prescribed Resonant Frequency.

The following approach also uses the formulation in Section 3.6 to transform from the equivalent circuit of Figure 58.a to the equivalent circuit of Figure 58.d, where the coupling of each resonator and its series resonant frequency is set by the filter designer.

At this point, it is worth to mention that a single resonant frequency for all the resonators is not possible (otherwise it would need a very wide range of impedances) when the filter needs to cover a wide passband. In that case, a set or groups of several series resonant frequencies will be selected.

To clearly explain the process, we will start by considering a unique resonant frequency, which will be referred as Approach III.1. Then, we will extend this method to consider several groups of resonant frequencies, which will be referred as Approach III.2. Note that this latter approach is very oriented to a practical implementation.

3.8.1 Approach III.1

1. Apply a conventional synthesis procedure - as outlined in (1), (58) and (59) to a general Chebyshev type response, to obtain a conventional transversal network, see Figure 48.
2. Apply circuit transformation on Figure 51 (branches) to obtain the equivalent circuit of Figure 53 for each branch. This is L_{S_i} and X_{S_i} for each resonator.
3. Apply element and frequency transformation from lowpass to bandpass following the set of equations (71)-(76), in order to obtain L_s , C_s , for each resonator.
4. Select the desired resonant frequency f_s of all resonators. Note that the configuration of the new BVD (Figure 58.d,e) only allows to move the initial resonant frequency – set by the initially synthesized L_s and C_s – to lower frequency. For that reason, a good practical application is to take as a desired f_s the lowest one ($f_{s_{min}}$) of the already synthesized resonators.

$$f_{s_{min}} = \frac{1}{2\pi\sqrt{C_s L_s}} \quad (106)$$

5. Since all resonators would have the same $f_s = f_{s_{min}}$, and we want all resonators to have the same coupling coefficient – namely 6.8% or other set by the designer-, so a given value of k_i , all resonators also need to have equal f_p . The value of the desired f_p can be found from:

$$f_p = f_{s_{min}} \sqrt{\frac{1+k_1}{k_1}} \quad (107)$$

6. Recall here that f_p cannot be changed from equivalent circuit of Figure 58.a to the equivalent circuit of Figure 58.d,e. So that the f_p of each resonator should be set on the initial step, Figure 58.a. To do that we can obtain the coupling set on Figure 58.a circuit, by:

$$k = \frac{1}{\left(\frac{f_s}{f_p}\right)^2 - 1} \quad (108)$$

Where f_s is the one defined by C_s and L_s and f_p is equal for all resonators (107). Note that the resulting k values are all different.

7. Now k is used to find the C_p values of each resonator, and the designing parameter α as:

$$(109)$$

At this point, we have all the information to find the values of the new resonators, this is C_6 , C_7 , L_3 and C_5 .

8. From the initial values of C_p , we can calculate the required value of the matching inductances $L_{shunted}$ by following step 5 of the procedure described in section 3.5.
9. As in previous case some additional $C_{residual}$ and $L_{residual}$ values might be required to completely match the synthesized response. To do that we need to perform step 7 of Approach II.

3.8.2 Approach III.2

The first three - 1), 2) and 3) - steps are equals to the ones in Approach III.1.

4. Then several frequencies f_s are selected. In practice, a good choice is to select the targeted frequencies from the synthesized ones, as in (106), resulting in $f_{s_{min},1}$, $f_{s_{min},2}$, ..., $f_{s_{min},N}$.
5. Then each resonator with an f_s , initially synthesized, between $f_{s_{min},I}$ and $f_{s_{min},I+1}$, has been modified using steps 5-9, in Approach III.1, to have a $f_s = f_{s_{min},I}$.

3.8.3 Example Approach III.1

The following example synthesizes the same frequency response that has been synthesized on the synthesis Approaches I and II. The filter frequency responses are detailed in Figure 61.a. Red and blue correspond to the filter response described by the characteristic polynomials, whereas in thick dash black and magenta is shown the response of the resulting filter topology. Note that both responses are in very good agreement. Figure 61.b shows the impedance of each individual resonator. This figure reveals that all resonators have the same coupling coefficient (6.8%) and also the same resonant frequencies. It is important to notice here that the values of the impedances of the resonators are very different, and might result in a very impractical implementation.

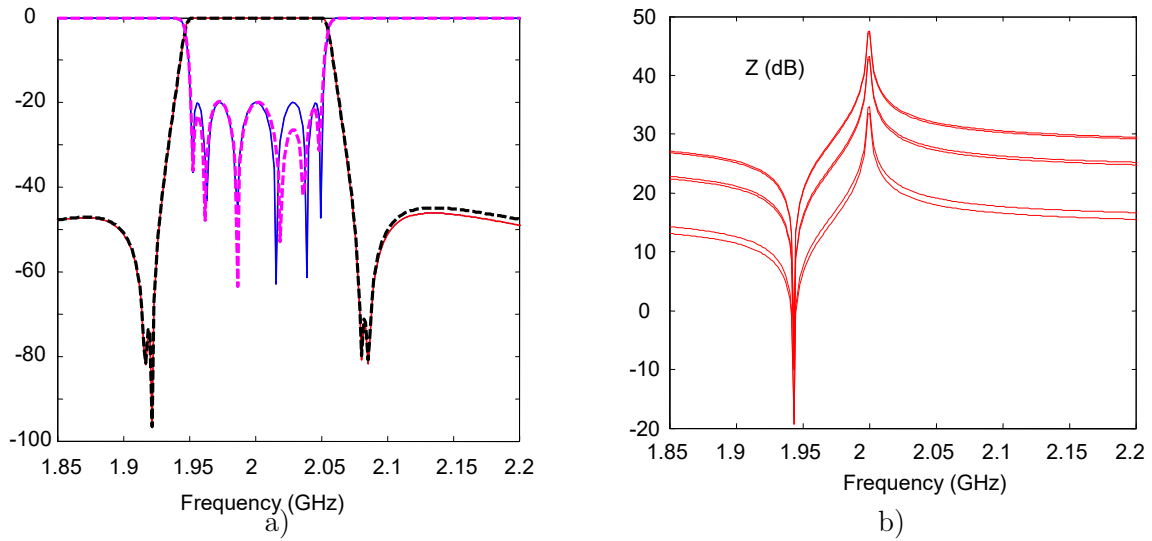


Figure 61. a) Filter response, b) impedance of each individual resonator.

3.8.4 Example Approach III.2

The following example synthesizes a filter response with wider bandwidth, 150 MHz of bandwidth instead of 100 MHz, by means of a 8th order filter. The normalized positions of the transmission zeros are maintained. The filter frequency responses are detailed in Figure 62.a. Red and blue correspond to the filter response described by the characteristic polynomials, whereas in thick dash green and cyan is shown the response of the resulting filter topology. Note that both responses are in very good agreement. Figure 62.b shows the impedance of each individual resonator. Results in Figure 62.b reveals that all resonators have the same coupling coefficient (6.8%) and the resonant frequencies correspond to a prescribed set.

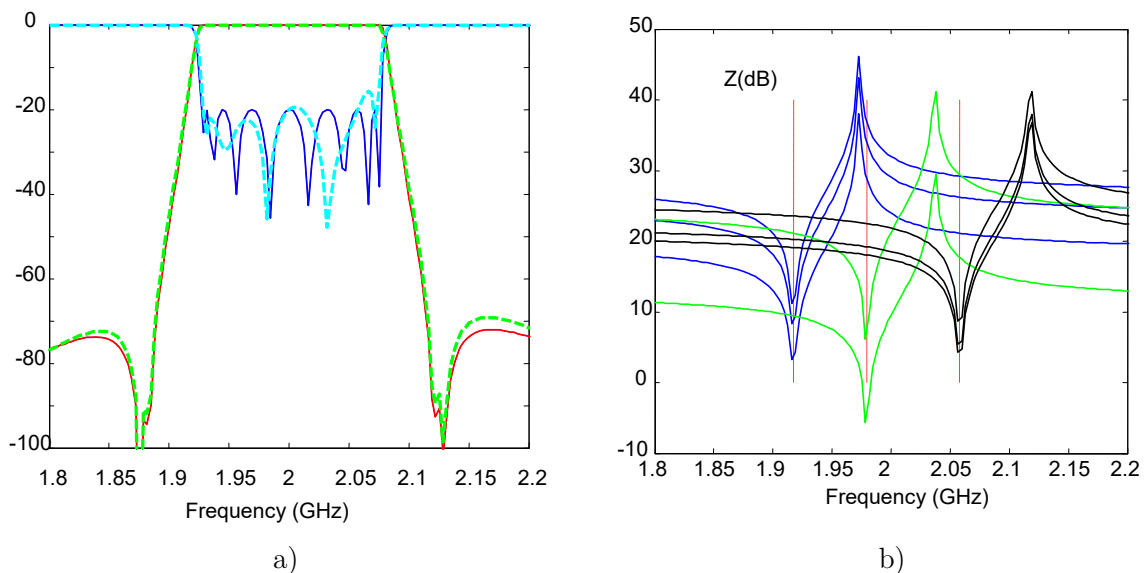


Figure 62. a) Filter response, b) impedance of each individual resonator.

3.9 Synthesis Procedure: Approach IV. Trade-off.

The following synthesis approach takes advantage of the two latter approaches presented on section 3.7 and 3.8, by using the flexibility of the formulation above (section 3.6) to have control on the impedance of the resonators forming the filter as well as on the resonant frequency of the resonators.

Note that in for practical purposes regarding manufacturing viability a designer would aim to find a solution with all resonators impedances (or sizes) within a certain range. Same happens with the set of different resonant frequencies which must be limited to a finite number (usually no more than 4 or 6).

To illustrate this approach, we will use the 100 MHz 6th order filter example evaluated in previous sections. The process outlines as:

- 1) Propose a range of suitable impedances
 - a) For the current example we select a range between 20Ω and 120Ω .

- 2) For each resonator of the filter we evaluate the corresponding resonant frequency for the whole range of impedances. This uses the formulation of Approach II, and obtains f_s for each impedance.
 - a) Figure 63, shows the f_s as a function of the prescribed impedance for each resonators.
 - b) Four families of f_s frequencies have been defined, $f_{s,1}$, $f_{s,2}$, $f_{s,3}$ and $f_{s,4}$.
- 3) From the selected resonant frequency families we obtain the required impedance of each resonator.
 - a) In this case the selected impedances are: 115 Ω , 35 Ω , 60 Ω , 60 Ω , 50 Ω and 50 Ω .
 - b) Note that a lot of flexibility would exist on families 2, 3 and 4 on the selection of the desired impedances.
- 4) Once the desired impedances are prescribed, the procedure of Approach II needs to be applied (see section 3.7)
 - a) Figure 64, shows the frequency dependence of the impedance of each resonator, where we can clearly identify each family.

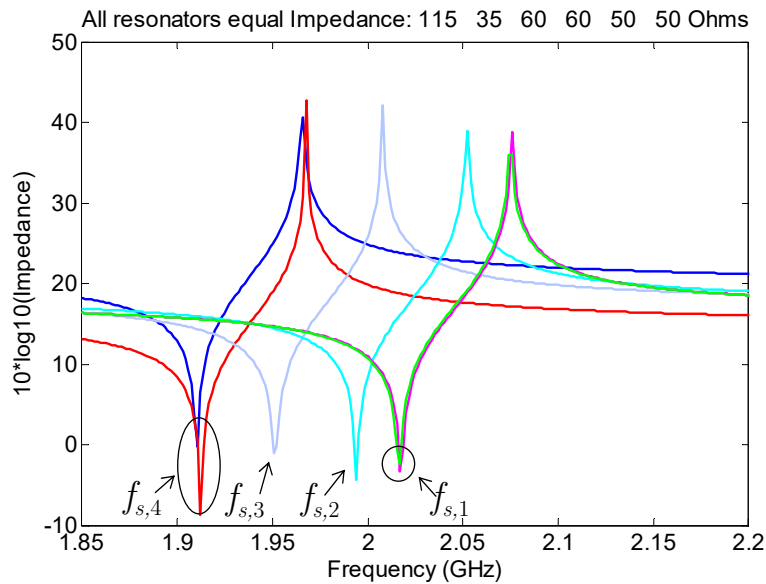


Figure 64. Impedance of each resonator.

To conclude with the example, Figure 65 below shows the frequency response of the synthesized transversal topology (cyan and green), along with the synthesized response.

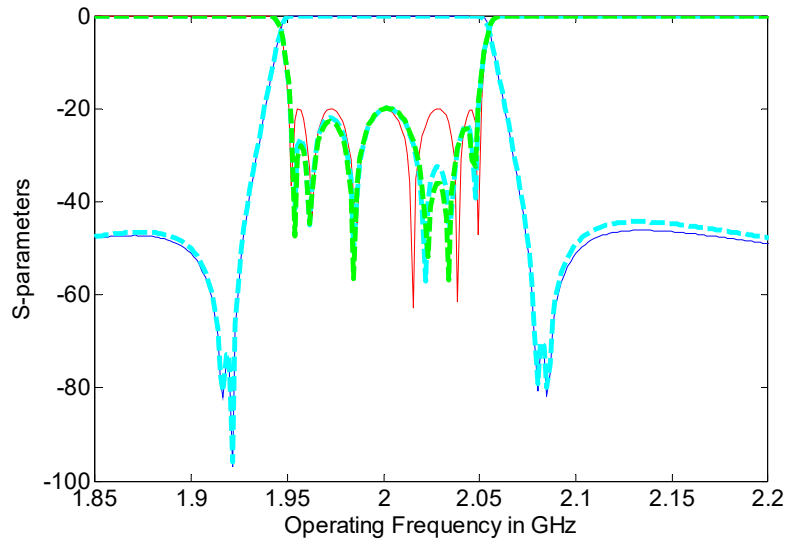


Figure 65. Filter response.

At this point, it is worth to mention that examples with much wider bandwidth response (200 MHz) have been performed following the same approach. The results for this case also yield to at least four necessary families of f_s , and the values of the required impedances are: 125Ω and 25Ω for family $f_{s,1}$, 60Ω for family $f_{s,2}$, 60Ω for family $f_{s,3}$ and 65Ω , for family $f_{s,4}$.

3.10 Advanced filter performances

This section illustrates two examples with advanced filtering responses. Those are responses that usually cannot be achieved (unless a way more complex circuits are used) with conventional ladder topologies. Both examples result from a synthesis response following any of the approaches outlined above, with a uniform coupling coefficient of 6.8%. Recall here that the coupling coefficient is prescribed by the designer, and by setting a different coupling coefficient the results would be very similar (in fact identical in the lowpass prototype).

The first example corresponds to a filter with very wideband response and with an arbitrary position of the transmission zeros. The filter bandwidth has been set to 200 MHz, and has been covered using only six resonators (note that this is not possible with a ladder configuration and uniform coupling coefficient of 6.8%). The transmission zeros have been located asymmetrically on both bands without the need of additional inductances.

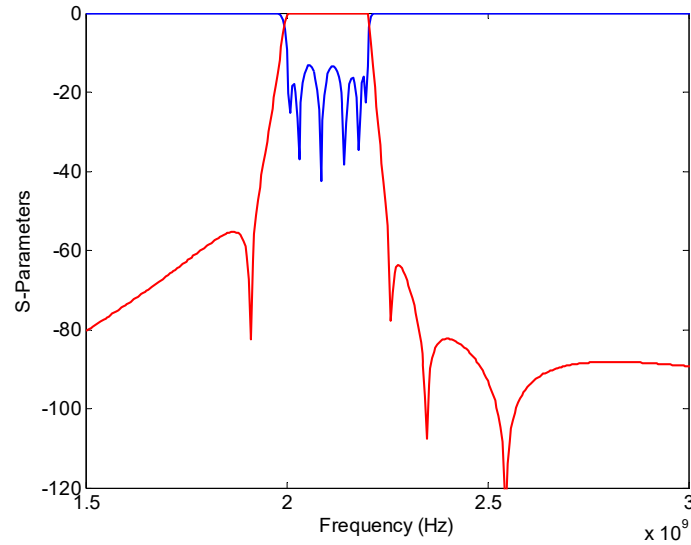


Figure 66. Filter response of a 200 MHz filter with arbitrary position of transmission zeros

The second example synthesizes a dual-band filter response. The total bandwidth of the filter is close to 300 MHz, with 80 MHz for the first band, 100 MHz for the second band, and around 120 MHz for the rejected band.

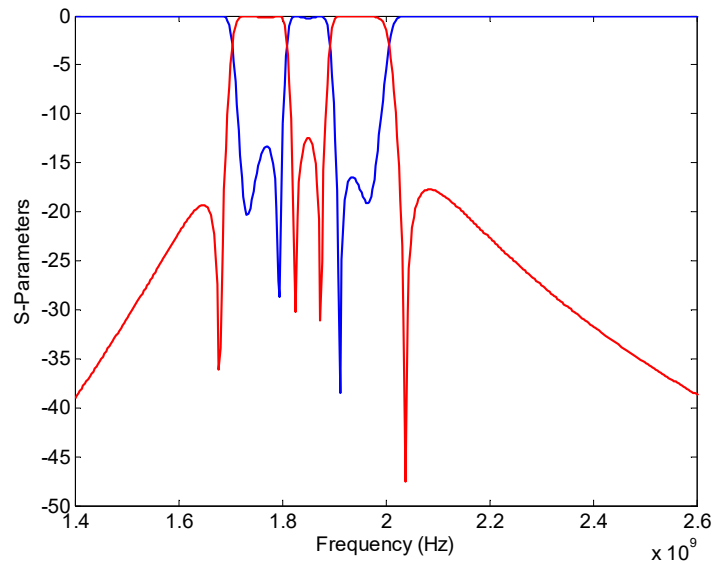


Figure 67. Filter response of a dual band filter.

3.11 Evaluation of the losses in a transversal filter configuration

This section evaluates the effects of the losses on the synthesized transversal topologies of preceding sections. Note that although those topologies exhibit almost equal frequency response, the impedances of the resonators may significantly differ, therefore requiring different

resonator sizes. As usually occurs in any resonator, the size affects the ability of the resonator to store energy, therefore giving rise to different quality factors.

The following analysis will use the size dependence of the resonator Q as stated in [53]. The lossy model of the resonators will also account for the electrode losses. The modeling of losses presented in this chapter refers and complements the model in section 1.7.4.

The quality factor of the acoustic resonance corresponding to a 50Ω resonator is set to $Q_a=1800$, and the quality factor corresponding to resonator of *infinite* size is set to $Q_{lim}=3000$. By defining a value η to account for the relative size [53]:

$$\eta = \sqrt{\frac{C_{tot}}{C_{ref_tot}}} \quad (110)$$

C_{tot} corresponds to the total capacitance of the resonator, which is C_p+C_s according to Figure 58.a and C_7+C_6 according to Figure 58.d. C_{ref_tot} , corresponds to the total capacitance of a 50Ω resonator, and is obtained following (96). The Q factor corresponding to each resonator for a given size Q_{ax} and the resistance, R_a , accounting for the losses in the acoustic branch of the BVD, are found by means of (21) and (22). This R_a value is then included as in Figure 68 for the corresponding resonators.

Additional lossy components need to be included to account for the electrode losses. This is usually modeled by placing a series R_s resistances as shown in Figure 68.b and Figure 68.d, which, although might have a slight dependence on size, is considered constant in this analysis. The value used for the analysis is $R_s=0.25\Omega$. No additional losses have been considered in the static branch. This comes from a *degradation factor* $gp=0$, that corresponds for a good resonator [53].

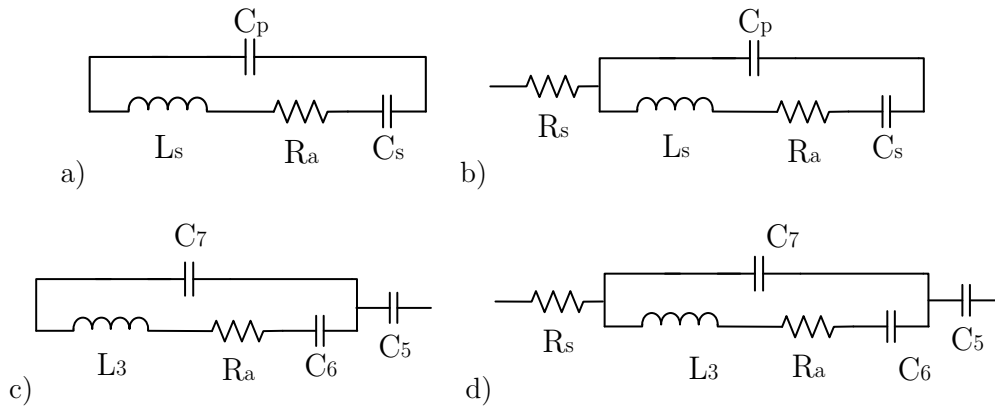


Figure 68. a) initially synthesized BVD with acoustic losses, b) initially synthesized BVD with acoustic losses and electrode losses, c) BVD after transformation with acoustic losses, d) BVD transformation with acoustic losses and electrode losses.

Figure 69 shows the results of including losses into the synthesized responses of previous sections. The figures on the left side (this is Figure 69.a and Figure 69.c) correspond to the case where only losses at the acoustic branch have been considered, this is $R_s=0$, whereas the figures in the right side include both losses on the acoustic branch and also the R_s term. The figure on the upper part outlined the details on the insertion losses and rounding at the band edges, whereas the figures in the lower part show the details on selectivity and transmission zeros location. Note that none of the figures show the reflection responses. The reason for that is that the return losses are barely affected by such amount of losses.

Both figures show, as a reference, the response of a lossless filter, and the response of a lossy filter evaluated from the characteristic polynomials. Note that the latter case assumes a uniform Q of the resonators. In that case we use the Q corresponding to 50Ω , which is 1800. Note as well, through the characteristic polynomials it is not possible to consider the effect of R_s .

For a better comparison between all synthesized responses the table below outlines the Q factor of each resonator and its corresponding impedance.

	App I	App II	App III	App IV		App I	App II	App III	App IV
Q_1	860	1800	854	1480	Z_1	670	50	670	115
Q_2	1120	1800	1200	1920	Z_2	310	50	241	35
Q_3	1227	1800	1220	1730	Z_3	230	50	230	60
Q_4	1231	1800	1222	1730	Z_4	234	50	230	60
Q_5	1130	1800	1661	1800	Z_5	315	50	73	50
Q_6	877	1800	867	1800	Z_6	677	50	684	50

Table 6. Values of Q and resonator impedance related to the different examples assessed for the losses evaluation of the transversal topologies.

Figure 69.a shows that the insertion losses and rounding obtained by evaluating the characteristic polynomials matches with the synthesized response from Approach II and Approach IV. Note that in both latter cases the Q factors (see table below) are around to 1800, at exception resonator 1 in Approach IV. In Approach I and Approach III, there is an increment of insertion losses and rounding effect due to the reduction of the Q factors. Note as well that in Approach III asymmetry is observed on the in-band response due to the asymmetry of the resonators and its location on the band. At this point it is also important to recall that approach III allows for several realization depending of the selection of the desired f_s . This would result as well in a different Q distribution.

Figure 69.c and Figure 69.d, outline analogous results than Figure 69.a and Figure 69.b, respectively, but for zoom out inspection. Both show similar effect on the transmission zeros, which now might be less deep depending on the Q distribution. Note that the loss of depth for the transmission zeros is not due to the amount of losses but it is for the compensation effect. This can be clearly seen from Approach II. In that case although the losses exist, since those are uniformly distributed the signal cancellation to create transmission zero is maintained. In all other cases, the deepness of transmission zeros is affected. Nevertheless, it is worth to mention that this effect might be different depending on the position of the transmission zero.

This last conclusion rises the important question on how the design, this is selection of the desired impedances and resonant frequencies, and distribution along the bandwidth, affects the filter performance due to the existence of losses.

As a last aspect to mention at this point is that losses of the external components, this is shunt inductances and series resonators, have not been considered in the previous analysis. Rigorous analysis would indeed require of such evaluation.

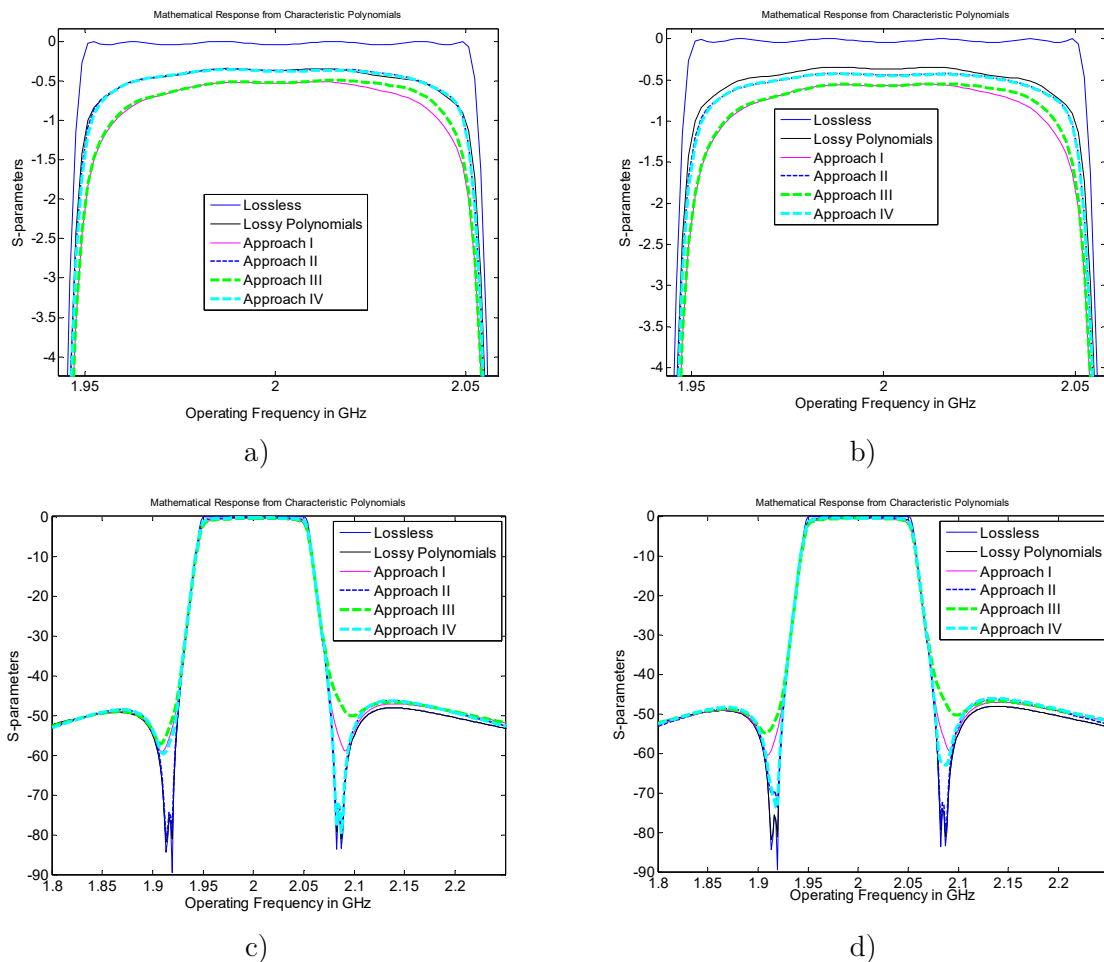


Figure 69. a) in-band effect due to only acoustic losses, b) in-band effect due to acoustic losses and electrode losses, c) effect on selectivity due to only acoustic losses, d) effect on selectivity due to acoustic losses and electrode losses.

3.12 Sensitivity analysis on transversal topologies

This section performs a sensitivity analysis of the topology of Figure 56 and Figure 59 for a order 6 filter, whose circuit parameters are listed in Table 6, respectively. In particular, the sensitivity analysis evaluates the effects of varying the impedance of the resonators and their resonant frequencies. To clearer unveil the effects of such deviation, losses are removed when evaluating the filter response.

According to our experience (Qorvo manufacturing process) on the development of acoustic filters based on BAW technology, some initial considerations need to be pointed out before showing the results of the analysis:

- Variation of the impedance of the resonator is mostly due to the manufacturing process and it happens in a uniform variation on the size of the resonators giving rise to variation up to a 1% of the resonator impedances.
- In contrast, variation of the resonating frequencies occurs randomly in the resonators, suffering a maximum deviation of up ± 1 MHz per resonator at the operating frequency of 2 GHz.

In order to evaluate the effects of both parameters we perform the analysis of each parameter separately.

3.12.1 Effects of the variation of the impedance

Figure 70 below, shows the effects of applying a uniform variation of the impedance of the resonator and also of the external elements (i.e., shunt inductors and series capacitors). Although a maximum variation of 1% could be expected, the analysis is also applied for a 5% in order to extend the analysis range. Blue lines correspond to the characteristic polynomial response where none variation of the impedances have been considered. Figure 71 shows a zoom-in of the in-band effects.

This analysis clearly reveals that the effects of considering a uniform variation of the impedance and all the circuit components forming the filter, barely affects the filter response. This fulfills in the near out-of-band rejection where the position of transmission zeros and deepness is maintained in both topologies, Figure 56 (App. I) and Figure 59 (App. II), and in the in-band ripple or return losses where slight deviations are observed.

Note that these results are indeed reasonable since with a uniform variation of the resonator impedances and the external components, each signal path of the transversal configuration provides the same contribution to the overall signal, but a higher reflected signal, which is very small due to the small impedance deviation considered in the analysis.

Figure 72 repeats the analysis of Figure 70, now without considering variation of the external components (i.e., shunt inductances and series capacitances), thus only variation of the resonators impedances is applied.

In contrast with the previous results, Figure 73 reveals that when the impedance of the external components is not changed accordingly with the impedance of the resonator, the response in the topology of Figure 56 deviates, especially on its near out-of-band rejection, and the position and deepness of the transmission zeros might change and might be significantly reduced.

Note again that this is consistent with the fact that the contribution of each path is differently changed, therefore the out-of-band cancellation does not hold any more. Note as well that this effect is more visible out-of-band where small effects on each path signal contribution need to be more precise, whereas the in-band effects are barely noticeable.

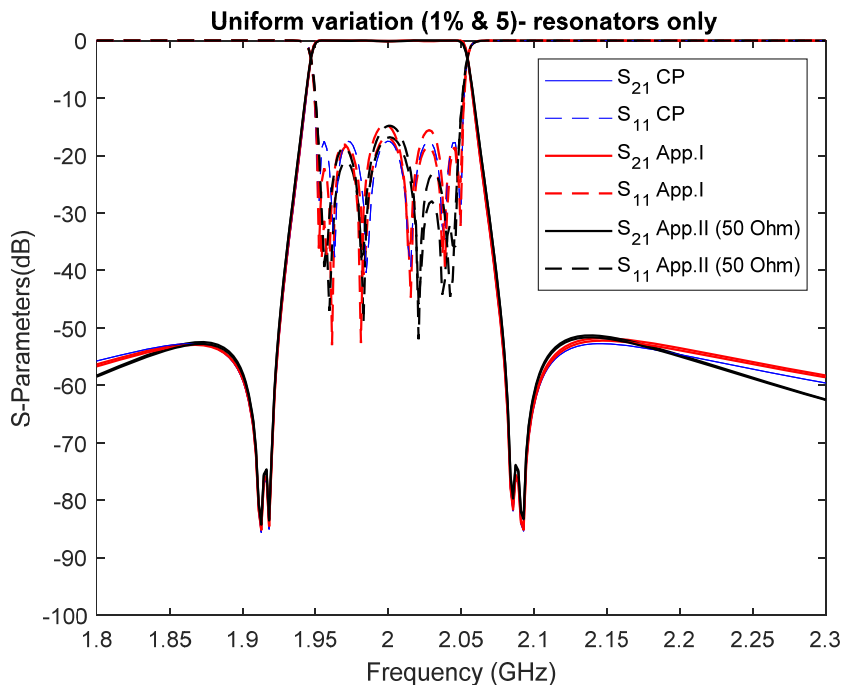


Figure 70. Frequency response considering a uniform variation of 1% and 5% of the impedance of the resonators and all other components of the filter. Legends are used to identify each response. The blue lines correspond to the characteristic polynomial response with none deviation of the impedances.

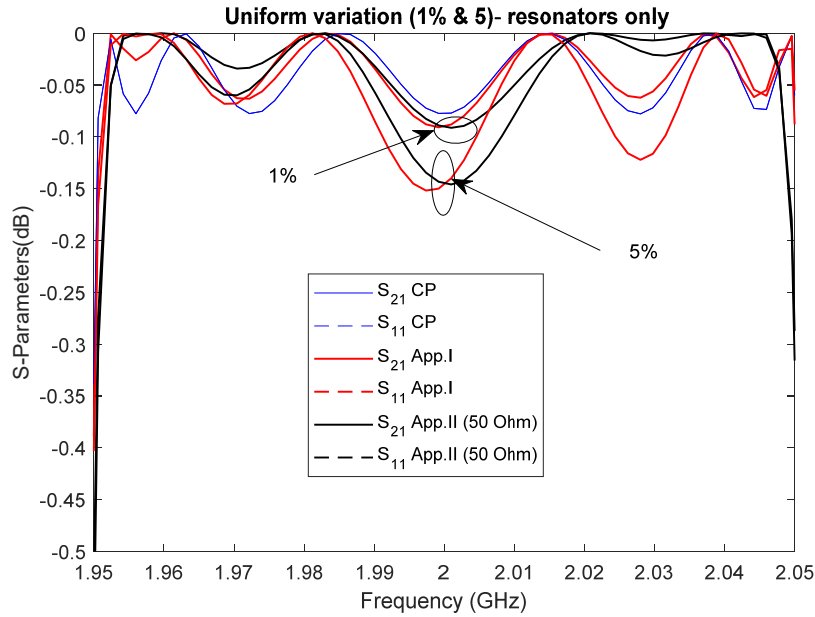


Figure 71. In-band details of the responses of Figure 70.

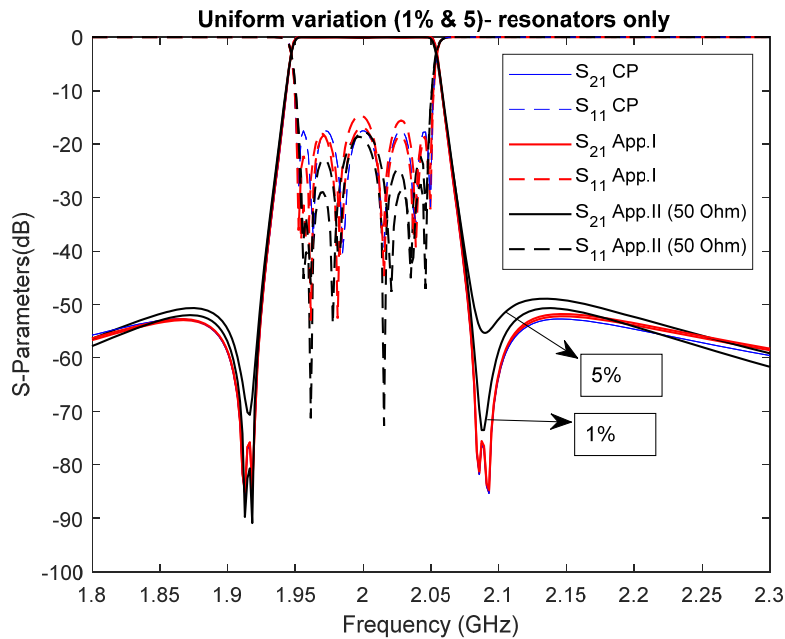


Figure 72. Frequency response considering a uniform variation of 1% and 5% of only the impedance of the resonators. Legends are used to identify each response. The blue lines correspond to the characteristic polynomial response with none deviation of the impedances.

Partial conclusion conclusions of this analysis are:

- When unbalancing effects are produced at the branches due to the deviation of the impedance, as the case of topologies following Figure 56 configuration, out-of-band

rejection is reduced and transmission zeros might be lost. Note however, that for 1% variation of the impedance this effects do not spoil the filter performance.

- The response can be recovered by applying the same variation factor to the external elements; these are C_5 capacitors and L_{shunted} inductance.
- This also allows to conclude that although the transversal configuration might be very sensitive, it is also very flexible and trimming process can be applied to recover the response.

It is also worth to recall here that the external network, including C_5 , C_{residual} and L_{residual} , might be potentially use to recovered the synthesized response by tailoring the contribution of each signal path.

3.12.2 Effects on the variation of the resonant frequency

As mentioned above the resonant frequency of each resonator forming the filter might deviate randomly in a +/- 1 MHz range. The figures below evaluate this effect. Instead of using a statistical analysis where hundreds of simulations are performed by means of applying random variation of the resonator frequency at the given +/-1 MHz range. We perform simulation where we apply +1 MHz or -1MHz deviation at several given resonators. This simple analysis allows to see the effects of having extreme variations at the resonant frequency of given resonators for unveil the worst cases.

Figure 73 to Figure 77 show different simulations. The variations applied at each simulation are indicated in the label of the figure by means of a vector. Each position of the vector corresponds to one resonator, and the value 1 means a deviation of 1 MHz, the value -1 means a deviation of -1 MHz and the value 0 means no deviation.

As in all previous cases, the analysis considers the topologies outlined in Figure 57 (red) and Figure 60 (black). Blue lines correspond to the characteristic polynomial response and they are used as a benchmark for comparison.

The first important conclusion from the simulations is that no differences can be observed between the two topologies under analysis (Figure 57 and 60), and both are equally affected by deviations on the resonant frequencies. A second conclusion is that the in-band performance is barely affected.

The simulations below also clearly show that the major effect occurs out-of-band, near the band edges on the position and deepness of the transmission zeros. When the position of transmission zeros changes, the rejection and sidelobe rejection accordingly changes.

It is also worth to note that the effects observed on Figure 74 are very similar to the effects occurring in Figure 76, but on the opposite sideband. Note that this is consistent with the fact that in a transversal configuration the resonators are distributed along the bandwidth, being the 1st resonator the one resonating closer to the lower band edge and the 6th resonator the one resonating closer to the upper band edge. Since the filter response is symmetric, the effects

of shifting the first and last frequencies up in frequency are equivalent dual to the effects of shifting the first and last frequencies down in frequency.

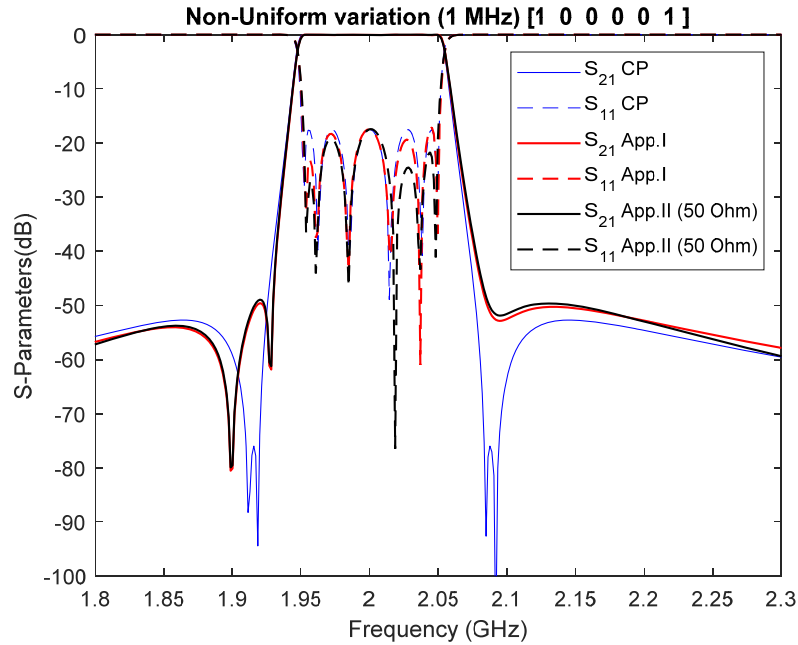


Figure 73.- Filter responses when a) +1MHz variation is applied to the 1st and 6th resonator. Legends are used to identify each response.

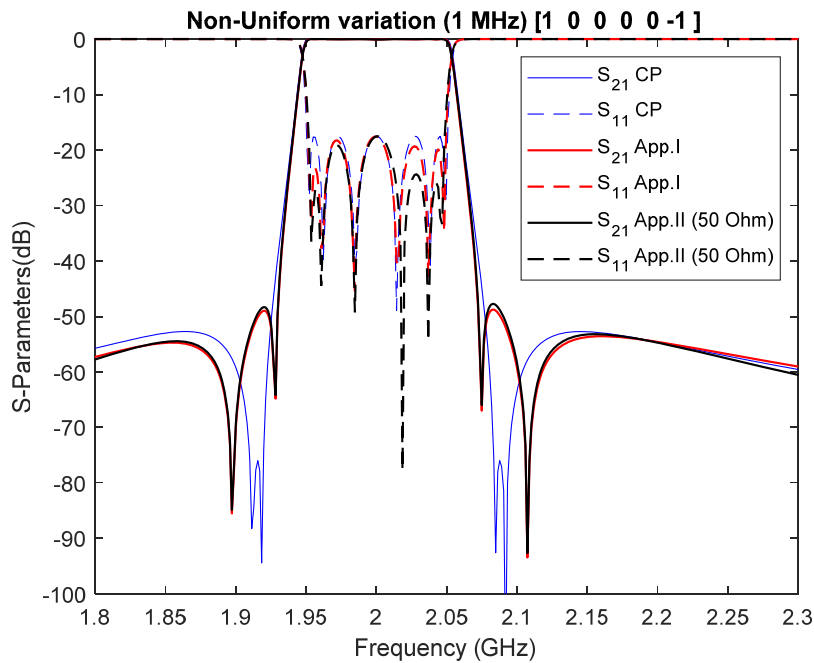


Figure 74. Filter responses when a) +1MHz variation is applied to the 1st and -1MHz variation is applied to the 6th resonator. Legends are used to identify each response.

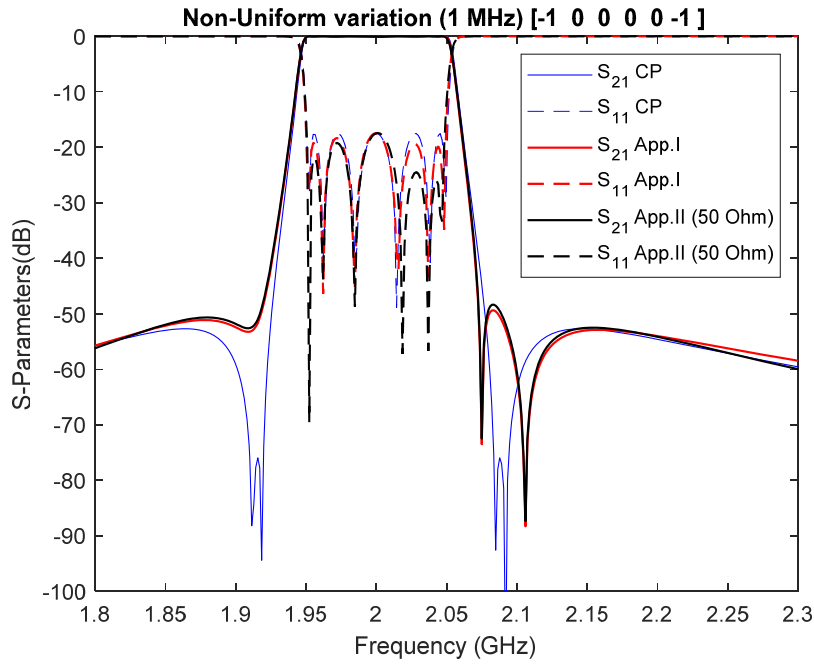


Figure 75. Filter responses when a) -1 MHz variation is applied to the 1st and 6th resonator. Legends are used to identify each response.

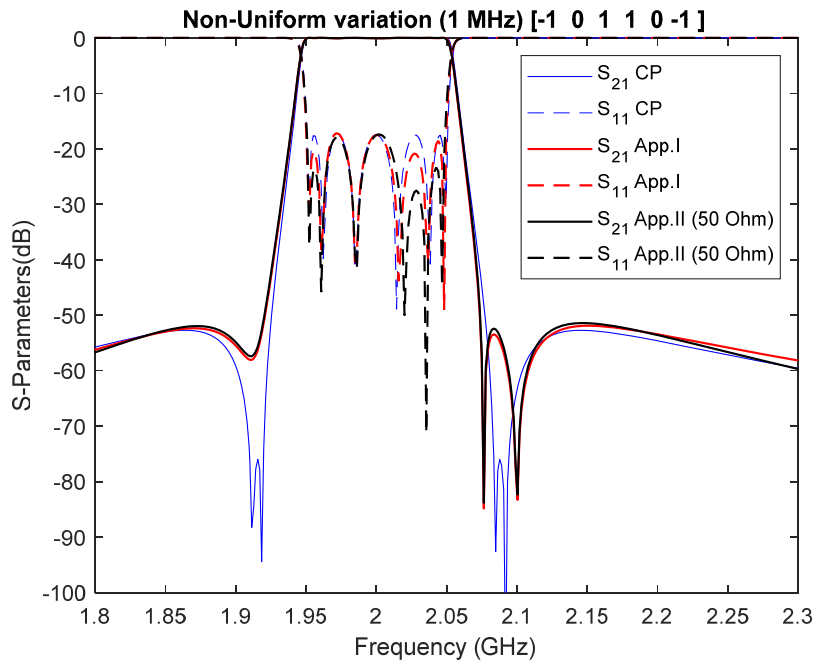


Figure 76. Filter responses when a) +1MHz variation is applied to the 3rd and 4th resonator, and a -1MHz variation is applied to the 1st and 6th resonator. Legends are used to identify each response.

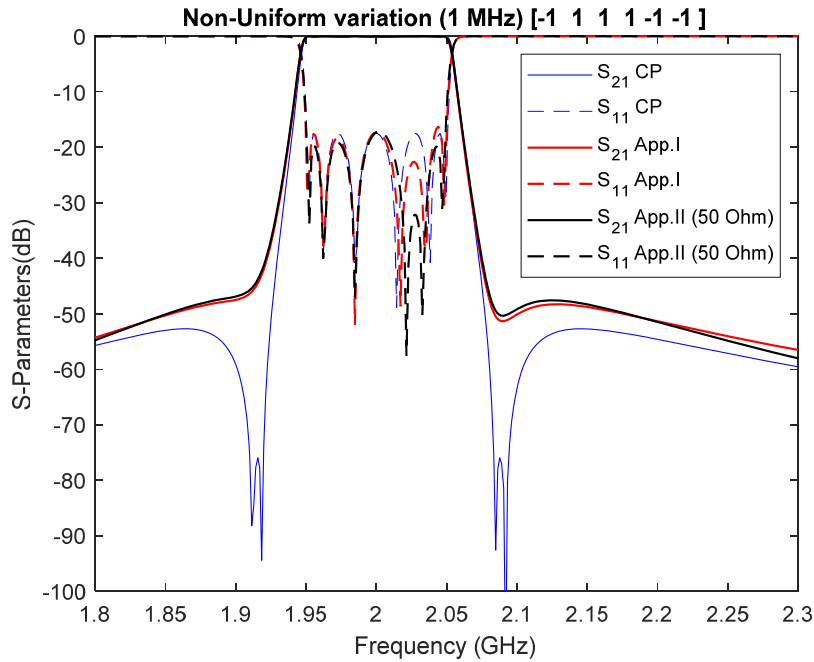


Figure 77. Filter responses when a) +1MHz variation is applied to the 2nd, 3th and 4th resonator and a -1MHz variation is applied to the 1st, 5th and 6th resonator. Legends are used to identify each response.

3.13 Effects of a non-ideal BALUN stage on the overall filter

As early noticed in the presentation of such novel topology, the existence of a transformer or BALUN stage at one end of the filter is mandatory to combine the contribution of the difference transversal branches for the final filter response. Indeed, this stage introduces a new degree of complexity for the implementation of such topologies, which could also affect the final performance of a real implementation.

Ideally, we would expect or need an ideal BALUN, this is a very wide band transformer fully balanced all over the frequency range and a phase shift of 180° . In practice this might become a real bottle neck for the full development of those topologies. Despite of that, the concept based on transversal topologies on acoustic wave filters can be applied on the different techniques used to develop acoustic wave resonator, this is in BAW, SAW, CRF and Stacked Crystal Filters (SCF) configurations. This latter statement might help to find the right niche for the development of transversal acoustic filters. For instance, SAW technology allows to obtain transformers with indeed acceptable performance BALUNs. On the other hand, the possibility to apply this concept into CRF configuration, where each resonator step produces a 180° degree shift, also opens the possibility to exploit the transversal configuration, or even on SCF where phase shift can be obtained by inverse polarization of the piezoelectric material.

Effects of a non-ideal BALUN are analyzed by means of the following equivalent circuit of Figure 78, where the parameters T_1 and T_2 refer to the coupling of each branch to the output port. An ideal BALUN results in $T_1=T_2=0.5$.

The analysis will consider to different simple cases. First when a non-unitary coupling exists, this is $T_1=T_2 \neq 0.5$, and second when a non-unitary signal ratio exists, this is $T_1 \neq T_2$.

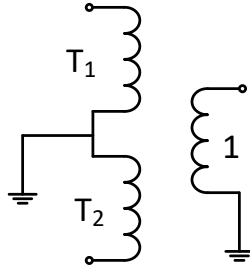


Figure 78. Equivalent circuit of the BALUN

3.13.1 Coupling (k_b) sensitivity

The coupling value is defined here as k_b as $k_b=T_1/0.5$. The following figures evaluate the cases for $k_b=0.95$, 0.8 and 0.75. Note that all these scenarios consider a fully balanced BALUN. This analysis has been performed with the circuit analysis software ADS (Advanced Design Systems) [58].

The results below reveal that the out-of-band performance is barely affected by the non-unitary coupling of the BALUN. This fulfils as well for the position and deepness of the transmission zeros. On the other hand, the in-band responses (or the return losses) in Figure 80, demonstrate the existence of a mismatch effect. From this figure, we can identify the different cases: the blue line corresponds to the case with $k_b=1$, the pink line $k_b=0.95$, the green line $k_b=0.8$, and the brown line $k_b=0.75$.

This effect can be easily recovered by changing the output matching impedance, which needs to be scaled by the value of k_b^2 [25]. This statement is demonstrated at the Figure 81 where all responses perfectly overlap.

This analysis has been replicated for the filter of order four with identical outcomes. The responses of the filter performance are shown in Figure 79 and 80, whereas Figure 81 outlines the results after applying the scaling factor k_b^2 to the output matching impedance.

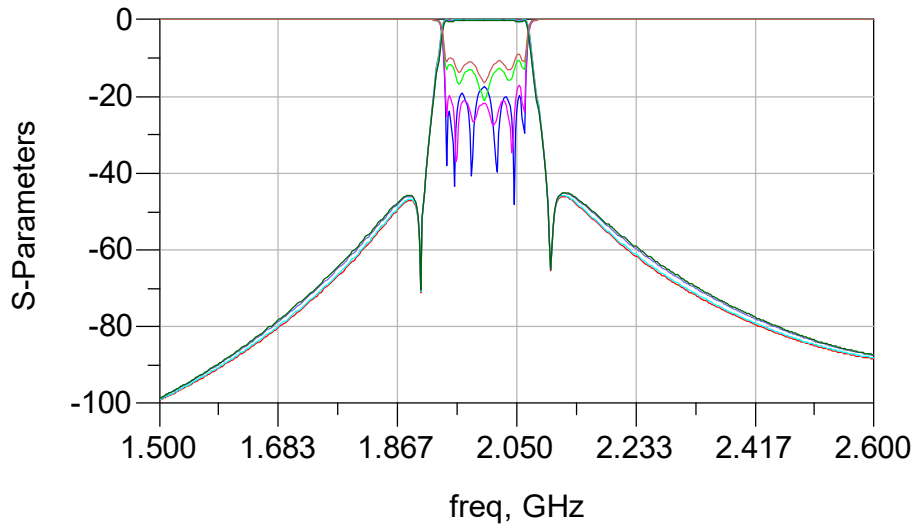


Figure 79. Response of a 6th order filter for coupling coefficients of $k_b=1, 0.95, 0.8$ and 0.75 .

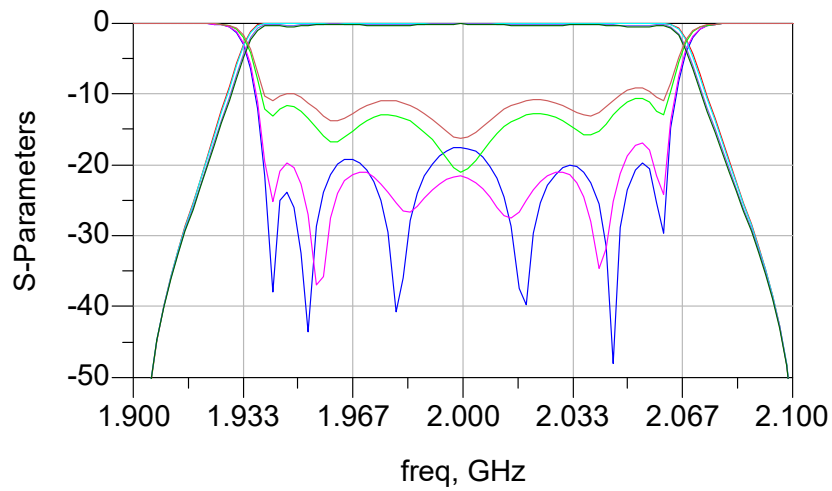


Figure 80. In-band details of the filter of Figure 80.

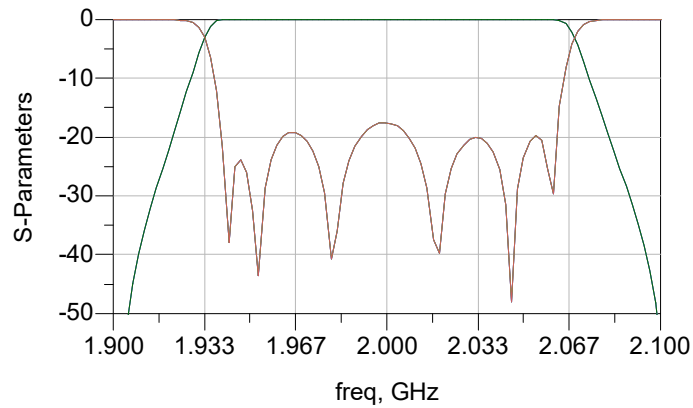


Figure 81.- In-band details of the filter when matching output impedance has been changed.

3.13.2 Signal ratio (a) sensitivity

The ideal value of balanced signal ratio is $a = T_1/T_2=1$. For this analysis we will perform simulation for $a = 0.98, 0.96, 0.94$. Such effects are outlined in Figure 82-83. This analysis has been performed with the circuit analysis software ADS (Advanced Design Systems) [58].

In contrast with previous subsection analysis, the unbalancing evaluated in this case strongly affects the out of band filter performance, due to the change on how each branch contributes to the output signal. This statement can be clearly observed in Figure 82 where the out-of-band rejection rises up to almost 20 dB for the different unbalanced cases. The caption of the figure indicates the corresponding a value. However, Figure 83 reveals that the unbalance effect barely affects the in-band response and return losses remains quite stable.

As in the previous analysis of the k_b -sensitivity, one might wonder if it is possible to recover the filter performance when unbalancing effects in the BALUN exist. The response is that the filter performance can be partially recovered. To illustrate that, Figures 84 and 85 show the responses of the filters of order six and four respectively, for the case of higher unbalancing effects, i.e., $a = 0.95, 0.9, 0.75$. As outlined in figures above, this would create an important reduction of the out-of-band rejection, however, this effect can be compensated by scaling the impedance of the resonators of the unbalanced branches by the factor a . By doing so, Figures 84 and 85 demonstrate that the out-of-band performance can be recovered at expenses of a degradation of the in-band performance.

The transversal topologies demonstrate that although being very sensitive to the balanced effect of each branch, they are also very flexible and the response can be somehow partially recovered, to still offer a good filter performance.

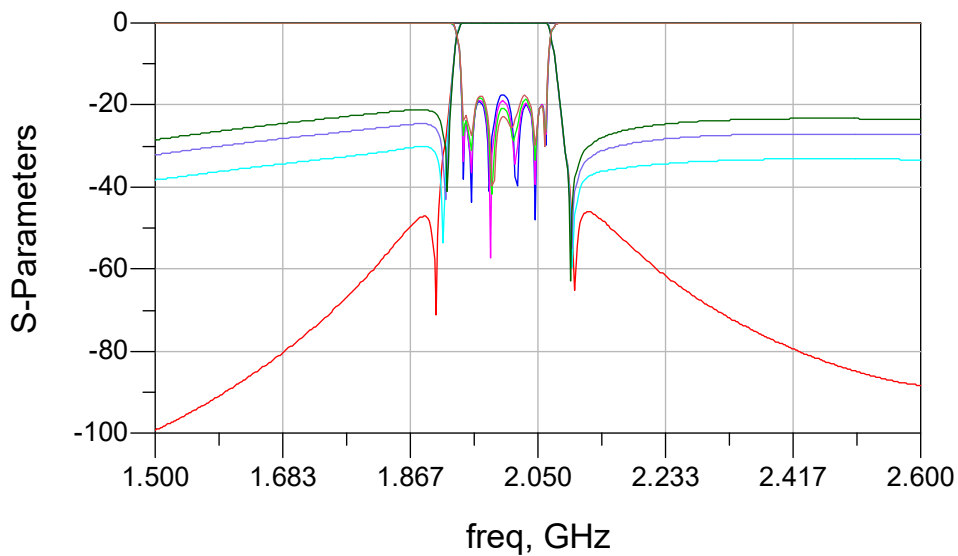


Figure 82.- Response of a sixth order filter for balance signal ratio $a= 1, 0.98, 0.96, 0.94$. The corresponding lines for the transmission coefficient are red, cyan, purple and dark green, respectively.

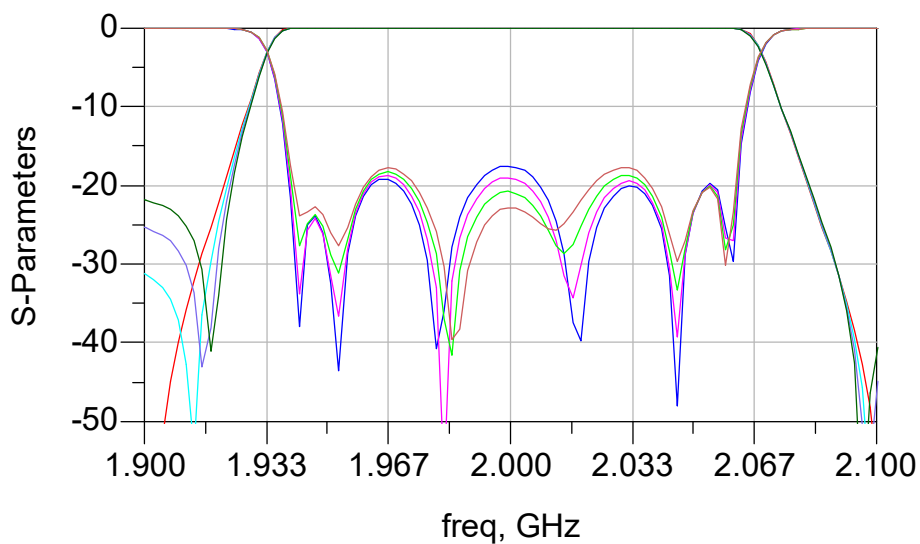


Figure 83. Return losses details for the responses of Figure 82.

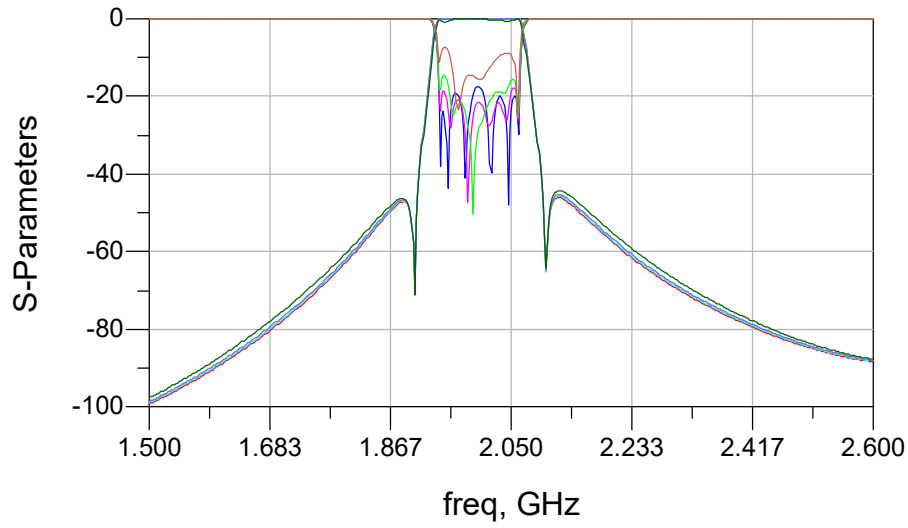


Figure 84.- Response of a sixth order filter for unbalanced signal ratio $a= 1, 0.95, 0.9, 0.75$.

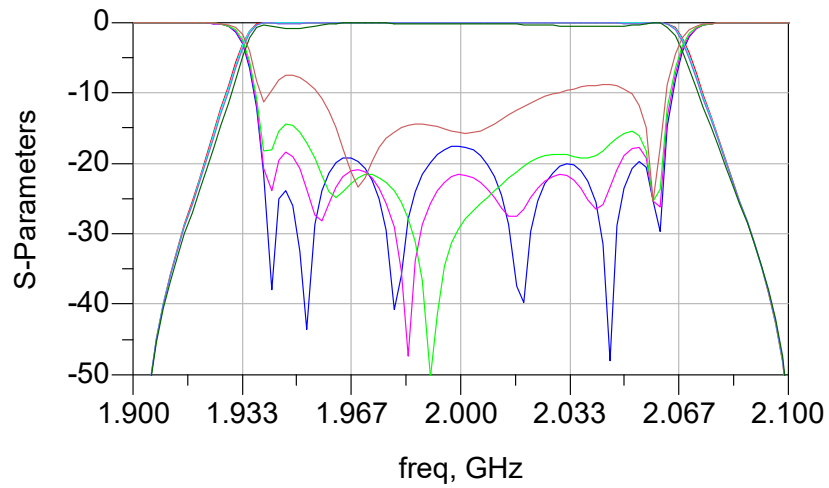


Figure 85.- Return losses details for the responses of Figure 84. The corresponding lines for the reflection coefficient are blue ($a=1$), pink ($a=0.95$), green ($a=0.9$) and brown ($a=0.75$).

Before ending this section, it is worth to recall that the effects of a non-ideal BALUN have not considered the frequency dependence of the BALUN which would indeed impact on the final filter response and might result in unrecovered filter performance.

3.14 Practical considerations

All the development detailed in previous sections show the potential and flexibility of the transversal topologies. Next chapter will explicitly report on some case studies for real applications along with some important implementation constrains. Before that the following sections advance some practical considerations.

In particular we evaluate the limitations and constrains of proposing a transversal topology without the inclusion of external capacitors. Note that this would result in a topology where flexibility on the impedance of the resonator neither its resonant frequency exists. We will see if the values of impedance are suitable from a direct synthesis procedure.

Then assuming that the fact of the inclusion of the external capacitors is necessary, this section will evaluate the suitability of the values obtained of C_5 . Also, the values of the always existing shunt inductance at the input and at the output will be discussed to see if it stays in a suitable range.

3.14.1 Non-external capacitors configuration

When no external capacitors are allowed the resulting impedance of the resonators directly depends on the synthesized values L_s and C_s , which in turn depend on the synthesized lowpass prototype values, the filter bandwidth and the operational frequency. The unique flexibility for selecting those values is therefore the synthesized characteristic polynomials.

On the other hand, the parameter k_b directly affects the resulting impedance through (79). Recall here that the value of k_b depends on the prescribed coupling coefficient by means of (78), and outlined in Figure 64. This figure indicates that lower coupling coefficients would give rise to lower values of impedances. Note that this is desired, since as we indicated in Section 3.5, the synthesis of transversal filters without external values might result in unsuitable high impedance values.

This last statement is quite significant since the designers always want to achieve higher electro-acoustic couplings. This achievement is not always trivial and there is even a rule of thumb that indicates that higher couplings result in lower Q. The possibility therefore of moving to lower couplings without affecting the achievable filter response might open the use of novel materials, and eventually a chance of applying this technology to new applications.

To qualitatively evaluate the values of the impedances as a function of the lowpass synthesized parameters we consider the case of a 4th order filter, without transmission zeros and BW= 200 MHz. For this particular case we evaluate the effects of proposing different values of return losses. Note that the dependence on the filter bandwidth is well specified by (79).

Figure 86 outlines the impedance of each resonator for a range of return losses that goes from 15dB to 35dB. The results show that the impedance values reduce when the return losses increases, and in this particular case is reduced half of their initial value. Recall however that higher return losses also means poorer selectivity, therefore a desired return losses value to achieve certain value of impedance might not be suitable for the electrical filter requirements.

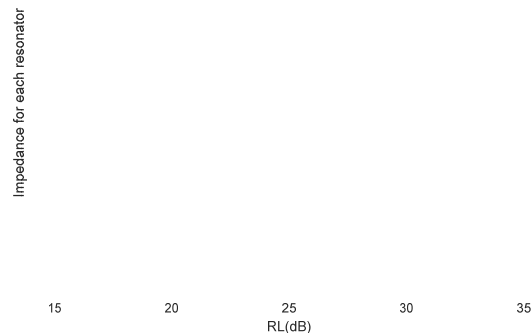


Figure 86. Impedance of each resonator as a function of the return losses (dB). Four order filter with 200 MHz bandwidth.

To further evaluate the dependence of the impedance with the filter response, the following figure (Figure 87) shows the impedance of the resonators for several order filters. The figure only shows the value of two resonators, one set at the edge of the passband and one set at the middle of the passband. It is assumed for all cases that there are no transmission zeros, return losses are fixed to 20 dB and the bandwidth is 200 MHz.



Figure 87. Impedance of each resonator as a function of the filter order.

The higher the order of the filter, the higher the impedance of the resonators, with a nearly linear dependence. This concludes as well that in order to keep low impedance values (suitable values) it is recommended to stay in low order filters, again therefore, with not very selective filter responses.

A way to overcome such constraint could be cascading several low order filters. This certainly would provide other advantages, such as the number of different resonant frequencies could be low. Outline of possible way to cascade low order filters could be as shown in Figure 88.

It is worth to mention that Figure 88.a presents a few advantages over Figure 88.b. On one hand in the case of implementing the topology all the filtering structure could go in a single chip. The BALUN stages would be off-chip. Additionally, the BALUN stages can be implemented to perform an impedance scaling, providing then any value of the impedance, making easier to match the filter at both ends.

3.15 Practical considerations - External capacitors and shunt inductors

External Capacitors:

For extension of the previous section, one may question whether the necessary values of the external capacitors are suitable in a real implementation. To answer that, we can refer to (101) and (102) that leads to $C_5 = C_3/(1 - \alpha)$, being $C_3 = C_s + C_p$ (see (20)). Then by recalling the equation of the impedance of the resonator $Z_0 = \frac{1}{2\pi f_s(C_s + C_p)}$, we can conclude that the value of C_5 depends on the impedance of the resonators as:

(111)

Note that when $\alpha=1$, the value of the desired impedance matches to the synthesized one (see (95), C_5 goes to infinite and therefore means there is a short circuit instead of a capacitance.

On the other hand, when the synthesized capacitance is very high and need to be significantly reduced the value of α is close to 0 and the value of C_5 can be found as:

(112)

In other words, when the initial impedance is very high the required capacitance is very small.

To illustrate this in numbers, Figure 89 shows the resonant frequency of the resonators as a function of the impedance of the resonator for the filter outlined in Figure 59. In square marks we indicate the value of impedances corresponding to $\alpha=1$.

Figure 89. Series resonant frequency as a function of the impedance of the resonator. In square marks are indicated the resonant frequencies and impedances when no external components are required.

The value of C_5 is shown below. It is possible to identify the values where $\alpha=1$, by the singularity of C_5 . Also, for values of impedances around 50Ω , the required values of C_5 are very suitable regarding their implementation (see Figure 91).

Figure 91. Details C_5 values as a function of the impedance of each resonator.

External shunt inductors:

The circuit transformation performed to go from a conventional transversal topology into a transversal topology based on AW resonators results in shunt inductances at the input and the output as outlined in section 3.5.

The value of this shunt inductance depends on the initially coupling coefficient of each resonator. As from the development detailed in the initial part of this chapter, these values depend on the filter bandwidth, on the synthesized lowpass circuit parameters (L_{Si}), and the final coupling coefficient desired at each resonator:

$$\frac{1}{L_{shunted}} \approx BW \sum \frac{k}{L_{Si}} = BW \sum \frac{k_1}{\alpha L_{Si}} \quad (113)$$

Figure 92 depicts the value of $L_{shunted}$ as a function of the impedance of the resonators, assuming in this case a uniform impedance of all the resonators. This case also synthesizes a uniform coupling coefficient for all resonators to 6.5%. From this figure we can see that for a uniform impedance of 50Ω the required inductance is in the order of a few nH, which places the inductance in the range of feasible values for this technology.

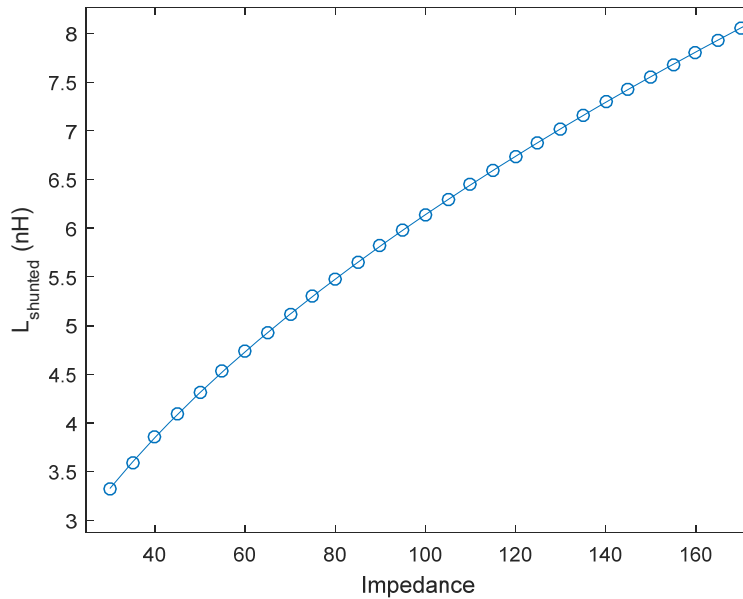


Figure 92. L_{shunted} value as a function of the impedance of the resonators (assumes a uniform impedance).

3.16 Conclusions

This chapter detailed on the most innovative part of this thesis by proposing and developing the synthesis procedure for a new topology of acoustic wave filters. The proposed topology is referred as transversal topology and can be applied to BAW and SAW filter configurations. Although not developed in this chapter the flexibility of this method certainly opens up the opportunity to be extended to the CRF configurations.

This novel topology proposes a new way of connecting the AW resonators to perform the filter response, which consists on electrically connecting all resonators directly from the input to the output, in such a way that the contribution of each transversal path is added at the output to offer the filter response. This new concept on acoustic filters allows to obtain filter responses not achievable with other filter configurations based on acoustic filters, such as:

- Very wideband filter response
- Multiband responses
- Responses with self-equalized in phase.

In addition to the advantages on the achievable responses, this new approach also offers some promising benefits from the implementation point of view. Those benefits are:

- The coupling coefficient of each resonator can be selected in advanced by the designer (prescribed).
- Allows flexibility on the impedance of the resonators.
- Allows flexibility on the resonant frequency of each resonator.

At this point is also important to outline some of the drawback or eventual limitations:

- Those topologies need a BALUN stage.
- Are sensitive to non-uniform deviation of the parameters defining each branch of the transversal configuration, such as resonant frequency and impedance of the resonators.

As it will be outlined in the last chapter of conclusions and future research lines, some modifications of the topology presented in this chapter can help to overcome some of the previous limitations.

At this point, it is also important to conclude that this new concept to synthesize acoustic wave filter may enable the use of less typical materials and lead to the use of new manufacturing techniques for their development, since constrains on the coupling coefficient do not affect the achievable responses, this in turn might give rise to the development of acoustic filters at other frequencies and therefore contributing to the expansion of this technology to other applications.

Next chapter completes some of the details on the proposed topologies by performing three case studies based on real filter electrical requirements and also accounting with some of the technological constrains.

CHAPTER 4

CASE STUDIES

This chapter details on some case studies corresponding to filter and multiplexer designs using the synthesis procedures described in chapters 2 and 3, for ladder filter topologies and transversal topologies, respectively. For the particular case of ladder topologies, a software tool has been developed with the aim to be used as a first step in a filter design process, by providing several topologies (solution space) for given filter electrical specifications.

Most of the examples presented below are based on real specifications of commercial filters or multiplexers. The presented designs do not only account for the initial mathematical response but also consider the implementation aspects, as the coupling coefficient of the resonators, impedances and resonant frequencies of the resonators. Evaluation of the losses are also considered in some cases.

4.1 Software for the synthesis of ladder filters

The tool includes all the mathematical formulation presented in Chapter 2 for the synthesis of ladder filters and it has been proposed as a user friendly interface where the designer would have the opportunity to obtain fast initial solutions of several synthesized networks. The aim of this subsection is then to present the main features of this tool.

Graphic User Interface – Ladder AW filter

The usual first step for a BAW/SAW filter designer would be to find a preliminary topology that meets some given specifications. A schematic ladder type filter will be drawn in some electronic design automation software giving initial values to the basic parameters of the elements placed on the circuit. For a BAW filter these usually will be:

- f_s , the resonant frequency of the acoustic resonators.
- C_0 , the static capacitance of the acoustic resonators.

- L_{gnd} , ground inductances that connects the shunt resonators to the common ground in the laminate.
- k_e^2 , electro-acoustic coupling coefficient.
- Additional external element values, - i.e. capacitors and inductances -, used to virtually modify the k_e^2 and/or to adapt the filter to the input/output port.

Several optimization iterations will be run in order to find the values of the parameters described above that makes the electrical response of the filter to meet the specifications. These values have been previously constrained within a certain range to make feasible the manufacturability of the filter.

After the preliminary topology is obtained, that is, the optimized values of the filter parameters provide a good solution, the designer may proceed to the next step. This should be to create an equivalent layout based on the optimized schematic that will give the initial appearance to the die. Along with the die a 3D model with all the layered filter structure, including pads, vias, laminate, etc. has to be created in order to perform accurate EM simulations of the overall device, including everything except, maybe, the packaging. But at this point the designer is already dealing with many issues that are out of the scope of the filter synthesis.

Unlike this typical methodology, the synthesis procedure manipulates a slightly different set of parameters due to its own mathematical nature. That is, the designer optimizes a ladder topology that will very unlikely provide with a frequency response that looks like a Chebyshev polynomial. This happens because the intrinsic relationships between all the parameters in the filter have to comply with a very particular set of conditions, which have been stated previously in this thesis, in order to reproduce a characteristic polynomial filtering shape.

So far, we have seen how varying the values of certain main parameters of the filter – order, transmission zeros, return losses, bandwidth, center frequency – we obtain a different topology for each new combination of all those values. One of the purposes of this work is to offer synthesized network ladder topology that can meet a set of given specifications. To this end a GUI tool has been created.

An overall view of one of the newest versions of the GUI is shown in the Figure 93. The GUI has been created using the MATLAB® platform. Different parts of the GUI have been numbered from 1 to 4, whose features are outlined latter along the text.

The GUI has grown up in size and functionalities little by little to be able to model more and more accurately the acoustic wave filter behavior up to the point that many features that are not related to the synthesis itself were added (losses of the BVD considering resonator size-dependent performance, optimization engine and more). Even a secondary window that allows to visualize the response of a group of multiplexed filters previously stored was created.

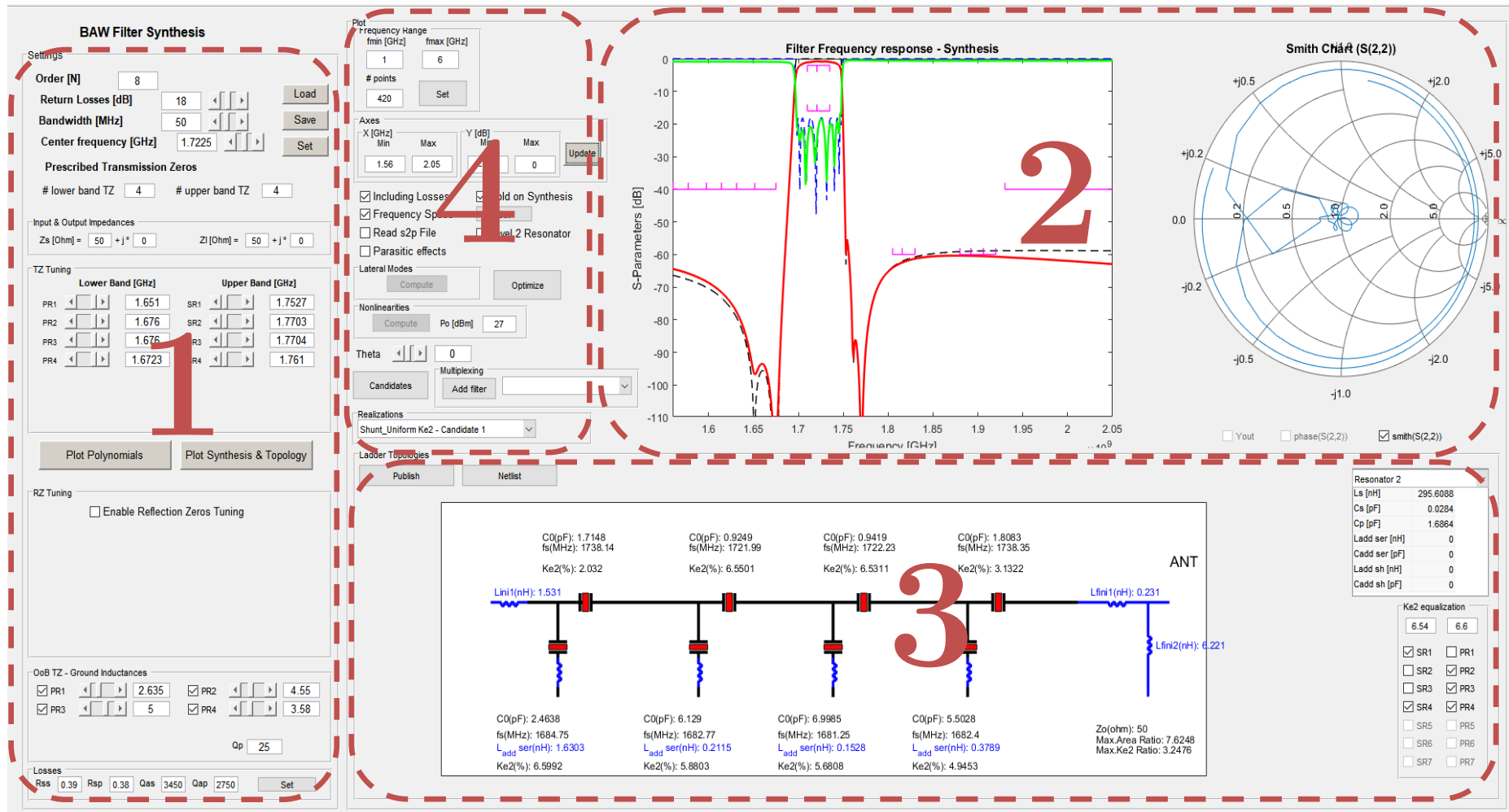


Figure 93. General Overview of the GUI Main Window

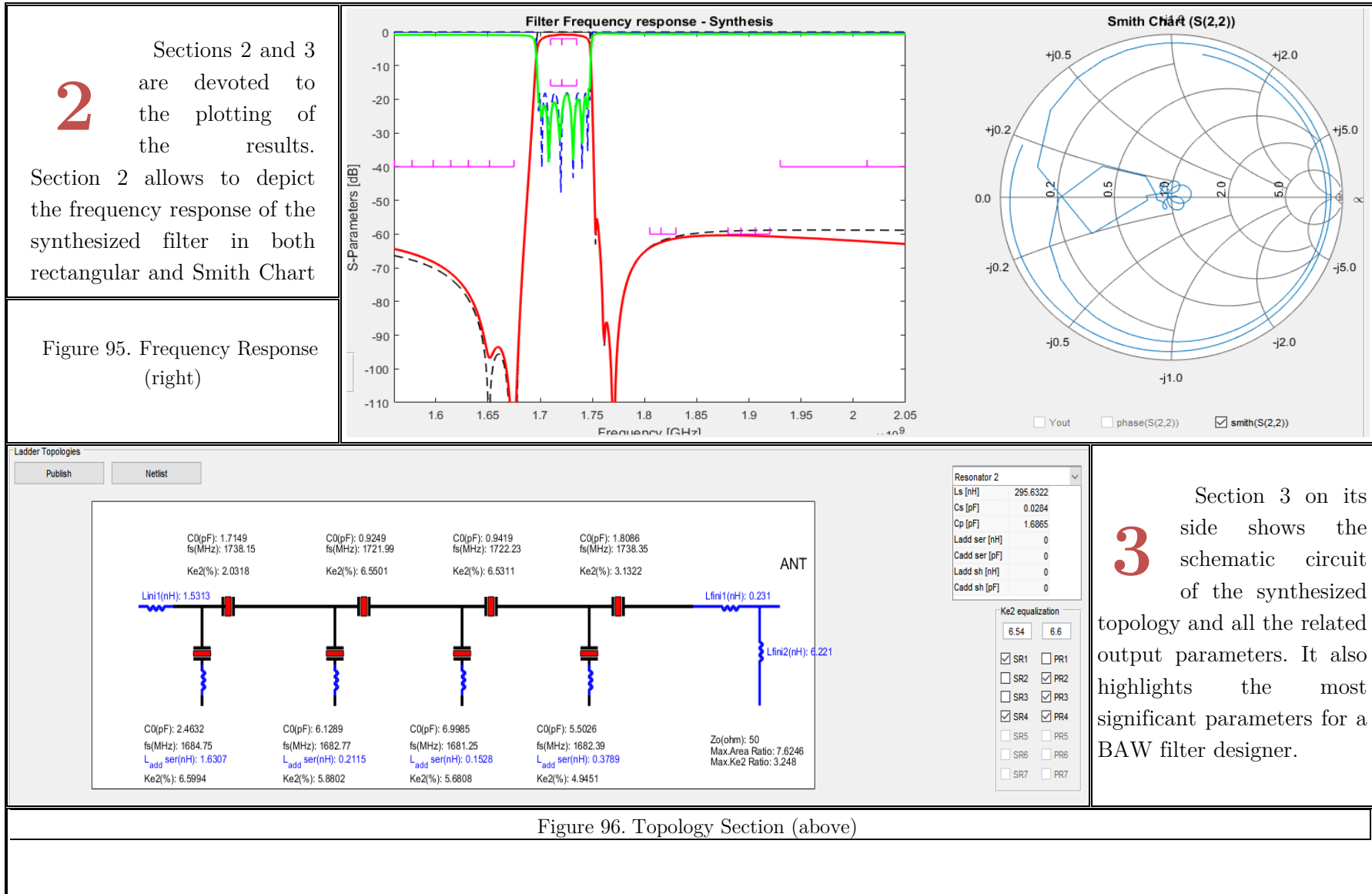
Figure 94 Settings Section.

the common ground of the filter. In this section we choose the frequency where we want to include a notch most likely in order to improve the out-of-band rejection or the Inter-Band isolation if the purpose of the filter is to be included in a multiplexer. Finally, it is possible to set the values of the parameters related to the losses of the filter, like the quality factor Q of the resonators and their input resistance, R_s , for both series and shunt resonators.

1 Settings Section. It involves the most significant input parameters that take part on the synthesis. That is the order of the filter, Return Losses value, Bandwidth, Center Frequency and position of the prescribed Transmission Zeros. Since the topology used is always ladder-type, the Transmission Zeros below the Lower Band Edge will be originated by the resonant frequency of the shunt resonators and the TZ above the Upper Band Edge will be originated by the anti-resonance of the series resonators. It is therefore necessary to specify exactly which TZ corresponds to each resonator. Also for the particular case of the odd order filters it is necessary to state the number of shunt resonators and series resonators that we want to place in the topology.

Additionally and also related with the synthesis, it is possible to modify here the values of the Reflection Zeros (RZ), which are the roots of the $F(s)$ characteristic polynomial. This may be convenient in order to fine-tuning the Return Losses (RL) or even the k_e^2 values of the resonator.

This section has other built-in features like setting the values of the out-of-band Transmission Zeros. As we stated previously, these are created by the inclusion of ground inductances between the shunt resonators and



4

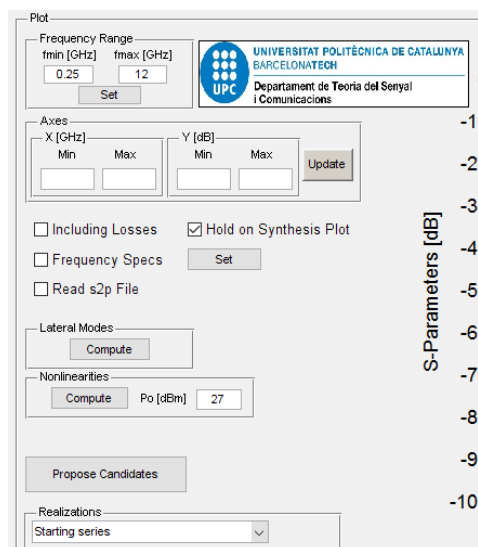


Figure 97. Screen shot for the input parameters of Section 4

Section 4 offers post-processing features for the synthesized networks. These allow for the evaluation of losses, lateral model and computation of the non-linearities. Additionally this section allows for selecting the proposed candidates (different topologies that result from the synthesis), inclusion of the filter specifications through a filter mask, and even to read previous designs save as .s2p files.

4.2 Case studies of ladder filters

The following subsection presents several case studies where ladder topologies have been synthesized to meet real filtering stages specifications. In particular three standalone filters have been synthesized and evaluated. A real triplexer scenario has been also considered, which latter has been extended into a quadplexer, in order to verify the suitability of the proposed approach. The synthesized values, these are impedances, series resonant frequencies and coupling coefficients of the resonators, are not always revealed for confidential issues, nevertheless the synthesized networks do not only meet the electrical requirement but also the technological requirements. This is, range of feasible impedances, frequencies and coupling coefficients.

4.2.1 Band 39 LTE

The first case study shows a very wideband filter covering the band 39 LTE. In particular, a high order filter $N=11$ in ladder configuration, synthesized by means of the element extraction technique and the software tool presented in previous section. The synthesized network has been evaluated by the software of previous section along with its implementation in AWR Microwave Office®, an RF & MW circuit design software powered by National Instruments, making use of the exact same parameters that the synthesis provided. However, in AWR a fairly more sophisticated model – regarding the SMR stack and the BVD model - is used for each resonator.

This model is QorvoTM proprietary and includes considerations related to non-linearities [59] [60], lateral propagation modes [44] and extended BVD model [53], therefore additional losses, parasitic effects and the quality factor dependence on the size and geometry of the resonators are taken into account.

Table 7. Specifications for the B39 Wideband filter and simulated values for the resonator stack and ground inductor losses.

Table 7 lists the specifications for the filter and the simulated values for the most representative parameters of the resonators as well as the losses considered for the external inductors. Figure 99 shows one topology that meets the specifications. This same topology has been replicated in AWR to make the comparison shown in Figure 98.

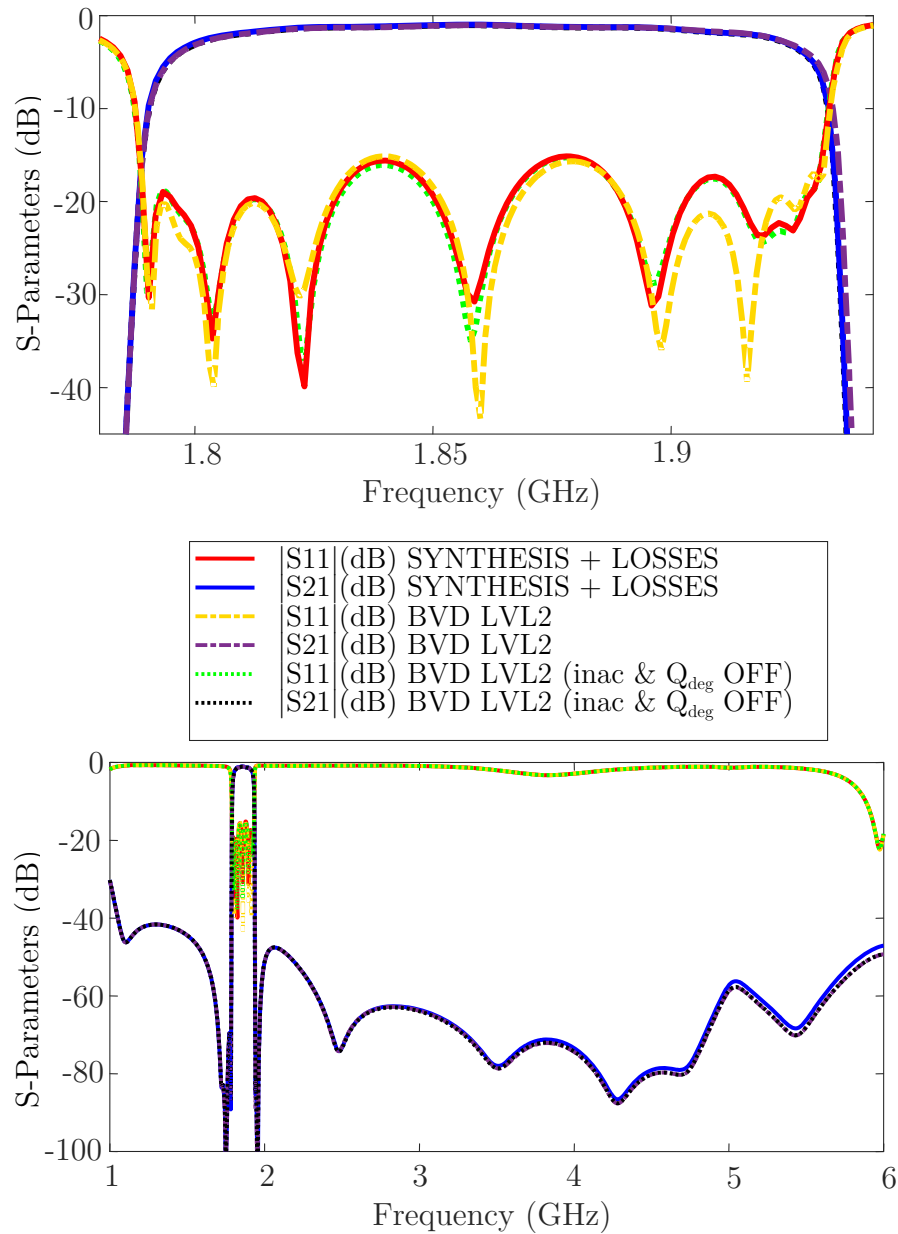


Figure 98. In-band frequency response (above) and Wide-Band response (below) of the synthesized B39 Wideband filter (solid red and blue) compared to the AWR simulation including the in-house Qorvo resonator model (dashed orange and purple) and also with the same model with the $inac$ and $qdeg$ variables disabled (dotted green and black) [53].

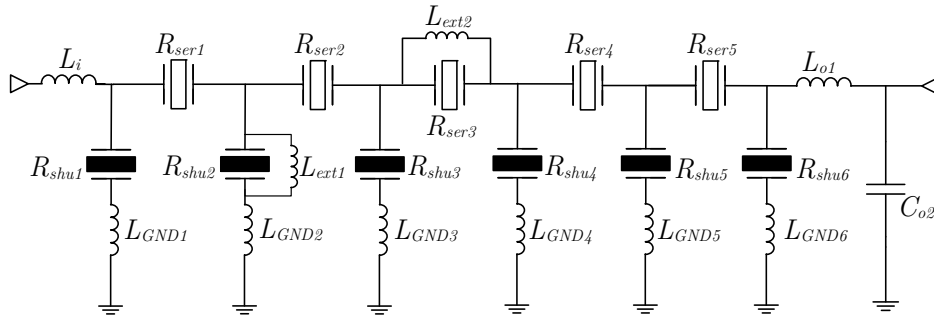


Figure 99. Synthesized topology for the B39 Wideband filter.

The synthesized values, including the inductance to ground values cannot be disclosed in this document.

4.2.2 Very stringent filters

The following case study consists of two markedly narrow bandwidth independent filters with very demanding skirt steepness. A lot of rejection is needed above passband for the filter number 1 and below passband for the filter number 2. Both solutions meet the specifications by means of a 9th order ladder filter.

Achieving a steep transition from the passband to the out-of-band skirt can be done usually by means of increasing the order of the filter response. However for these particular cases where the bandwidth is quite narrow as well, high orders are in practice synonym of having some very low k_e^2 and small synthesized resonators.

We can recall how the absolute value of the impedance varies between the resonance and the anti-resonance along the frequency axis for both the shunt and the series resonators. Whether the filter bandwidth gets narrower the impedance variations take place in a much short frequency range, that is f_s and f_p are closer to each other. Therefore the k_e^2 value is low.

Even if we think of placing some of the TZ far from the band to get good k_e^2 values for the synthesized resonators it has to be taken always into account that there are certain specifications to be met. For example, demanding skirt steepness will require some TZ placed very close to the passband. On the other hand, placing all the TZ very close to the band to achieve the steepness is counter-productive in order to meet the near band rejection specifications; therefore, it is convenient to choose wisely their locations.

In order to compensate this, we increase the bandwidth of the synthesis, that is, we use an initial input bandwidth for our polynomial frequency response fairly wider compared to the value stated on the specifications (let's say double for this particular example) and shift conveniently the center frequency.

In addition, we can include shunt capacitors to all those synthesized resonators that still have a low k_e^2 value after the synthesis

Steep Filter 1		
Requirement	Specification Value (dB)	Frequency Range (MHz)
Passband		
Return Loss (RL)	>14	2400-2429
Insertion Loss (IL)	< 2.5	
Rejection		
Near-out-of-band Rejection	>50	2437-2483.5
Far-out-of-band Rejection	>30	<2300
	>20	2520-6000
Steep Filter 2		
Requirement	Specification Value (dB)	Frequency Range (MHz)
Passband		
Return Loss (RL)	>14	2447-2474
Insertion Loss (IL)	< 2.5	
Rejection		
Near-out-of-band Rejection	>50	2400-2439
Far-out-of-band Rejection	>30	<2300
	>20	2500-6000

Table 8. Specifications for the very demanding skirt steepness filters

Table 9. Simulation values of the resonator stack and ground inductor losses for the filters of the case study 4.2.2.

Table 8 shows the frequency specifications for each of the two filters. Table 9 shows the simulated values for the most representative parameters of the resonators. It also shows the

constraints regarding the feasibility and suitability of the filter elements. That is, the expected maximum and minimum size of the resonators. Finally, Table 10 details on the synthesized values corresponding to the resulting topologies detailed in Figure 100 and Figure 101, for filter #1 and filter #2, respectively.

The frequency responses of the synthesized filters are outlined for in-band and out-of-band response in Figures 102-105. Description of each figure are detailed in the corresponding figure caption.

Table 10. Circuit parameters corresponding to the synthesized topologies in Figures 100 and 101.

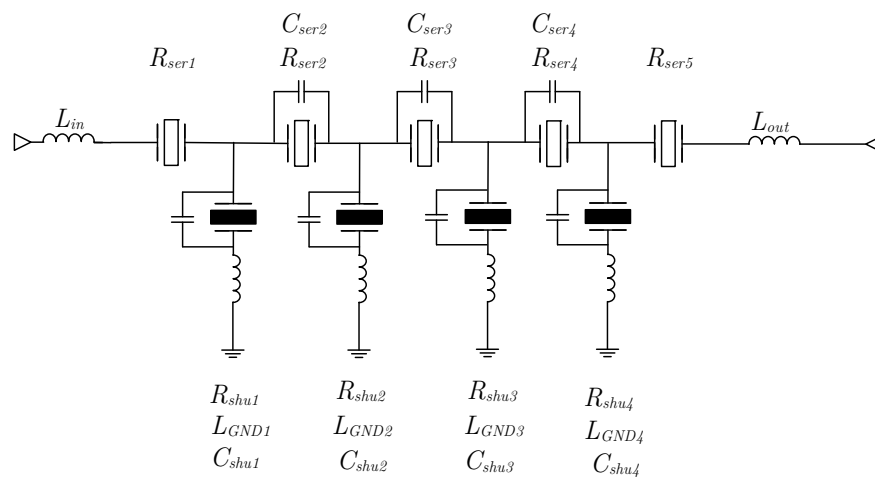


Figure 100. Synthesized network for filter #1

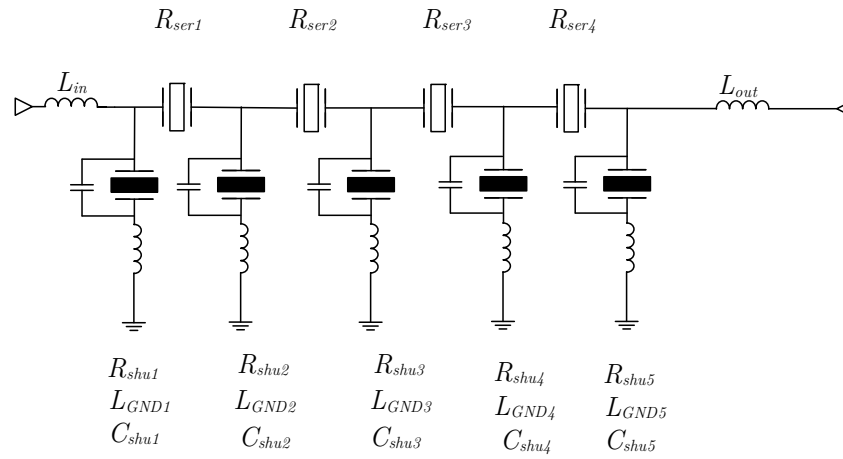


Figure 101. Synthesized network for filter #2

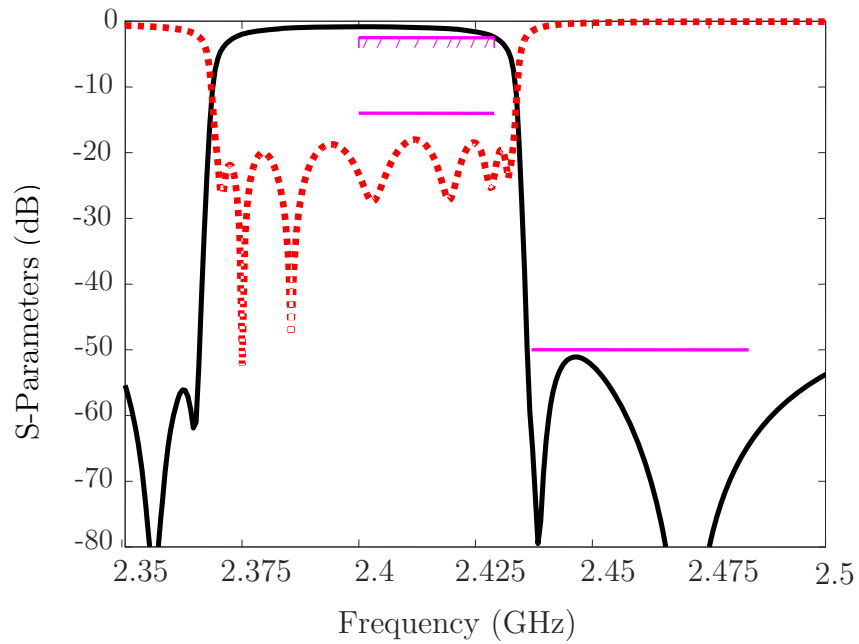


Figure 102. In-band frequency response of the synthesized steep filter #1

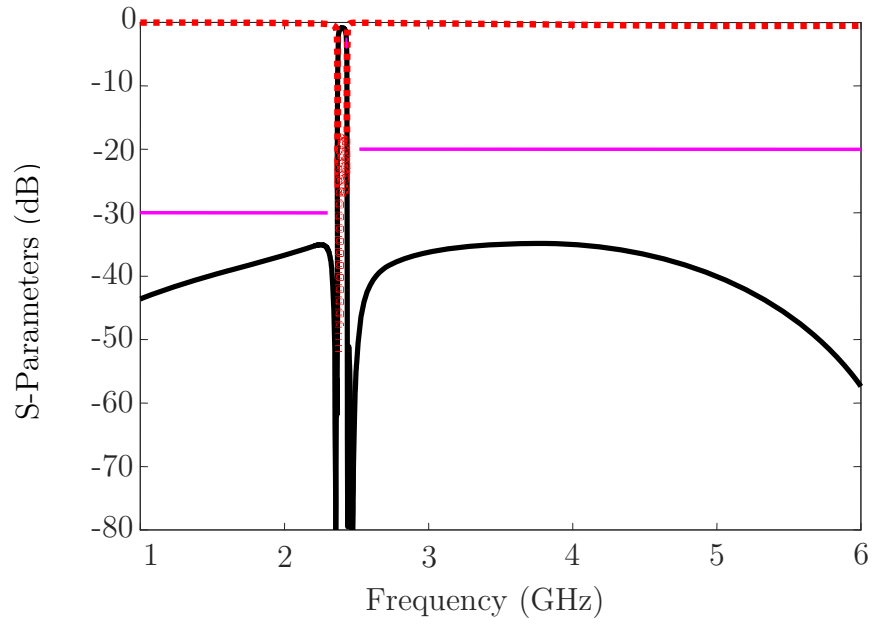


Figure 103. Out-of-band frequency response of the synthesized steep filter #1

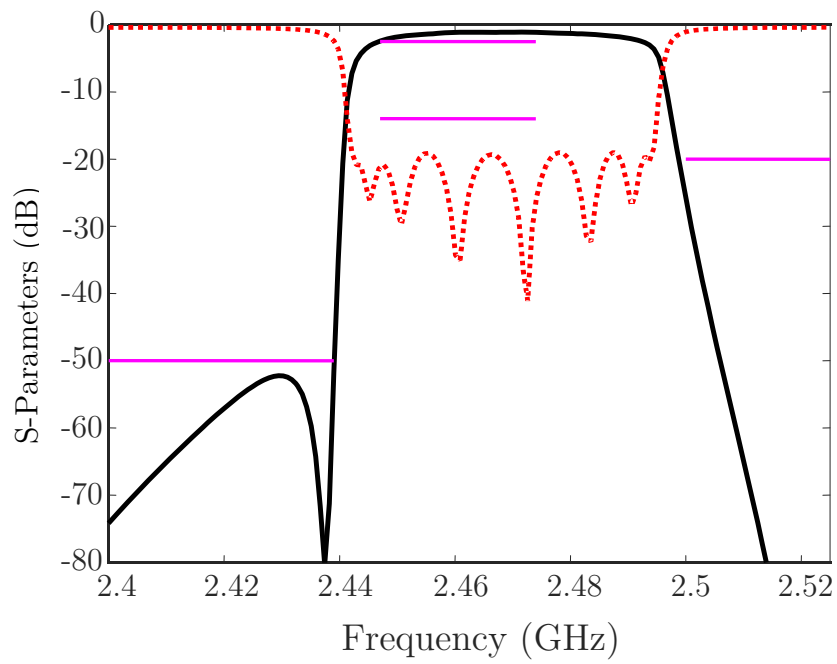


Figure 104. In-band frequency response of the synthesized steep filter #2

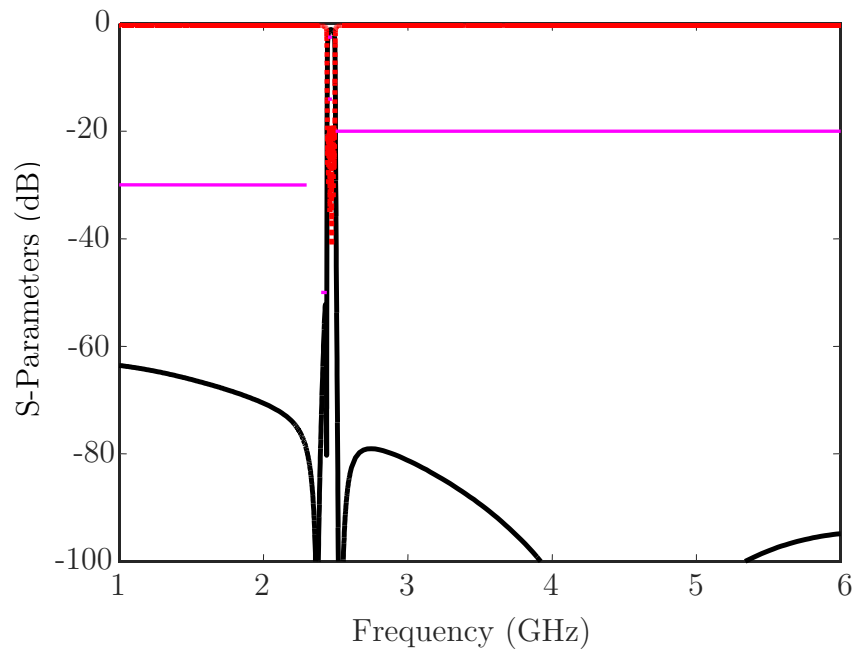


Figure 105 Out-of-band frequency response of the synthesized step filter #2

4.2.3 Multiplexers

Multiplexing has been since many years a largely used technique in MW/RF Front End Modules (FEM) to receive and transmit, sharing the antenna, different frequency bands at the same time. While Carrier Aggregation (CA) becomes inevitable to provide faster data services and mobile devices are intended to communicate on multiple LTE bands simultaneously –in many occasions, closely spaced in frequency-, the need for a more compact and elegant solution welcomes the use of multiplexers to address the challenge.

The major requirement for a multiplexer consists on providing the best achievable isolation between and within bands whilst keeping every single filter corresponding to each band well matched to the antenna. Minimizing insertion loss is always expected to maintain good reception [61] [62] [63].

Among the key features of multiplexers, compactness, design simplicity and reduced cost can also be listed. Therefore, it is no wonder that the use of multiplexer solutions becomes more and more important as the number of bands that operators aggregate increases.

When we face the design of a multiplexer, based on acoustic filters or not, we have to deal with the fact that connecting different filters to a common port (e.g. antenna port) most likely will change the load that every respective filter is terminated with. This is a major issue because we design every single filter to be well matched typically to a 50Ω antenna but now we have those 50Ω added to a few arbitrary loads with different frequency dependencies. This may cause unacceptable degradation on the filter performance even for slight changes of its termination load.

The most classic solutions have come up through the attempts to overcome the multiplexer design issues for a wide range of different filter technologies and architectures. In many occasions they place elements like hybrid couplers or circulators or they may involve *manifold* structures interconnecting the filters with many low-loss transmission lines [63]. Optimization techniques may get involved in order to make every filter to behave as similar as possible to an open circuit at the corresponding center frequencies of the other filters.

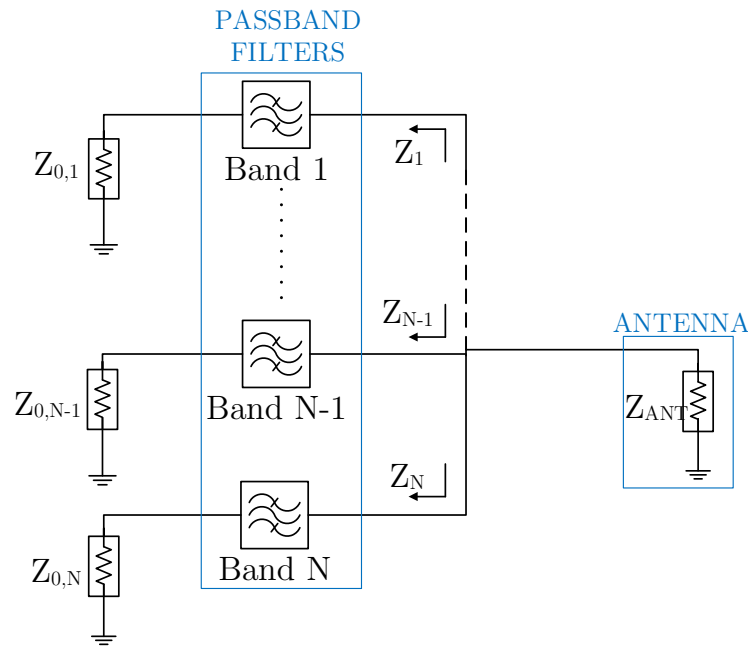


Figure 106. Scheme of an N-order multiplexer.

However, the element extraction synthesis allows facing the design in a systematic manner thus obtaining synthesized single filters which have great performance and at the same time have small affectation to the antenna load at those critical frequency ranges without either having to add a subsequent phase shift or any other kind of element. It goes without saying that the more filters you involve the higher the complexity of the problem. Therefore, the extraction element may show its limitations as the order of the multiplexer increases. Nevertheless, it has proven to be very useful for triplexers and quadplexers. In this work the followed approaches using the element extraction synthesis technique are two and the results are shown hereinafter. These two approaches are referred as *Phase approach* and *Output impedance approach*, both outlined in Sections 4.2.1.4 and 4.2.1.5, respectively.

Figure 106 shows a generic diagram of a multiplexer and Figure 107 shows the equivalent circuit including the perspective of one single filter loaded with the remaining filters and the antenna.

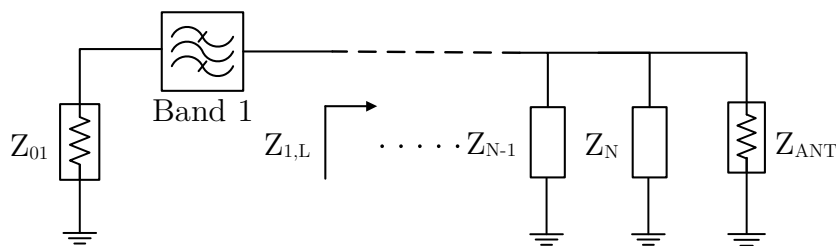


Figure 107. Equivalent circuit of an N-order multiplexer outlining the input impedance seen from the filter number 1.

According to the previous circuit in Figure 107 the following expression states the impedance that loads the filter i , which ideally should be equal to Z_{ANT} .

$$Z_{i,L}(f) = \frac{1}{Y_{ANT}(f) + \sum_{j=1, j \neq i}^N Y_j(f)} \quad (114)$$

When we analyze the overall system electrically, the port where all the filters are connected to the antenna is typically called the antenna port. In a subsystem level of analysis this port can be interpreted as either the input port of the filters (which makes sense in terms of the RX signal path that goes from the antenna through the filter) or the output port of the filters (which makes sense in terms of the TX signal path from the previous stages of the filter, such as a power amplifier, through the antenna).

This later choice also agrees with the concept of “direction” in which the filter has been synthesized using the element extraction technique. Therefore, and in order to avoid possible misunderstandings we must clarify that the naming criteria here has been the following:

- i. We name “filter output admittance” to the admittance of each filter seen from the antenna and they are expressed as Y_{out} .
- ii. We name “Port 2” or “output port of the filter” to the port connected to the antenna and its S-parameter is therefore S_{22} .

4.2.4 Phase (S_{22}) Approach

This approach is based on the observation of the S_{22} parameter of the filter. The S_{22} parameter of every filter taking part in the multiplexer gives information about which electrical impedance is seen from the antenna. This parameter can be also interpreted as the reflection coefficient of a 50Ω terminated filter considering the antenna port as the input port. It can be helpful either to depict the S_{22} on the Smith Chart (SC) or the *Phase* S_{22} itself vs frequency for this purpose.

We know that a value of the depicted S_{22} parameter placed on the right side of the SC means a high impedance for that particular frequency. This would be equivalent to behave as an open

circuit. The equivalent *Phase* S_{22} on that SC location would be close to $2\pi k$ where $k = 0, 1, \dots, n$ for any frequency value.

Therefore, if we pay careful attention to the S_{22} parameter while we design our filter we can try to make it fall close to the open circuit position of the SC for the center frequencies of the remaining filters. Equivalently we can try to make *phase* S_{22} take a value that is a multiple of $2\pi k$ [rad] for those frequencies.

If this consideration is taken while designing all the filters, at the end we will get that each filter have small affectation on the impedance of the remaining filters at their respective working frequency bands. Therefore, despite of having an antenna loaded with several filters, for the frequency band number 1 the signal will see a clear path to the filter 1, which will have a proper reflection coefficient and it will see a high reflection for the remaining filters. For the frequency band number 2 the signal will see a clear path to the filter 2 which will have a proper reflection coefficient and it will see a high reflection for the remaining filters and so on.

4.2.4.1 Triplexer and quadplexer examples with Phase (S_{22}) Approach

As we have mentioned previously when we are looking for the best synthesis for a filter we must keep in mind all the constrains related to the filtering characteristics, i.e. IL, RL, Out-of-Band rejection, and also additional requirements related to the practical implementation, i.e. size of the resonators, suitable k_e^2 values, size of the external elements, etc. When we are trying to find a good candidate filter for a multiplexer we need to add a new constrain to the problem. Thus we synthesize each filter trying to achieve as well a certain value of *phase* S_{22} at the center frequency of the other filters.

Case Study I. B3-B39 Triplexer example

The triplexer will serve the bands comprised between 1.71GHz and 1.735GHz (within the LTE Band 3 UL), 1.805GHz and 1.83GHz (within the LTE Band 3 DL) and 1.88GHz and 1.92GHz (LTE Band 39 itself).

Table 11 shows the goal specifications for the multiplexer frequency response and Table 12 shows the values of the parameters for each filter.

Requirement	Specification Value (dB)	Frequency Range
Return Loss (RL)	>15	In-Band
Cross Isolation	>65	Inter-Band
Out-of-Band Rejection	>45	1 to 6 GHz
Insertion Loss (IL)	<2	In-Band

Table 11. B3-B39 Triplexer Frequency Specifications

Requirement	B3UL	B3DL	B39
k_e^2 [%] serie	6.54	6.44	6.46
k_e^2 [%] shunt	6.60	6.50	6.49
Q serie	3450	2450.5	2648.2
R serie	0.39	0.38	0.36
Q shunt	2750.2	2750.2	2948.7
R shunt	0.38	0.39	0.37
C0min [pF]		0.8	
C0max [pF]		3	
External C max [nH]		1.5	
External L max [nH]		5	

Table 12. Simulation values for the stack of each band, and constrains related to the area of the resonators as well as to the external components for the Triplexer case study.

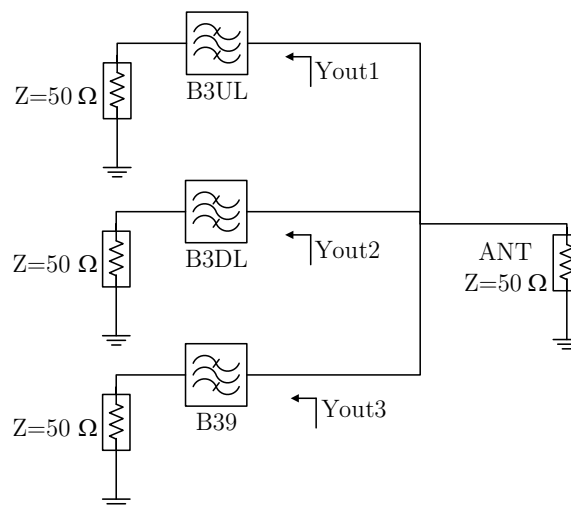


Figure 108. Scheme of the B3UL-B3DL-B39DL/UL triplexer.

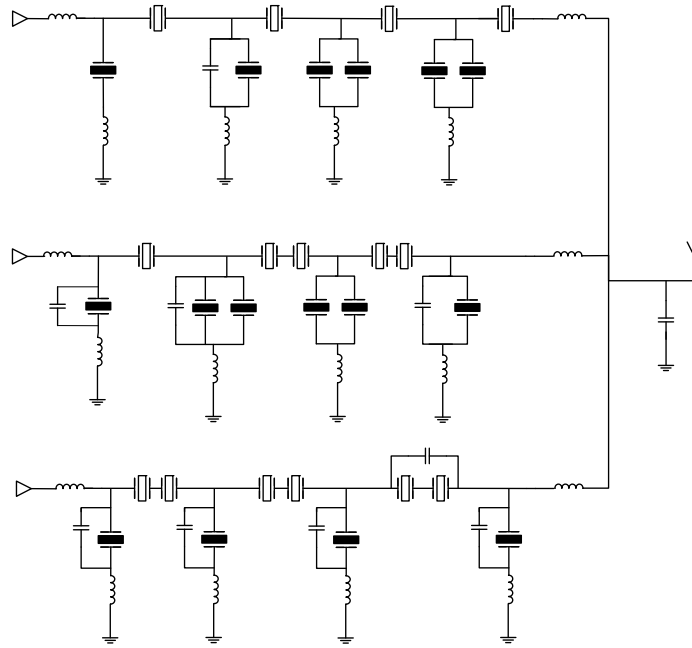


Figure 109. B3UL-B3DL-B39DL/UL triplexer topology following the approach described in paragraphs above. The following table, Table 13, details on the values of circuit components, where the output port is the antenna. The numbering starts by the input ports. Note as well that the overall output shunt capacitance corresponds to the addition of all output shunt capacitances.

Table 13. Summary of the resultant values of all the filters synthesized for the triplexer example, including k_e^2 , C_0 and f_s of each resonator and values of the external elements.

Figure 110 below shows the resulting triplexer response corresponding to the topology of Figure 109, with the corresponding values of Table 13.

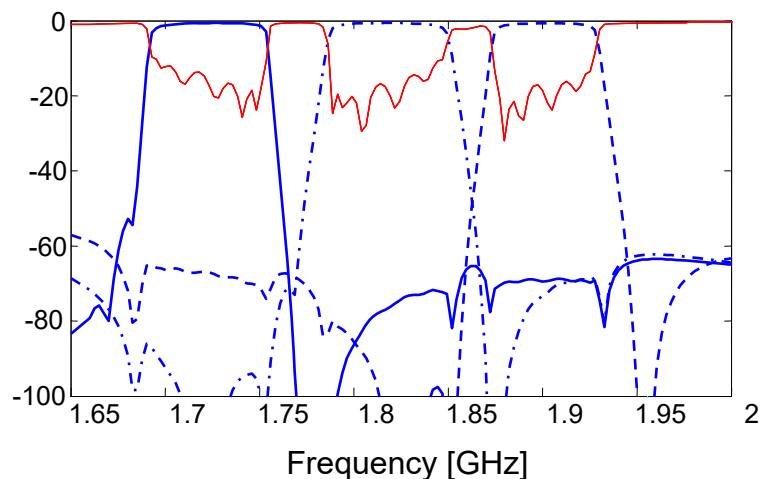


Figure 110. B3UL-B3DL-B39DL/UL triplexer response following the approach above.

Case Study II. Extended B3-B39 quadplexer example

In order to prove the validity of the phase approach and starting from the results of the B3-B39 triplexer we add a 4th band to extend the previous solution to a quadplexer configuration. This 4th band doesn't correspond to any LTE band as this solution represents a purely academic example. In that sense and in order to provide the scenario with some homogeneity the filter is synthesized aiming a 30MHz bandwidth (B3UL and B3DL filters are 25MHz and B39 is 40MHz) and a center frequency separation to its adjacent filter (B39) similar to the others (85MHz).

The achieved solution consists of a 7th order filter directly connected at the antenna port to the previous triplexer solution. Figure 111 shows the topology of the whole quadplexer along with its

corresponding values, detailed in Table 14. The values of the shunt capacitance of the B3DL has been slightly modified from 1.9 pF to 2.63 pF. Note that the values of Filters B3UL and B39 does not change. Figure 112 and 113, detail on the lossless and lossy responses of the final quadruplexer design, respectively.

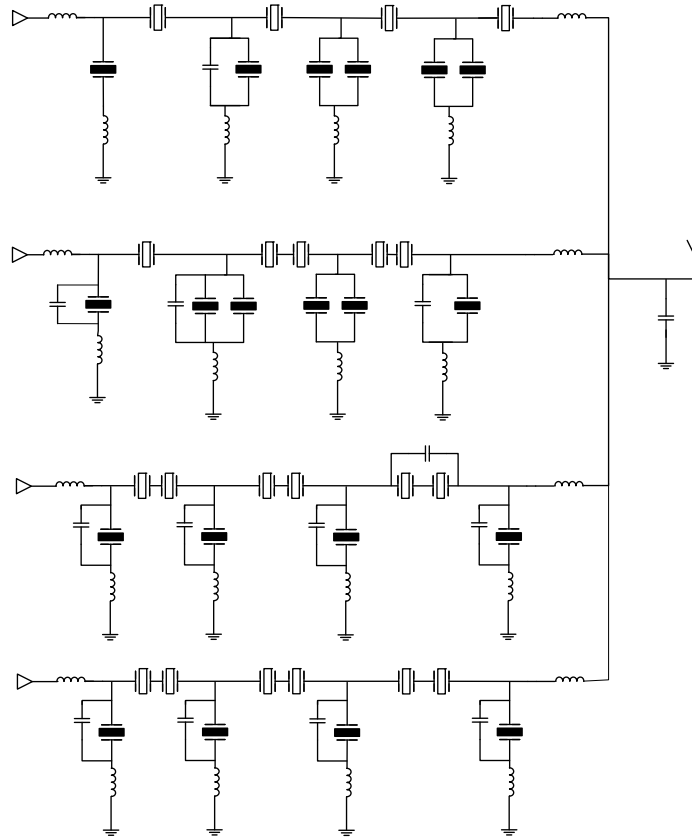


Figure 111. Quadruplexer topology following the approach described in paragraphs above. The following table, Table 14, details on the values of circuit components, where the output port is the antenna. The numbering starts by the input ports. Note as well that the overall output shunt capacitance corresponds to the addition of all output shunt capacitances.

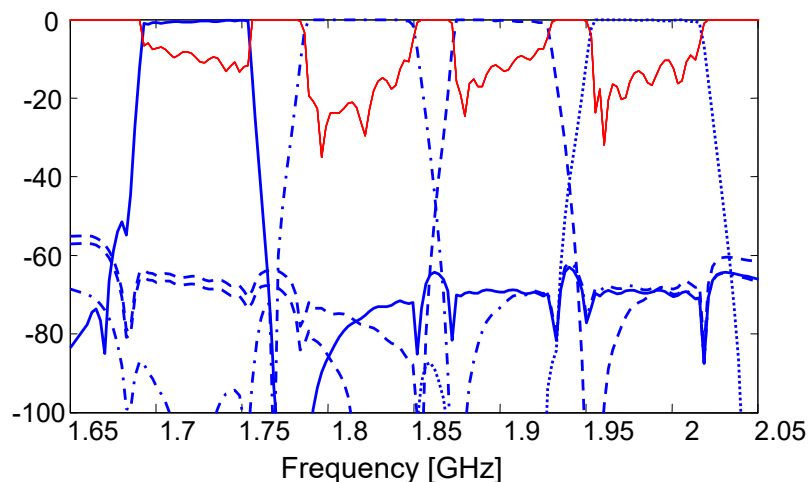


Figure 112. B3UL-B3DL-B39DL/UL+New filter Quadplexer.

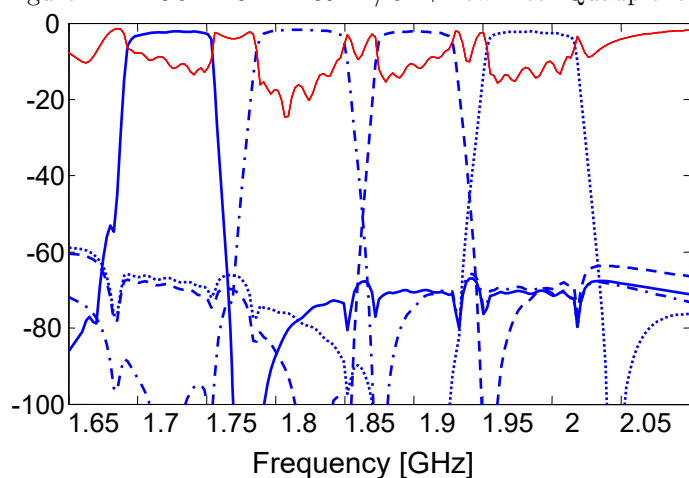


Figure 113. B3UL-B3DL-B39DL/UL+New filter Quadplexer. Losses are evaluated afterwards.

4.2.5 Output admittance approach

Alternatively, we could follow an approach based on the observation of the output impedance or admittance of the filter. This approach is similar to the previous one. Rather than obtaining high impedances for each filter at the rest of the frequency bands the aim of this approach would be to satisfy a set of equations.

For simplicity it is more convenient to work with admittances. For a triplexer case we would have a set of 3 independent equations, one for each of the 3 filters. Ideally, this equation system should comply the following equations:

$$\{Y_1(f) + Y_2(f)|_{f=f_3} = 0, \quad Y_1(f) + Y_3(f)|_{f=f_2} = 0 \quad \text{and} \quad Y_2(f) + Y_3(f)|_{f=f_1} = 0\}$$

In practical terms this means that the overall admittance at the antenna port for a certain frequency would be equivalent to the antenna's admittance. That is for each frequency band the

remaining filters have theoretically no effect over the overall impedance which we are loading the filter with.

4.2.5.1 Triplexer and Quadplexer examples with output admittance Approach

Case Study I. B3-B39 Triplexer example with Output admittance approach

Table 15 below lists the resulting parameters of the synthesized filters, including the external components. The corresponding triplexer response for both, narrowband and broadband scope are detailed in Figure 115. Figure 114, outlines and the topology corresponding to the table below.

As we know during the last steps of the element extraction for every single filter, that is, after the last resonator is synthesized, there is some reminder impedance that needs to be managed to achieve a proper adaptation to the corresponding termination load (here the antenna port). This impedance can be extracted in several different ways according to its value.

Probably the best way to adapt every filter intended to be part of the multiplexer to the antenna port consists of a small series inductance followed by a shunt inductance. The small series inductance provides a convenient solution in terms of losses, size and manufacture ease. Besides all the shunt inductances can be added in a single inductance of equivalent value which will be also smaller (again reduces losses and size) without degrading the overall performance.

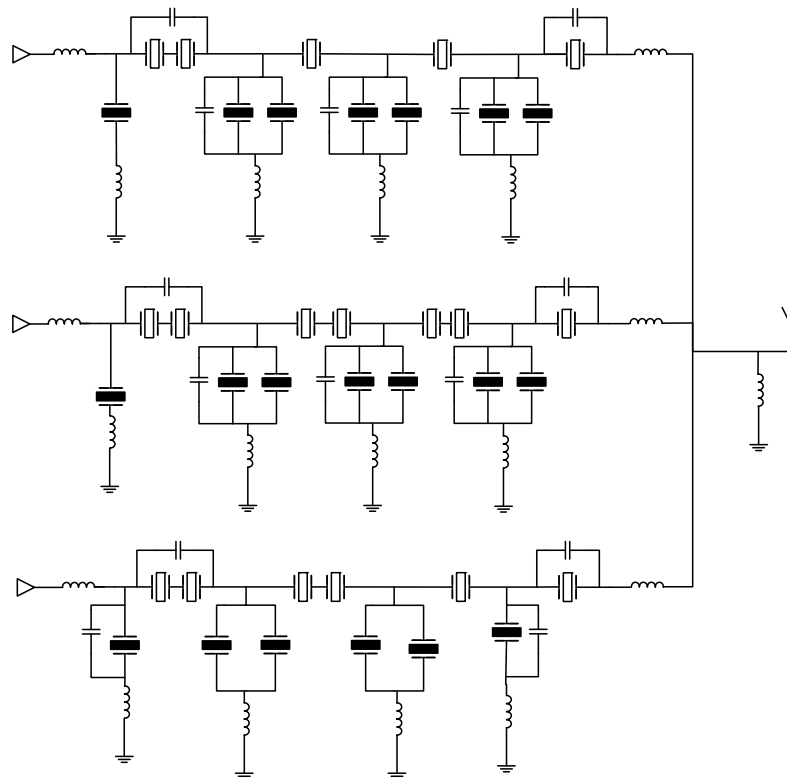


Figure 114. Detailed circuit of the synthesized triplexer.

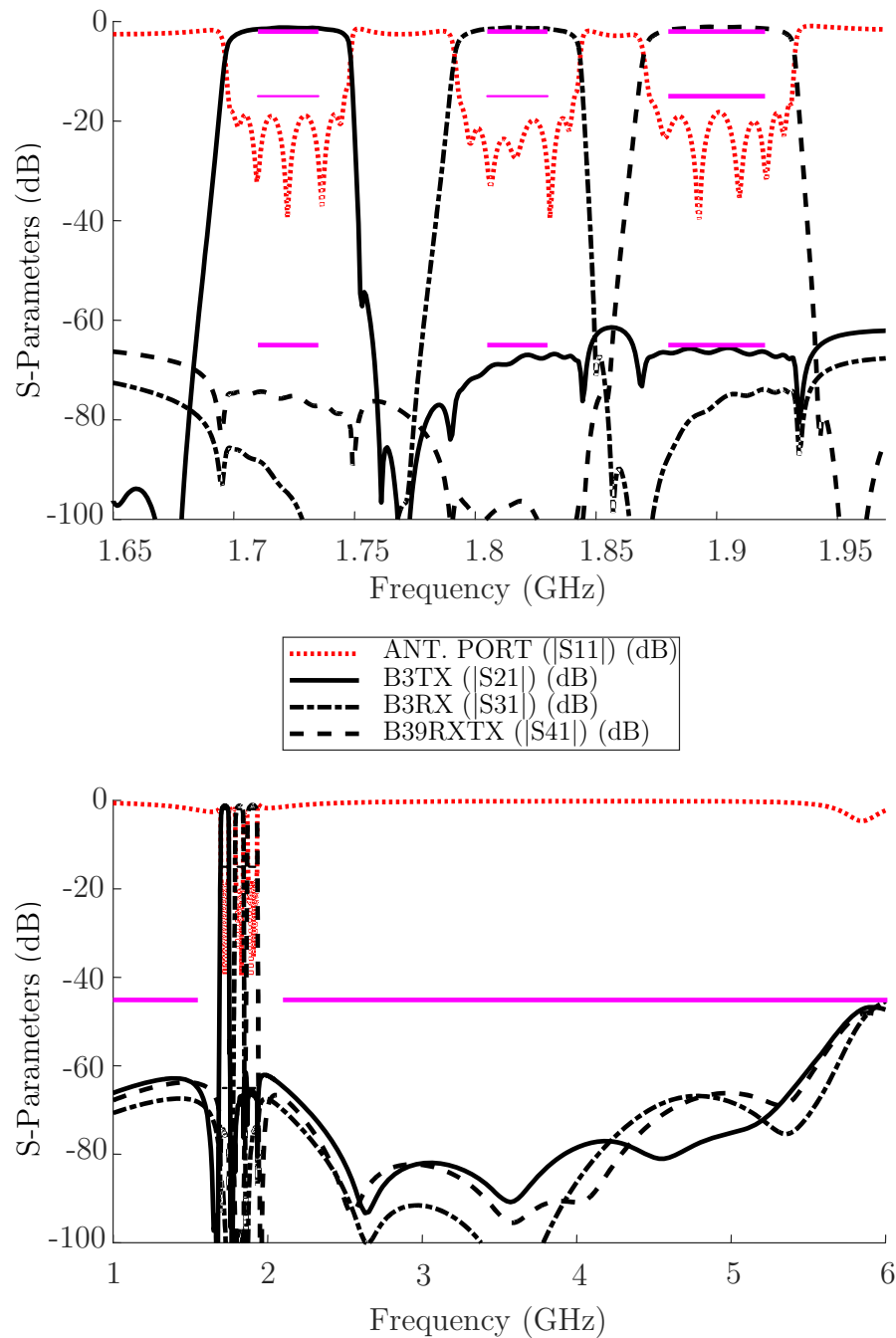


Figure 115. In-band and Inter-band Frequency response of the synthesized triplexer (above). Wide-band Frequency response of the synthesized triplexer (below).

Case Study II. Extended B3-B39 quadplexer example

As in previous approach section 4.2.1.4, the triplexer case has been extended to a quadplexer, with identical specifications than in previous case, section 4.2.1.4.1.

The achieved solution consists of a 6th order filter directly connected at the antenna port to the previous triplexer solution. The B3UL filter needs to be slightly modified in order to achieve the desired overall performance but the B3DL and B39 filter remain exactly the same.

Table 16. Summary of the resultant values of the additional filter and the modified B3UL filter synthesized for the quadplexer example, including k_e^2 , C_0 and f_s of each resonator and values of the external elements.

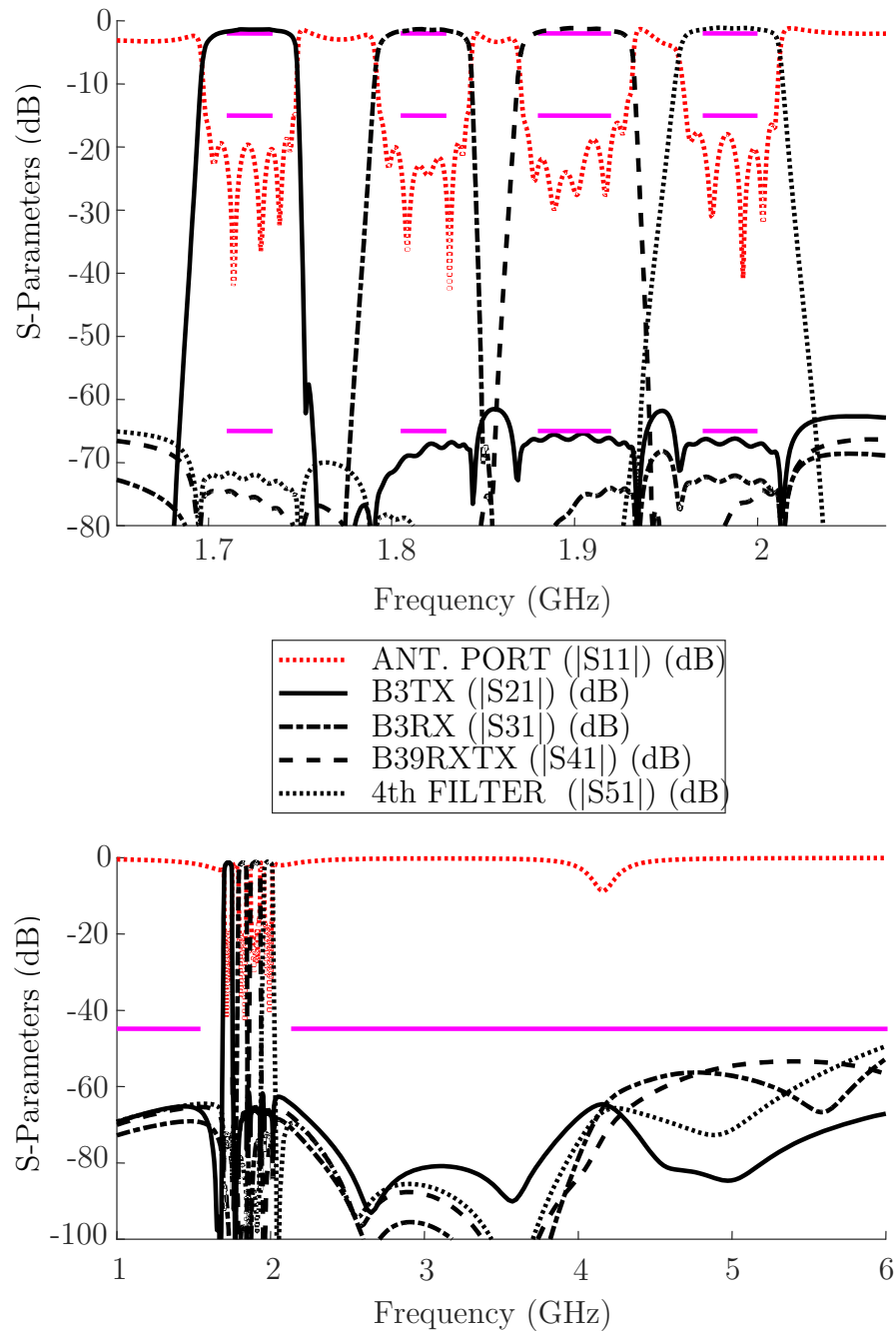


Figure 116. In-band and Inter-band Frequency response of the synthesized quadplexer (above). Wide-band Frequency response of the synthesized quadplexer (below).

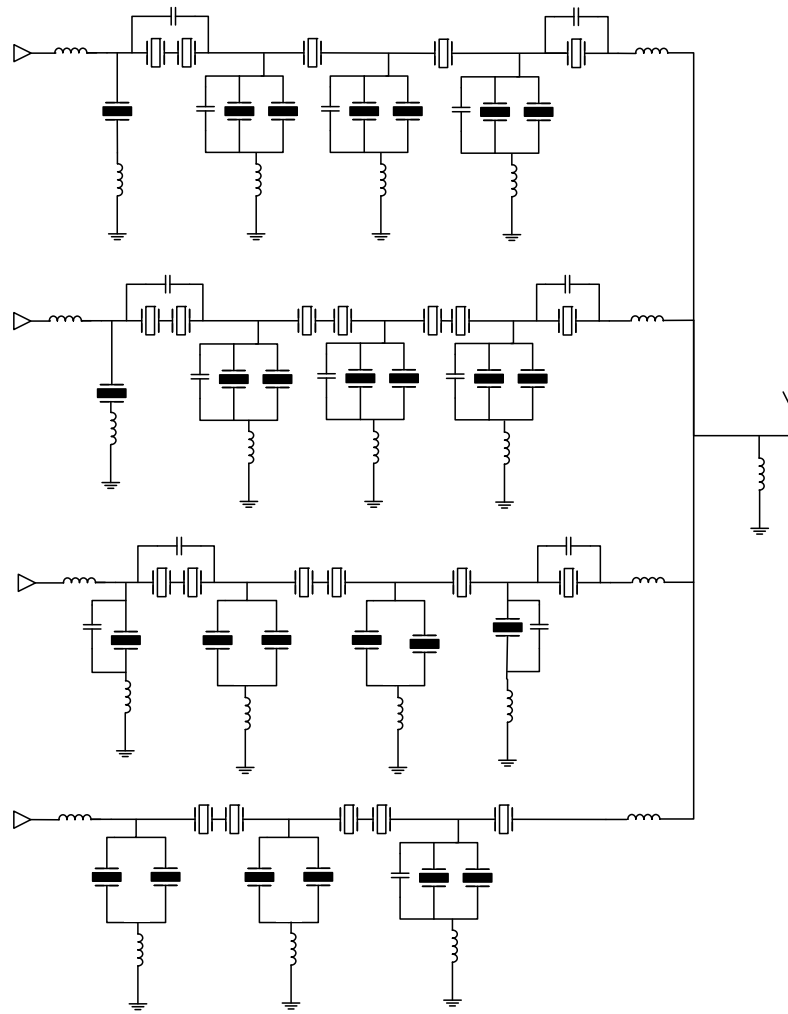


Figure 117. Detailed circuit of the synthesized quadplexer.

4.3 Case studies on transversal filters

Along Chapter 3 we demonstrate the benefits of synthesizing a transversal network for achieving responses hardly achievable with all other used topologies on the development of acoustic wave filters. Below we present three synthesized responses corresponding to real filter specifications of current and future licensed bands. Two of the examples would correspond to filters implemented with BAW technology and one would correspond to a filter implemented with SAW technology. The application in these two different technologies will further confirm the utility of the proposed novel topologies.

4.3.1 Band 71 - SAW configuration

This example corresponds to the RX Band 71. Details on the filter performance and implementation constrains are presented before the proposed transversal topology. In this case and due to the operating frequency, a SAW configuration will be assumed.

4.3.1.1 Band 71 - Specifications

Below are listed the most critical values of the specifications. Since Band 71 is a band has been recently licensed, not all the specifications are fully detailed. For this reason for instance the insertion loss value is not defined, and therefore the effects or losses are not evaluated in this example.

Passband RX:

- 615 to 654 MHz
- Max 14 dB Return Losses

Rejections:

- 30 dB from 604 to 610 MHz
- 40 dB below 604 MHz
- 55 dB for TX Band (661 MHz to 700 MHz)
- 35 dB above 700 MHz to 2.7 GHz

4.3.1.2 Band 71 - Implementation constrains

Some initial constrains regarding implementation aspects of the final topologies are:

4.3.1.3 Band 71 - Analysis and Synthesis

The filter response has been synthesized following the Approach IV, detailed in section 3.9. This approach outlines the relation between the impedances of the resonator and their resonant frequencies for a prescribed coupling coefficient. In this case we use a uniform coupling coefficient of 7.5%.

Figure 118 shows the resonant frequency dependence for each resonator as a function of their impedances. The square marks indicate the impedance and series resonant frequency required for each resonator in the case of non-external capacitors (C_5) want to be included in the final topology. Note that outlined in section 3.5, Approach I, this would require very high impedance resonators, nevertheless those are within the range of achievable impedances.

Impedance

Figure 118. Series resonant frequency as a function of the impedance of the resonator. In square marks are indicated the resonant frequencies and impedances when no external components are required.

Along with Figure 119, it is worth to indicate the value of C_5 required in the case of moving to a different value of impedance of the resonator. Note that this figure exhibits a singularity at the impedance points where no C_5 is needed (see Figure 119). Complimentarily, Figure 120 shows a zoom-in to the suitable values of the impedances showing the suitable values of C_5 .

Figure 120. Details C_5 values as a function of the impedance of each resonator.

As fully detailed in Chapter 3, the transversal topology requires of shunt inductances at the input and at the output of the filter. These shunt inductances come from the circuit transformation used to go from the conventional transversal network to the transversal network based on AW resonators. Moreover, these values depend on the initially incrustrated direct couplings, which those in turn depend on the prescribed coupling coefficient and on the prescribed impedances of the resonators. Figure 121 shows the required inductance values for a uniform coupling coefficient of 7.5% as a function of the impedance of the resonators. This particular case assumes all the resonators with uniform impedances, nevertheless this clearly illustrate the feasibility of these values, which for the case of 50Ω impedances would result in an inductance of 4 nH.

Finally Figure 122 shows the synthesized frequency responses by using the circuit parameters defined by the figures above for the case of assuming no-external capacitors, which corresponds to the lines labeled by Approach I and for the case of assuming uniform impedances to 50Ω for all resonators, labeled in the figure as Approach IV. Note that for the latter case, C_5 values as indicated in Figure 120 will be required.

Both responses would meet the specifications, at expenses of not applying any additional effect, such as losses, and the existence of lateral mode effects, which in any case will be more harmful in the case of smaller (higher) impedance resonators.

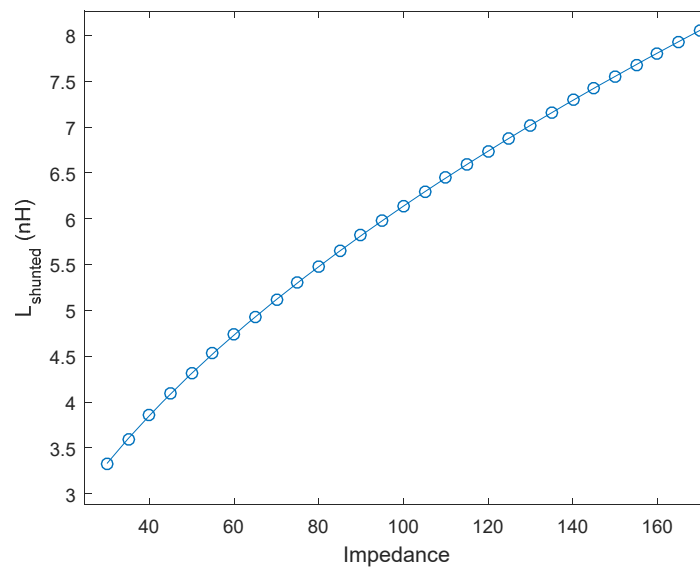


Figure 121. $L_{shunted}$ value as a function of the impedance of the resonators (assumes a uniform impedance).

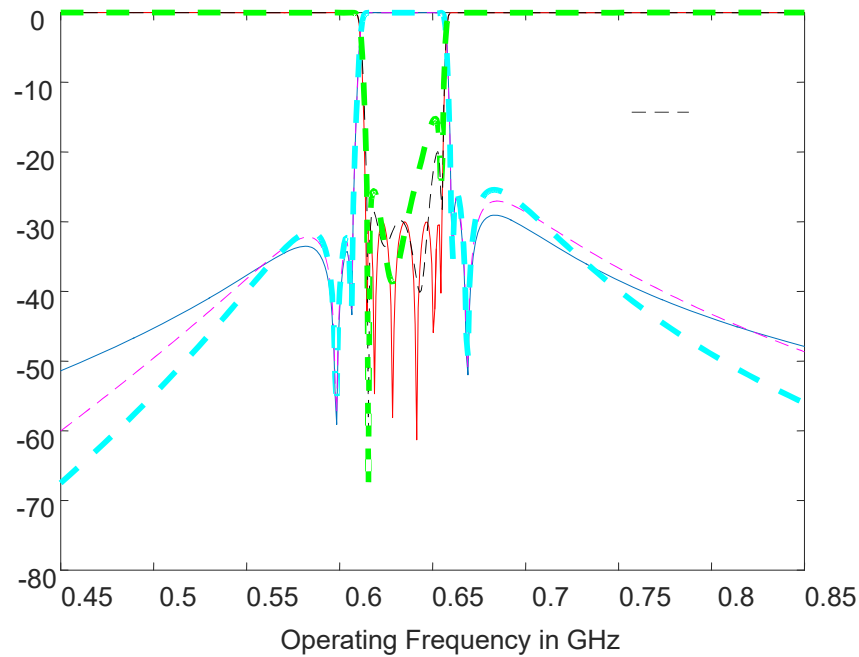


Figure 122. Synthesis response by means of a transversal topology. In blue and red solid line are, respectively, indicated S_{21} and S_{11} by evaluating the lossless distributed parameters. Pink and black dashed lines correspond to S_{21} and S_{11} the synthesized response with Approach I. Blue and green dashed thick lines correspond to S_{21} and S_{11} the synthesized response with Approach IV.

4.3.2 Band 41 - BAW configuration

This example corresponds to the RX Band 41. Details on the electrical requirements and implementation constraints are outlined before the synthesized response. In contrast with previous case the current filter would be implemented in a BAW configuration. Losses and other parasitic effects will be considered in this case.

4.3.2.1 Band 41 - Electrical performance requirements

The following table summarizes the frequency response requirements:

Frequency (MHz)	Min (dB)	Max (dB)	Parameter	Notes
2496 – 2690		-3	$S(2,1)$	<i>Insertion Loss</i>
2496 – 2690	17		$S(1,1)$ & $S(2,2)$	<i>Return Loss</i>
1710 – 1785	62		$S(2,1)$	B3Tx
1805 – 1880	62		$S(2,1)$	B3Rx

1920 - 1980	62	S(2,1)	B1Tx
2110 - 2200	62	S(2,1)	B66Rx
1850 - 1915	62	S(2,1)	B25Tx
1930 - 1995	62	S(2,1)	B25Rx
2400 - 2448	50	S(2,1)	ISM
2448 - 2471	60	S(2,1)	ISM
4992 - 5380	60	S(2,1)	H2
3500 - 6000	40	S(2,1)	<i>High Freq. Attenuation</i>

Table 17. B41 Filter Frequency Specifications

4.3.2.2 Band 41 - Implementation constrains

- Coupling range: 8% - 6.3%
 - A preferred solution is uniform coupling 6.3%
- Achievable impedances: 20 Ohm – 200 Ohm
 - High impedance resonator however present larger lateral mode effects (or BR).
 - In practice it is good to stay on resonators close to 50 Ohms
- All filters have to be input and output matched to 50 Ohm

In addition to the previous considerations in this case the filter will be evaluated considering a more complete model than the conventional BVD. This model, detailed in section 1.7, accounts for the area of the resonators, aspect ratio, Q factors and other resonator features. Values of the extended BVD model [53] used in this example and for this frequency range are listed in table below.

Parameter	Value	Units	Notes
k_e^2	6.30	%	<i>Coupling Coefficient</i>
A_{ref}	11400	um ²	<i>Area of reference resonator</i>
$inac$	0.06		<i>Inactive area of the reference resonator</i>
Q_m	929		<i>Q of the reference resonator</i>
Q_{lim}	3108.3		<i>Q of a very large resonator</i>
$qdeg$	0.6		<i>Power of degradation for Q</i>
R_s	0.68	Ohm	<i>Series Resistance</i>

AlN_{thick}	0.85	um	<i>AlN layer thickness</i>
ϵ_{r_AlN}	10.4		<i>AlN relative dielectric constant</i>

Table 18. Simulation values for the stack of the Band 41 filter.

Since the final proposed topology will contain external capacitors and inductors, their non-ideal effect such as losses, are quantified by means of Q_C and Q_L , respectively, in the Table 19. The table below also ranges the values of suitable capacitors, and the number of different resonant frequencies to be performed.

Parameter	Min.	Typ.	Max.	Units	Notes
C_{stat}	0.4		4	pF	<i>Range of static capacitors</i>
Q_L		20			<i>Quality factor for external</i>
Q_C		100			<i>Quality factor for external</i>
$\#f_s$	1		5		<i>Number of different resonant frequencies</i>

Table 19. Constrains related to the area and f_s of the resonators as well as to the external components for the Band 41 filter.

4.3.2.3 Band 41 - Analysis and Synthesis

Below, Figures 123 and 124 present the designing curves that meet the filter specifications of the previous section. Filter responses from the characteristic polynomials, transversal configuration without external elements and transversal configuration with all uniform resonators to 50Ω , are depicted in Figure 125.

At this point, it is worth to mention that such a wide band response and required selectivity at the lower side band would require at least 11 resonators in a ladder configuration.



Figure 124. a) Details C_5 values as a function of the impedance of each resonator. b) $L_{shunted}$ value as a function of the impedance of the resonators (assumes a uniform impedance).

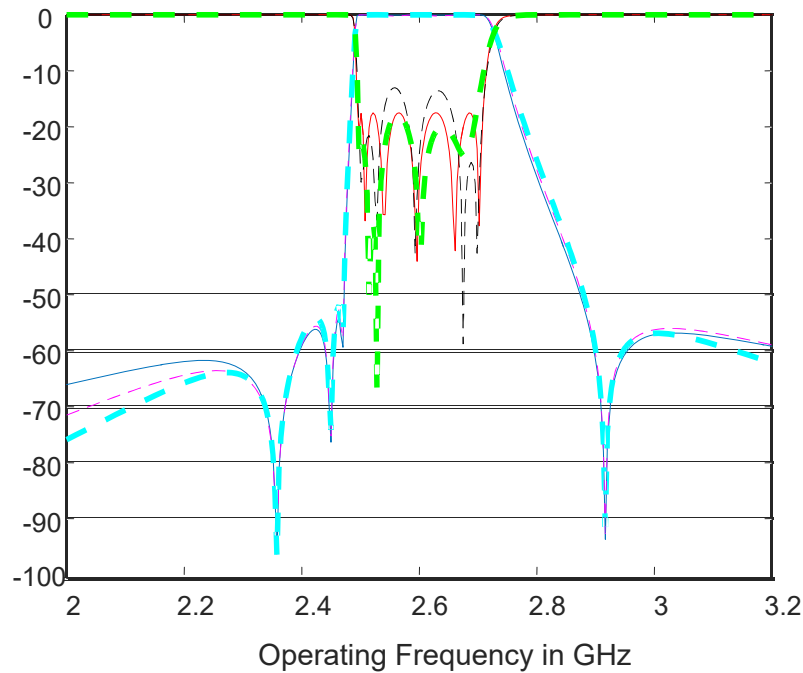


Figure 125. Synthesis response by means of a transversal topology. In blue and red solid line are, respectively, indicated S_{21} and S_{11} by evaluating the lossless distributed parameters. Pink and black dashed lines correspond to S_{21} and S_{11} the synthesized response with Approach I. Blue and green dashed thick lines correspond to S_{21} and S_{11} the synthesized response with Approach IV.

To move forward to a practical implementation, Figures 126 and 127 show a new synthesized response considering the losses of all the components forming the transversal network when each acoustic resonator is modeled by means of an extended BVD model [53]. Figure 126 shows the broadband response and Figure 127 details on the in-band insertion losses.

The initially proposed polynomials, indicated in red, are not identical to the previous case. The reason for that is because when the response above is evaluated with lossy components, due to sensitivity reason (see section 3.12) the electrical requirements are not met. The response corresponding to the characteristic polynomials have also been evaluated considering losses. In this case as uniform $Q=Q_m$ above have been used to calculate the dissipative value σ (see section 1.6).

Note that both responses do not perfectly overlap due to sensitivity reason, and although both would meet the specifications, the synthesized response offers less selectivity at the lower side band. The mask corresponding to the electrical requirements is indicated in black lines.

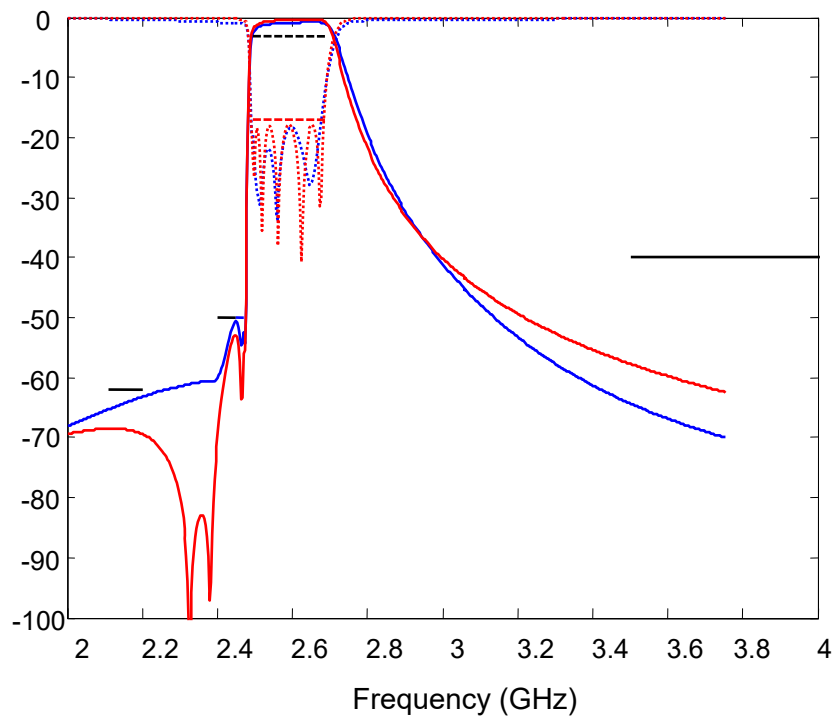


Figure 126. Broad band response of the synthesized response (blue), along with the lossy characteristic polynomials in red. The electrical filter requirements are indicated in black.

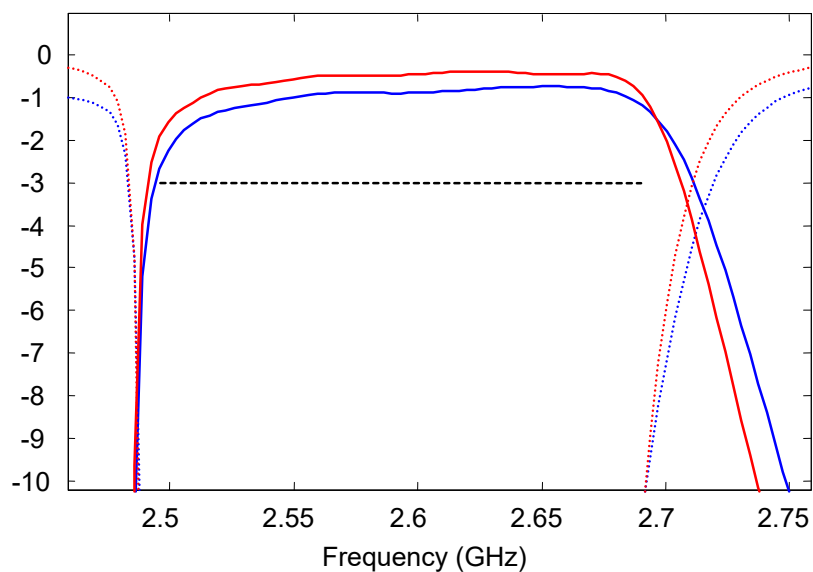


Figure 127. Details on the in-band insertion losses

The following table lists the values of the six resonators forming the transversal topology. As per the transversal topology, three of the six resonators need to be connected to one branch of the BALUN and the other three to the other branch. Those are not arbitrary, and in this case R1, R3 and R5, would go to the same branch and R2, R4 and R6 to the other branch.

Table 20. Summary of the resultant values of the synthesized Band 41 filter, including k_e^2 , C_5 , impedance and f_s of each resonator and values of the external elements.

4.3.3 Band 25- BAW configuration

The last example corresponds to the Band 25. As in previous cases, electrical and implementation requirements are presented before proposing a synthesized topology. In this case a BAW configuration is assumed.

4.3.3.1 Band 25 – Specifications

Frequency	Min(dB)	Max(dB)	Parameter	Notes
1930 - 1995		-2	S(2,1)	<i>Insertion Loss</i>
1930 - 1995	17		S(1,1) & S(2,2)	<i>Return Loss</i>
1850 - 1915	62		S(2,1)	B25Tx
1710 – 1780	62		S(2,1)	B66Tx
2500 – 2570	62		S(2,1)	B7Tx
2305 - 2315	62		S(2,1)	B30Tx
2496 – 2690	62		S(2,1)	B41
2400 - 6000	40		S(2,1)	<i>High Freq Attenuation</i>

Table 21. B25 Filter Frequency Specifications

4.3.3.1.1 Band 41 - Implementation constrains

Table 23. Constrains related to the area and f_s of the resonators as well as to the external components for the Band 25 filter.

4.3.3.1.2 Band 41 - Synthesis & losses evaluated afterwards

Figures 128 and 129, depict the broadband and the in-band response of the synthesized network. Losses are evaluated considering only losses in the resonators (and uniform Q) and losses considering also the effects of the external components, these are the series shunt capacitors and shunt input and output inductances.

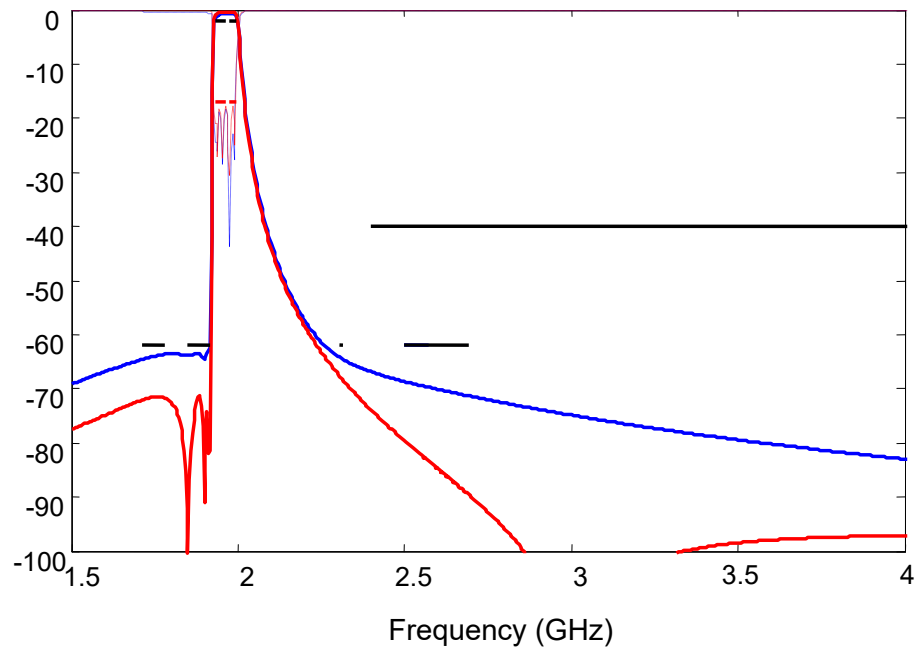


Figure 128. Broad band response of the synthesized response (blue), along with the lossy characteristic polynomials in red. The electrical filter requirements are indicated in black.

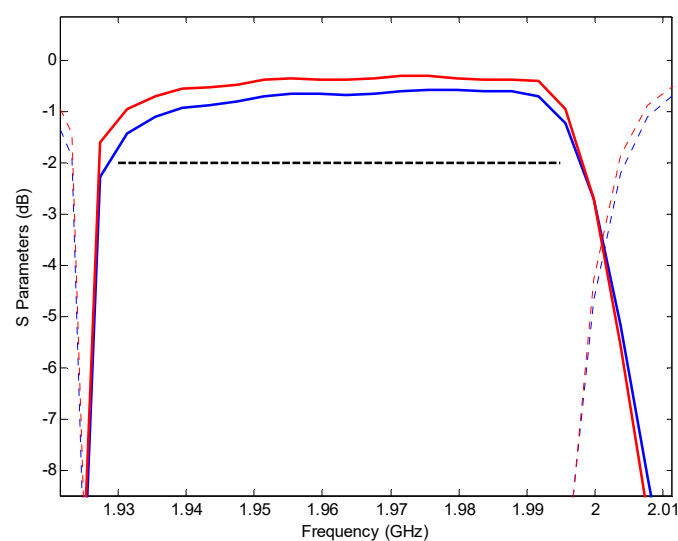


Figure 129. Details on the in-band insertion losses

The following table lists the values of the six resonators forming the transversal topology. As per the transversal topology, three of them need to be connected to one branch of the BALUN and the other three to the other branch. Those are not arbitrary, and in this case R_1 , R_3 and R_5 , would go to the same branch and R_2 , R_4 and R_6 to the other branch.

Table 24. Summary of the resultant values of the synthesized Band 25 filter, including k_e^2 , C_5 , impedance and f_s of each resonator and values of the external elements.

4.4 Conclusions

This chapter demonstrates the validity of the methodologies developed in Chapter 2 and 3, for ladder and transversal topologies, respectively. Both methodologies are applied to real cases where the electrical requirements and implementation constrains are considered along.

The method to synthesize ladder networks demonstrate to be very useful to provide topologies even in cases where the electrical constrains are very stringent and somehow non-trivial to be achieve in a ladder topology where the electro-coupling coefficient affects the filter bandwidth and selectivity of the filter, by means of the position of transmission zeros. All the synthesized networks with this topology have been implemented by the use of the software tool outline in section 4.1.

The ultimate case corresponding to the ladder topology corresponds to a triplexer specification, where stringent constrains on selectivity and isolation between channels have been achieved with the proposed solution. To further illustrate the validity of the software and methodology, this triplexer has been extended to a quadplexer case showing the flexibility and comprehensiveness of the method.

Novel transversal topologies have been evaluated for three cases. One case required the use of a SAW configuration, whereas the other two cases required the used of BAW configurations. All the specifications in these cases correspond to novel systems where not exist a product yet. Transversal topology demonstrates to be a suitable topology for giving response to the new stringent requirement. In some of those cases, such electrical requirement cannot be achieved with a ladder configuration with 6.8% of coupling coefficient. The transversal topology met those specifications with a reduced number of resonator (6 resonators). In these cases, we also observe however that the sensitivity might be an important drawback on the implementation of those filters.

CHAPTER 5

CONCLUSIONS AND FUTURE RESEARCH LINES

This last chapter gathers the conclusion of the research activities developed along this work and outlines some of the future research lines resulting from the activities pioneered in this work, mainly by the novel proposed transversal topology.

5.1 Conclusions

A general conclusion of this work is that we succeed with the objectives outlined in the introduction, by developing a comprehensive formulation and defining a systematic synthesis procedure for the design of AW filters. This certainly helps and speeds up the development of AW filters and therefore will help to further expand the use of the acoustic technology on the development of high-performance microwave filters and multiplexers.

To list in more detail the conclusions of the different part of the thesis, we consider the two main blocks of this work. First the synthesis approach for the well-established topology of ladder filter and then all the achievements and conclusions corresponding to the novel proposed topology of transversal acoustic filters.

Synthesis of ladder filters:

As a main conclusion of this part and major achievement is the development of a software package tool for the synthesis of ladder filters. This software contains all the mathematical formulation, circuit transformation and some implementation considerations to provide a set of potential filter candidates that are complained for a given electrical requirements. This code also allows the design of multiplexing structure by the definition of a step by step procedure. Although out of the scope of this work, this code also include the ability to evaluate some other undesired

effects always existing in a filter based on acoustic wave filters, such as nonlinear effects [59] and lateral modes effects [44].

This software also includes some practical features that help into the design process, as it is the variation of the synthesized values and the evaluation of the electrical response afterwards.

The possibility to provide such a useful tool response is due to the achievements/conclusions on the mathematical formulation and definition of a synthesis procedure. Those could be listed as:

- Definition of the characteristic polynomials responding to a ladder topology based on AW resonators.
- Definition of a lowpass prototype equivalent circuit that emulates the behavior of a BVD model.
- Definition of the recipe that allows to go from the mathematical formulation to the ladder network
- Definition of circuit transformations to obtain more suitable topology for a final implementation
- Demonstration of the utility of the proposed approach.

Synthesis of Transversal AW filters:

The definition of a novel topology for the design of AW filters has been created along with all the mathematical formulation and circuit transformation to clearly outline a synthesis process. Before listing the conclusions and achievements of this part, it is worth to mention that the novelty and promising applications and benefits of the proposed topology, result on the filling of a **US patent as a joint invention between UPC and Qorvo**.

The transversal topology demonstrates to be an **innovative topology** on the synthesis and design of Acoustic Waveguide (AW) filters, in both Surface AW (SAW) and Bulk AW (BAW) configurations, which allows to obtain high performance filter with **arbitrary response**, not achievable with the current state of the art electro-acoustic topologies.

The **novelty** of the new proposed topology extends on:

- The topology:
 - The topology itself is novel for acoustic filters
 - The topology allows to obtain the filter response without dependency of the acoustic coupling coefficient. This is a very novel aspect, since would allow to apply this topology with different and novel materials.
 - Flexibility on selecting the impedance (size) of the resonator.
 - Flexibility on selecting the resonant frequency of the resonators. This aspect is also very significant since have a direct impact on the layer thicknesses of the different resonators and therefore a huge impact on the fabrication process and cost.

- Filter response
 - The filter bandwidth does not depend on the resonator electro-acoustic coupling.
 - Location of transmission zeros is arbitrary, not limited to the resonator electro-acoustic coupling and it does not require additional external elements.
 - Self-equalized filter response is achievable without additional external elements.
 - Advance filter responses, such as multiband responses, are also achievable.

It is also worth to conclude at this point that the transversal topology has been evaluated under real scenarios in Chapter 4, that verify the innovative points above.

PUBLICATIONS AND OUTCOMES

Contribution to journals

- i. C. Collado, M. González-Rodríguez, J.M. González-Arbesú, J. Mateu, J. Verdú, A. Hueltes, *Feed-Forward Technique to Measure the reflection Coefficient under CW high power signals*; IEEE Transaction on Microwave Theory and Techniques, vol. 66, no 10, pp. 4627-4633, 2018
- ii. C. Collado, J. Mateu, D. Garcia-Pastor, R. Perea-Robles, A. Hueltes, S. Kreuzer, R. Aigner; *Nonlinear effects of SiO₂ Layers in BAW Resonators*; IEEE Transaction on Microwave Theory and Techniques, vol. 66, no 4, pp. 1773-1777, 2018
- iii. J. Mateu, C. Collado, A. Hueltes, J.M. O'Callaghan, D. Garcia-Pastor, R. Perea-Robles, N. Joshi, X. Lu, N. Orloff, and J.C. Booth; *Comprehensive Circuit Model of Auto-limiting Superconductor Devices*; IEEE Transaction Applied Superconductivity, vol. 27, no. 5, pp., 2017.
- iv. Hueltes, E. Rocas, C. Collado, J. Mateu, N. Orloff, J.C. Booth, D. Garcia-Pastor, R. Perea-Robles; *Three-Port Frequency-Selective Absorptive Limiter*; IEEE Microwave and Wireless Components letters, vol. 27, no. 5, pp. 479 – 481, 2017.
- v. Carlos Collado, Alberto Hueltes, Eduard Rocas, Jordi Mateu, James. C. Booth, J.M. O'Callaghan, J. Verdu; *Absorptive Limiter for Frequency Selective Circuits*; IEEE Microwave and Wireless Components Letters, vol. 24, no. 6, pp. 415 - 417, June 2014
- vi. Alberto Hueltes, Jordi Verdu, Carlos Collado, Jordi Mateu, Eduard Rocas, J.L. Valenzuela; *Filtenna Integration Achieving Ideal Chebyshev Return Losses*; Radioengineering. vol. 23, no. 1. pp. 362 – 368, April 2014.
- vii. Eduard Rocas, Jordi Mateu, Carlos Collado, Alberto Hueltes, Jordi Verdú, C. Billard, J.B. David, A. Reindhardt; *Nonlinear Performance of BAW Filters Including BST Capacitors*; Radioengineering. vol. 23, no. 1, pp. 369 – 374, April 2014.

Contribution to conferences

- i. J. Mateu, C. Collado, A. Hueltes, R. Perea-Robles, R. Aigner, N. Khlát, *Acoustic Wave Filters for Enhanced Performance*, 2018 IEEE International Ultrasonic Symposium (IUS).

- ii. J. Mateu, C. Collado, A. Hueltes, R. Perea-Robles, D. Garcia-Pastor, M. González-Rodríguez, J.M. Gonzalez-Arbesú, *Outline process from the synthesis towards the nonlinear modeling of BAW filters*, 2018 IEEE/MTT-S International Microwave Symposium- IMS.
- iii. J. Mateu, C. Collado, A. Hueltes, *Novel topology for enhanced response of acoustic wave filters* , IWWMF-2018, ESA Sept. 2018
- iv. D. Garcia-Pastor, M. Gonzalez-Rodríguez, C.Collado, J.Mateu, J.M. Gonzalez-Arbesu, A. Hueltes, S. Kreuzer, R. Aigner; *Nonlinear effects of Electrode and Bragg Reflector Materials in BAW Resonators*; IEEE International Ultrasonics Symposium, Washington, DC, USA, Sep 2017.
- v. Eduard Rocas, Carlos Collado, Jordi Mateu, Alberto Hueltes, Jordi Verdu, Robert Aigner; *A Lateral Modes Model for Membrane BAW Resonators*; IEEE International Ultrasonics Symposium, Chicago, IL, USA, Sep 2014.
- vi. Eduard Rocas, Carlos Collado, Jordi Mateu, Alberto Hueltes, Jordi Verdú, Robert Aigner, James. C. Booth; *Performance of BAW Resonators at Cryogenic Temperatures*; IEEE International Ultrasonics Symposium - UFFC, Prague, Czech Republic, Jul 2013.
- vii. Carlos Collado, Jordi Mateu, Alberto Padilla, Alberto Hueltes, Juan M. O'Callaghan, Cristoph Ernst; *Practical Considerations in the Design of Lossy Cavity Filters*; International Workshop on Microwave Filters, CNES, Toulouse, France, 2012.
- viii. *Eduard Rocas, Carlos Collado, Robert Aigner, J.C. Booth, Jordi Mateu, Alberto Hueltes; A consistent methodology to characterize BAW resonators; IEEE International Ultrasonics Symposium, Dresden, Germany, Oct 2012.*

Patents

- i. TITLE: Acoustic Wave Filters in Transversal Configuration.
INVENTORS: J. Mateu, C. Collado, A. Hueltes, R. Aigner, N. Khlal
APPLICATION NUMBER: 2867-2184P - Priority Country/Date: USA/2017.
- ii. TITLE: Método y sistema de medida de parámetros eléctricos de dispositivos de radiofrecuencia bajo condiciones de alta potencia.
INVENTORS: C Collado, J Mateu, J M. González, A Hueltes, M González, D García, R Perea
APPLICATION NUMBER: P2017300571 - Priority Country/Date: Spain/2017.

Software: Synthesis of Ladder Acoustic Wave filterssoftware

Authors: A.Hueltes, J. Mateu, C .Collado; Signal Theory and Communications Dept - Universitat Politècnica de Catalunya (UPC). Copyright: ©2017 Universitat Politècnica de Catalunya (UPC)

Description: The software package is powered to synthesize filters based on Acoustic Wave Resonators using the classical General Chebyshev polynomials where prescribed Transmission Zeros and prescribed Insertion Loss are the two most characteristic input parameters. This software is on one hand able to synthesize topologies that provide with filtering responses from different order filters, bandwidths, center frequencies, return losses and position of the transmission zeros. Also is able to provide the user with several network topologies for a particular given response. It allows to manipulate not only all the parameters involved in the synthesis but many other parameters related to additional post-synthesis features like evaluating the effect of losses, add external lumped elements or interconnect stored synthesized filters in a multiplexer solution. It provides with a lot of flexibility and show the effect of each modification instantaneously.

Secondments:

- i. INSTITUTION: National Institute of Standards and Technology (NIST), Boulder, CO (USA), Oct 2016 - Dec 2016.
ATTENDING AS: Guest Researcher. Collaboration with the Radio Frequency Technology Division on Measurements Systems and Modeling for advanced filters and multiplexers.
- ii. INSTITUTION: QORVO Inc, Apopka, FL (USA), May 2016 - July 2016.
ATTENDING AS: Engineering Trainee. Collaboration with the R&D and Advanced Filter Design Team. Training on BAW Filters design workflow.

APPENDIX 1: Demonstration of Equivalent Circuits

The procedure to go from the conventional transversal network into a transversal network based on BAW resonators is based on the insertion of additional cross couplings that compensate each other. This implies that some of the couplings need to be negative. The negative coupling can be also transformed into BVD resonators, by the inclusion of a transformer.

The formulation above demonstrates that the circuits of Figure 52b and 53b are equal.

The following set of equations A.1-A.5, outline the ABCD and Y matrix of basic building blocks used in such transformations, those are a series impedance Z_{series} , and admittance inverter J and a transformer (-1) T.

$$ABCD_{Z_{series}} = \begin{bmatrix} 1 & Z \\ 0 & 1 \end{bmatrix} \quad A.1$$

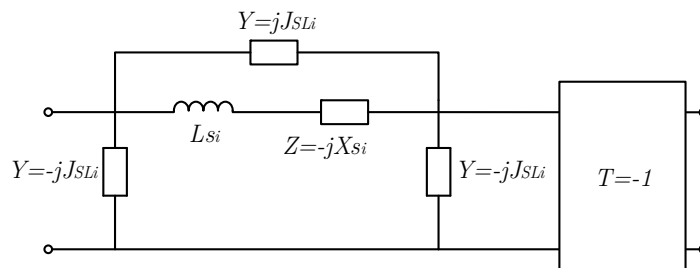
$$ABCD_J = \begin{bmatrix} 0 & \frac{1}{jJ} \\ -jJ & 0 \end{bmatrix} \quad A.2$$

$$ABCD_{T=-1} = - \begin{bmatrix} 1 & 0 \\ 0 & 1 \end{bmatrix} \quad A.3$$

$$Y_J = \frac{1}{jJ} \begin{bmatrix} 0 & 1 \\ 1 & 0 \end{bmatrix} \quad A.4$$

$$Y_{Z_{series}} = \frac{1}{Z} \begin{bmatrix} 1 & -1 \\ -1 & 1 \end{bmatrix} \quad A.5$$

Circuit 1: The first circuit corresponds to network described in Figure 53b and recall below.



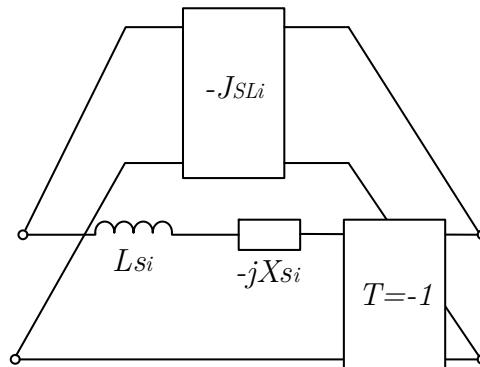
The overall ABCD matrix of such network is obtained by A.8 through the following calculations:

$$Y_{TOTAL} = Y_{Z_{series}} + Y_J = \begin{bmatrix} \frac{1}{Z} & \frac{1}{jJ} - \frac{1}{Z} \\ \frac{1}{jJ} - \frac{1}{Z} & \frac{1}{Z} \end{bmatrix} \quad \text{A.6}$$

$$ABCD_{TOTAL} = \frac{1}{\frac{1}{jJ} - \frac{1}{Z}} \begin{bmatrix} -\frac{1}{Z} & -1 \\ \frac{1}{jJ} - \frac{1}{Z} & -\frac{1}{Z} \end{bmatrix} \quad \text{A.7}$$

$$ABCD_{TOTAL} * ABCD_{T=-1} = \frac{-1}{\frac{1}{jJ} - \frac{1}{Z}} \begin{bmatrix} -\frac{1}{Z} & -1 \\ \frac{1}{jJ} - \frac{1}{Z} & -\frac{1}{Z} \end{bmatrix} \quad \text{A.8}$$

Circuit 2: Analogously the circuit of Figure 52b, recall below, results in the ABCD matrix developed through A.14.



$$ABCD_{Z_{series}} * ABCD_{T=-1} = - \begin{bmatrix} 1 & Z \\ 0 & 1 \end{bmatrix} \quad \text{A.9}$$

$$ABCD_J * ABCD_{T=-1} = - \begin{bmatrix} 0 & \frac{1}{jJ} \\ -jJ & 0 \end{bmatrix} \quad \text{A.10}$$

Transforming the above into Y matrices,

$$Y_{J_{T=-1}} = \frac{-1}{jJ} \begin{bmatrix} 0 & 1 \\ 1 & 0 \end{bmatrix} \quad \text{A.11}$$

$$Y_{Z_{series_{T=-1}}} = \frac{1}{Z} \begin{bmatrix} 1 & 1 \\ 1 & 1 \end{bmatrix} \quad \text{A.12}$$

$$Y_{TOTAL_{T=-1}} = Y_{Z_{series_{T=-1}}} + Y_{J_{T=-1}} = \begin{bmatrix} \frac{1}{Z} & -\frac{1}{jJ} + \frac{1}{Z} \\ -\frac{1}{jJ} + \frac{1}{Z} & \frac{1}{Z} \end{bmatrix} \quad \text{A.13}$$

$$ABCD_{TOTAL_{T=-1}} = \frac{1}{-\frac{1}{jJ} + \frac{1}{Z}} \begin{bmatrix} -\frac{1}{Z} & -1 \\ \frac{1}{j^2} + \frac{2}{Z^2} & -\frac{1}{Z} \end{bmatrix} \quad \text{A.14}$$

The previous and simple circuit analysis demonstrates that the network of Figure 52b is identical to the Figure of 53b.

References

- [1] 3GPP, "LTE; evolved universal terrestrial radio access (E-UTRA); user equipment (UE) radio transmission and reception," Tech. Report. 3GPP TS 36.101, version 10.17.0, 2015.
- [2] G. Hueber, "Cost-Efficient High-Volume Transmission," *Microwave Magazine, IEEE*, pp. 26-46, 2015.
- [3] P. W. Andreas Link, "Golden Age for filter design," *Microwave Magazine, IEEE*, vol. 16, n° 7, pp. 60-72, 2015.
- [4] T. Bauer, "A Bright Outlook for Acoustic Filtering," *Microwave Magazine*, vol. 16, n° 7, pp. 73-81, 2015.
- [5] T. Gillenwater, "Evolution of the Smartphone," *Microwave Journal*, February 2017.
- [6] R. Ruby, "The 'how & why' a deceptively simple acoustic resonator became the basis of a multi-billion dollar industry," de *IEEE 30th International Conference on Micro Electro Mechanical Systems (MEMS)*, Las Vegas, NV, USA, 2017.
- [7] R. Muller, RF 5G for Dummies, Special Edition, John Wiley & Sons, 2016.
- [8] L. Miller, Carrier Aggregation Fundamentals for Dummies, Special Edition, John Wiley & Sons, 2016.
- [9] R. Ruby, "A Snapshot in Time: The Future in Filters for cells phones," *IEEE Microwave Magazine*, vol. 16, n° 7, pp. 46-59, 2015.
- [10] W. Mason, Physical acoustic principles and methods, Academic Press, 1964.
- [11] K. M. Lakin, "Thin film BAW filters for wide bandwidth and high performance applications," de *IEEE MTT-S International Microwave Symposium Digest*, Fort Worth, TX, USA, 2004.
- [12] K. Lakin, "Thin film resonator technology," *IEEE Transactions on Ultrasonics, Ferroelectrics, and Frequency Control*, vol. 52, n° 5, pp. 707-716, 2005.
- [13] K. Lakin, "Thin film bulk acoustic wave filters for GPS," vol. 1, pp. 471-476, 1992.
- [14] R. Ruby, P. Bradley, D. Clark, D. Feld, T. Jamneala y K. Wang, "Acoustic FBAR for filters, duplexers and front end modules," de *IEEE MTT-S International Microwave Symposium Digest*, Fort Worth, TX, USA, 2004.
- [15] R. Ruby, J. Larson, C. Feng y S. Fazzio, "The effect of the perimeter geometry on FBAR resonator electrical performance," de *IEEE MTT-S International Microwave Symposium Digest*, Long Beach, CA, USA, 2005.
- [16] G. G. Fattinger, A. Volatier, M. Al-Joumayly, Y. Yusuf, R. Aigner, N. Khlal y M. Granger-Jones, "Carrier aggregation and its challenges - or: The golden age for acoustic filters," de

- IEEE MTT-S International Microwave Symposium (IMS)*, San Francisco, CA, USA, 2016.
- [17] P. Warder y A. Link, "Golden Age for Filter Design: Innovative and Proven Approaches for Acoustic Filter, Duplexer, and Multiplexer Design," *IEEE Microwave Magazine*, vol. 16, n^o 7, pp. 60-72, 2015.
- [18] R. Aigner, "RF-MEMS filters manufactured on silicon: key facts about bulk-acoustic-wave technology," de *Topical Meeting on Silicon Monolithic Integrated Circuits in RF Systems*, Grainau, Germany, 2003.
- [19] R. Aigner, J. Kaitila, J. Ella, L. Elbrecht, W. Nessler, M. Handtmann, T.-R. Herzog y S. Marksteiner, "Bulk-acoustic-wave filters: performance optimization and volume manufacturing," de *IEEE MTT-S International Microwave Symposium Digest*, Philadelphia, PA, USA, 2003.
- [20] R. Aigner, "SAW and BAW technologies for RF filter applications: A review of the relative strengths and weaknesses," de *IEEE Ultrasonics Symposium*, Beijing, China, 2008.
- [21] R. Aigner, "Filter technologies for converged RF-frontend architectures: SAW, BAW and beyond," de *Topical Meeting on Silicon Monolithic Integrated Circuits in RF Systems (SiRF)*, New Orleans, LA, USA, 2010.
- [22] R. Aigner, "Tunable Filters? Reality Check. Foreseeable Trends in System Architecture for Tunable RF Filters," *IEEE Microwave Magazine*, vol. 16, n^o 7, pp. 82-88, 2015.
- [23] K.-Y. Hashimoto, *RF Bulk Acoustic Wave Filters for Communications*, Artech House Publishers, 2009.
- [24] G. Matthaei, *Microwave Filters, Impedance Matching Networks and coupling structures.*, Norwood, MA: Artech House, 1980.
- [25] R. Cameron, *Microwave filters for communication systems. Fundamentals, design and applications.*, Wiley-Interscience, 2007.
- [26] E. Atia, "Narrow-band multiple-coupled cavity synthesis," *IEEE Transactions on Circuits and Systems*, vol. 21, pp. 649-655, 1974.
- [27] J-S Hong, *Microstrip Filters for RF/Microwave Applications*, John Wiley & Sons, 2001.
- [28] I. Hunter, *Theory and Design of Microwave Filters*, IEE Electromagnetic Waves Series 48, 2000.
- [29] M. Yu, "Predistortion Technique for Cross-Coupled Filters and its application to satellite communication systems," *IEEE Trans. On Microwave Theory and Techniques*, Vols. %1 de %251, No. 12, Dec. 2003.
- [30] I. Hunter, "Passive Microwave Receive Filter Networks Using Low-Q Resonators," *IEEE Microwave Magazine*, Sept. 2005.
- [31] M. Yu, "Shrinking Microwave Filters," *IEEE Microwave Magazine*, pp. 40-54, 2005.
- [32] J. Mateu et al, "Direct synthesis of lossy filters: Use for 4th order filter with uniform Q distribution," de *International Workshop on microwave filters*, Toulouse, 2009.
- [33] J. Mateu et al., "Synthesis of 4th order lossy filter with uniform Q," de *International*

- microwave symposium*, 2010.
- [34] A. Shirakawa, J.-M. Pham, P. Jarry y E. Kerherve, "Bulk acoustic wave coupled resonator filters synthesis methodology," de *European Microwave Conference*, Paris, France, 2005.
 - [35] J. Fan, M. Chatras y D. Cros, "Synthesis Method for BAW Filters Computation," de *IEEE 13th International Conference on Electronics, Circuits and Systems (ICECS)*, Nice, France, 2006.
 - [36] S. Giraud, S. Bila, M. Chatras, D. Cros y M. Aubourg, "Bulk acoustic wave filter synthesis and optimization for UMTS applications," de *European Microwave Conference*, Rome, Italy, 2009.
 - [37] E. C. López, "analysis and Design of Bulk Acoustic Wave Filters Based on Acoustically Coupled Resonators," Universitat Autònoma de Barcelona (UAB), 2011.
 - [38] M. J. Blasco, "A coupling matrix vision for mobile filtering devices with micro-acoustic wave technologies. A systematic approach.," Universitat Autònoma de Barcelona (UAB), 2015.
 - [39] A. R. G. Bonastre, "RF Filters and Multiplexers Based on Acoustic Wave Technologies with Ladder-Type and Cross-Coupled Topologies," Universitat Autònoma de Barcelona (UAB), 2016.
 - [40] J. Verdú, I. Evdokimova, P. d. Paco, T. Bauer y K. Wagner, "Synthesis methodology for the design of acoustic wave stand-alone ladder filters, duplexers and multiplexers," de *IEEE International Ultrasonics Symposium (IUS), 2017*, Washington, DC, USA, 2017.
 - [41] I. Evdokimova, A. Gimenez, J. Verdú y P. d. Paco, "Synthesis of ladder-type acoustic filters in the band-pass domain," de *2017*, Nuremberg, Germany, IEEE 47th European Microwave Conference (EuMC).
 - [42] E. Rocas, C. Collado "Unified model for bulk acoustic wave resonators," de *International Ultrasonic Symposium*, 2009.
 - [43] E. Rocas, C. Collado "Electro-Thermo-Mechanical Model for Bulk Acoustic Wave Resonator," *IEEE Trans. on Ultrasonic, Ferr and Freq. Control*, vol. 60, nº 11, 2013.
 - [44] C. Collado, et al "A lateral modes model for BAW resonator," de *International Ultrasonic Symposium*, Chicago, 2014.
 - [45] J. Kaitila, M. Ylilammi, J. Ella y R. Aigner, "Spurious resonance free bulk acoustic wave resonators," de *IEEE Symposium on Ultrasonics*, Honolulu, HI, USA, USA, 2003.
 - [46] J. Kaitila, M. Ylilammi, and J. Ellä, "Resonator structure and a filter comprising such resonator structure," *Patent Number 6812619*, November 2004.
 - [47] J. Mateu, C. Collado, A. Hueltes, R. Aigner, N. Khat "Filter circuits having acoustic wave resonators in a transversal configuration, 2867-2184," PATENT, 2018.
 - [48] J. Mateu, et al "Acoustic Wave filter for enhance performance," de *International Ultrasonic Symposium*, Kobe, Japan, 2018.
 - [49] I. H. a. J. R. B. S. Senior, "Synthesis of lossy filters," *32nd Eur. Microwave Conference, Milan, Italy*, pp. 401-404, 2002.
 - [50] D. Pozar, *Microwave Engineering*, Wiley & Sons, 1998.

- [51] E. Kreyszig, *Advanced engineering mathematics*, John Wiley & Sons, 1972.
- [52] J.Larson, R. Ruby "Modified Butterworth-Van Dyke circuit for FBAR resonators and automated measurement systems," de *IEEE Ultrasonic Symposium*, San Juan de Puerto Rico, 2000.
- [53] R. Aigner, "Extende BVD Model - Level 2- Qorvo Property".
- [54] M. Van Valkenburg, *Network analysis*, Prentice-Hall, 1955.
- [55] F. Gantmacher, *The theory of matrices*, New York: The Chelsea Publishing Co, 1959.
- [56] J-S.Hong, "On the performance of HTS microstrip Quasi-elliptic function filters for mobile communications," *IEEE Transaction on microwave theory and techniques*, vol. 48, n° 7, p. 1240, 2000.
- [57] S. Amari, "Singlets, cascaded singlets and the nonresonating node model for advanced modular desing of elliptic filters," *IEEE Microwave Wireless Components Letters*, vol. 14, pp. 237-239.
- [58] Keysight, "Advanced Design systems (ADS)".
- [59] C. Collado, et al. "Nonlinear Effects of SiO2 layers in bulk acoustic Wave resonators," *IEEE Transactions on Microwave Theory and Techniques*, vol. 66, n° 4, pp. 1772-1779, 2018.
- [60] S. Shim, D. Feld "A General nonlinear Mason Model and its application to piezoelectric resonators," *International Journal of RF and Microwave Computer-Aided Engineering* , vol. 21, 2011.
- [61] M. Cristal, "A technique for the design of multiplexers having contiguous channels," *IEEE Transaction Microwave Theory and Techniques*, vol. 12, pp. 88-93.
- [62] Rodhes, Levy, "A generalized multiplexer theory," *IEEE Trans. Microwave Theory and tehcniques*, vol. 27, pp. 99-110, 1979.
- [63] Rhodes, Levy, "Design of general manifold multiplexer," *IEEE Trans. Microwave Theory and tehcniques*, vol. 27, pp. 111-123, 1979.